1

FATIGUE OF FLUID-SUPPORTED THICK-WALLED CYLINDERS.

By

David Charles Harvey.

A thesis submitted for the degree of

DOCTOR OF PHILOSOPHY

of the University of London

and also for the

DIPLOMA OF IMPERIAL COLLEGE

Department of Mechanical Engineering

Imperial College of Science and Technology

London S W 7.

COPY NO. 2

ABSTRACT

One of the major problems in the development of hydrostatic extrusion as a production process is the design of vessels to withstand high repeated pressures for adequate economic life. It is suggested that vessels prestressed by a layer of pressurised fluid have advantages over conventional designs and two particular examples of such fluid supported vessels are where the support pressure is either static or cycles in phase with the internal pressure.

A fatigue press has been built and special purpose test rigs constructed for the application of combined repeated internal pressure and static or dynamic fluid support pressure to cylinder test specimens in En25 steel. Fatigue tests have been carried out over a wide range of stress conditions and at lives up to 10^5 cycles. The tests have demonstrated that both static support and dynamic support vessel systems are reliable and that good fatigue performance is obtained.

The results of the fatigue tests are presented on a shear stress range/mean shear stress basis for the design of vessels in En25 steel. For the design of yielded En25 vessels elastic-plastic analysis is necessary to use design curves presented on a shear strain range/mean shear strain basis. In both elastic and yielded cases the design curves embrace as wide a range of conditions as would be encountered in the design of either fluid supported or traditional compound vessels.

For high endurance vessel design in a material for which extensive cylinder fatigue data are not available a method is presented which predicts the fatigue limit pressures under all the test conditions employed. For design in the mortal fatigue region in the absence of cylinder fatigue data a simplified fracture mechanics approach is presented which is in good agreement with the experimental results.

ACKNOWLEDGEMENTS.

I wish to thank Dr. B. Lengyel and Professor J.M.Alexander for their constant help and encouragement, Mr. P.G. Ashford for many helpful discussions, and Mr. R.A. Baxter for valuable assistance in the experimental work. Thanks are also due to Rolls-Royce (Bristol Engine Division) for financial help and to the Science Research Council for supporting the project.

LIST OF CONTENTS

LIST OF FIGURES

Note: The letter P indicates a figure which is in the pocket at the end of the thesis.

LIST OF TABLES

NOTATION

Symbols are usually defined on their first appearance in the text or in a diagram. The following reference list contains the commonly occurring symbols.

K ratio	(outer diameter)/(inner diameter)
a, b	bore radius, outer radius
c	elastic-plastic interface radius
r	any radius
p	pressure
p_i, $p_{i_{max}}$	internal pressure, maximum internal pressure
p_o, $p_{o_{max}}$	external pressure, maximum external pressure
p_e	endurance pressure
p_c	clamping pressure
p_h	hydraulic pressure
$p_{collapse}$	collapse pressure
$\sigma_1, \sigma_2, \sigma_3$	principal stress components
$\sigma_\theta, \sigma_r, \sigma_z$	principal hoop, radial, and axial stress components
$\sigma_{1_{max}}$ etc.	maximum principal stress components
$\sigma_{\theta\ effective}$	effective hoop stress
$\sigma_{\theta\ Lamé}$	Lamé hoop stress

$\Delta\sigma$	asymptotic stress range
$\epsilon_1, \epsilon_2, \epsilon_3$	principal strain components
$\epsilon_\theta, \epsilon_r, \epsilon_z$	principal hoop, radial, and axial strain components
ϵ_p	plastic strain component
ϵ_{el}	elastic strain component
$\Delta\epsilon$	strain range
τ	shear stress $= \frac{\sigma_\theta - \sigma_r}{2}$
τ_{range}	range of shear stress
τ_{mean}	mean shear stress
τ_y	shear yield stress
γ	shear strain
γ_r, γ_o	shear strain at radius r, and outer radius
$\Delta\gamma$	shear strain range
u_r	displacement in radial direction
E	Young's modulus
G	Shear modulus
ν	Poisson's ratio
T	torque
J	polar moment of area
K_I	stress intensity factor
K_C	fracture toughness

ΔK	range of stress intensity factor
N	number of cycles
N_f	total number of cycles to failure
a_a, a_c, a_r	initial, final, and rth cycle crack lengths
$\frac{da}{dN}$	crack growth rate

CHAPTER 1.

INTRODUCTION.

1.1 Background to the Work.

In recent years the industrial application of hydrostatic extrusion has received increasing attention. Considerable effort has been directed towards developing hydrostatic extrusion as a production process. Orthodox hydrostatic extrusion is limited both in the length of product which can be extruded and in the rate of operation as the process has to be interrupted to feed in a new billet. While no practicable continuous method of hydrostatic extrusion is yet proven, both the principle and a particular method of semi-continuous hydrostatic extrusion has been the subject of work at Imperial College.

The semi-continuous hydrostatic extrusion process has been described by Alexander and Lengyel (1), and later papers (2,3) by the same authors have dealt with particular problem areas involved in the development of hydrostatic extrusion as a production process. The process involves the repeated clamping, extrusion, and release of short lengths of continuous feedstock, and the main problems in developing a semi continuous hydrostatic extrusion machine are,

(i) the design of containers for very large cyclic pressures with sufficient fatigue life.

(ii) the development of feed stock clampling devices.

(iii) the development of static and dynamic seals.

(iv) the investigation of high pressure fluids.

The work described in this thesis is chiefly directed towards an investigation of the first problem area, the fatigue life of containers subject to high cyclic pressures. Initially a design study was carried out by Lengyel, Burns and Prasad (4) to compare six different container designs, monobloc, multi-ring shrink or taper fit, strip wound over a solid liner, strip wound over a segmented liner, and concentric compound cylinders with static or dynamic fluid pressures between them. The study considered a design pressure of 150 $Tonf/in^2$ (2.3 GN/m^2) with a container life of 10^5 cycles. The design study indicated that if the assumptions made about fatigue behaviour proved correct then the design with static interface pressure was most attractive. A container life greater than 10^5 cycles would not be needed for a hydrostatic extrusion press, and it could be uneconomic to strive for anything higher. In two-shift working, the extrusion press running at say 5 cycles per minute, 10^5 life would represent a liner change once in every six weeks, very good by any standard. Also under production conditions damage other than fatigue is almost bound to occur over a period of six weeks and thus the liner of an 'infinite-life' container could need replacing in any case at this stage. The economic advantages of hydrostatic extrusion over conventional metal-working processes such as wire drawing are greatest at the highest pressures. A pressure of 150 $Tonf/in^2$ (2.3 GN/m^2) is probably a conservative limit as the pressurising plunger is supported over most of its length by hydrostatic pressure.

Lengyel and Alexander (2) have investigated container designs for 220 $Tonf/in^2$ (3.4 GN/m^2) cyclic pressures. Two designs with cyclic interface pressure referred to as 'floating liner' and 'floating die' were proposed. Both designs provide a means for generating a supporting pressure on the outside of the liner. The supporting pressure is always proportional to the internal pressure and is determined by area ratio considerations. By suitable design it can be ensured that no tensile stresses occur in the liner, thus enabling the use of hard brittle materials. This can of course be achieved by static supporting pressure but in that case the range of shear and other stresses is much greater than for dynamic support pressure and this could be detrimental in fatigue.

Fluid supported cylinders have many other advantages in addition to the considerations of stress distribution and fatigue behaviour. These may be listed as follows:

(i) The inner liner may be easily removed for inspection or replacement. There is no inherent limitation on the length of a fluid supported container. This is not true of compound vessels involving interference fits between mating cylinders, where a large hydraulic press may be needed to separate the components.

(ii) The dimensional accuracy of the surfaces in contact with the supporting fluid can be of normal hydraulic engineering practice. Extreme precision to tolerances of the order of 0.0001 in (0.0025 mm) is needed for shrink and taper fit construction.

(iii) There is no temperature limitation as in shrink fit containers to the extent of the preload which can be achieved and there is no danger of components suddenly springing apart as in taper fit construction.

(iv) The magnitude of preload achieved by fluid support can be accurately known and maintained.

Also the uniformity of interface loading can be guaranteed except for the region close to the seals where special precautions are needed. Work by Burns and Crossland (5) and Burns and Parry (6) has shown that even under the most careful laboratory conditions shrink fit cylinders are subject to significant axial stresses and the magnitude of the preload conditions can not be predicted accurately. Shrink fit, taper fit, wire wound, and autofrettaged cylinders also suffer from the problem that pressure cycling may result in redistribution of stresses so that the preload conditions at the bore of the vessel are not maintained.

(v) There is a greater chance than with other designs of detecting the failure of a fluid supported liner before further damage occurs. It is simple to monitor an interface fluid pressure signal and to use this signal as part of a fail - safe system within the control system of the extrusion press.

(vi) As there is no metal to metal contact between the liner and outer cylinder of a fluid supported vessel there is no danger of fretting damage which could greatly reduce fatigue resistance. Allowance has to be made for fretting in the design of wire wound containers and in the design study by Lengyel et al (4) this amounted to a fatigue safety factor of three.

(vii) An advantage of the fluid supported construction in the context of hydrostatic extrusion is that the fluid pressure provided or generated can be used to perform secondary functions such as extrusion back pressure or to actuate clamping devices.

Fluid supported cylinders have disadvantages which should not be overlooked in an assessment of vessel designs for hydrostatic extrusion. In the case of dynamic support construction the vessel is considerably more complex than other containers, there are a number of moving components, seals, and check valves subject to fatigue which must reduce the overall reliability of the system. The static support vessel is much simpler although a high pressure pumping system is required. Such systems are now available commercially. The accurate winding of wire or strip under carefully controlled tension however is a difficult mechanical problem and costly capital equipment is needed. In this respect wire winding appears less favourable than a static support system. Seals are a problem in any fluid supported vessel not only in ensuring minimum leakage and long life, but also in the introduction of undesirable stress discontinuities with serious implications for brittle materials with low tensile strength.

From the previous discussion it should be clear that fluid supported vessels are very suitable for high pressure applications such as hydrostatic extrusion. There is a need however for fatigue tests to be carried out on fluid supported vessels before large scale design is attempted. The purpose of these tests would be to develop fluid supported vessels from a basic idea to a reliable working stage and to gather fatigue information which can be used in the subsequent design of large scale hydrostatic extrusion vessels or high pressure vessels for other fatigue applications. The development of fluid supported vessels would produce information about related topics such as the performance of static and dynamic seals, high pressure check valves, and accurate repeatability of pressure over long time periods, and the effect of vessel geometry. Such information and the fatigue data would be of considerable value not only in hydrostatic extrusion work but in general high pressure technology. Developments such as fast cycling isostatic compaction, high pressure chemical processes, and metal cutting by high pressure fluid jets all demand this information for the design of safe reliable equipment.

The advantages listed earlier of the fluid support principle over other methods of vessel design apply perhaps even more strongly when a fluid support vessel is used as a fatigue specimen. It is possible to investigate a wide range of accurately known, uniformly applied, and constant loading conditions. These are essential requirements for fatigue testing which are not satisfactorily met by other vessel designs. The various elastic fatigue stress conditions which can be achieved in both dynamic and static supported vessels have been discussed by Harvey and Lengyel (7), and recently Crossland (8) has proposed the use of combinations of internal and external pressure to investigate the fatigue of thick-walled cylinders. The most significant feature of fluid supported cylinder fatigue tests is that such tests permit the investigation of the separate effect of the important fatigue parameters, an impossibility with monobloc cylinders and an impracticable proposition with compoound cylinders.

1.2. The Process of Fatigue.

The process of failure by fatigue is currently considered to be divided into a number of stages which may be identified (9) as crack initiation, slip band crack growth, crack growth on planes of high tensile stress, and final fracture. Fatigue initiation occurs in slip bands which result from partially reversible slip motion on a few favourably oriented slip planes governed by shear stress. Slip - band crack growth, termed Stage I crack growth by Forsyth (10), entails the deepening of the initial crack on planes of high resolved shear stress. This mode of propogation may be absent in a highly stressed specimen or or it may involve up to 90% of the life in a low stress test. Crack growth on planes of high tensile stress known as Stage II growth is the most familiar mode and produces by far the largest area of fatigue fracture surface. The surface often shows characteristic macroscopic progression marks or striations. The Stage II mode may occupy only 10% of the life to failure in a low stress long life test (high cycle fatigue) whereas in a short life test (low cycle fatigue) it may occupy 100% of the life. The low cycle and high cycle fatigue processes are identical metallurgically and the differences in behaviour in these regimes stem from the different proportion of the life to failure spent in the two stages of crack propogation. For example the inherent scatter in the results of high cycle fatigue tests may be attributed to the large fraction of the life spent in Stage I crack propogation where microstructural variations are significant. The final fracture in fatigue occurs when Stage II cracks have weakened the component to the extent that the gross stress can no longer be supported and unstable fast fracture results.

In the engineering analysis of fatigue a clear distinction is made btween low and high cycle fatigue. The dividing line between the two regimes usually occurs at about 10^4 to 10^5 cycles and may be attributed partly to the different loading cycles employed in laboratory fatigue testing. High cycle fatigue is normally characterised by constant load amplitude cycling, and low cycle fatigue by constant strain amplitude cycling. In high cycle fatigue the usual elastic relations between stress and strain are valid, whereas in low cycle fatigue macroscopic plasticity is involved and the stress/strain relationship is non-linear and further complicated by the cyclic strain hardening or softening characteristic of the material (11).

Ideally a designer needs the knowledge to design against fatigue in a material for which perhaps only static properties or at best standard laboratory fatigue data are available. The complexity of the fatigue process is such that reliable design from static properties will probably never be achieved although design using standard data such as zero mean stress rotating bending can be attempted. There is a vast amount of information (12, 13) to call upon particularly in the high cycle fatigue regime, and at present the technique consists of gathering together an appropriate series of modifying factors to add the influences of mean stress, type of loading, size effects, stress concentrations, surface finish, environment and so on to the basic fatigue data. The literature in low cycle fatigue is also considerable although the Manson-Coffin Law (14) has rationalised the fatigue behaviour of a wide range of materials and some success has been achieved in relating fatigue to static properties (11). Low cycle fatigue is not as sensitive to the influences of the factors mentioned earlier but allowances can be made for such effects where necessary.

One of the most important influencing factors in the context of the present work is the effect of a multiaxial stress system in fatigue. The various criteria governing static failure under complex stress have been applied to fatigue and it is usually argued that as fatigue failures propagate from a free surface where one principal stress is zero it is sufficient to consider biaxial stresses only. Forest (12) discusses the work of a number of investigators and shows that a von Mises shear strain energy criterion most closely represents the available data, although there are a number of exceptions. Gough et al (15) proposed an empirical elliptical relation to predict the fatigue strength under the important engineering combination of bending and torsion. In low cycle fatigue, work has also concentrated on biaxial fatigue and a von Mises equivalent strain relationship has been applied (11) to relate biaxial fatigue results to the basic Manson-Coffin Law. Pascoe (16) has suggested that for design purposes fatigue results for all states of strain could be displayed on a single plot. Pascoe's work showed that low cycle biaxial fatigue is adequately represented by the Manson-Coffin Law although the constants are dependent upon the state of strains as well as the strain amplitude. Low cycle biaxial fatigue data from other sources along with uniaxial data is used by Pascoe to plot contours of equal life on the basis of the two principal strains.

Recently much attention has been devoted to the fracture mechanics analysis of fatigue. Fracture mechanics is the study of the mechanics of crack growth starting from an initial crack or flaw. It therefore goes straight to the heart of the fatigue process and can be regarded as a more fundamental approach than phenomenological studies to understanding fatigue. In fracture mechanics the stress field in the region of a crack is described by the stress intensity factor K_I and values of K_I are now known for a wide range of cracked configurations (17).

The subscript, I, denotes the opening mode of crack surface displacement which is the most common mode of fatigue crack propogation. When K_I reaches a critical value K_c known as the fracture toughness of a particular material then the crack extends, usually catastrophically. The final fracture stage in the fatigue process may occur in this manner. However the concept of the stress intensity factor can be used in the study of 'sub-critical' crack growth mechanisms such as fatigue and stress corrosion which cause slow crack growth at stress intensity factors below K_c (18). Paris and Erdogan (19) and more recently Frost et al (20) have shown that the fatigue crack growth rates for a large body of experimental data can be related to the range of stress intensity factor, ΔK , by an expression of the form,

$$\frac{da}{dN} = B(\Delta K)^m \qquad (1.1).$$

where B and m are constants.

Once a designer is armed with a master curve of da/dN against ΔK for a particular material he can then predict the crack growth rate in any cracked body from a knowledge of the appropriate stress intensity factor. This is the chief attraction of the fracture mechanics approach to fatigue.

1.3. The Repeated Pressure Fatigue of Thick-walled Cylinders.

Manning (21) and Crossland (8) have both reviewed the literature on thick-walled cylinders subject to repeated internal pressure. Manning's contribution contains an interesting account of events leading up to the commissioning of the first pulsating pressure fatigue rig, but covers only the earlier work on the subject up to 1963. Crossland's review published in 1970 is currently the most comprehensive account available. It contains in addition a review of other fatigue tests carried out under fluid pressure. The present review includes both low cycle and high cycle fatigue work and treats the subject chronologically. Naturally some of the work has already been reviewed by Manning or Crossland but it is important to present a complete picture to highlight the significance of more recent work and the outstanding gaps in our knowledge.

A large percentage of all thick-walled cylinder fatigue results has been obtained with the 'Bristol' pulsating pressure fatigue machine. Details of the design of this machine were given along with the first results by Morrison et al.[1] (22) in 1956. The machine operates by reciprocating a crank-driven ram inside a closed volume of fluid in a closed ended test cylinder. To-day the machine is able to run at speeds up to 1,000 cycles/min, and apply cyclic pressures up to 50,000 lbf/in^2 (345 MN/m^2). Repeated pressure fatigue tests were carried out by Morrison et al [1] on 1 in (25.4 mm) bore cylinders of En.25 steel heat treated to a nominal ultimate tensile strength of 56 $Tonf/in^2$ (865 MN/m^2) sometimes referred to as 'soft' En.25. After the cylinders had been machined to the correct dimensions, and the bores honed to a mirror finish the cylinders were vacuum stress relieved. The cylinder K ratios ranged from 1.4 to 2.0 and it was found that the results were most closely grouped together within a narrow band if plotted on the basis of maximum shear stress rather than the maximum tensile hoop stress. However the nominal repeated shear stress value at the fatigue limit was surprisingly low compared with the fatigue limit shear stress in torsion. This could be attributed perhaps to the effect of hydrostatic tension in a closed-ended cylinder or to the penetration of micro-cracks by high pressure oil. Further tests were reported by Parry[1] (23) on a wider range of K ratios, from 1.2 to 3.0, and also on the effects of a 0.6 in (15.2 mm) bore and longer gauge length, honing and rubber protection of the bore. The results confirmed the maximum repeated shear stress criterion of failure. The smaller bore and increased gauge length appeared to have no influence whereas honing after, rather than before, stress relieving, and bore protection both had a significant strengthening effect. As such a wide range of K ratios and corresponding hydrostatic tensile stress states had then been tested it was argued that the initial shear stress could hardly be affected by the magnitude of the hydrostatic tensile stress. It was also concluded that the effect of both honing, and bore protection was to prevent the high pressure oil from penetrating micro-cracks.

Considerable new thick-walled cylinder fatigue data for En.25 steel and a range of other materials was presented in 1960 by Morrison et al[2] (24). It was found that autofrettage and nitriding significantly improved the fatigue resistance of En.25 cylinders, and that the benefits of autofrettage were greater for the larger K ratios. Autofrettaged cylinders could be strengthened still further by rubber protecting the bore. Fatigue results for En.25 heat treated to an ultimate tensile strength of 68 Tonf/in^2 (1050 MN/m^2), a 3% chromium steel known as Hykro, and 0.15% carbon steel all confirmed the maximum repeated shear stress criterion at the fatigue limit, and all exhibited a similar measure of disagreement with the respective torsional fatigue limits. The fatigue resistance of Hykro cylinders was improved substantially by nitriding although some of the improvement may have been due to yielding and resultant autofrettage. Yielding was also blamed for the poor agreement on a shear stress basis of the results for various K ratio cylinders in both austenitic stainless steel and titanium. DTD.364 aluminium alloy cylinders results have no true fatigue limit. In conclusion Morrison et al[2] suggested as a simple design rule that the permissable repeated shear stress at the fatigue limit for a thick-walled cylinder is given by one third of the ultimate tensile strength.

The fatigue strength of cylinders with cross-bores was considered by Morrison et al[3] (25) and experimental results were presented for En.25 cylinders of 2.25 K ratio with $\frac{1}{8}$ in (3.2 mm) and 3/16 in (4.8 mm) diameter crossbores. It was shown that the reduction in the fatigue strength could be estimated by a simple stress concentration factor approach.

The results of a low cycle fatigue investigation on open-ended thick-walled cylinders was reported in 1963 by Davidson et al (26). The cylinder material was SAE 4340 steel, which is fairly similar to En.25, heat treated to an ultimate tensile strength of 71.5 Tonf/in^2 (1104 MN/m^2). Repeated internal pressure tests were performed on cylinders of K ratios ranging from 1.4 to 2.0 in both the non-autofrettaged and fully-autofrettaged conditions. The test rig for pressures up to 80,000 lbf/in^2 (552 MN/m^2) operated from an intensifier system and fatigued four specimens at the same time. However the maximum cycle speed was only 20 cycles/min. For pressures up to 150,000 lbf/in^2 (1034 MN/m^2) a Harwood intensifier system was used with an even slower cycle speed of 10 cycles/min. The results were presented on the basis of a normalised principal stress difference function and it was observed that the fatigue resistance was increased by autofrettage and that the benefit increased with decreasing operating stress level and increasing K ratio.

The second low cycle fatigue investigation on thick - walled cylinders was presented in 1965 by Austin and Crossland (27). The test material was En.25 in the soft 56 Tonf/in^2 (865 MN/m^2) condition. Plain 1 in (25.4 mm) bore cylinders of 1.4 and 1.8 K ratio, and cross bored cylinders of 2.25 K ratio were subjected to repeated internal pressures up to 40 Tonf/in^2 (618 MN/m^2) in a closed ended condition. The test rig consisted of a hydraulically operated jack which reciprocated a plunger through a conventional hydraulic seal within the test specimen.

The plain cylinder results were plotted against life on the basis of the maximum elastic shear stress range, and on the basis of maximum hoop stress range. In the mortal region the agreement between the two fatigue curves was closest on the hoop stress plot although illogically the 1.4 K ratio cylinders appeared to live longer than the 1.8 K ratio cylinders. For that reason the shear stress criterion was preferred.

Further thick-walled cylinder and ancillary tests on soft En.25 and other materials were also reported in 1965 by Parry[2] (28). The En.25 results showed that there was no size effect within the range of bore diameters from 1 in to 0.375 in (25.4 mm to 9.5 mm), and that there was little difference in the fatigue lives of cylinders with radial or tangential cross-bores. Autofrettaging cross- bored cylinders greatly increased their fatigue strength even to the extent of compensating completely for the detrimental effect of the cross-bore. The other materials covered in the investigation were 13% Cr En.56 steel, 18% Ni - Co - Mo maraging steel, 1% Cr ball race steel En.31, beryllium copper, and tungsten carbide. The En.56 cylinders were tested in various tensile strength conditions and it was shown that the higher tensile strength cylinders had lower fatigue strength due probably to the poor transverse fatigue properties of this material. Maraging steel was also a disappointing performer at long lives in spite of its very high tensile strength. There is little to comment on the cylinder fatigue results for En.31 and beryllium copper, and no cylinder fatigue results could be obtained for tungsten carbide.

As yet no serious attempt had been made to predict cylinder fatigue behaviour from basic fatigue information such as from rotating bending tests. Hannon (29) proposed an empirical relation

$$\cancel{P_e = \left\{ (HW)\,(MS)\,(SB) \right\} S_f \left(1 - \frac{1}{K^{2}}\right) \left\{ \frac{1}{3} \right\} \qquad (1.2)}$$

$$p_e = \left[(HW)(MS)(SE)\right] S_f \left(1 - \frac{1}{K^2}\right)\left(\frac{1}{\sqrt{3}}\right) \quad (1.2)$$

where the endurance pressure (p_e) is predicted from the rotating bending fatigue limit stress (S_f) and a von-Mises equivalent stress function. Also included are factors which correct for hydrodynamic wedging (HW), mean stress (MS) and size effect (SE). Although Hannon obtained quite g od agreement with the fatigue results published by Morrison et al[2] (24) doubt has been expressed by Burns and Parry (6) on the validity of the correction factors.

In 1967 Blass and Findley (30) published results of pulsating pressure fatigue tests in the region of 10^5 cyclic life on thick-walled cylinders of 1.414 K ratio in SAE 4340 steel (similar to En.25 in the soft condition). A special sub - press had been used to apply pulsating in - phase axial tension or compression, which permitted the influence of the intermediate principal stress on fatigue to be investigated. Over a range of axial stresses from a tensile value equal to the bore hoop stress to a compressive value equal to the internal pressure the experiments showed that the intermediate principal stress had no influence on cylinder fatigue. This important finding meant that in En.25 steel at lives of about 10^5 cycles there was no reason to expect any difference in the fatigue behaviour of open-ended and closed-ended cylinders.

A number of papers (6 , 31-34) on the subject of thick-walled cylinder fatigue were presented in September 1967 at the High Pressure Engineering Conference arranged by the Institution of Mechanical Engineers. En.25 was again the favourite test material. One of the most significant contributions from the point of view of the present work was by Burns and Parry (6). These authors described long endurance fatigue tests using a Bristol machine on monobloc En.25 cylinders with deliberately raised minimum cyclic pressures, and on duplex shrink fit cylinders to investigate the effect of mean shear stress on fatigue behaviour. Results also obtained on cylinders of 0.15% carbon steel. The K ratios tested were 1.4 and 2.0 in the case of the high base pressure tests and 1.2 in the case of the inner cylinder of the compound cylinders. A plot of range of shear stress against mean shear stress for a life of 10^7 cycles showed that the safe range of bore shear stress decreased as the mean shear stress increases providing that cyclic softening does not occur. However there was no agreement with either push-pull or torsion fatigue results plotted on the same graph, and it was suggested that the high pressure fluid in contact with the cylinder bore may be one factor which accounted for the discrepancy. Another factor which could provide a partial explanation was the magnitude of the tensile normal stress on planes of maximum range of shear stress, or simply the maximum tensile stress.

Frost and Burns (31) subjected 1.62 K ratio cylinders of En.25. to static internal pressure and push-pull fatigue along their longitudinal axis. The purpose of the tests was to investigate the effect of Tellus 15 oil and mercury on the fatigue behaviour. It was concluded that at high endurances the fatigue strength was unaffected by either fluid at pressures up to 32,000 lbf/in^2 (221 MN/m^2). The fatigue limit was reduced with increased internal pressure but this was due to the higher static stresses and not the particular pressure medium.

Thick-walled cross-bored cylinders of 2.25 K ratio in En.25 steel heat treated to three ultimate strength conditions 63, 83.5 and 112 Tonf/in^2 (973, 1290 and 1729 MN/m^2) were subjected to repeated internal pressure by Crossland and Skelton (32). The authors used a modified version of the testing machine described by Austin and Crossland (27) and obtained failures at lives from 10^2 to 10^6 cycles. At the fatigue limit the harder cylinders lasted longer whereas at short lives the softer cylinders had the greater fatigue resistance. The harder cylinders were also subject to catastrophic fast fracture at failure and this led the authors to emphasize the importance of fracture toughness of the cylinder material and fracture mechanics analysis of crack propagation for the safe use of high strength materials.

Austin et al (33) carried out a comprehensive series of tests in the range 10^3 to 10^5 cycles on open-ended cylinders of a gun steel similar to SAE 4330 which had been heat treated to between 79 and 88 Tonf/in^2 (1220 and 1359 MN/m^2) ultimate tensile strength. The cylinder K ratios were 1.2, 1.5, and 2.0 and both smooth and rifled bore specimens were tested. Tests were carried out on cylinders which had been autofrettaged by means of an oversize swaging mandrel, and also cylinders with chromium plated bores. The authors found that the results from different K ratio cylinders correlated best on the basis of maximum hoop stress. Autofrettage was observed to increase fatigue resistance more for rifled than for smooth bore cylinders and generally more improvement was obtained with increasing K ratio. There was a slight reduction in the fatigue strength of cylinders with chromium plated bores.

Jones and Tomkins (34) investigated the low endurance fatigue of very thick-walled cylinders. The cylinder K ratios were 3, 5 and 7, and the material used throughout was En1A steel. The specimens were fatigued in the range 10^3 to 5.10^4 cycles in an open-ended condition by using a testing machine to reciprocate a sealed piston within the bore of the test cylinder. Most cylinders were tested at pressures above the collapse pressure and therefore considerable plastic expansion took place early in the life before a steady state was reached but nevertheless the final failure was by fatigue. The authors proposed a number of mathematical models to represent the shakedown of stress in the cylinders to a steady state. Using these models with plastic analysis of the cylinder and cyclic stress / strain data for the cylinder material it was possible to predict the steady state strain range, and finally to predict the cyclic life from the Manson-Coffin Law. The prediction of the experimental results was reasonably good although the method was complex for design purposes. Jones and Tomkins were the first to present a logical analysis enabling prediction of low endurance cylinder lives from basic fatigue data, and it is significant that no allowance was made in the analysis for the oil effect.

The first results of fatigue tests carried out on fluid supported thick-walled cylinders were described in 1968 by Harvey and Langyel (7) 'Soft' En25 steel cylinders of 1.4, 1.8 and 2.0 K ratio were subjected in a special sub-press to repeated internal and external pressure. A few monobloc tests were also reported for comparison. It was concluded from the limited evidence that the reduction in maximum tensile hoop stress achieved in the fluid supported tests had not influenced the permissable range of shear stress.

A review of failure criteria for the pulsating pressure fatigue of thick-walled cylinders was presented in 1969 by Marsh and Haslam (35). The review confirmed the maximum shear stress criterion at the fatigue limit but suggested that a maximum principal strain criterion was more correct in the mortal region. However the authors also mention the idea of using Gough's combined stress criterion in conjunction with stress components which have been modified to account for the oil pressure effect. Experimental results of 1.2 K ratio En.26 cylinders to pulsating pressure were also presented and shown to be in good agreement with the results of earlier workers.

In a further report Haslam[1] (36) expressed Gough's combined stress criterion in principal stress form, and proposed that the oil effect should be represented by a simple function (n p), where n is constant and p the fluid pressure, added to the conventional Lame hoop stress to give an 'effective' hoop stress which should then be used in Gough's criterion. It was argued that if the cylinder bore were protected from the direct effects of the fluid pressure then clearly (n) must be zero. The results of pulsating pressure fatigue tests on protected bore cylinders of 1.2 K ratio in En26 steel were presented by Haslam[2] (37) in 1970, and it was confirmed that the fatigue behaviour could in fact be predicted from the rotating bending fatigue limit by use of Gough's criterion and the simple Lamé principal stresses. The best value for the oil effect factor (n) was found by analysis of all the known experimental results to be $(5 / K + 1)$. Very good agreement was obtained between the predicted and experimental fatigue limits for a wide variety of materials and K ratios.

The fatigue behaviour of thick-walled cylinders in the low endurance region was also investigated by Haslam[3] (38). Use was made of a simplified fracture mechanics approach on the basis of the fatigue crack growth rate equation (1.1) mentioned in Section 1.2. By integrating equation (1.1) the number of cycles (N) required to propagate an initial fatigue limit crack through the wall thickness of the cylinder can be found. A very simple stress intensity factor was used and the governing stress assumed to be the effective hoop stress determined earlier by Haslam[2] (37) which takes account of the oil effect. The fatigue curves predicted by Haslam were in good agreement with his own experimental results for En.26, and also with previous work by Morrison et al[2] (24), and Austin and Crossland (27) for En.25, Hykro, and 0.15% carbon steel over a range of K ratios from 1.2 to 3.0. Less satisfactory agreement was obtained for aluminium alloy DTD.364 and titanium cylinders results but relatively few experimental data were available in the mortal region. Haslam recommended that the method of prediction should be limited to repeated internal pressures below those required to cause yielding in the hoop direction at the bore.

In conclusion, there is considerable experimental evidence for a maximum shear stress criterion of failure for the high endurance fatigue of thick-walled cylinders in ductile materials. The range of shear stress at the fatigue limit is much lower than would be expected from standard fatigue tests and the difference can be attributed to the combination of the effects of mean stress and the high pressure oil in contact with the bore. The importance of mean stress was shown by tests on autofrettaged cylinders, compound cylinders, and cylinders with high minimum pressure, and the oil effect was revealed by rubber-protecting the bores of monobloc cylinders. Tests have also shown that the magnitude of the axial stress has no effect. The most satisfactory way yet found to predict the fatigue limit of monobloc cylinders from standard fatigue data is to employ Gough's combined stress criterion of failure in conjunction with Lamé stresses modified to account for the oil pressure effect and known as 'effective' stresses. In this way the oil effect is quantified empirically but is still imperfectly understood.

Less experimental data are available in the low endurance fatigue region and both maximum shear stress and maximum hoop stress criteria have received support. The stress ranges are treated as purely elastic even beyond yield and no analysis is normally made of the state of mean stress, despite its importance as a fatigue parameter. A linear elastic fracture mechanics approach again using 'effective' stresses has resulted in good predictions of monobloc cylinder fatigue behaviour in the mortal region provided the cyclic behaviour is predominantly elastic. When considerable yielding takes place a full shakedown analysis of the repeated stress state and the application of the Manson - Coffin Law may be necessary.

1.4 Objectives and Programme of Work.

The broad objective of the work was to investigate the fatigue behaviour of fluid supported thick-walled cylinders over a range of lives up to 10^5 cycles. The particular justification for the work was to provide design information on the feasibility and fatigue performance of fluid supported vessels for semi-continuous hydrostatic extrusion.

The figure of 10^5 cycles was judged to be an economic life expectation for an extrusion vessel and there was no intention to gear the investigation specifically towards a study of low cycle fatigue. Fluid supported vessels have applications outside hydrostatic extrusion, and the fatigue data from testing fluid supported vessels can be applied to other prestressed vessel designs. In fact a more general aim of the work was to provide for the first time reliable fatigue criteria for a range of lives and stress conditions of considerable importance in prestressed vessel design. It was hoped also that the tests might throw some light on the little understood fatigue strength reducing effect of high pressure oil in contact with the bore of a cylinder subject to repeated pressure fatigue.

Two particular designs of fluid support vessel were of interest; one with static external pressure and the other with dynamic external pressure in phase with the cyclic internal pressure. It was intended that work should not only reveal the merits of these designs on the basis of fatigue but also on practical grounds such as mechanical reliability and sealing performance. While not a primary objective of the work practical information from the tests would be very valuable to the designer concerned with high pressure fatigue. It was decided that this first venture into fluid supported vessel fatigue would be made at relatively modest cyclic internal pressures up to 50 $Tonf/in^2$ (772 MN/m^2) with a material for which considerable fatigue data including thick-walled cylinder fatigue already existed, namely En.25 steel in the 'soft' 56 $Tonf/in^2$ (865 MN/m^2) ultimate tensile strength condition. By limiting the pressure conditions it would be possible to reduce the scale of the test rigs and employ fairly simple components for end plates outer vessels, and tie rods. Hopefully in this way fatigue failures in components other than the test specimens would be avoided. It was decided to test cylinders in the open-ended condition as this is the most convenient arrangement for fluid support vessels and is of most interest in hydrostatic extrusion. By using En.25 steel it would be necessary to perform a minimum of ancillary tests as a vast body of information was already available to assist in the analysis of fatigue results.

Before testing could start a considerable quantity of test equipment had to be gathered together. The programme of work was divided into the following broad stages.

1. Design and build. (a) Fatigue press.
   and (b) Static high pressure pumping system.
2. Design and build. (a) Dynamic support test rig
   and (b) Static support test rig

   Arrange high pressure measuring system and recording system, and means of calibration.
3. Ancillary mechanical property tests on En 25 material.
4. Fatigue tests on monobloc, and fluid supported cylinders.
5. Analysis of results.

CHAPTER 2.

THE FATIGUE PRESS.

2.1 Design Considerations.

The overall aim of the present work was to develop principles on which the design of a hydrostatic extrusion production machine could be based. Vessel fatigue behaviour was to form the heart of the work but it was intended that in addition information on seal performance, high pressure instrumentation, and press performance would be gathered. It was, therefore, important that the fatigue testing machine used in the test work should operate in a manner representative of a potential production machine. Such a machine would be likely to operate at a slow cycling rate and with a typical container life of 10^5 cycles.

The first design decision concerned the maximum cyclic pressure which the press would be required to generate. It was felt that this pressure should be in the range of 150 to 200 Tonf/in^2 (2.3 to 3.1 GN/m^2) for future work on very high strength vessels. The simplest method of generating pressure would be to reciprocate a plunger within seals inside the test rig itself. In this way the number of components subject to fatigue would be kept to a minimum, and a variety of different testing designs could be accommodated. The maximum plunger load which the press could be required to produce was the next consideration. If the plunger diameter were very small then the press load and the scale of the press would also be small. However considerations of buckling and the need to lead electrical wires through the plunger led to a compromise minimum plunger diameter of $\frac{3}{8}$ in (9.5 mm). The minimum press capacity could then be fixed at 20 Tonf (199 kN). This meant that allowing for 10% friction losses a pressure of 164 Tonf/in^2 (2.53 GN/m^2) could be generated with a $\frac{3}{8}$ in (9.5 mm) diameter plunger. It was decided that in a simple test rig a 1/2 in (12.7 mm) working stroke would suffice but for complicated rigs with internal movements such as a floating liner rig 1 in (25.4 mm)or more could be necessary. A further requirement beyond the basic working stroke was the facility to withdraw the plunger approximately 4 in (102 mm) to clear the test rig.

Having established the essential features of the press the possible driving systems were reviewed. The choice lay between a mechanical crank operated system and a hydraulic system. The main feature of a crank driven system would be a high cycle speed, up to 600 cycles/min against 60 cycles/min for a hydraulic system, but high speed would not necessarily be an advantage in the present application. For example a cycle speed of 600 cycles/min would be quite unrepresentative of a hydrostatic extrusion machine, and would dictate the use of a non-rubbing seal such as the Morrison seal. It was felt however, that the use of synthetic rubber seals would be inevitable in both the test rig and in a hydrostatic extrusion machine because of their simplicity and ability to accommodate misalignment.

A hydraulic press could easily provide the requirement of long stroke capability with a short working stroke, whereas this would be much more awkward to incorporate in a mechanical system. The accurate maintenance of test rig cyclic pressures would be affected in a hydraulic system by variation in seal friction. In a mechanical press cycling with constant stroke amplitude changes in the compressibility of the high pressure fluid with temperature would also influence the accuracy of the testing pressure. In addition to a change in compressibility seal leakage would affect the peak pressure if the stroke were fixed. It was felt that seal friction in the cylinder of a hydraulic press would stabilise after a short period of use and that the frictional variations in the test rig seals would be less significant than the compressibility and leakage effects in a mechanical system.

In conclusion the hydraulic operated press had most to offer for the test rig of vessel designs for hydrostatic extrusion at high cyclic pressures and lives up to 10^5 cycles.

The speed advantage offered by a crank operated mechanical press would be both unnecessary and undesirable for this work. A hydraulic system could be constructed from commercially available components, and would remain flexible if modifications or extensions were needed. Very slow or incremental pressurisation of the test rig for a burst test for example would be an additional facility provided by a hydraulic press.

2.2 Construction of the Press.

The overall layout of the fatigue press is shown in Fig.2.1, and on the photgraph Fig. 2.2. The press frame and hydraulic cylinder, the hydraulic valve gear, and a separate electrical control cabinet are mounted on a 1/2 in (12.7 mm) thick mild steel table. The table is supported by a welded angle framework which contains the 80 gallon (364 litre) oil tank and the hydraulic pump gear. An electric motor is flange mounted to the pumps and extends from the back of the unit. A separate pump and motor unit for supplying and replenishing high pressure fluid to the test rig is mounted above the hydraulic valve gear in the top compartment of the press.

The press frame, which houses the rig under test, consists of 19 in. (483 mm) square x $2\frac{7}{8}$ in (73 mm) thick top and bottom plates held in position by four 2.1/2 in (63.5 mm) diameter columns. The spacing between the columns is 12.1/2 in (318 mm) which limits the width of test rig which can be accommodated. To ensure good paralleslism

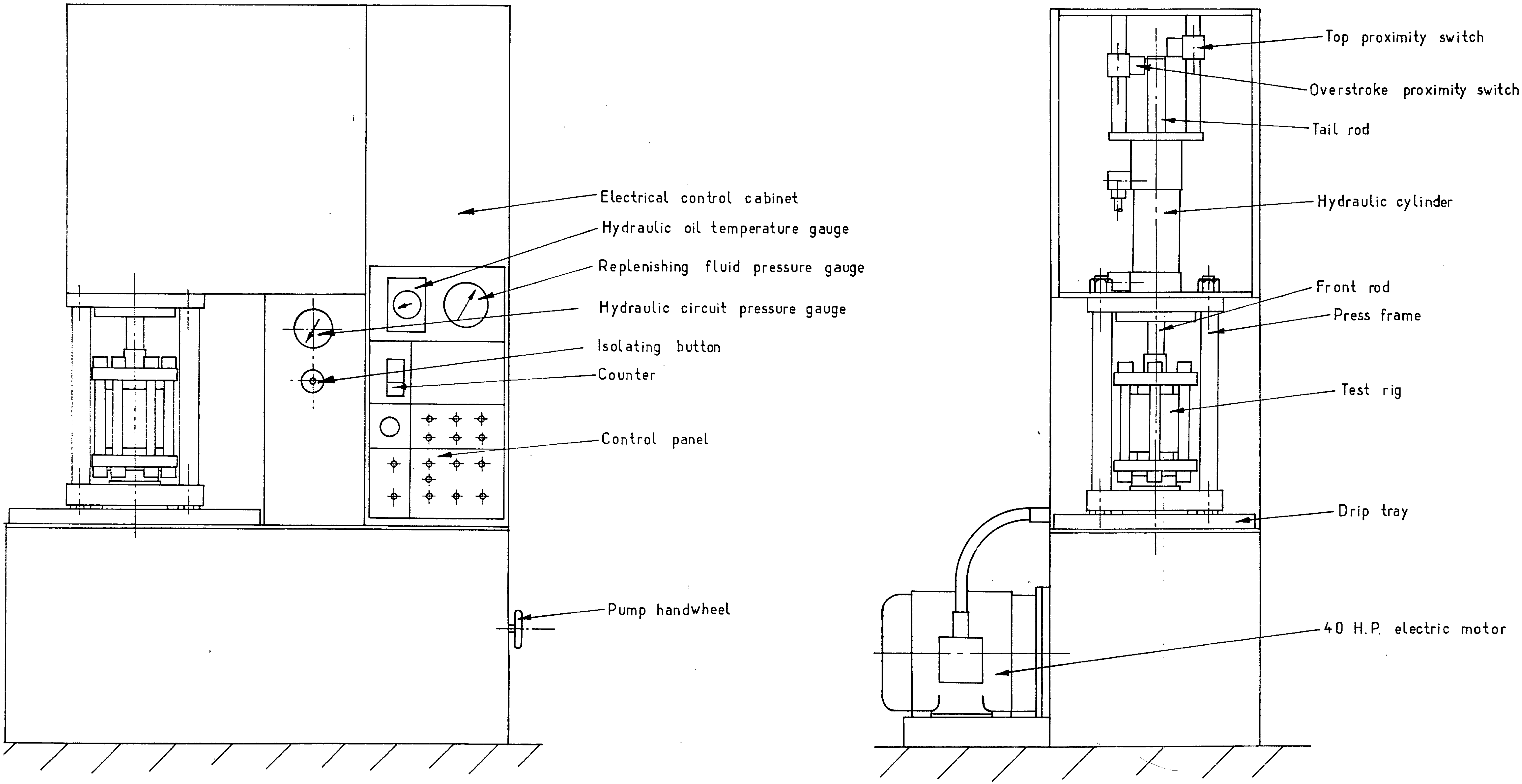

fig.2.1 20 Ton f. FATIGUE PRESS

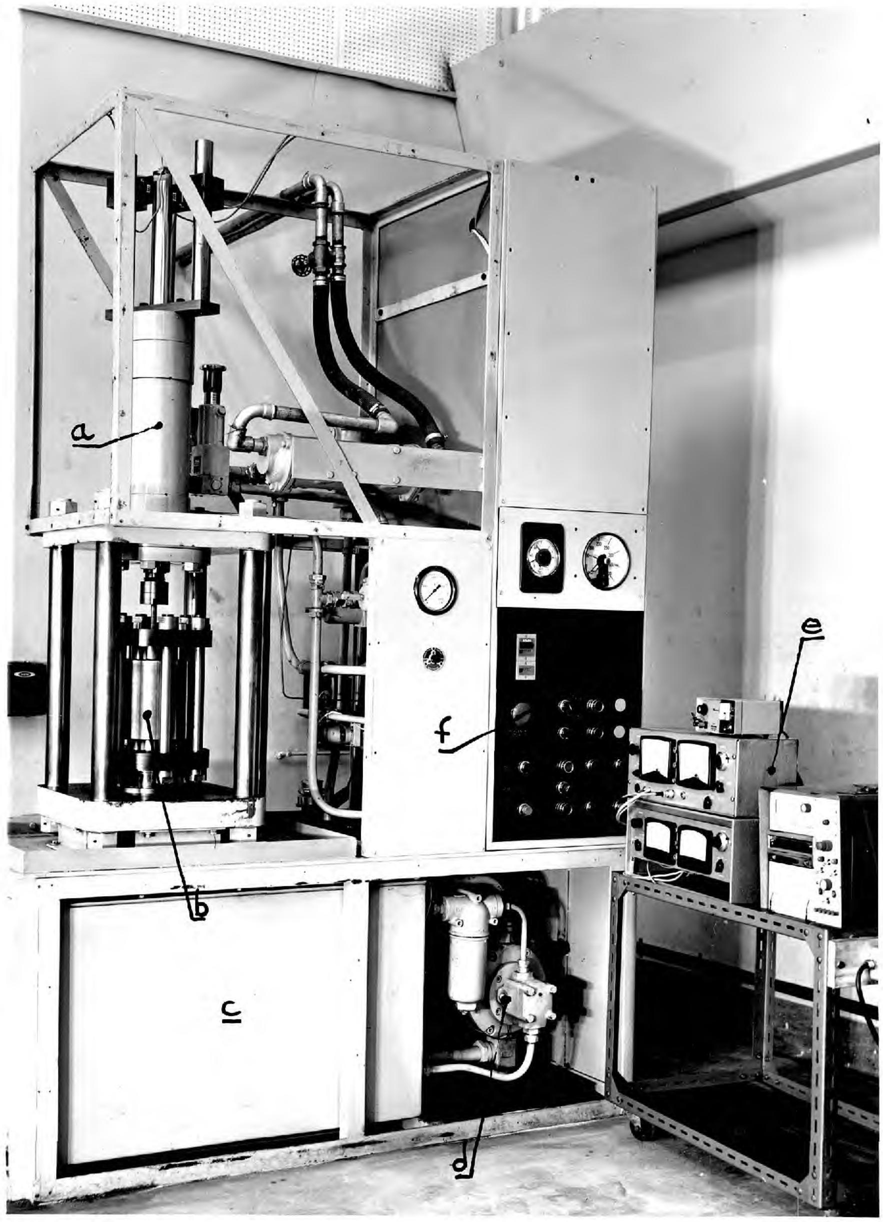

Fig. 2.2 General View of the Fatigue Press.

(a) Hydraulic Cylinder.

(b) Test Rig.

(c) Oil Tank.

(d) Pump Gear.

(e) Instrumentation for Recording Pressure.

(f) Electrical Controls.

between the plates the columns were accurately shouldered at each end, and variations in length between shoulders held within 0.001 in (0.025 mm). 2 in. B.S.F. nuts locked in position on assembly provide rigid clamping under the full press load. The test rig rests on the bottom plate and may be clamped down if required. The top plate supports and locates the hydraulic cylinder. The cylinder, which was custom built by Eland Engineering Co. Ltd., is double ended with a 5 in (127 mm) bore, a 2.1/2 in (63.5 mm) diameter hard chromed rod top and bottom, and a maximum working pressure of 3,500 lbf/in^2 (24.1 MN/m^2). A 1/4in diameter hole through the centre of the rods provides a passage for electrical leads or for replenishing fluid to the test rig if required. The maximum stroke is 6 in (152 mm) and in the fully retracted position the daylight between the front rod and the bottom plate is 20 in (508 mm). Two proximity switches are mounted on opposite sides of the tail rod on vertical pillars. They may be adjusted and locked in position as required.

2.3 Hydraulic Equipment.

A graphical diagram of the hydraulic circuit is shown in Fig 2.3. The equipment was supplied by Towler Bros. Ltd. and assembled by Rae and Stephens Installations Ltd. Oil is supplied to the system by swashplate pump P.V. at a rate variable between 0 and 60 in^3/sec (984 cm^3/sec) and up to a maximum system pressure of 3,500 lbf/in^2 (24.1MN/M^2). The flow rate is adjusted by a hand wheel extending at the side of the press. Vane pump P.F. provides a fixed delivery of 9 in^3/sec (148 cm^3/sec) at 250 lbf/in^2 (1724 KN/M^2) for pilot operation of the main control valve V.1. Filter FL.2. ensures the cleanliness of the pilot supply while FL.1. filters the oil as it is returned to the tank. The oil used is Shell Tellus 27, and a heat exchanger HE ensures that the oil temperature is kept below 60^{o}C.

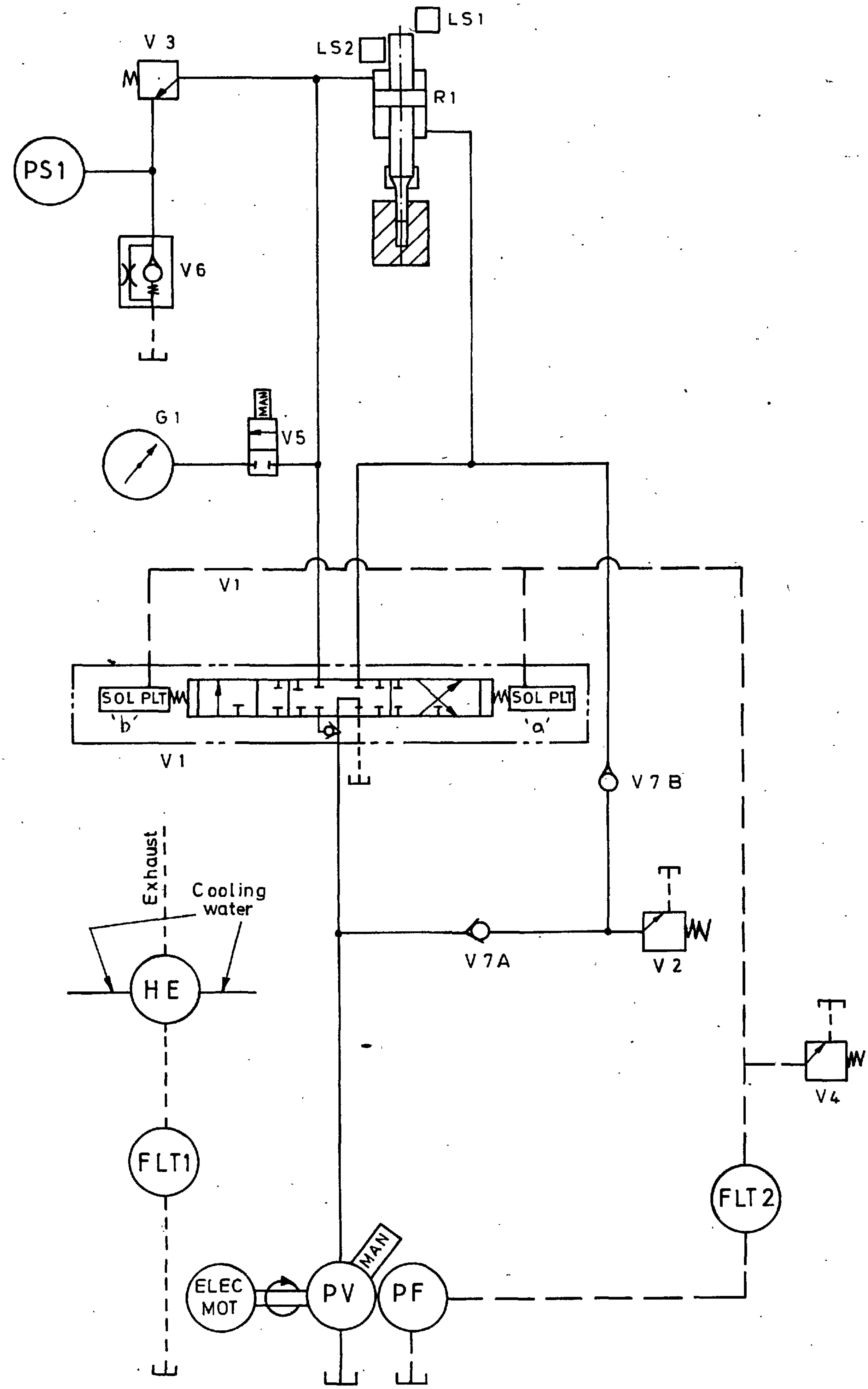

Fig 2.3 HYDRAULIC CIRCUIT OF FATIGUE PRESS

In operation pilot pressure is supplied to both ends of the main control valve spool holding it in the neutral position shown in Fig. 2.3. When solenoid 'a' is energised pilot pressure is exhausted from that end of the spool and the spool moves over to the right toward 'a'. Oil then flows from P.V. to the top annulus of hydraulic ram R.1. while oil trapped below R.1. is returned to tank. The ram travels downwards until the system pressure reaches the setting of relief valve V.3. Oil then spills back to tank via the check valve V.6. which creates a back pressure of 100 lbf/in^2 (689 KN/M^2) to close the pressure switch contacts P.S.1. This pressure switch provides the signal for the reversal of the stroke when cycling. At any stage of press operation the hydraulic pressure in the system may be read on the pressure gauge G.1. by pressing the isolator button V.5.

If the ram is to tavel up solenoid 'b' must be energised to allow pilot pressure from 'a' to push the spool across to the left. However, in this case the spool is restrained by an internal anti-surge piston from complete changeover until fluid pressure in the pipework and top annulus of the ram has dissipated through a small clearance to a value lower than the pilot pressure. The spool then moves fully over and supply from P.V. is directed to the underside annulus of R.1. The ram will travel up to the top of its stroke unless limit switch L.S.1 is arranged to provide a signal to halt or reverse the ram at some intermediate position.

An adjustable stop is provided on the main control valve to control the position at which spool motion is arrested by the anti-surge piston. In this way the rate at which pressure may be dissipated can be controlled , a feature of considerable importance when fatigue testing a pressure vessel.

2.4 Replenishing Pump.

The supply of replenishing fluid to the test rig is provided by a Savery APP 349 Pump and Motor Set mounted above a 5.gallon (23 litre) storage tank. The pump can deliver at 10 gallons/hour (45.4 dm^3/hr) and the delivery pressure may be adjusted by a built-in relief valve up to a maximum of 300 lbf/in^2 (2068 KN/M^2). A Vokes 10 micron filter ensures the cleanliness of the fluid supplied to the test rig. Shell Tellus 27 was used as the test rig fluid for the work described in this report. The delivery pressure,,normally 250 lbf/in^2 (1724 KN/M^2) is indicated on a pressure gauge fitted with electrical contacts and mounted on the main Press Control Panel. The minimum contact is usually set at about 200 lbf/in^2 (1379 KN/M^2). Having switched on the 240 V supply the pump may be started by pressing the white START button on the control panel. The button must be held pressed until the pressure exceeds 200 lbf/in^2 at which point a holding relay is latched. If due to excessive leakage or lack of fluid the pressure fell below 2001bf/in^2 (1379 KN/M^2) the pump would automatically cut out.

2.5 Electrical Controls.

The electrical control system was supplied as a custom built wired up unit by Brookhirst Igranic Ltd. It employs for the purposes of controlling the press a static switching system known as 'Bi-Stat'. In this system conventional circuit devices such as relays and timers are replaced by static units devoid of electrical contacts, and in which limit switches are based on contactless proximity elements. Amplifiers operated by this system serve to energise the contactors or solenoids of the normal system. The life of the static units is independent of the unmber of operations, clearly an advantage for fatigue press operation. A schematic diagram of the control circuit is shown in Fig 2.4P. This will not be described in detail but reference will now be made to the following important control features.

1. A normally open proximity limit switch L.S.1. defines the top reversal position of the ram.
2. A normally-open pressure switch P.S.1, with conventional microswitch contacts defines the bottom reversal position of the ram.
3. A normally-closed proximity limit switch L.S.2., detects when the ram overstrokes past the normal P.S.1. reversal position. This happen when there is a seal failure, leakage, or fatigue failure in the test rig.
4. A normally-open pressure switch P.S.2, detects the malfunction of a separate high pressure pumping rig.
5. A Total Counter records the number of cycles from the start of a test.
6. A Preset Counter signals completion of a preset number of cycles by closing of normally open contacts.
7. A Thermometer Regulator indicates the temperature of the hydraulic oil in the storage tank.

To operate the controls the main isolator switch is first switched on. The motor can then be started by pressing the PUMP ON button and the pumps will deliver oil which is directed by the main control valve back to tank. The main selector switch may be turned either to HAND or AUTO and the corresponding indicator lights will illuminate.

In HAND it is possible to move the ram by pressing the UP or DOWN buttons which energise the appropriate solenoids. Then the button is released the control valve returns to neutral and the ram is held in position. The control switches L.S.1, L.S.2, P.S.1 and P.S.2. are all fully operational in both HAND and AUTO.

However, when setting up it is sometimes useful to overide L.S.2., and this may be done by changing the upper selector switch from NORMAL to L.S.2. OVERIDE. It is impossible to cycle the press unless the selector is returned to NORMAL.

In AUTO two control buttons are in command CYCLE START and CYCLE STOP. Having first set L.S.1., L.S.2, the relief valve V.3, and the pump speed, CYCLE START may be pressed. The ram will then reciprocate between P.S.1. and L.S.1. limits and will continue to do so until stopped by the operator or one of the automatic cut outs.

The operator would normally halt the machine by pressing CYCLE STOP which will return the ram to its top L.S.1 position and leave the pumps running. By pressing EMERGENCY STOP or PUMP OFF the pumps will cut out and the ram will stop immediately.

Automatic halting of the press occurs under any one or a combination of the following circumstances:-

1. Ram overstrokes - L.S.2. contacts open.
2. Pumping Rig pressure faulty - P.S.2. contacts close.
3. Preset count complete - contacts close.
4. Oil temperature above 60°C - contacts open.

Two engraved indicator lights L.S.2. and P.S.2, are illuminated when either or both of these faults occur in operation. The lights are held on after the press has stopped so that the operator immediately knows the cause. When the fault has been corrected the RESET button is pressed to switch off the fault lights.

2.6. Press Performance.

Reference was made earlier to the decompression facility of the main control valve. This feature provides a very important control on the press particularly in the situation when a pressurised column of fluid acting like a spring continues to offer a substantial restoring force on the return stroke. Without decompression in the main valve the ram would return at great speed and cause considerable shock in the pipework. However, by adjusting the decompression screw the return speed can be reduced to match the down speed. There is still some minor shock when the spool finally moves over completely at a line pressure of 250 lbf/in^2 (1724 KN/M^2). With a 5/8" (15.9 mm) diameter plunger this corresponds to an internal test rig pressure of about 5 $tonf/in^2$ (77 MN/m^2). The effect of this pressure is to make the ram speed up for the last stage to the top L.S.1. position. If the working stroke of the plunger were small the time taken for this last stage in the return stroke would be of the same order as the response time of the valve. In these circumstances the press runs erratically and the pressure will not return to zero every cycle. The problem is solved by increased the working volume of fluid in the test vessel. If a base pressure of 5 $tonf/in^2$ (77 MN/m^2) or more is applied to the cycle then the problem does not arise.

The only component in the system which gave serious trouble was the pressure switch. Originally a diaphragm operated pressure switch was fitted but the degree of wear and internal damage sustained after as few as 100,000 cycles often rendered the switch inoperable. Eventually a Lockheed pressure switch of the spring loaded plunger type was substituted and has proved entirely satisfactory,

Variations in friction conditions at the main hydraulic ram and plunger seals were not detectable provided a period of warm up allowed along with a short period of running in at low pressure.

CHAPTER 3.

HIGH PRESSURE PUMPING RIG.

3.1 Design Considerations.

The basic requirement was to provide a self contained, portable and automatic means of generating a high static pressure which could be delivered to a test rig in the fatigue press. In spite of occasional minor leakage from the test rig pressure would need to be kept constant within say $\pm$ 3% for periods up to 100 hours continuous running. Using commercially available components the maximum pressure was limited to 200,000 lbf/in^2 (1379 MN/m^2) for a high pressure intensifier, pipework, and valve gear.

To generate this pressure the low pressure side of the intensifier would need to be supplied at 12,500 lbf/in^2 (86 MN/m^2). This pressure could be provided either by an electrically driven high pressure pump, or an air-hydraulic pump operated from low pressure shop air or gas bottle. An electrically driven pump could run continuously and dump excess fluid through a relief valve, or operate intermittently as determined by a pressure switch. Continuous running involves unnecessary wear and tear on the pump and relief valve while intermittent operation has the disadvantage of a large pressure-on pressure-off differential possibly greater than $\pm$ 3%. An air-hydraulic pump would introduce increased friction loss in the intensification system and this could be subject to variation. However, it was decided that an air-hydraulic pump system was the better choice.

3.2 Description of the Rig.

A graphical diagram for the pumping system is shown in Fig. 3.1P and a general view of the rig is shown in the photograph Figure 3.2. The unit consists of a two tiered trolley, the upper shelf containing the intensifier and associated high pressure piping

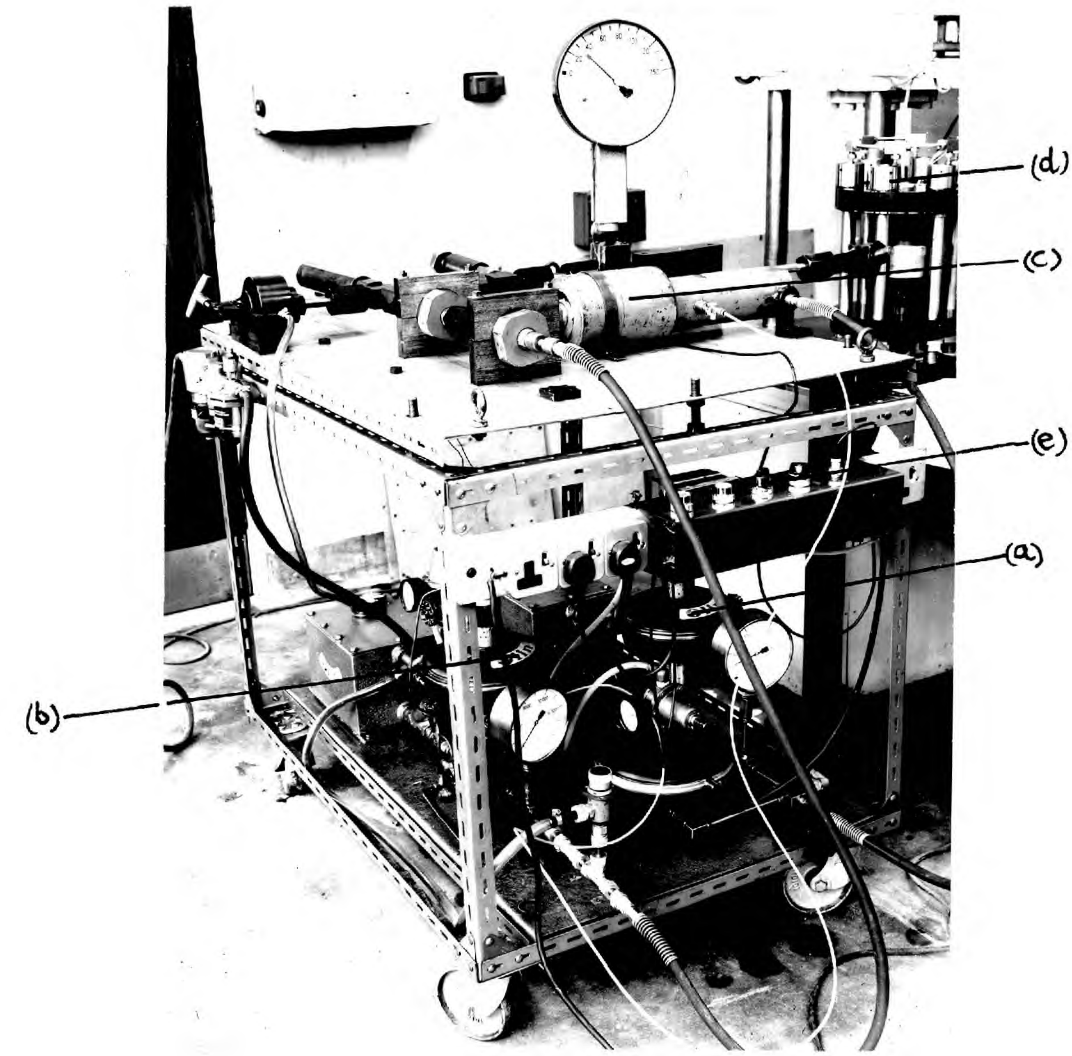

Fig. 3.2 General View of the High Pressure Pumping Rig.

(a) Drive Pump.

(b) Charge Pump.

(c) Intensifier.

(d) Test Rig.

(e) Electrical Controls.

and fittings, and the lower two air-hydraulic pumps, the control gear and separate fluid reservoirs. Flexible high pressure hoses connect the two levels and the height of the upper shelf may be adjusted to suit a particular testing rig.

The 200,000 lbf/in^2 (1379 MN/m^2) intensifier was supplied by Harwood Engineering Co. Inc. It has a nominal intensification ratio of 16 : 1 a 4 in (102 mm) stroke, and a capacity of 1.22 in^3 (20 cm^3) stroke. The 200,000 lbf/in^2 (1379 MN/M^2) fittings and valves were also supplied by Harwood. The two-air hydraulic pumps are identical, 'Olinair Junior' pumps with a nominal pressure ratio of 244 : 1, a maximum working outlet pressure of 15,000 lbf/in^2 (103 MN/M^2) for 60 lbf/in^2 (414KN/M^2) inlet pressure, and a delivery of 0.31 in^3 (5.1 cm^3) per stroke. The pumps with the control gear and reservoirs were supplied by Olin Mathieson Ltd.

One of the pumps acts as a drive pump on the low pressure side of the intensifier while the other serves as a charge pump on the high pressure side. The charge pump is necessary to prime the high pressure system at a moderate pressure, to reduce the number of strokes needed to achieve a high pressure, and also to drive back the intensifier at the end of its stroke.

Referring to the graphical diagram Fig 3.1Pthe operation of the rig is as follows. When the unit is switched on the solenoid shut off valve V.1. allows filtered air at 80 lbf/in^2 (552 KN/M^2) to be admitted to the main air-operated control valve V.2. In its normal position, as shown in Fig. 3.1, V.2. then directs air via a pressure regulator P.R.1. and speed control valve V.3. to the charge pump P.1. The supply pressure to the charge pump is 40 lbf/in^2 (276 KN/M^2) and the pump draws high pressure fluid from tank T.1. and delivers it at 10,000 lbf/in^2 (69 MN/M^2) to the intensifier and high pressure equipment through check valves

V.9. A. and B. Esso Univis P.38 is normally used as a high pressure fluid. The intensifier piston is pushed back and when fully retracted the pressure rises sharply at the charge pump. On the inlet side this pressure is sufficient to withdraw the latch pin L. and allow the actuator A to operate poppet valves V.4. and V.5. At the same time the internal check valve of the pump is unseated so that any high pressure leakage can drain back to tank. V.5. directs pilot pressure to the main control valve V.2., while V.4. exhausts air remaining in the charge pump line.

V.2. now directs the air supply to the drive pump P.2. and to the unloader valve V.7. The unloader valve consists of a shut off valve operated by the piston assembly of an air hydraulic pump. Air supplied to V.7. is regulated by P.R.3. to 20 lbf/in^2 ($138 KN/m^2$) and at this value the valve can check a hydraulic pressure of 35,000 lbf/in^2 ($241 MN/m^2$). When the charge pump P.1. is in operation the valve is not supplied with air and will allow fluid driven back by the intensifier to drain to tank.

The air to drive pump P.2. passes through regulator P.R.2. and speed control valve V.6.. P.2., drawing Shell Tellus 27 oil from reservoir tank T.2., drives the intensifier forward and pressure is gradually built up in the system until the pump stalls. At this point all the piston and friction forces are balanced and the high pressure generated by the intensifier will be nominally 16 x 244 = 3,904 say 4,000 times the regulated air pressure setting of P.R.2. . Clearly P.R.2. must be adjusted with caution. The intensifier may reach the end of its stroke before stall conditions are established. In this case a probe extending into the intensifier barrel will operate poppet valve V.8. and the air supply holding the actuator, A, forward will be exhausted. The Latch Pin L. will re-engage and V.4, V.5 and V.2. will revert to their normal starting positions. Air is once again directed to P.1., and the whole cycle will be repeated until equilibrium pressure conditions are established. A rupture disc assembly is fitted to protect the low pressure side of the intensifier from pressures in excess of 15,000 lbf/in^2 (103 MN/m^2)

An additional check valve V.12 and high pressure relief valve V.13 were incorporated in the circuit after difficulties with the flexible hose. It was found that the hose contained such a large colume of fluid that the charge pump P.1., which is not fitted with an outlet check valve, could not raise the pressure beyond 3,000 lbf/in^2 (20.7 MN/m^2). Check valve V.12 overcame this problem but relief valve V.13 was also necessary as a safety measure against possible high pressure leakage from V.9.A.

3.3 High Pressure Equipment.

The supply of high pressure fluid to a test rig is controlled by two way angle needle valve V.11., Fig. 3.1P An identical valve V.10 can release the pressure in the high pressure system and test rig when required and allow the fluid to drain back to Tank T.1. The safety of the equipment is catered for by a high pressure safety assembly. This contains a pin which will fail in shear at 200,000 lbf/in^2 (1379 MN/m^2). Alternative pins can be fitted to fail at lower pressures. Pressure measurement is performed in two separate ways. A manganin cell provides an accurate and permanent record of pressure on the ultra-violet recorder, while a 150,000 lbf/in^2 (1034 MN/m^2) Budenberg Gauge gives a visual indication of pressure and incorporates a pressure switch P.S.2. for the fatigue press. The pressure switch consists of a reed switch mounted on a perspex arm pivoted at the centre of the Gauge dial glass. The arm may be swung to any position of the dial and locked in position. A small permanent magnet is attached at the end of the pointer which is counterbalanced. The reed switch contacts close when the pointer magnet passes underneath. Fortunately almost all the moving parts of the gauge mechanism are non-ferrous, and the presence of the small magnet has only a minor effect on gauge calibration. The manganin cell houses a manganin coil and thermocouple attached to terminals in a screwed end plug. The cell has a 10in (254 mm) long 3/4in (19mm) diameter bore and acts as a high pressure reservoir to damp out cyclic pressure variations which may be set up by elastic deflections within the test rig in fatigue.

3.4 Electrical Controls.

The Electrical controls are installed in a panel at one end of the pumping rig as can be seen on the photgraph Fig. 3.2. A schematic circuit diagram is shown on Fig. 3.3. Initially the reed switch arm on the Budenberg gauge is set to the required pressure. The selector switch is set to OVERIDE and the START button is pressed, The signal lamp will illuminate indicating that shut off valve solenoid V.1. is energised and the rig will start to operate by first charging the system and then by driving the pressure gradually higher. When the required pressure is near, pressure regulator P.R.2. should be carefully adjusted so that the drive pump stalls when the pressure is reached. The reed switch contacts will now close and the selector switch may be changed to NORMAL. The external connection from the fatigue press which is plugged in on the control panel is now presented with closed contacts and the fatigue press may be started. If during operation the pumping rig pressure fell or rose beyond the reed switch operating band of $\mp$ 4,000lbf/in^2 (27.6 MN/m^2) both the pumping rig and the fatigue press will be immediately brought to a halt. Neither may be re-started until the fault is corrected.

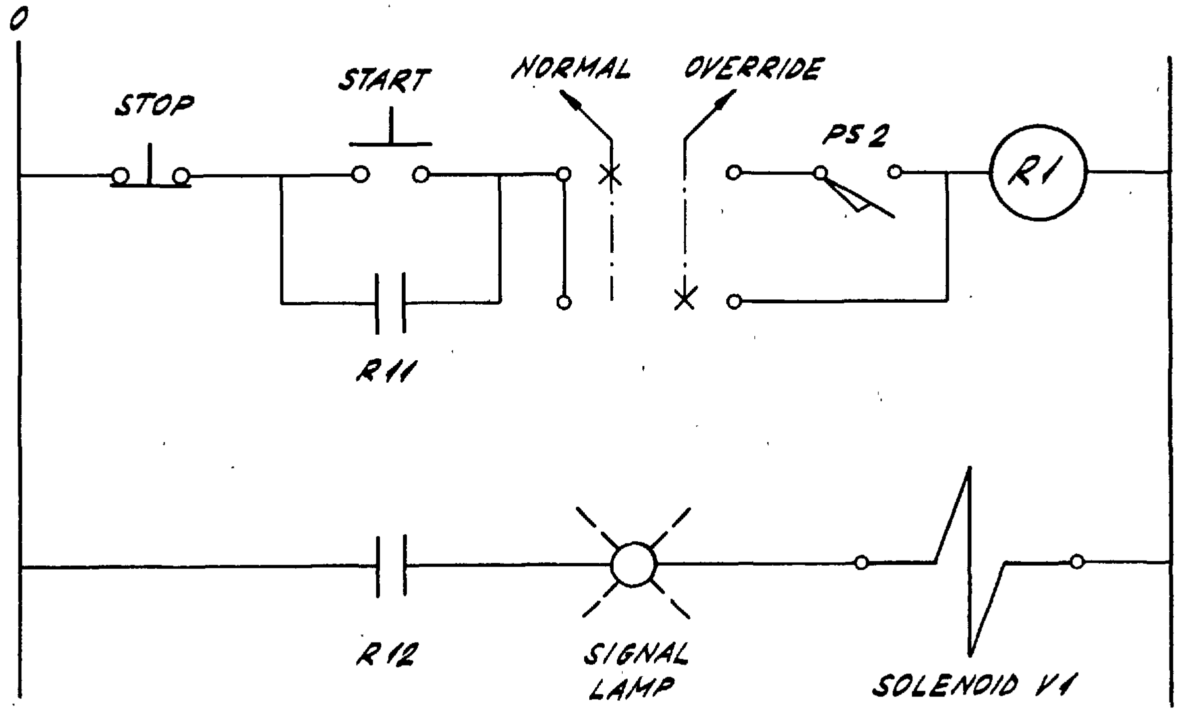

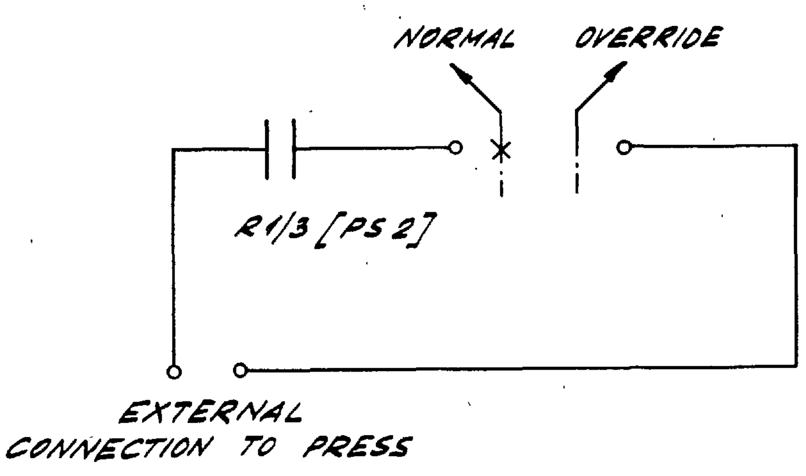

FIG. 3.3 PUMPING RIG CONTROL CIRCUIT

CHAPTER 4.

DYNAMIC SUPPORT RIG.

4.1. Preliminary Design Considerations.

The basic requirement of the dynamic support test rig was to generate simultaneous repeated internal and external fluid pressures on a hollow cylindrical fatigue specimen. In addition the following features had to be accommodated:-

1. The ratio of maximum external pressure to maximum internal pressure should remain constant during a test, but be simply adjustable when required from test to test.
2. The axial stress in the test specimen should be as near zero as possible to give true 'open-ended' stress conditions.
3. The internal and external pressures should be inter-dependent so that if leakage occurs in one region pressure cannot be built up in the other unless the plunger over-strokes, which should immediately halt the press.
4. Facilities must be provided to measurement of internal and external pressures, and for the replenishment of fluid during the test.

Fig. 4.1. illustrates a schematic method of fulfilling the basic requirements. A plunger generates internal pressure p_i which is fed to a pressure reducer. The low pressure side of the reducer then provides the external pressure p_o for the test specimen. If leakage occurred in the high pressure system p_o could not be generated, and if leakage occurred in the low pressure system the plunger would overstroke before any pressure could be built up. The design of Fig.4.1 could work equally well in reverse with direct generation of external pressure p_o and intensification to give p_i. However, in practice either scheme has the weakness of subjecting components of the rig to more severe ~~fatigue than the~~ fatigue conditions than the specimen itself.

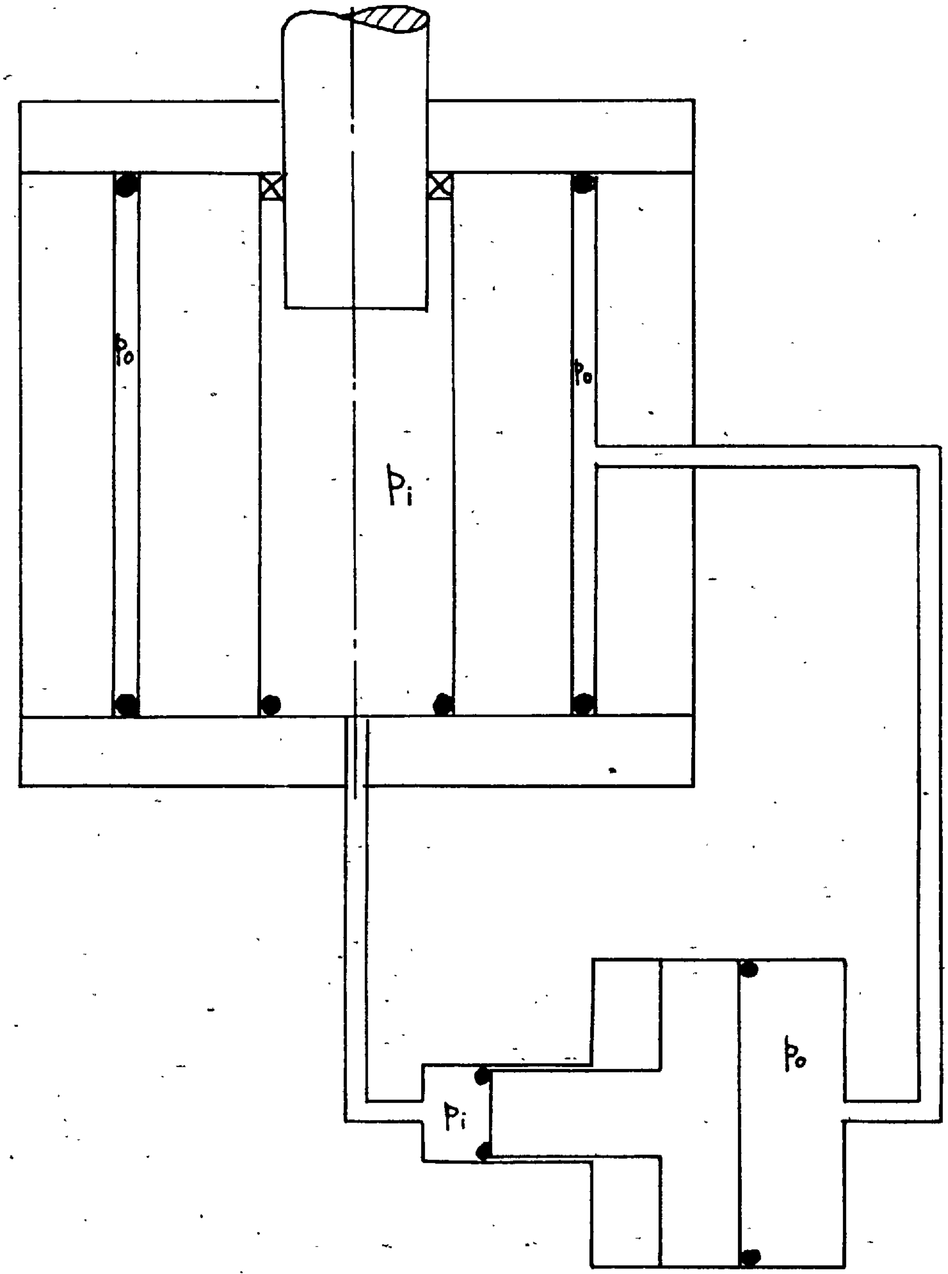

FIG 4.1 SCHEMATIC DYNAMIC SUPPORT SYSTEM

It was clearly necessary to incorporate the pressure modifying system internally such as in the designs put forward by Lengyel and Alexander (2) under the headings floating die and floating liner. These designs were suggested as possible solutions to the vessel fatigue problem in semi-continuous hydrostatic extrustion. Adaptations of the designs for dynamic support fatigue testing are shown in Figs. 4.2 and 4.3. (The floating die design has been called floating piston in the present context).

In the floating piston arrangement, Fig 4.2, internal pressure built up by the plunger acts on the floating piston to create external pressure Po. The nominal pressure ration is given by:-

$$\frac{Po}{Pi} = \frac{A_1}{A_2 - A_3}$$

By changing the tail diameter of D_3 of the floating piston the area A_3 may be changed and the pressure ratio altered to a new value.

In the floating liner design pressure built up by the plunger acts on the end piston which is rigidly attached to the specimen. The whole specimen - end piston assembly moves down to create external pressure Po. Once again the nominal pressure ratio is given by:-

$$\frac{Po}{Pi} = \frac{A_1}{A_2 - A_3}$$

which may be adjusted by changing the end piston to a different D_3 diameter.

The test specimen in both designs has been indicated as a hollow cylinder separate from associated components for ease of manufacture and so that the other components are not replaced

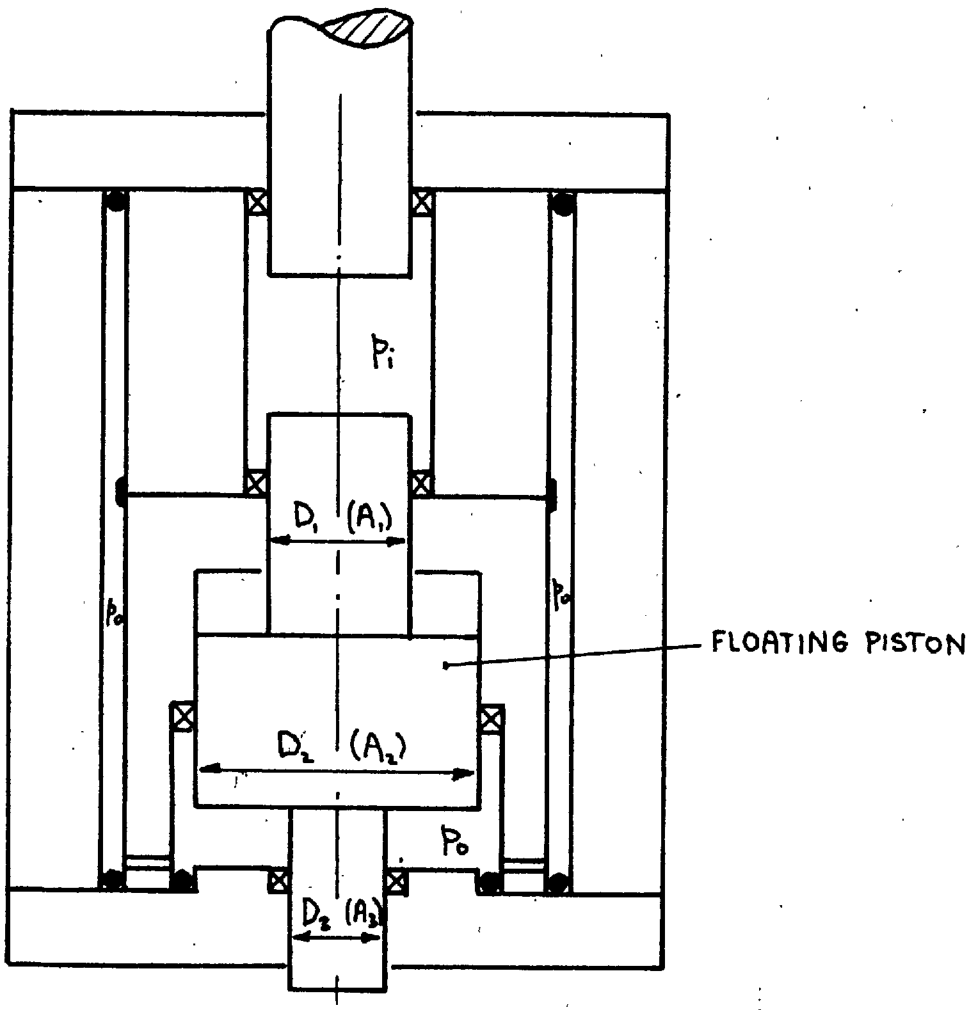

FIG. 4.2 FLOATING PISTON DESIGN

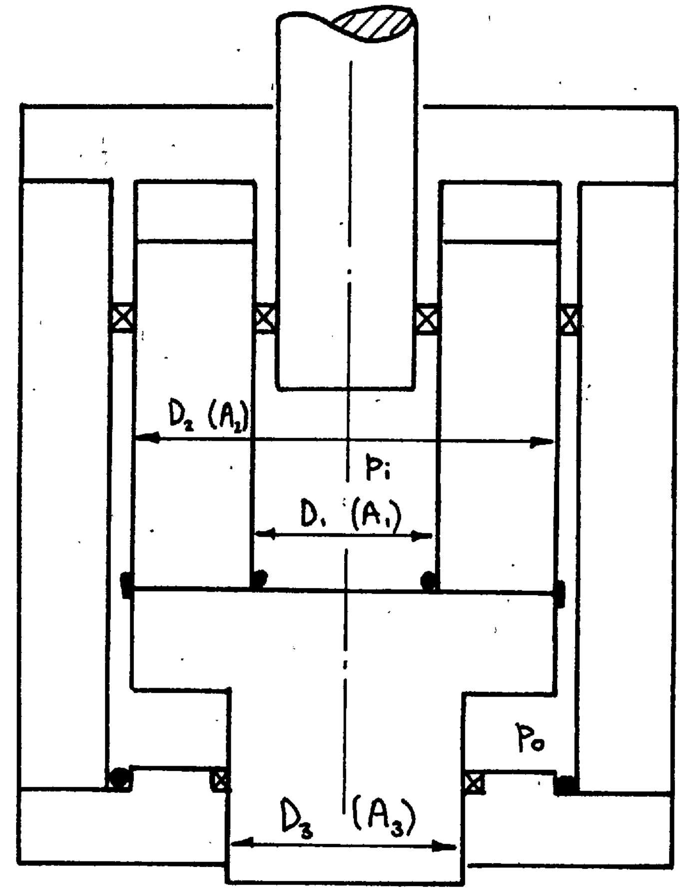

FIG. 4.3 FLOATING LINER DESIGN

every test. However, this does create a sealing problem at the lower end of the specimen, and in the case of the floating liner design a problem of attachment of moving parts. In comparing the two designs the possibility of fatigue failure in components other than the test specimen is an important consideration. The piston chamber of Fig 4.2 is subject to bending fatigue due to the repeated pressure end load on the upper seal, ~~to repeated pressure fatigue of the radial drillings~~, and to stress concentration at the middle piston seal. The end piston of Fig 4.3 is also subject to bending fatigue but it is possible for the construction to be relatively massive to minimise the stress levels. The floating liner design has a smaller number of dynamic seals but as the specimen itself reciprocates fretting of the specimen at the seals may initiate fatigue cracks. This could probably be avoided by locally enlarging the outside diameter of the test specimen, in the region of the seals. In fact it is common practice to design fatigue specimens with enlarged ends and a central necked portion to ensure failure occurs in a region of known stress distribution away from stress concentrations.

Considering the points described earlier the floating liner design was chosen on balance as the more attractive of the two designs. The remainder of this section will deal in greater detail with specific features of the floating liner design.

4.2 The Problem of Axial Tensile Stresses.

Necking a floating liner specimen as shown in Fig. 4.4a has one unfortunate aspect. The action of the external fluid pressure on the annular area of the top end will introduce a uniform tensile axial stress in the gauge length of the specimen given by

$$\sigma_z = \frac{(A_3 - A_2)\,Po.}{(A_2 - A_1).}$$

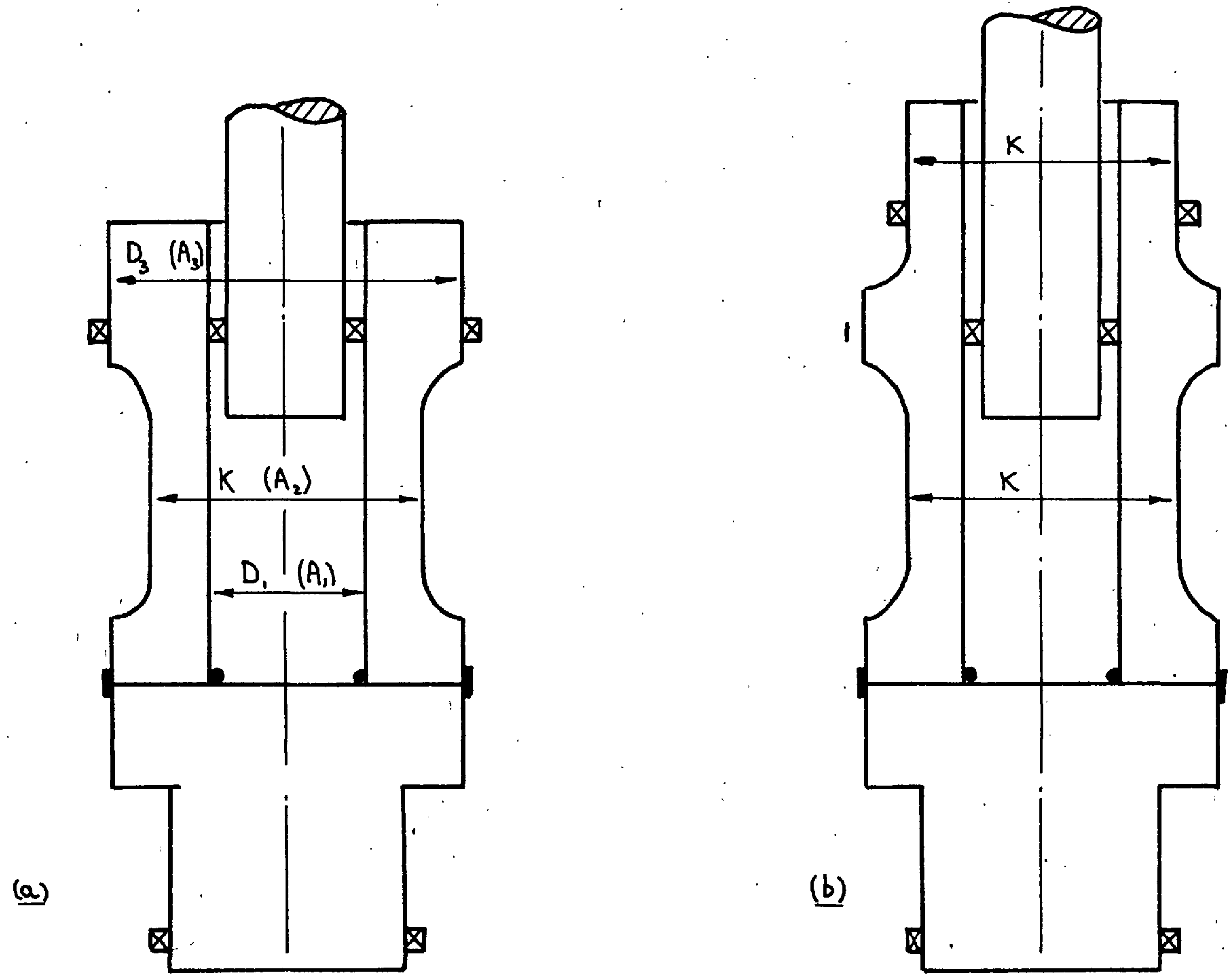

FIG. 4.4 ALTERNATIVE FLOATING LINER DESIGNS

The problem does not exist in a plain specimen or even in one with an enlarged bottom end, but one possible design where an enlarged top end is retained is shown in Fig 4.4.b. By displacing the internal and external seals and sealing the outside diameter of the specimen at the gauge diameter axial tensile stresses are avoided. This method was in fact adopted for the static support test rig but it is less satisfactory for the dynamic support case. As can be seen in Fig. 44.(b) both the specimen and the plunger are significantly longer, and the plunger has an increased unsupported length. It was decided to adopt the necked design of Fig 4.4 (a) with a D_3 diameter of 2.1/4 in and a maximum K diameter of 2 in (50.8 mm) but initially the test conditions and geometry would be arranged to ensure the axial tensile stress was always the intermediate principal stress.

4.3 Sealing and clamping the specimen and end piston.

The test specimen internal pressure can be sealed conventionally by an 'O' and mitre ring as shown in Fig 4.5, but the sealing arrangement for the external pressure is more difficult. A face seal between the specimen and end piston would be an unsatisfactory solution as very high separating loads would need to be contained. Even the simple radial 'O' ring shown in Fig. 4.5 could result in significant separating loads due to the imperfect squareness of the corner of the specimen at the joint. Thus some clamping pressure is needed between the components to prevent intrusion of the 'O' ring. This clamping pressure can be arranged very conveniently merely by increasing the diameter of the lower end of the specimen as in Fig 4.5. Providing an initial low pressure clamp and seal is arranged then as Po is built up a clamping load of $Po\frac{\pi}{4}(D_2^2 - D_1^2)$ is automatically applied to the joint face giving a clamping pressure.

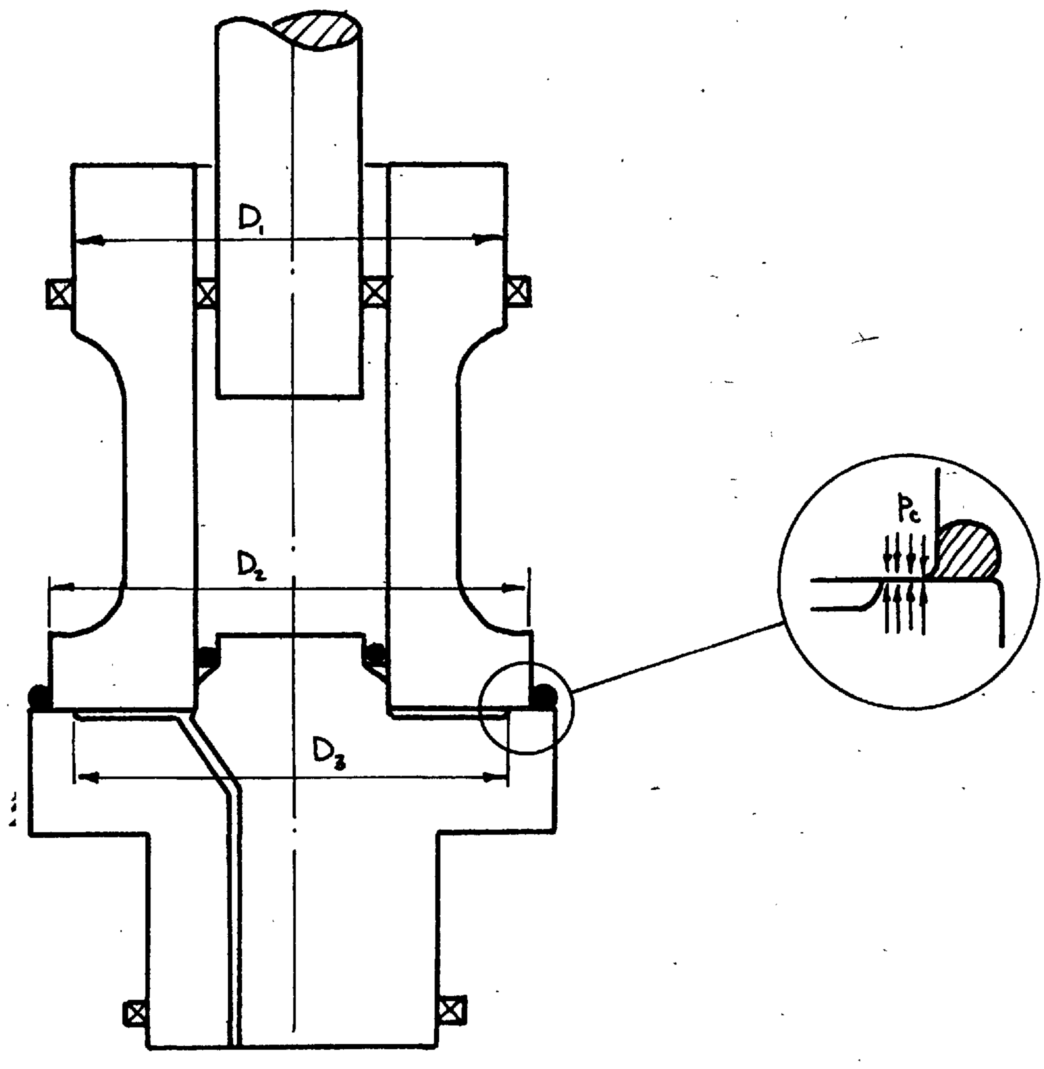

FIG. 4.5 DETAILS OF SEALING ARRANGEMENT

$$P_c = P_o \left[\frac{D_2^2 - D_1^2}{D_2^2 - D_3^2} \right]$$

If $D_3 > D_1$ then $P_c > P_o$ and under these conditions the joint is entirely self-sealing and no 'O' ring is needed. However, in practice it was decided to retain the 'O' ring because of the difficulty of providing reliable low pressure seal.

4.4 Design Details and Development of the Rig.

4.4.1. Outer Vessel.

The outer vessel is a monobloc cylinder of EN.30.B. Steel 8 in. (203 mm) outside diameter, 3 in. (76 mm) bore and 8 in (203 mm) high heat treated to 100 tonf/in^2 (1544 MN/m^2) U.T.S. A 3 in (76.2 mm) plain bore is necessary to accommodate the hydraulic seal around the specimen upper diameter of 2.1/4 in (57.2 mm) As can be seen by reference to Fig 4.6 this arrangement ensures that the fluctuating end load is resisted by the end plates rather than by the vessel itself. The alternative of housing the seal in a groove cut into the vessel bore was considered less favourable from a fatigue point of view because of the introduction of stress raisers. The bore of the vessel was honed and polished to a surface finish of 3 to 5 μin (0.076 to 0.127 μm) C.L.A. to improve its fatigue resistance. The pressure to yield the bore of the outer vessel is about 34 tonf/in^2 (525 MN/m^2) and under ideal conditions one can be confident that this pressure could be repeated for about 10^5 cycles at the most. However, as the vessel must be sure to outlive a number of tests of 10^5 cycles endurance a more conservative pressure limit of 25 tonf/in^2 (386 MN/m^2) has been set. This limit could be increased by autofrettaging the vessel if necessary.

4.4.2. End Plates.

The loading on the end plates consists of two elements, firstly the internal pressure (Pi) acting on an annular seal area of 0.48 in^2 (3.1. cm^2), and secondly the external pressure (Po) acting on an annular seal area of 3.09 in^2 (19.9 cm^2) The Maximum Po = 25 Tonf/in^2 (386 MN/m^2) and if the maximum pi = 50 Tonf/in^2 (772 MN/m^2) the total end load is approximately 101 tonf (1005 KN), The end plates and closures are all made from 100 Tonf/in^2 (1544 MN/m^2) U.T.S. EN.30B, and the end plates are 12 in (305 mm) outside diameter x 1.3/4" thick (44.5mm) while the top and bottom end closures are 5 in (127 mm) outside diameter x 2 in (50.8mm) thick. The maximum bending stress in the top end plate, which also has a 3 in (76.2 mm) diameter central hole and is the more highly stressed component, under a 100 Tonf/ (996 KN) end load can be calculated approximately as 33 Tonf/in^2 (510 MN/m^2) at the inner edge.

As the Goodman relationship indicates that even a transverse specimen of 100 Tonf/in^2 (1544 MN/m^2) U.T.S. EN.30B can withstand a repeated bending stress of 0-54 tonf/in^2 (0-834 MN/m^2) the plates should be quite safe whether prestressed or not. However, when the whole assembly of vessel end plates, and tie rods is considered prestressing does become important not only to increase fatigue resistance but also to minimise deflections and preserve the rigidity of the assembly under load.

4.4.3. Prestressing the Assembly.

The principles of prestressing against fatigue are well known (13) and can be applied straight fordwardly to the test rig assembly. Prestressing achieves a reduction in the amplitude of the fluctuating tensile loading on the tie rods at the expense of introducing a fluctuating compressive load in the vessel itself. If, after prestressing, a working load P is applied to the end plates the proportion of extra load applied to the tie rods is

$$P_1 = \frac{1}{\left(1 + \frac{K_v}{K_t}\right)} P.$$

Where K_v = characteristic stiffness of the vessel.
and K_t = characteristic stiffness of the tie rods.
To minimise P_1 the ratio K_v/K_t must be as large as possible. It should be noted that the proportion P_1/P is dependent only on the stiffness ratio of the components and not on the magnitude of the initial preload. Where this does not have a bearing is in the magnitude of external load which can be carried without separation of the joint faces. This condition is given by

$$P = \left(1 + \frac{K_t}{K_v}\right) Q.$$

Where Q = preload,
If separation takes place the tie rods are subjected to a greatly increased rate of loading which should be avoided. Unfortunatl y to maximise P for a given Q the ratio K_t/K_v must be as large as possible which conflicts with the previous requirement for minimum tie rod loading. However, because of the seriousness of dynamic loads in practice it was decided that the preload Q should be at least as great as the maximum anticipated external load P max and that K_v should be much larger than K_t. The evaluation of K_v and K_t is complicated by the effect of the end plates and closures which act partly as the outward tie rod load transmitting system and partly as the inward load transmitting system through the vessel. As an approximation the end closures are taken ~~as~~ with the vessel as the inward load transmitting system and the end plates with the tie rods as the outward load transmitting system.

The maximum anticipated external load has already been established as 100 Tonf/ (996KN) and the preload should now equal that figure, that is the six tie rods should each carry a preload of 17 tonf (169 KN), say. Taking a stiffness ratio $K_v/K_t = 5$ one sixth of an 100 Tonf (996 KN) applied external load is taken by the tie rods that is 16.7 Tonf (166KN) total, or approximately 2.8 Tonf (28KN) per tie rod. The tie rods threads are 1.1/4" B.S.F. and a fluctuating load of $\pm$ 1.4 Tonf (14 KN) produces a core stress of $\pm$ 1.45 tonf/in^2 ($\pm$ 22 MN/m^2). In fact for material of 60 - 65 Tonf/in^2 (927 - 1004 MN/m^2) U.T.S. chosen for the tie rods a fluctuating fatigue limit of $\pm$ 3 Tonf/in^2 ($\pm$ 46 MN/m^2) can be expected (13) so that even for maximum load conditions we have a safety factor of 2.

4.4.4. Tie Rods and Hydraulic Nuts.

The six tie rods are of 1.1/4" in (31.8mm) diameter S.97 steel threaded 1.1/4" B.S.F. at the ends. The thread run out is carefully relieved to minimise the stress concentrations.

The nuts, also of S.97 Steel, are spherically radiused and bear on matching lapped seats in the end plates. Originally twelve conventional nuts were fitted and these were tightened in sequence by long arm spanners. This turned out to be very laborious and one could never be confident about either the magnitude or the uniformity of the preloads induced. The top six nuts were consequently replaced by hydraulic nuts marketed by G.K.N. Ltd under the Trade Name Pilgrim (A pun on the name of their invenor Mr. T.W.Bunyan). The body of the Pilgrim nut is threaded internally as usual but a deep annular groove is cut into the lower face of the body to take a hollow rubber 'O' ring. A hydraulic connection into the 'O' ring is provided from the top face of the body. A separate piston plate engages in the groove from below against the 'O' ring and provides the bearing surface for the nut. Initially the assembly is tightened sufficiently to take up the slack in the system by hand or gently with a spanner. Hydraulic pressure supplied to the 'O' ring then separates the nut body and piston plate thereby tensioning the tie rod. To lock in the pretension shims are inserted in to gap between body and piston and the hydraulic pressure can then be released.

The six Pilgrim nuts are ganged together in series by a single high pressure supply line from an S.K.F. No. 226400 hand operated oil injector which can supply up to 42,000 lbf/in^2 (290MN/m^2) fluid pressure. The Pilgrim nuts are of En 16.T. Steel designed for a maximum fluid pressure of 30,000 lbf/in^2 (207 MN/m^2) which acts on a piston area of 1.375 in^2 (8.86 m^2) to give a maximum preload of 18.4 tonf (183 KN) In fact 28,000 lbf/in^2 (193 MN/m^2) is sufficient to generate the required preload of 17tonf (169 KN). Initially a pressure gauge is used during pretensioning so that the correct shim thickness for the nuts could be established. It was found that bending of the plate had created a non uniform gap and tapered shims varying from 0.040 in (1.02 mm) at the innermost point to 0.047 in (1.19 mm) at the outermost point had to be made. To save unnecessary pumping a set of thinner shims was also made for relatively low pressure tests where the maximum preload was not required.

4.4.5. Fretting.

One of the troubles experienced early in the development of the rig was severe fretting of the contact areas between the end closures and the outer vessel, and to a lesser extent between the end plates and closures. Initially this was attributed to the rather ineffective prestressing achieved by spanner tightening of the tie rod nuts. It was thought that rather large relative movements were taking place between contacting surfaces under load. In fact with hydraulic prestressing and higher contact stresses the fretting was worse and other remedies were sought. Molybdenum disulphide grease had no effect and the use of a soft packing material such as P.T.F.E. layer was unacceptable because of the reduction in stiffness K_v, which would result. However, tinning the contacting surfaces with Fry's K. No.90 Solder Paint at about 200°C and wiping the flux and excess solder off with a tissue proved entirely satisfactory, and fretting was eliminated for a considerable period of use. Eventually when the tinning wore thin the process could be repeated.

4.4.6. Displacement Problems.

Fig. 4.7 shows in simplest detail the bore of the test specimen with a core tube, the pressurising plunger and the seal. At stage (i) the bore is full of fluid and the plunger is at the top position. Stage (ii) shows an imaginary situation where the floating liner assembly has been pulled down to a distance 'a' to create the correct external pressure, and the plunger has merely followed to maintain the initial entrapped volume of fluid without generating any internal pressure.

Thus the plunger displacement $b = \frac{0.785}{0.305} a = 2.57 a$ (4.1.

At stage (iii) the plunger has moved a further distance 1/3 taken to be the displacement required to generate the correct internal pressure.

Thus total plunger movement $C = \frac{L}{3} + 2.57 a.$ (4.2).

the distance $d. = \frac{2.L.}{3.} - 1.57 a \quad 0.$ (4.3)

$$\text{therefore } \frac{2.L}{3.} \geqslant 1.57.a. \qquad (4.4)$$

The analysis serves to highlight a number of important points. Firstly as the plunger compensating displacement, b, is over 2.1/2 times the assembly displacement, a, the latter must clearly be kept to a minimum. Equation (4.4) indicates that for a given value of a a certain minimum internal length L is essential to avoid bottoming of the plunger, and

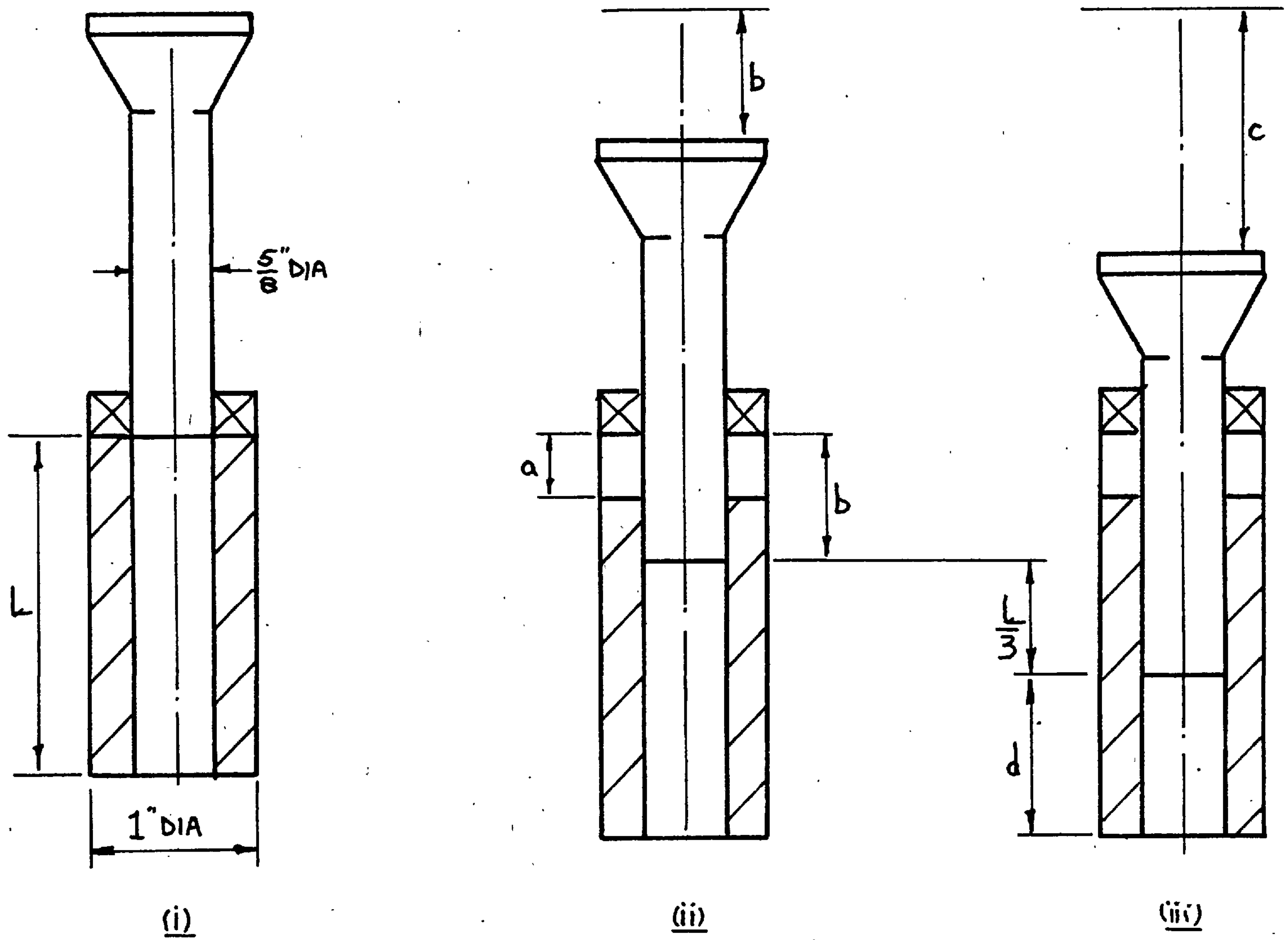

FIG. 4.7 DISPLACEMENT OF SPECIMEN AND PLUNGER

the normal procedure of shortening $\underline{L}$ to reduce the plunger stroke can not be followed. In operation a further constraint may be necessary for the reliable actuation of the overstroke limit switch that is the total stroke $\underline{c}$ must not exceed $\underline{l}$. This is to ensure that if there is a leakage and no internal pressure is built up the plunger can not force the assembly downwards undetected.

Thus from (4.2) $l \geqslant \frac{L}{3} + 2.57.a.$ or $\frac{2.L}{3.} \geqslant 2.57.a.$ (4.5)

or if a specific differential $\underline{e}$ is required

$$\frac{2.L}{3.} = 2.57a + e. \qquad (4.6)$$

As an example consider an assembly displacement a = 0.5 in (12.7mm) and a differential $\underline{e}$ = 0.25 in (6.35 mm) then from (6) L = 2.3 in (58.4mm) and the working stroke of the plunger c = 2.05 in (52.1.mm). Only by reducing the plunger displacement can this stroke be reduced to a more acceptable value.

It was with the above considerations in mind that at one stage during the development of the rig mercury was tried as an external working fluid. However considerable difficulties in handling, and in sealing the inlet check valve led to the rejection of the idea and a return to hydraulic oil. One possibility would be to use rubber as the pressure transmitting medium, but because of considerable doubt as to the integrity with which rubber could transmit pressure hydrostatically this was not explored.

4.4.7. Sealing between specimen and end piston.

Mention has been made earlier of the self clamping action between the test specimen and end piston. However in spite of this in the practical design of Fig.4.6 it has been necessary to use an 'O' ring and claping sleeve to give favourable low pressure conditions. The sleeve is a substantial component and has the disadvantage of riding up and down with the specimen and piston in operation. Although it takes no part in pressurising it must have unhindered passage through the fluid thereby reducing the efficiency of external pressurisation and increasing the working stroke of the assembly. A serious attempt was therefore made to attach the test specimen and end piston together without a sleeve. Theoretically if the two components were glued together sufficiently strongly to resist assembly loads and provide an initial seal they would continue to seal and hold together in operation.

Araldite A.U.1., a high strength hot-setting epoxy adhesive, and Loctite 307 high tensile adhesive, were both tried with limited success. The assemly would operate satisfactorily for a few hundred cycles and then the bond would fail and the components separate. The only explanation for this seemed to be possible severe bending stresses on the joint due to misalignment or lack of concentricity which fatigued the joint after a relatively small number of cycles. Soldering of the two components with Fry's K No.90 Solder Paint was also tried with little more success than the adhesives, although one test did run to over 2,000 cycles before the bond failed.

CHAPTER 5.

STATIC SUPPORT RIG.

5.1 Preliminary Design Considerations.

As in the chapter describing the dynamic support rig it is appropriate to define at the outset what is required of the static support rig. The main requirement is to subject a hollow cylindrical specimen to repeated internal fluid pressure and a simultaneous constant external fluid pressure. Open-ended conditions are required and thus the axial stress in the specimen should be as near zero as possible. Also the magnitude of the external pressure must be adjustable from test to test. This is a relatively simple matter if the external pressure is supplied from a separate finely controlled pumping source but electrical interlocks will be necessary to ensure the system fails safe. It is possible that the external pressure could be generated automatically within the rig as in the dynamic support rig, and that the pressures could be interdependent. In that way internal pressure could not be built up unless the correct external pressure was present at the same time, and the system inherently fails safe. To put this into practice involved two considerations. Firstly, the maximum internal pressure must reach balanced equilibrium with the static external pressure, and secondly, a check valve must be provided to hold the external pressure constant. The first requirement is met by either the floating liner or floating piston designs mentioned in Chapter 4, but the second could not be applied to the floating liner and only with considerable difficulty to the floating piston.

An interesting self generating static support vessel has been suggested by Prasad (39) and is shown in Fig. 5.1. As the plunger strokes downwards for the first time pressure is built up equally inside and out because of the radial check valve drilling. When the plunger

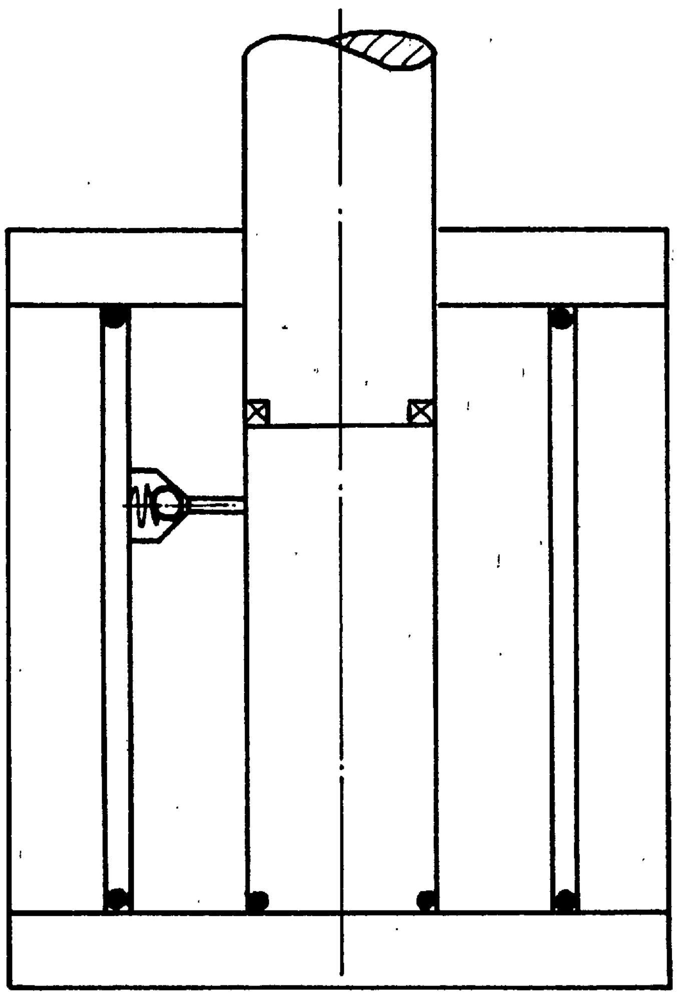

FIG. 5.1

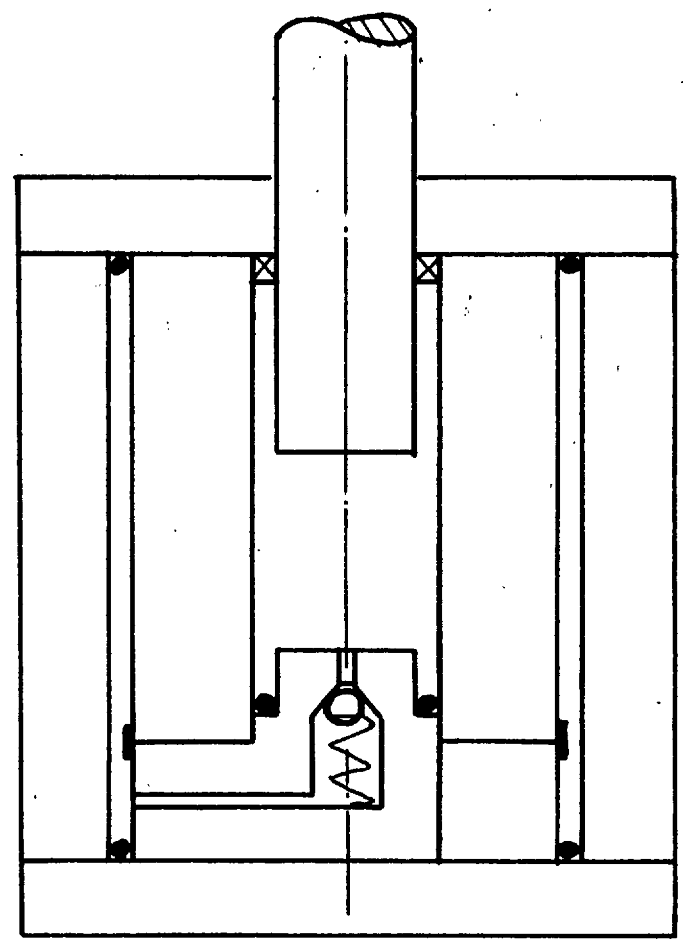

FIG. 5.2

FIGS. 5.1 AND 5.2 SELF GENERATING STATIC SUPPORT DESIGNS seal passes the drilling the external pressure is held by the check valve but the plunger can continue to build up to the required pressure. Thus the position of the radial drilling with respect to the stroke of the plunger determines the external pressure that can be built up. Unfortunately this design is severely handicapped by practical difficulties and will not strictly fail safely.

One self generating static support system which could have practical application, although not for the test rig in question, is shown in Fig. 5.2. The static external pressure is simply equal to the maximum repeated internal pressure and clearly success will depend upon the fatigue life under these circumstances. Enough has now been said about self generating static support systems to indicate that for an effective test rig resort will have to be made to an external pressurising system.

The introduction of the pressurised fluid to the test rig from an external source may be achieved via the end closures or through the wall of the outer vessel. The latter method was chosen for simplicity and in the knowledge that the outer vessel although weakened by a radial drilling would be adequate for a series of tests on EN.25 specimens.

5.2. Elimination of axial stresses.

Fortunately in the present case it is possible to eliminate with confidence all axial stresses in the central gauge length of the test specimen, although local axial stresses will be present in the bore at the seals due to the pressure discontinuity. Fig. 5.3 shows three alternative specimens and sealing arrangements, all employing the simple principle that at least one end of the specimen must be sealed on the outside at the specimen gauge diameter. Functionally just one end treated in this manner is sufficient as in Fig. 5.3.a., but a more favourable design is possible if both ends are so arranged as in Fig.5.3.(b).

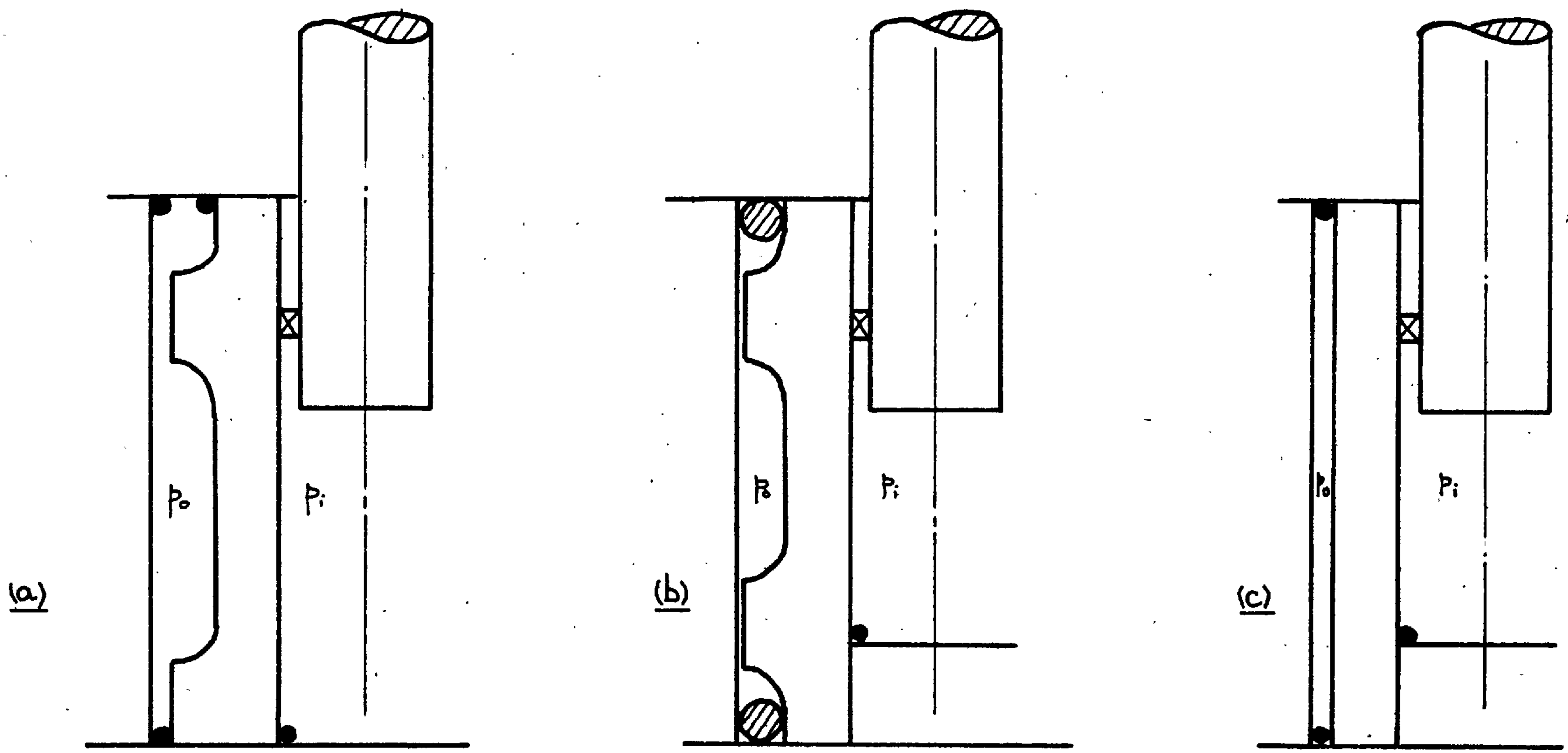

FIG 5.3 ALTERNATIVE SEALING ARRANGEMENTS

The bore of the outer vessel can be smaller and end loads reduced. The initial specimen design followed the arrangement of Fig. 5.3.(b) although the final design was a plain cylinder as in Fig 5.3. (c). It will be noticed that the external and internal seals are displaced so that radial displacements due to the repeated internal pressure have less influence on the external seals.

5.3. Design Details and Development of Rig.

5.3.1. General Features.

Fig 5.4P shows the general arrangement of the static support rig. The end plates, tie-rods, nuts and method of prestressing are common to both static and dynamic rigs, and the reader is referred to section 4.4 for further details.

5.3.2. Outer Vessel and Support Ring.

The outer vessel is a monobloc 100tonf/in^2 (1544MN/m^2) U.T.S. En 30.B. steel cylinder 6 in (152 mm) diameter (outside), 2 in (50,8mm) bore, and 6 in (152 mm) high. A 1/16th in (1.66 mm) diameter radial drilling penetrates the wall centrally and is countersunk at the outside to accept a standard high pressure olive. Care was taken to radius the intersection of the drilling with the main bore to minimise the stress concentration. The working life for the vessel may be taken as an extreme case of low cycle fatigue, say 200 cycles at the most. Crossland & Skelton (32) found that closed ended En.25 cylinders 2.25 K. ratio heat treated to approximately 100 Tonf/in^2 (1544 MN/mm^2) U.T.S. with two 5/32 in (4 mm) diameter radial cross bores withstood a repeated pressure of 40 Tonf/in^2 (618 MN/mm^2) for 200 cycles. The intersection of the cross-bore was not radiused and thus in the present case one could reasonably expect a repeated pressure of 50 Tonf/in^2 (772 MN/m^2) say to be contained.

The support ring is of En.8. steel, 8 in (203 mm) outside diameter, 2.3/4 in (69.9 mm) high, and is a close sliding fit on the outer vessel.

5.3.2. External Pressure Variation.

Elastic displacement of the outside surface of the test specimen due to the repeated internal pressure imposes a pressure fluctuation around the desired static external pressure. This can not be tolerated in a rig devoted to careful work on fatigue although it might be quite acceptable in practical situation. There are two obvious solutions, firstly, the external fluid volume can be increased, and secondly, a very compressible fluid can be used. Little can be done about fluid compressibility because of the need for speedy pumping and the safety of the apparatus, and Esso Univis P.38 was generally used. The external fluid volume was enlarged considerably by including a long 3/4 in (19.1 mm) bore vessel in the high pressure supply line from the pumping rig. In this way pressure fluctuations were kept below ± 5%.

CHAPTER 6.

PRESSURE MEASUREMENT AND INSTRUMENTATION.

6.1 Measurement of High Repeated Pressures.

In the earlier chapters dealing with the dynamic and static support rigs reference was made to manganin gauges for internal and external pressure measurement. The intention in this chapter is to present a detailed account of the technique of pressure measurement using a manganin gauge and also to assess the alternative methods of pressure measurements and indciate the reasons for preferring the manganin gauge method. A recent review of high pressure measuring devices by de Malherbe and Firth (40) lists the following three available methods:

1. dead weight gauges, 2. elastic deformation gauges and 3. gauges whose electrical resistance is affected by pressure. Little attention is given in the paper to the important question in the present work of thefgtigue performance of pressure gauges.

6.1.1. Dead Weight Gauges.

The dead weight gauge is a primary standard and as such is essential in any high pressure laboratory. However, it is strictly a static instrument and not applicable to the dynamic pressure conditions in the fatigue test rigs. Fawcett (41) has proposed using a sensitive dynamic gauge, in conjunction with a dead weight tester to measure varying pressures, but to lead the dynamic pressures from the test rig to the dead-weight tester would involve subjecting components of the test rig to more severe fatigue conditions than the test specimen itself. It is this last factor which also eliminates many of the elastic deformation gauges from further consideration.

6.1.2. Elastic Deformation Gauges.

Elastic deformation gauges are secondary measuring instruments and include the Bourdon gauge, a vessel which has been strain gauged, and the bulk modulus cell. The Bourdon gauge contains a flattened or elliptical tube formed into a spiral, helix, or 'C' shape, which tends to straighten under pressure. It is a robust and reliable instrument up to as much as 70,000 lbf/in^2 (483 MN/m^2). However, under fatigue conditions Mason (42) has shown that the life is severely limited. The eccentric-tube type of pressure gauge is similar to the Bourdon tube and may again be 'C' shaped or at higher pressures straight. Pressures up to 200,000 lbf/in^2 (1379 MN/m^2) are possible although not under fatigue condition. The simplicity and reliability of a Bourdon type of gauge is very attractive and it may be used in a repeated pressure fatigue rig provided the gauge is isolated from the repeated pressure by a check valve. In this way the gauge reads only the maximum pressure of the cycle, and means must be provided for bleeding-off high pressure oil occasionally to re-check the pressures. This principle was used by Austin and Crossland (27) for repeated pressures up to 40 Tonf/in^2 (618 MN/m^2). The check valve block clearly needs to be carefully designed and fairly massive to avoid fatigue failures. This would be extremely difficult to accommodate in the fluid support test rigs and would be a certain trouble-spot. Also the method was unacceptable on the grounds that a complete record of rising and falling internal and external pressure was considered essential for a fatigue machine.

The Bristol repeated pressure fatigue machine (22) uses a different type of elastic deformation gauge. A strong thick walled cylinder which has been externally strain gauged is assembled in series with the test cylinder and is subject to the same repeated pressure conditions. The strain gauge output gives a secondary measure of pressure once the pressure measuring cylinder has been calibrated against a dead weight tester. The method has been very successful and ± 0.5% accuracy is claimed, but clearly the method is limited to fairly low pressures where it is still possible for a monobloc cylinder to have infinite life. This could not be said of fluid support test rigs and the method can not be considered viable. One possibility as far as measurement of external pressure is concerned would be to attach strain gauges to the outer diameter of the outer vessel, but as the vessel is so massive signals would be low and if the vessel became autofrettaged measurements could not be relied on over a long period,

Manning (21) has suggested that strain gauges could be installed in the bore of a thick walled closed ended vessel which enters the high pressure environment so that pressure is exerted on the outside surface. The strain levels would be larger and fatgue life much improved but the same limitations apply regarding autofrettage and space consumption. Another possibility is to attach strain gauges to the bore of the outer vessel or test cylinder within the fluid pressure environment. The main objection to this is in the difficulty of maintaining an effective strain gauge bond over long periods, in a dynamic fluid pressure environment. Pressure compensation of the strain gauges is necessary and Kudo and Nakane (43) have shown that this becomes a complex procedure only suitable for static conditions.

The bulk modulus cell described by Newhall & Abbot (44) has the advantage of robustness and a good fatigue life could be expected. A hollow cylinder, closed at one end and open to the atmosphere at the other end, is installed within the vessel and the application of pressure to the outside surface of the cylinder causes contraction. A central probe senses the movement to give a secondary measurement of pressure.

Typically for 100,000 lbf/in^2 (689 MN/m^2) external pressure a 2 in. (50.8 mm) long cylinder contracts 0.003 in (0.076 mm). Although the gauge had the advantage from a fatigue point of view cycling in a compressive regime, the maximum pressure will be severely limited if plastic cyling is to be avoided.

6.1.3. Electrical Resistance Gauges.

The last class of pressure gauge is that of the resistance gauge sensitive to applied pressure. The manganin coil is the best known example of such gauges and was used extensively by Bridgman (45). Manganin is a generic term used to describe a number of copper-manganese-nickel alloys used for high quality precision resistors. A typical composition is 83% Cu., 13% Mn, and 4% Ni. The material is chosen for its extremely low temperature coefficient of resistance, high resistance stability, and low thermal e.m.f. with respect to copper. As far as high pressure work is concerned manganin had the added bonus of providing a large positive pressure coefficient of resistance 380.10^{-6} per $tonf/in^2$ ($24.7.10^{-6}$ per MN/m^2).

The idea of using manganin as a pressure gauge Bridgman attributed to Lisell (46). Bridgman's gauge was a 120 ohm coil of double silk-covered manganin wire 0.005 in (0.13 mm) diameter. The wire was doubled and wound non-inductively on itself into a coreless toroid of about 0.39 in (10 mm) diameter. A seasoning operation followed by exposing the coil to a temperature of 140°C for six to ten hours. Bridgman established the linearity of his manganin gauge as within 0.1% to 84 $Tonf/in^2$ (1,300 MN/m^2) and to within 0.15% to 194 $Tonf/in^2$ (3,000 MN/m^2).

It was also mentioned earlier that manganin has an extremely low temperature coefficient of resistance but this in fact holds only for a relatively small temperature range, and the material is characterised by a steep parabolic resistance temperature curve outside this range.

The peak temperature of the parabola may be shifted for higher temperature operation by altering the composition, for example shunt manganin which normally has a higher operating temperature is of the composition 85% Cu., 10% Mn, 4% Ni. and 1% Fe. In a dynamic pressure situation which is accompanied by corresponding temperature variations it may not be possible to remain within the flat topped region of the parabola. To overcome this problem a gold chromium alloy has been proposed by Darling & Newhall (47) but the pressure coefficient of resistance is less than half that of manganin and manufacturing and attachment problems have precluded its general use. Temperature compensation of a manganin coil may be achieved by using two coils one of which is subject to the pressure and temperature of interest and the second of which is outside the pressure environment but still subject to the temperature by conduction through the vessel wall. This can clearly only work in a static situation where sufficient time can elapse for thermal equilibrium, and in fact is not strictly precise because the temperature coefficient of resistance varies with pressure. The practice is however employed in commercial manganin cells, and will give some protection against day to day variations in ambient temperature. In a dynamic pressure situation a possible solution could lie in a self compensating gauge similar to the self compensating strain gauge, where two carefully chosen wire materials having similar but opposite temperature coefficients are connected in series, but this is no easy matter. A compromise solution lies in recording simultaneously the pressure and temperature at the same point in the high pressure fluid. A temperature correction can then be made subsequent to the manganin gauge pressure reading.

Measurement of temperature in a high pressure environment is itself not simple, as pressure affects the thermal e.m.f. generated by a given temperature difference,. Bundy (48) tested eight common thermocouple metals at pressures up to 466 tonf/in^2 (7,200 MN/m^2) and showed that for a chromel-alumel thermocouple the correction for 100°C temperature difference at 65 Tonf/in^2 (1,000 MN/m^2) was less than 0.5°C. This inaccuracy may be considered negligible when the temperature reading is being used for a secondary correction to the pressure reading.

Considering the application of manganin gauges for pressure measurement within the test rigs it emerges clearly as the best method. The gauge can be made very small and accommodated in a complex rig without the need for valves or external pressure connections. It is accurate and can be simply connected in a Wheatstone Bridge to give sufficient output to drive an ultra-violet recorder without amplification. Unlike any of the elastic deformation gauges there is no serious hysteresis or fatigue problem in the gauge itself. Electrical connections have to be made via sealed terminals which are themselves subject to substantially compressive cycling conditions so that there should be little chance of fatigue failure. The only significant disadvantage of the manganin gauge is its fragility and this can be improved by winding on a former and using robust connecting leads to the terminals.

6.2. Details of Manganin Gauges, Thermocouples and Terminals.

6.2.1. The Manganin Gauge.

The Manganin wire used throughout the present work came from a single reel of standard quality Stabilohm 43 resistance wire made by Johnson Matthey & Co. Ltd. The composition is approximately 85% Cu., 11% Mn., and 4% Ni., and the nominal diameter of the wire is 0.004 in (0.10 mm). The wire is insulated with an epoxy based sythetic enamel known as Diamel which is extremely flexible and to be preferred to the silk winding used in the past. Stablohm 43 has the usual flat topped parabolic relationship between variation in resistance and temperature, and the peak temperature value (T_p) can be controlled by the manufacturers within the range 15°C to 35°C. The Nominal T_p of 'standard' quality wire is 25°C with a tolerance of ± 15°C but the T_p of 'premium' quality wire can be controlled to within ± 2.1/2% of a number of values within the range 15°C to 35°C. If high temperatures are anticipated during pressurisation then a high T_p value is clearly advisable to remain within the flat part of the parabola. In fact if temperatures in excess of 60°C are to be encountered the use of manganin wire itself becomes questionable, and alloy such as Stabilohm 133 a modified version of an 80/20 nickel chromium alloy may be preferred.

The procedure for making a gauge consisted initially of cutting an approximate 78 in (2 m) length of Stabilohm 43 wire. The wire was then carefully shortened until the resistance was 100 ±1 ohms, and wound on a Tufnol bobbin of the design shown in Fig.6.1 (a). The two ends of the wire were soldered to the terminal strip araldited on to the bobbin. The terminal strip has printed circuit copper terminals on a fibre glass backing and is sold for strain gauge work by Welwyn Electric Ltd. An alternative version of the bobbin shown in Fig.6.1 (b) is suitable for rigid attachment by a central screw to a plunger so that no strain is put on the connecting wires. The arrangement can be seen in the photograph Fig 6.2.

It had been the practice of Bridgman and other workers to double the wire before winding to minimise inductance effects. However, this doubling inevitably meant a 180° bend in the wire which would certainly cause considerabl localised hardening with possible side effects on stability. Winding without doubling as was the case in the present work has not been found to introduce undesirable inductive noise. This is hardly surprising as the coil is normally well shielded by substantial steel components. To stabilise the resistance of the gauge after winding the manufacturers recommend annealing at 140°C for at least 10 hours preferably in a neutral

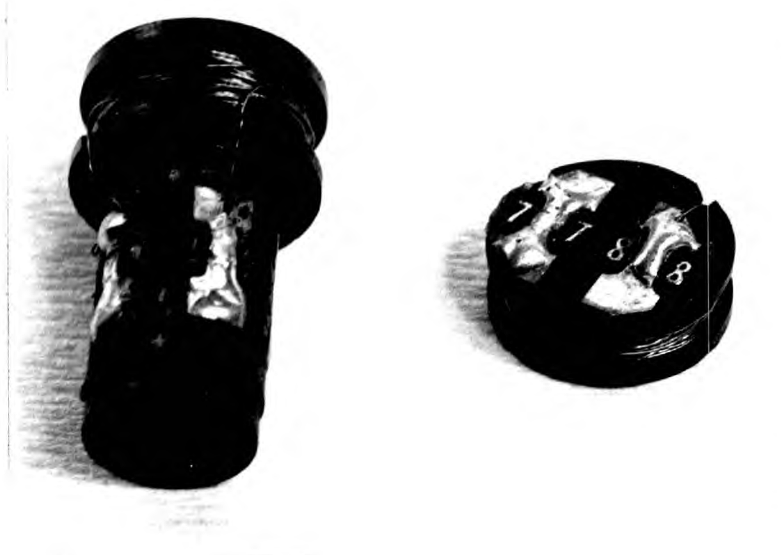

Fig. 6.1. Manganin Coil Bobbins.

Fig. 6.2. (a) Pressurising Plunger with Manganin Gauge and Thermocouple.

(b) Plain Pressurising Plunger.

atmosphere. Undoubtedly this is a wise precaution although it was not always carried out rigorously in the present work. No short term resistance instability could be observed in coils which had not had the recommended anneal,. Pressure cycling is also advised before calibrating a manganin gauge and it was convenient and simple to do this using the fatigue press.

6.2.3. Terminals and Thermocouples.

The design employed for electrical terminals for both manganin and thermocouple connections was originally devised by Amagat who used a thin conical shell of ivory between the electrode and the body of the vessel. In the present case shown in Fig. 6.3, the insulator is a standard component made by Smith's Industries Ltd., in alumina ceramic. The terminal material must be sufficiently hard such that it will not extrude under pressure and in the case of the manganin coil terminals hardened and tempered silver steel was used. The thermocouple terminals, however, were made of the individual thermocouple alloys to overcome the problem of additional thermal e.m.f.'s which would be introduced by coupling to steel terminals.

Both the terminals and the sockets were machined by conventional methods as precisely as possible in the soft unhardened state. After hardening the insulator was first lapped into the socket until the surface contact was uniform, and at this point the insulator tended to stick in the socket. The terminal could then be lapped into the insulator in situ. It will be noticed from Fig 6.3. that the insulator rests entirely within the socket and is not assembled proud of the top surface. This is an important feature to ensure the uniformity of stress conditions in the brittle ceramic. Normally before the first pressurisation a thin layer of araldite was applied to the top of the insulator to ensure an initial seal and effective bedding down within the socket.

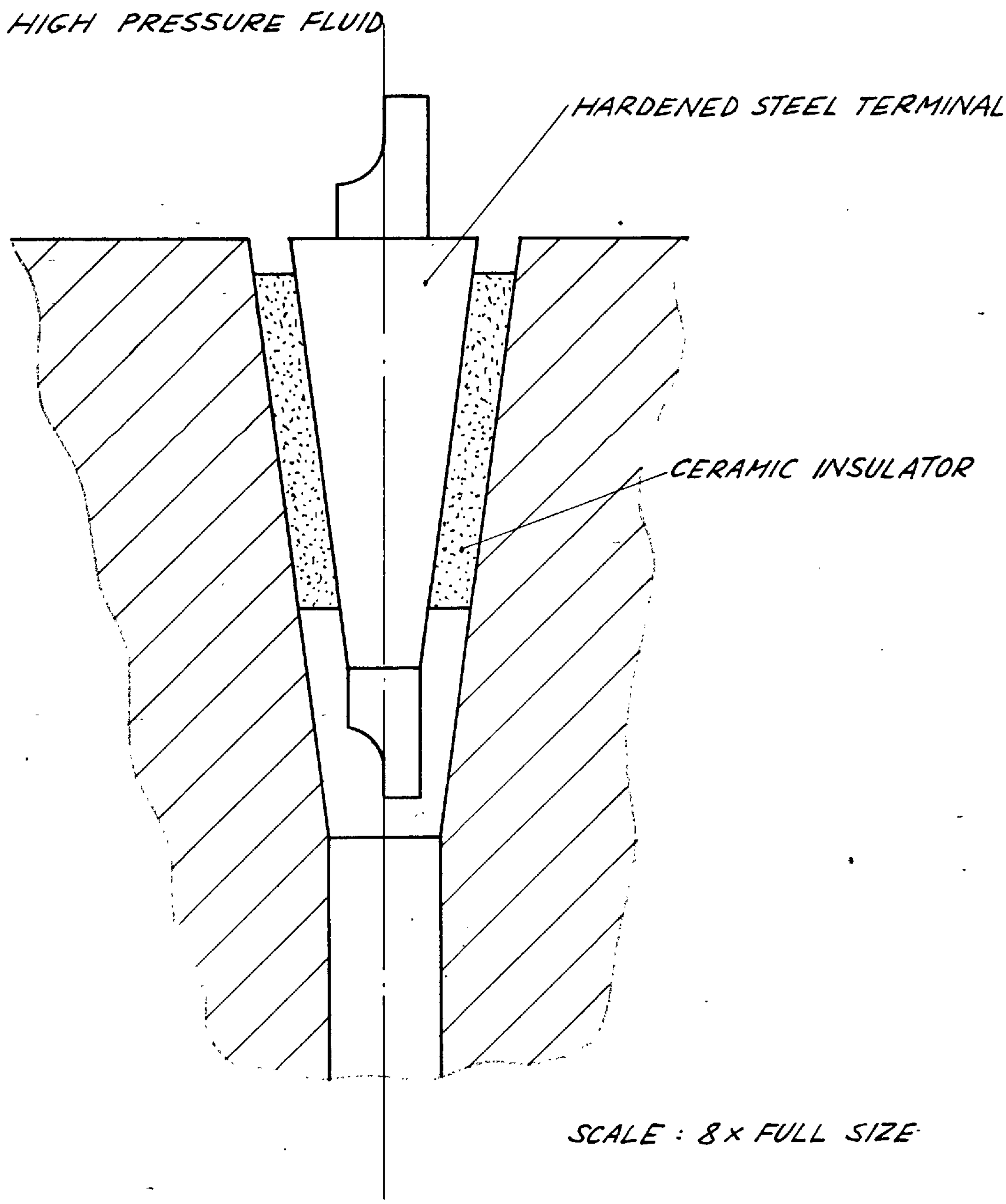

FIG. 6.3 ARRANGEMENT OF TERMINAL AND INSULATOR

It was sometimes found that after a few thousand pressure cycles an insulator had cracked, but invariably the cracks did not leak under pressure and the arrangement was satisfactory for many more tests. The Photograph Fig. 6.4., shows a typical cracked insulator on the four terminal end piece from the static support rig. The manganin coil has been removed but the thermocouple can still be seen. Eventually if a terminal or insulator was giving trouble and had to be replaced the process of extraction was very difficult unless individual back holes were provided. This was done wherever possible, for example in the static support rig, Fig 5.4., but could not be arranged when terminals were placed in a plunger, One minor problem associated with the terminals was short circuiting towards the end of a long fatigue test of 100,000 cycles or more. It was found that minute particles of phosphor bronze which had worn from the plunger mitre ring had collected in the annular well above the insulator and eventually provided a short circuit path. This could probably be avoided by filling up the well with araldite.

The use of four terminals in a 5/8 in (15.9 mm) diameter plunger creates difficult design problems because of the extremely limited space. Chandler (49) has suggested an alternative more compact method of introducing a number of electrical wires. A single steel cone is made with a number of longitudinal slots just sufficiently large to accomodate say 0.015 in (0.38 mm) diameter wires. The wires are bonded in the slots with an epoxy resin and the whole insert bonded in a matching socket in the vessel. The mthod was tried in the present case for an assembly of four wires in a plunger, butfound unsatisfactory in fatigue. One of the wires invariably extruded or snapped after only a few hundred cycles and it is impossible to replace one wire without extracting the whole assembly and starting again. In a static situation

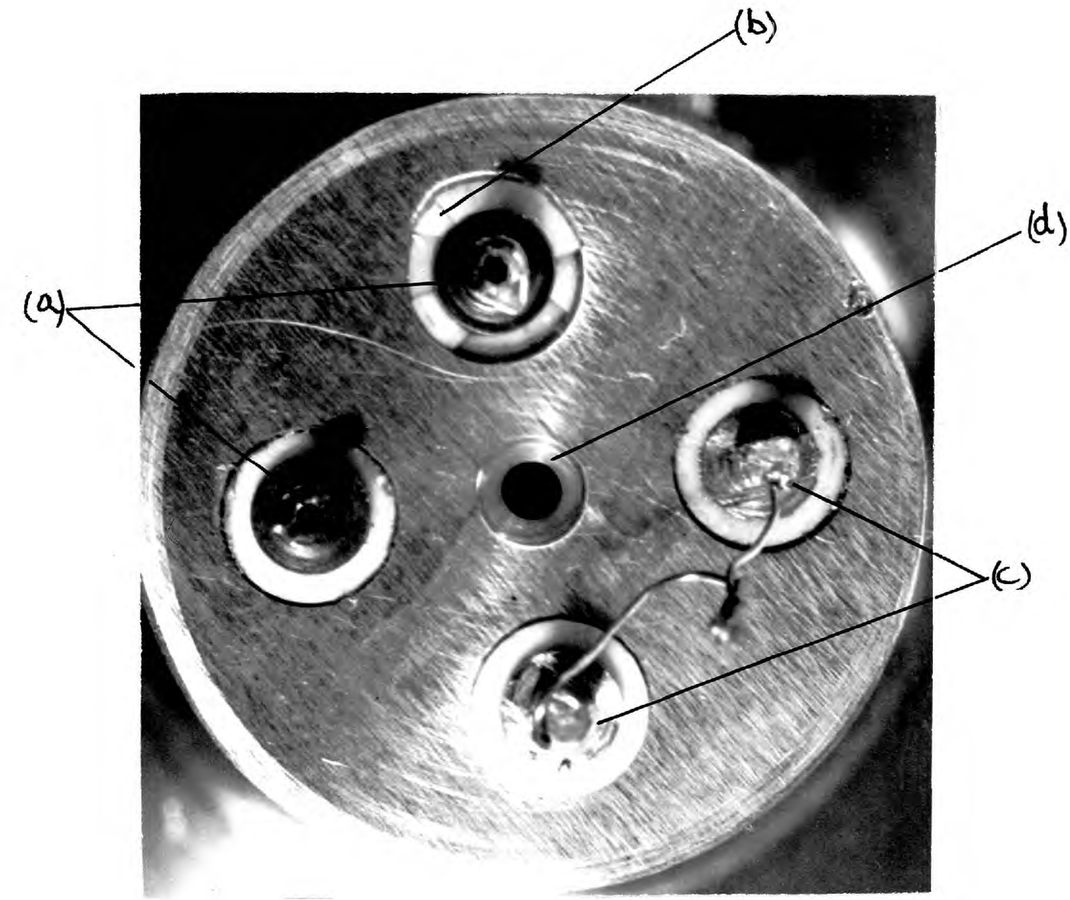

Fig. 6.4. Four Terminal Assembly with Cracked Insulator.

(a) Manganin Coil Terminals.

(b) Cracked Insulator.

(c) Thermocouple Terminals.

(d) Check Valve Seat.

the method appears to be satisfactory but was not developed further for the fatigue rigs.

Commercial Chromel-Alumel 32 S.W.G. thermocouple wire was used for all temperature measurements, and the terminals were individually made from 1/4in (6.4mm) diameter Chromel and Alumel rods. These materials are much softer than the silver steel used for the manganin gauge terminals but no extrusion problems were encountered at the pressures achieved in the present test programme.

6.3. Instrumention and Recording Equipment.

The general layout of instrumention and recording equipment is shown in the photograph Fig 2.2. It consists of two pressure units, one each for internal and external manganin gauges, a variable D.C. supply unit and an ultra-violet recorder, The pressure units are based on an arrangement described in detail by Barton (50). The circuit diagram for the units is shown in Fig. 6.5, but in the test programme no use was made either of the amplifier or the direct indicating meter. What remains is a Wheatstone bridge circuit with the manganin gauge forming one quarter of the bridge, and the usual controls for balancing the bridge and adjusting the supply voltage to control output. The output is in fact quite sufficient to drive the recorder galvanometers without amplification. For calibration a fixed 'set-calibration' resistor R.7 can be switched in the circuit to give a state of unbalance corresponding to a known pressure. It was arranged that different R.7 resistors could be installed appropriate to the particular pressure range required. Both pressure units were driven from a single Microreg type 300 Transistor variable power supply made by Weir Electronics Ltd. This instrument provides D.C. output from 0 to 25 volts with low noise and drift free performance. Normally it was required to supply about 6 volts to the pressure units.

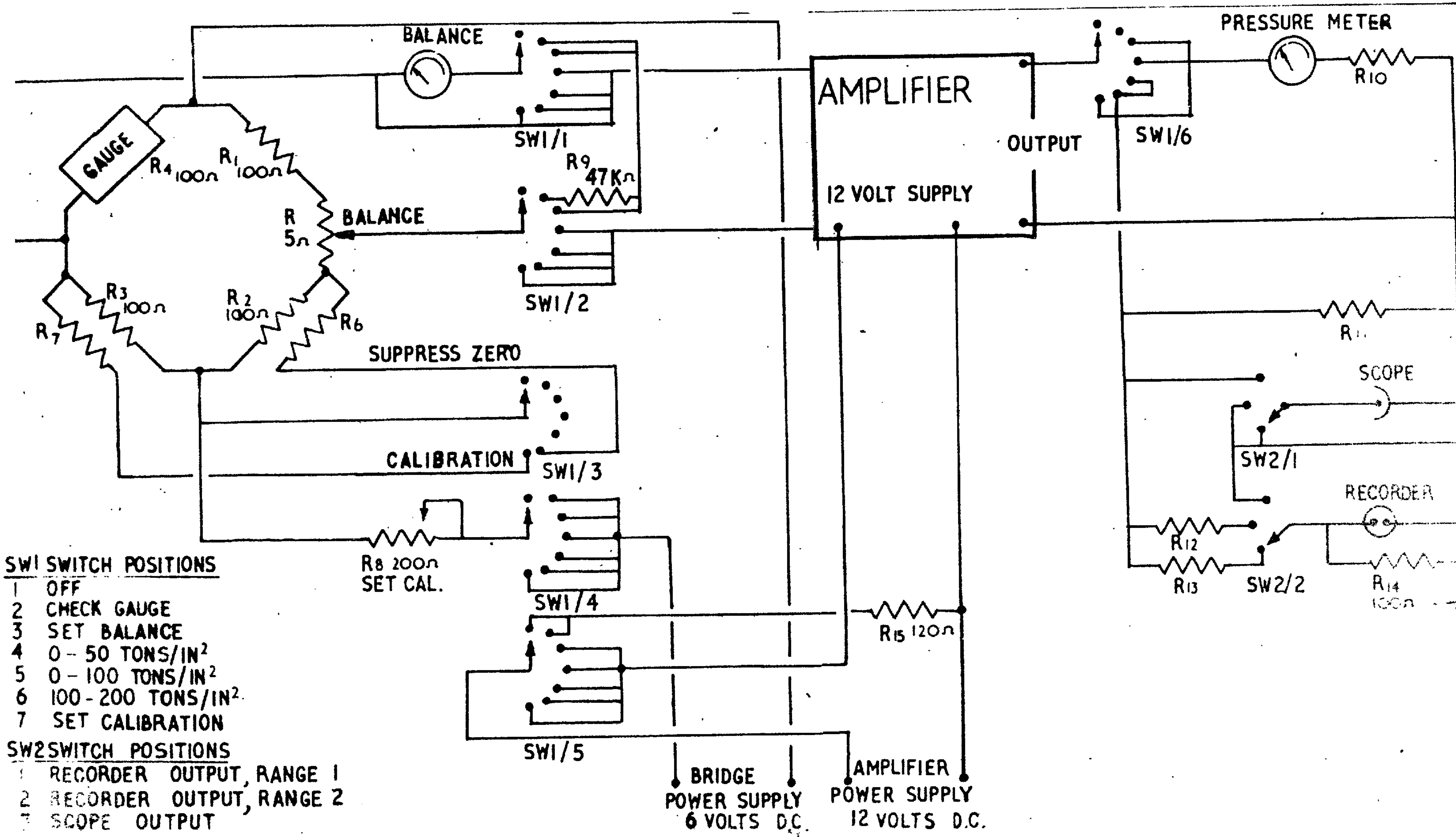

SW1 SWITCH POSITIONS
1 OFF
2 CHECK GAUGE
3 SET BALANCE
4 0 – 50 TONS/IN^2
5 0 – 100 TONS/IN^2
6 100 - 200 TONS/IN^2
7 SET CALIBRATION

SW2 SWITCH POSITIONS
1 RECORDER OUTPUT, RANGE 1
2 RECORDER OUTPUT, RANGE 2
3 SCOPE OUTPUT

FIG. 6.5 CIRCUIT DIAGRAM OF PRESSURE UNIT

The output from the pressure units was fed to an S.E. Laboratories (Engineering) Ltd. Type 3006 ultra-violet oscillograph with six galvanometer channels. The instrument is fitted with a slow speed gearbox giving paper speeds from 0.2 in (5.1 mm)/min to 5 in (127 mm)/S. The slowest speed enables the recorder to be left running throughout a test for a complete permanent record on 6 in (150 mm) wide direct print paper. The recorder is fitted with Type A.100 galvonometers having a nominal sensitivity of 0.0037 mA/cm with a tolerance of $\pm$ 10%. Because of the possibility of sensitivity variation between galvanometers care was taken to assign a particular galvanometer to a particular channel and to a particular pressure measuring unit. The galvanometers were not regarded as interchangeable.

The thermocouple output was also fed directly to the recorder a reference cold junction being maintained nearby in an ice filled vacuum flask. As it was necessary for current to be drawn from the thermocouple to drive the galvanometer the standard temperature/ e.m.f. charts could not be used and thermocouples had to be calibrated.

6.4. Calibration Technique.

In the early part of the test programme a dead weight tester was not available and manganin gauges were calibrated against a 150,000 lbf/in^2 (1,034 MN/m^2) Budenberg pressure gauge, which itself had been calibrated by the National Physical Laboratory. A square section vessel, as described by Lengyel and Alexander (1), was used with the manganin gauge installed at one end of the horizontal bore and the Budenberg gauge connected at the other end, with an intersecting vertical bore for the pressurising piston. The whole assembly was installed in a testing machine, the vessel filled with fluid and pressurised incrementally up to a maximum of 80,000 lbf/in^2 (552 MN/m^2) and released. A recording was made on ultra-violet paper of the manganin coil galvanometer deflection at each pressure increment, and also of the 'set-calibration' deflection. In a subsequent fatigue test the 'set calibration' deflection would be adjusted to the same value as in the calibration test so that the actual fatigue test pressures could be read from the calibration chart. In this way non-linearity of the galvanometer at large deflections was not a problem.

It was possible to perform elevated temperature calibrations by installing the square section vessel in a thermostatically controlled oil bath. Three calibrations were carried out at 19°C and 70°C and it was found that the three calibration lines diverged slightly as the pressure rose. However, by assuming that the elevated temperature calibration lines were parallel to the room temperature line and displaced only by the temperature effect at atmospheric pressure a maximum error of about 1% was introduced at 70°C and 70,000 lbf/in^2 (483 MN/m^2). It should be mentioned that during these elevated temperature calibration tests the temperature of the oil in the Budenberg gauge was also high which may have distorted the calibration curves.

Much more accurate room temperature calibration became possible later in the test programme when a 200,000 lfb/in^2 (1379 MN/m^2) Harwood controlled clearance piston gauge was installed. Details of this dead weight tester have been fully described by Johnson & Newhall (51). A thick-walled monobloc cylinder of 100 Tonf/in^2 (1544 MN/m^2) U.T.S. En 30.B. was connected to the dead weight tester and contained a sealed terminal block for the manganin gauge under test and thermocouple which was supported by a screwed plug. The complete instrumentation trolley was brought to the dead weight tester and allowed to warm up for an hour before starting the calibration. Zero readings were taken and the 'set-calibration' deflection adjusted to a convenient value, usually 6 or 12 cm. Correct weights for the first pressure increment were applied to the piston and the drive pressure built slowly up to a value just short of balance. The piston was then set spinning by an electric motor and the jacket pressure was increased to a value known to give the correct support. The drive pressure was increased again very gently until balance was achieved and the piston floated to the top of its stroke. After a short time a dial indicator showed that the piston was beginning to fall and having noted that the temperature had stabilised a recording of the galvanometer was made. The pressure was taken at this point to be simply $\frac{\text{total load on piston}}{\text{piston area}}$ and more exact corrections were not applied. It was assessed that these corrections were smaller than the accuracy with which it was possible to read the galvanometer deflection. The whole procedure described above was repeated for a number of pressure increments up to 100,000 lbf/in^2 (689 MN/m^2). On release of pressure and after time had elapsed for thermal equilibrium the galvanometer deflection was closely watched for an accurate return to the original zero. In exceptional cases this did not occur and the calibration was repeated, or if still troublesome the gauge was scrapped. A typical gauge calibration curve is shown in Fig. 6.6.

Thermocouple calibration was carried out by immersing the thermocouple in oil in a beaker and heating uniformly to two or three different temperatures which were measured accurately at the same time by a mercury in glass thermometer. The galvanometer deflections could then be related to known temperatures and because of good linearity intermediate temperatures could be measured accurately

For the purpose of temperature compensation calculations for the pressure measurements a series of temperature tests were also carried out at atmospheric pressure on the manganin gauge.

The gauge was coupled in the normal way to a pressure unit and an initial 'set-calibration' deflection was noted so that as the coil heated up the output from the bridge could be expressed as a pressure correction. A plot of this correction is shown in Fig. 6.7.

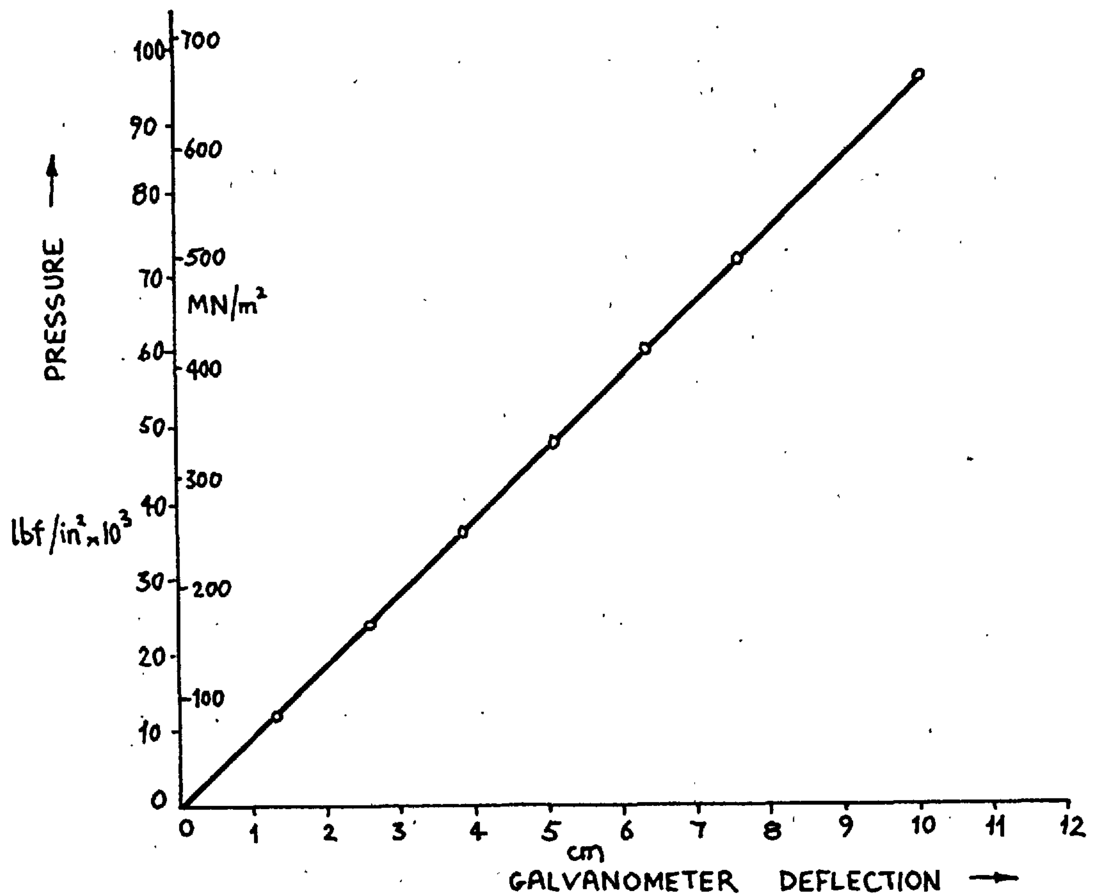

FIG. 6.6 MANGANIN GAUGE CALIBRATION CURVE

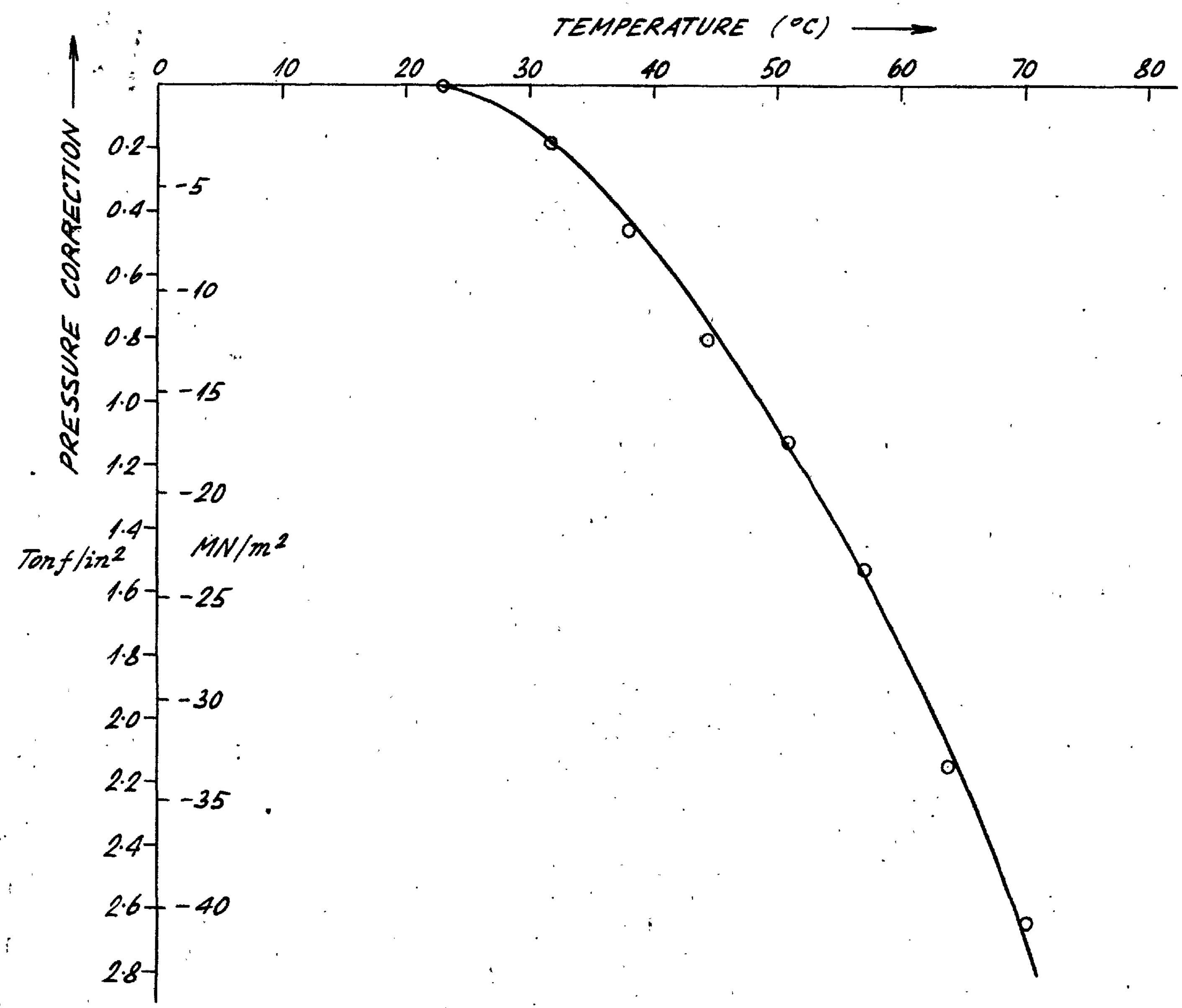

FIG. 6.7 MANGANIN GAUGE PRESSURE CORRECTION FOR ELEVATED TEMPERATURES.

CHAPTER 7.

MATERIAL AND SPECIMENS.

7.1 Test Material and Cutting up Procedures.

The material used for the test programme was a 2½% nickel-chromium-molybdenum steel to British Standard Aircraft Material Specification 2S96B. The more familiar designation of this steel is EN.25 to British Standard Specification 970:1955. The material was supplied in the form of eleven 2½ in (63.5 mm) diameter 12ft (3.7 mm) long rolled bars all from a single cast. The bars were heat treated by the steel maker by oil quenching from 840°C and tempering at 660°C to give a U.T.S. of approximately 58 Tonf/in^2 (896 MN/m^2). The chemical composition of the steel is shown on an inspection certificate. Appendix 2 issued by the supplier Aircraft Materials Ltd. The certificate also shows typical mechanical properties although detailed hardness, tension and torsion tests were carried out as part of the test programme.

Fig. 7.1 shows the indentification system and cutting up procedure used on the five bars of steel involved in the test programme. The 12ft. (3.7 mm) nominal length bars were first cut up into 3 ft. (0.9 mm) lengths numbered as shown in Fig 7.1., and the first and last 6 in (152 mm) length of each bar were discarded as untypical material. The remaining material was divided up as shown between dynamic support fatigue specimens, static support fatigue specimens, hardness, tensile and torsion specimens.

7.2. Fatigue Specimen Geometry and Manufacture.

Fig. 7.2 shows the geometry adopted for the dynamic support specimen. The shape was chosen firstly to satisfy functional requirements defined in Chapter 4 and secondly to correspond broadly to the specimen shapes used by Morrison et al. (24) and Austin and Crossland (27). The static support specimen Fig. 7.3 (a) was designed on the same principles although the later version of the specimen Fig.7.3 (b) arose initially from a need to simplify the shape for faster manufacture

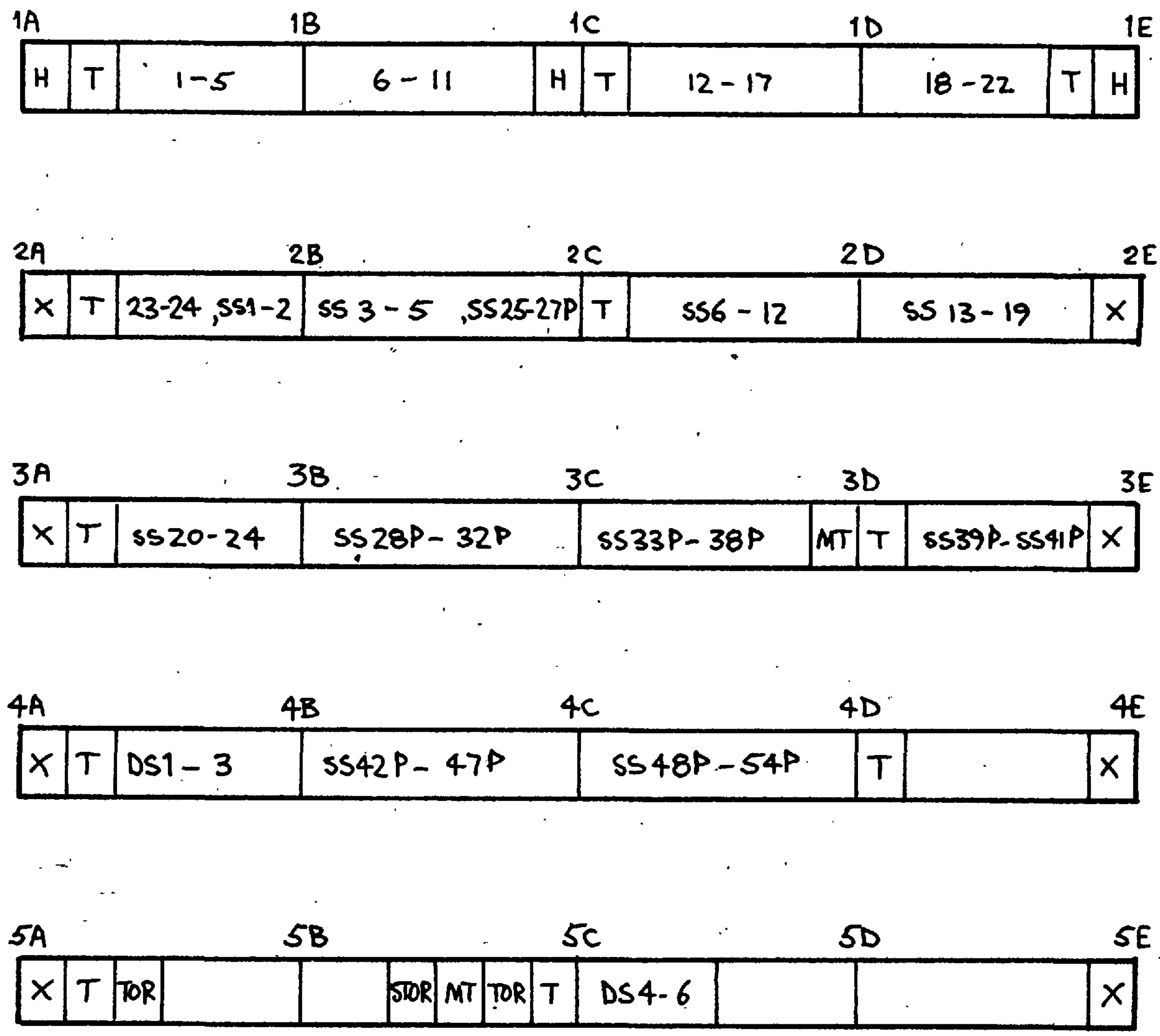

KEY

PLAIN DIGITS : FIRST SERIES MONOBLOC AND DYNAMIC SUPPORT CYLINDERS
SS DIGITS : NECKED STATIC SUPPORT CYLINDERS
SSP DIGITS : PLAIN STATIC SUPPORT CYLINDERS
DS DIGITS : SECOND SERIES DYNAMIC SUPPORT CYLINDERS
H : HARDNESS SPECIMEN
T : TENSILE SPECIMEN
MT : MINIATURE TENSILE SPECIMEN
TOR : TORSION SPECIMEN
STOR : SMALL TORSION SPECIMEN
X : DISCARDED BAR END

FIG. 7.1 TEST MATERIAL CUTTING UP AND IDENTIFICATION DIAGRAM

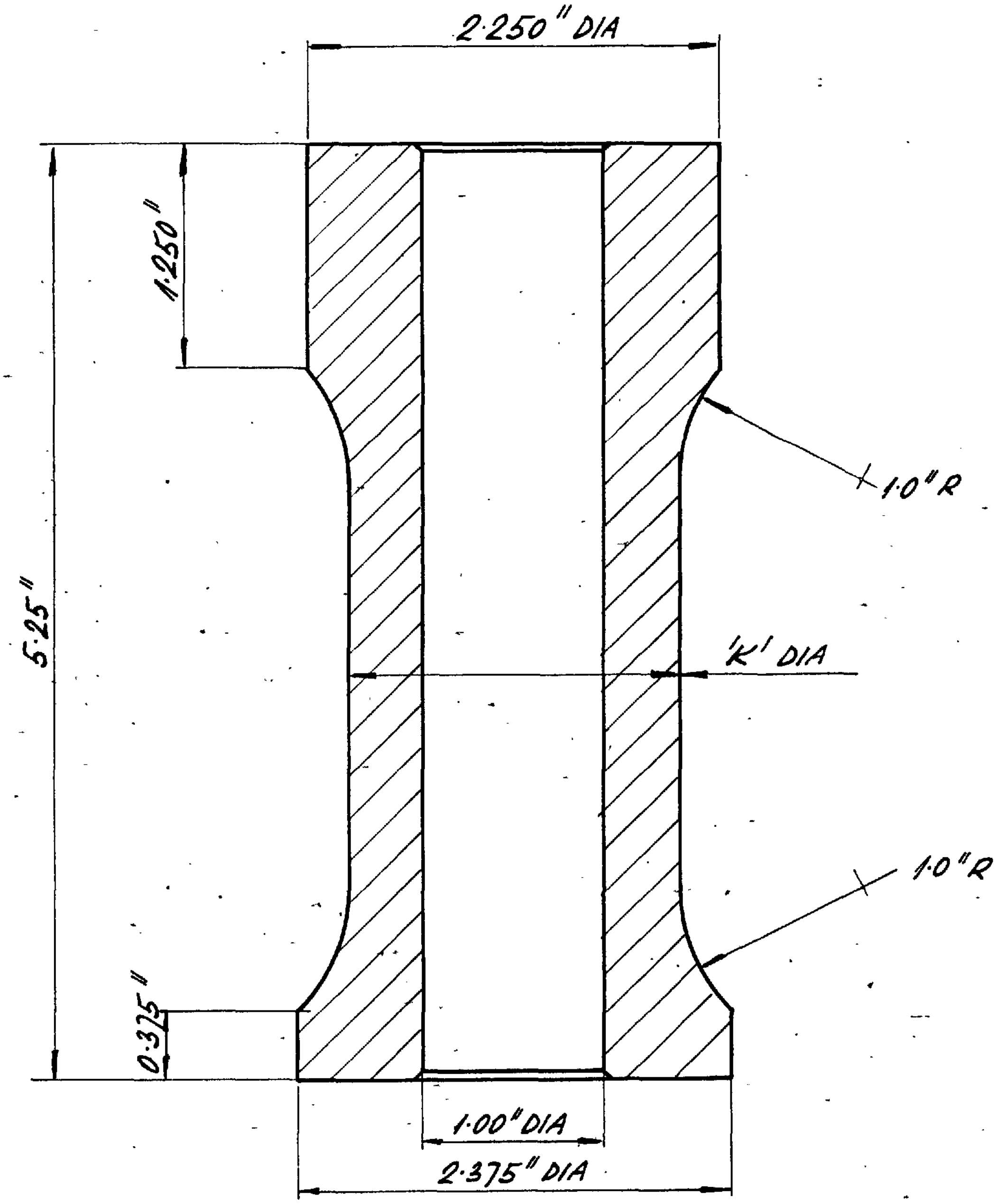

FIG. 7.2 DYNAMIC SUPPORT TEST SPECIMEN

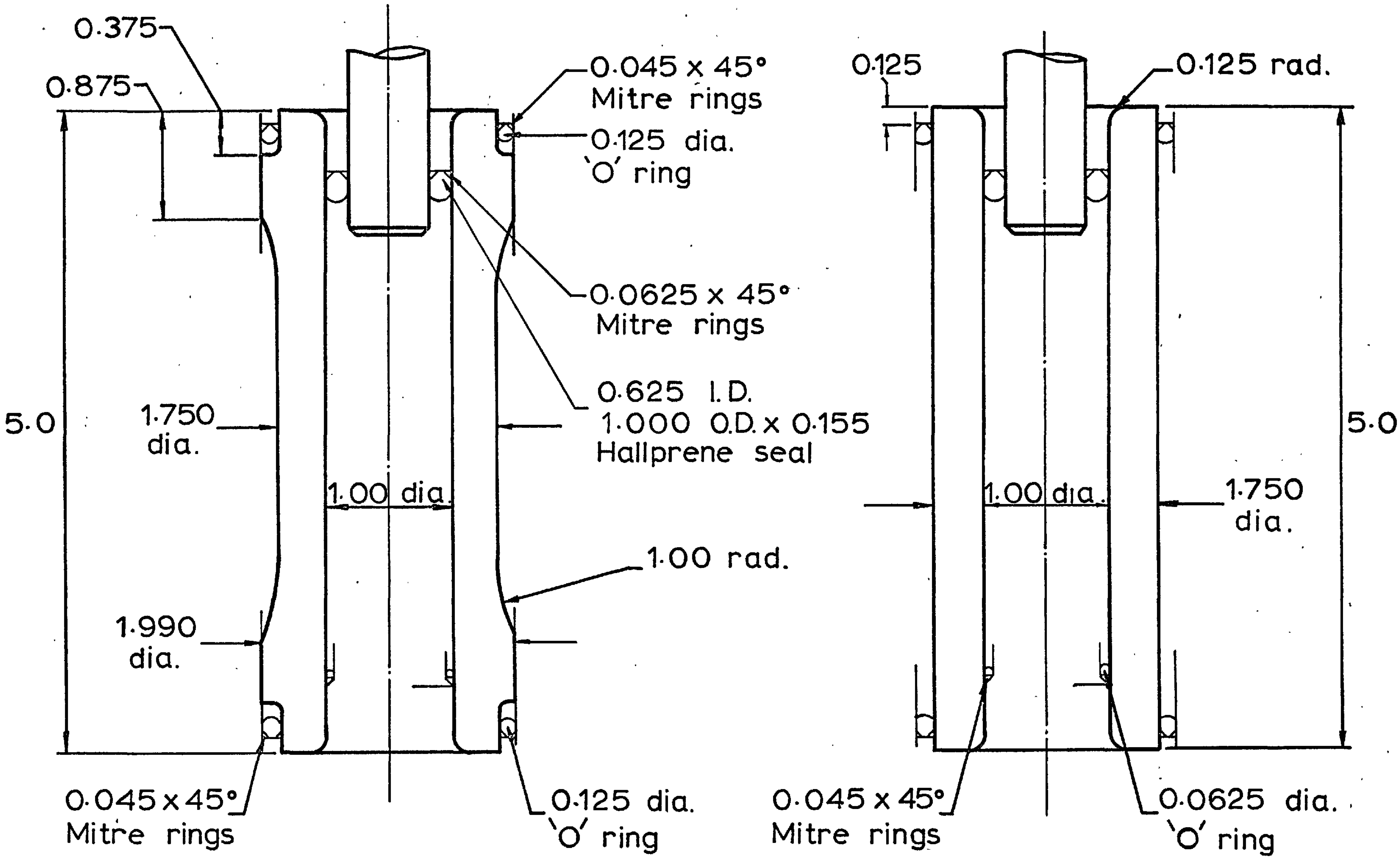

NECKED DESIGN a. FIG. 7.3 STATIC SUPPORT TEST CYLINDERS b. PLAIN DESIGN

Finite element stress analysis was subsequently carried out on the specimens to assess the effects of geometry and pressure discontinuities at seals which showed that the simpler design was quite adequate as a fatigue specimen. Details of the finite element analysis are given in Chapter 10.

All fatigue specimemts were manufactured to the following sequence:-

(i) A slug of material was sawn from one of the 3.ft. (0.9 mm) lengths taking care to preserve identification marks.

(ii) The slug was drilled and fine bored on a centre lathe to within 0.020 to 0.025 in (0.51 to 0.64 mm) of the final diameter. It was not safe to go nearer to the final size than this because of the difficulty in smooth boring the test material. Excess material was also rough turned from the outside at this stage although no attempt was made to profile the outside diameter.

(iii) The bore was coarse honed to within 0.004 or 0.005 in (0.10 or 0.13mm) of the correct size and a careful visual check made to ensure that no serious boring marks remained.

(iv) A well cleaned and greased expanding mandrel was inserted in the bore and set up between centres in a copying lathe. The outside diameter was then fine turned to the correct profile and the ends faced to give the required length. The outside surface was also lightly papered with fine emery cloth to improve the finish.

(v) The bore was fine honed to the correct diameter with a surface finish of 4 to 6 μin (0.10 to 0.15 μm) C.L.A.

(vi) Diamond lapping ensured a final mirror like bore with a surface finish of 2 to 4 μin (0.05 to 0.10 μm) C.L.A.

(vii) The specimen was normally inspected at this stage for dimensional accuracy surface finish, and concentricity, and a visual and magnetic check made for cracks in the bore. An identification number was etched on the end of the specimen.

(viii) The specimen was finally subjected to the following stress relieving treatment in vacuo,

(a) Heat slowly and uniformly up to 600 $\pm$ 10°C under high vacuum, 5.10^{-5} torr / (6.7 MN/m^2), taking 2 to 3 hours to reach the maximum temperature.

(b) Soak for 1 hour at 600 $\pm$ 10°C.

(c) Allow to cool slowly and uniformly to room temperature.

The stress relieving was performed by Edwards High Vacuum Ltd., and a typical run sheet is shown in Appendix 3

(ix) To preserve the specimen against corrosion before testing a liberal coating of white vaseline was applied.

7.3 Ancillary Test Specimens and Conditions.

7.3.1. Hardness Tests.

A systematic check of hardness variation along the length of a bar and across the section was carried out on bar No.1. The specimens were simply 3 in (76 mm) long cylinders with flat ground ends taken from the middle and two ends of the bar as shown in the cutting up Diagram Fig. 7.1.

7.3.2. Tension Tests.

Two sizes of tension specimen were employed. The larger, shown in Fig 7.4., was only suitable for longitudinal test pieces but had a gauge length to which an extensometer could be attached. The smaller specimen, shown in Fig 7.5., was suitable for both longitudinal and transverse test pieces and was modelled on a Hounsfield No.1. Specimen. No extensometer was available for this specimen and the measurement of crosshead displacement had to be relied upon. It can be seen from ~~Fig7.4 and~~ Fig 7.5. that the specimen were taken from bar material away from the centre

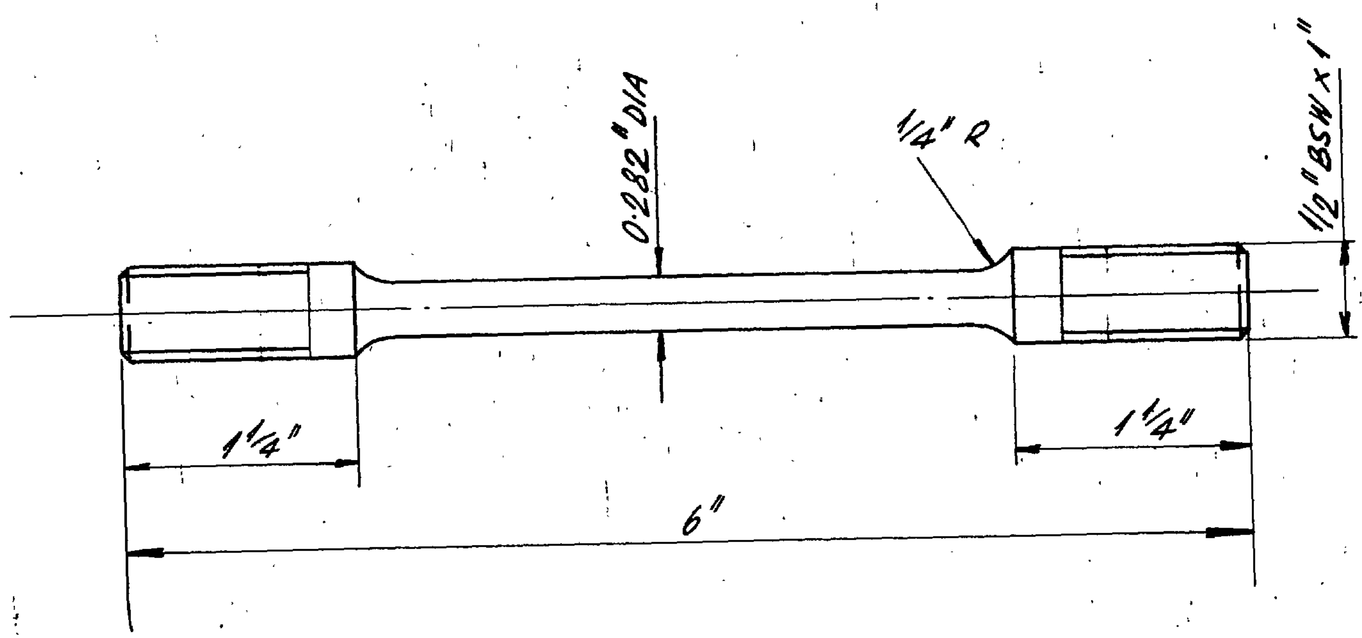

FIG. 7.4 LARGE TENSION SPECIMEN.

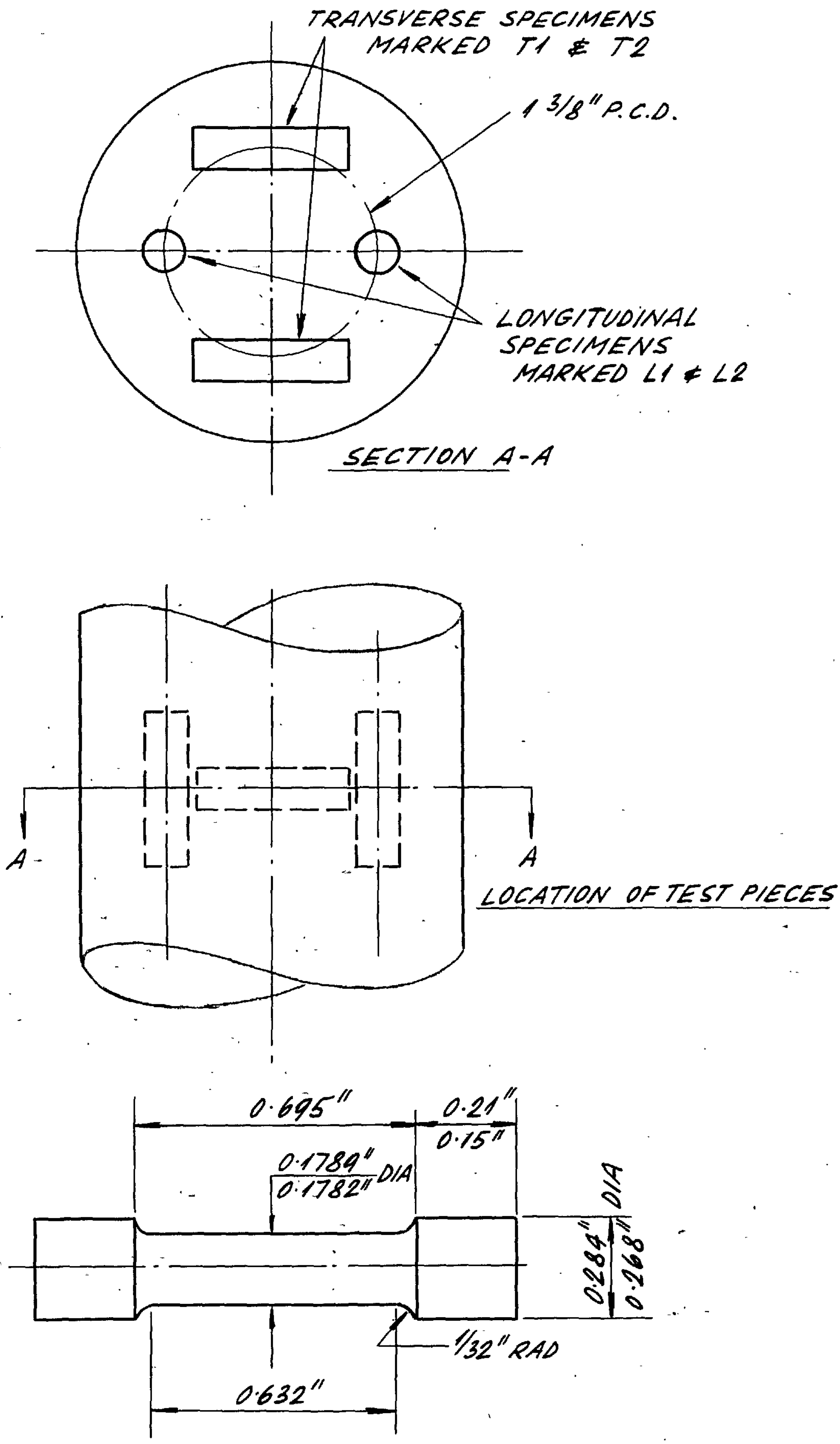

FIG. 7.5 HOUNSFIELD No 1 TENSILE TEST PIECE.

at a radius typical of the fatigue specimen cross section. The small specimens were intended to reveal the longitudinal and transverse tensile properties of the material whereas the large speciments were to indicate material property variation from bar to bar. It can be seen from the cutting up Diagram Fig 7.1. that large tension specimens were taken at one end and away from the ends of every bar.

The large specimens were tested in a Dennison Model T.42C2 testing machine using the 11,000 lbf (49 KN) range setting. This machine was fitted with an autographic recording facility which was used in conjunction with a Wiedman-Baldwin K.S.M-D. Extensometer. This extensometer is fitted with two linear variable differential transformers, one to cater for elestic and small plastic strains, and the other to cater for large plastic strains, over a gauge length of 2 in (50.8 mm) Autographic records of load against extension were obtained during the tension tests. When testingthe higher extensometer sensitivity was used initially, but soon after yield had occurred the lower sensitivity was used for the remaining extension up to failure.

The small longitudinal and transverse speciments were tested in an Instron testing machine using the 5,000 lbf (22 kN) range. A crosshead speed of 0.02 in/min (0.51 mm/min) was used and again an autographic loade-extension curve was obtained. However, on this occasion the extension referred to the crosshead displacement.

7.3.3. Torsion Tests.

A number of torsion tests were carried out on bar No.5. Initially two large solid torsion speciments were made to the shape shown in Fig. 7.6., which was a reduced diameter version of the standard specimen normally used on a 15,000 lbf in (1.7 kN m) Avery Type 6609 C.G.C. Torsion Testing Machine. The ends of this specimen are so large that the specimens were cut from the centre of the bar. Four strain gauges were attached to the centre portion of each specimen equally spaced around the circumference and aligned on 45° helix guide lines. The

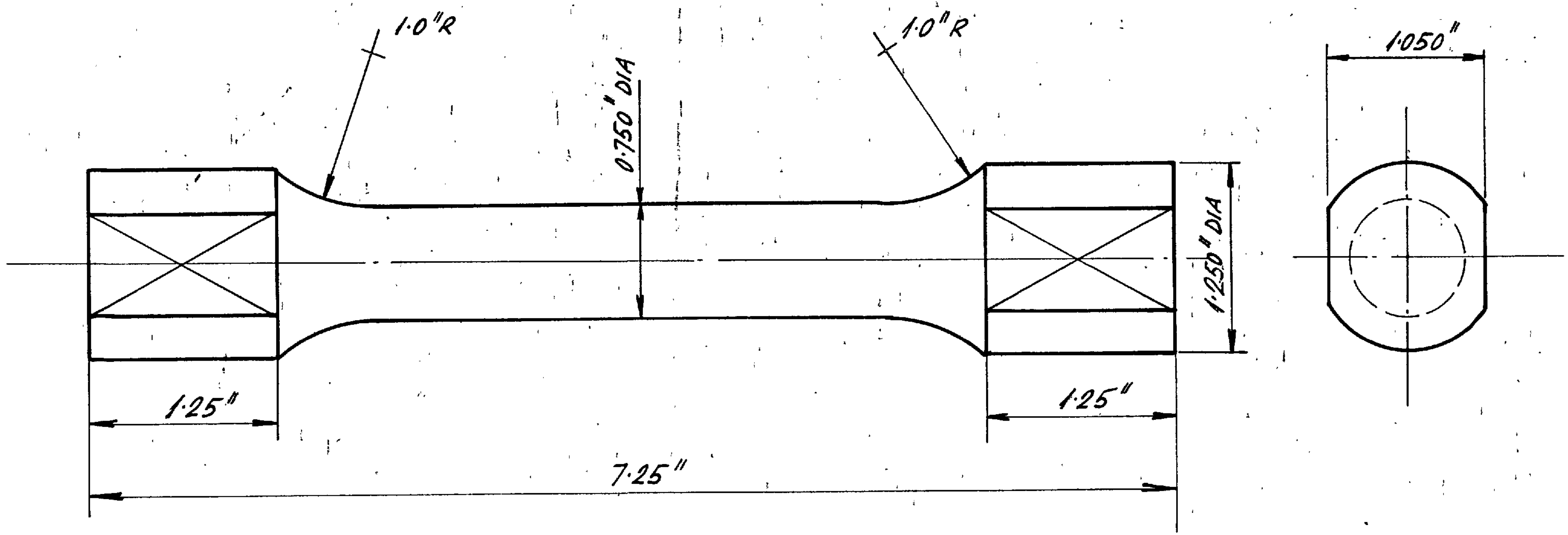

FIG. 7.6 LARGE TORSION SPECIMEN.

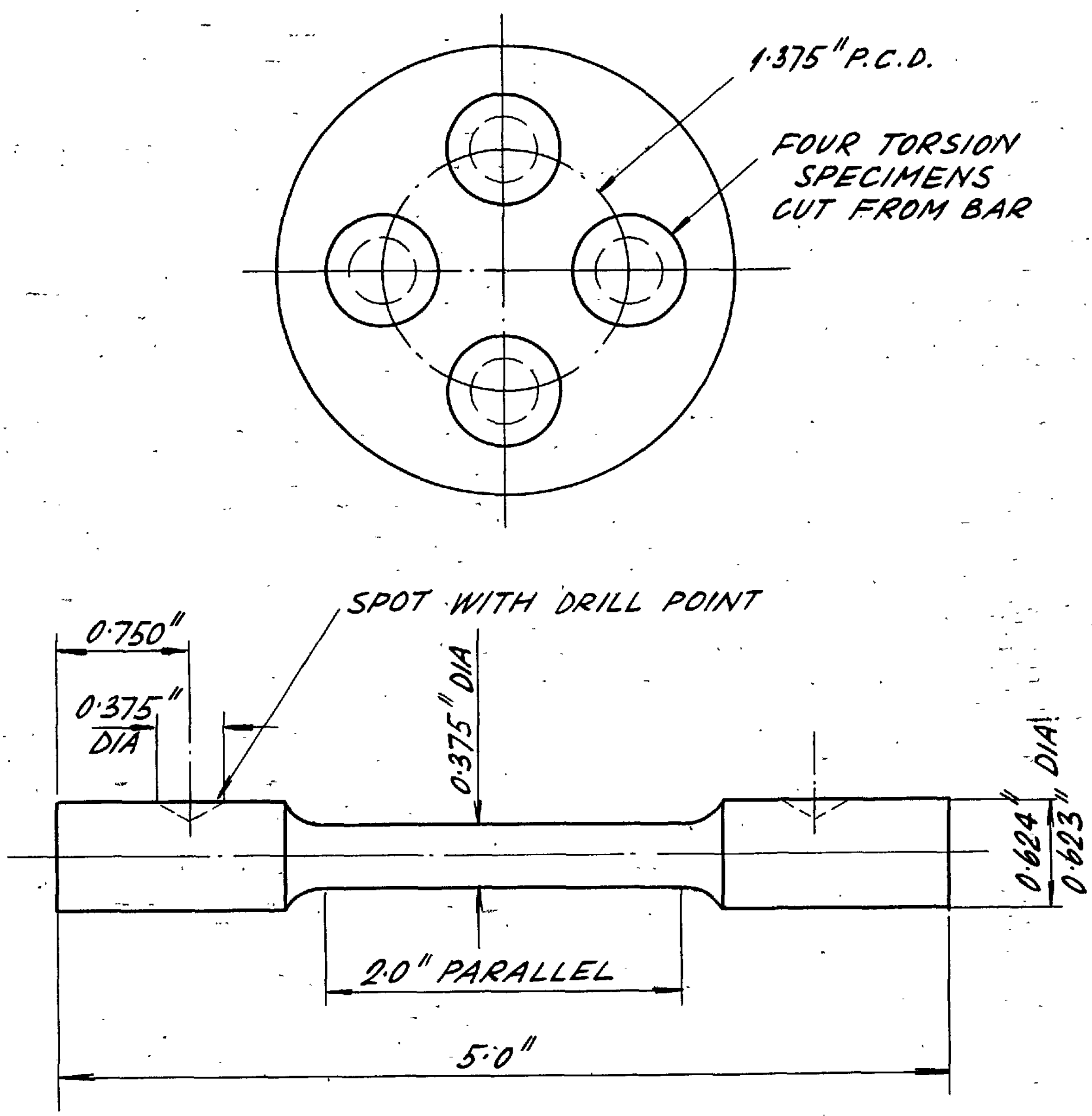

FIG. 7.7. SMALL TORSION SPECIMEN.

directions of the helices alternated so that the four gauges were strained in tension, compression, tension, and compression respectively. The gauges were connected via a selector box to a Budd direct reading strain indicating bridge. A torsiometer was also fitted to the specimen to indicate large angular displacements beyond yield. It consistedof two clamping rings spaced 3 in (76.2 mm) apart and carrying a protractor scale and pointer.

It was felt desirable to carry out torsion tests on material away from the centre of the bar which would be more representative of the material in the fatigue specimens. A much smaller fatigue specimen was required and the design shown in Fig 7.7 was adopted. Two driving collars were made in 100 Tonf/in^2 (1544 MN/m^2) U.T.S. En. 30.B. material of the same external shape as the ends of the large specimen but with an accurate bore to slide over the ends of the small specimen. The driving collars were radially drilled and tapped 3/8 in B.S.F. and a 'W' point grub screw was used in each to engage in the conical dimples at the two ends of the specimen. In this way the specimen could be used in the existing driving grips of the 15,000 lbf in (1.7 KN m) Avery Machine. Two strain gauges were attached to the smaller specimen and the torsiometer was modified to suit the 1.7/8" (47.6 mm) gauge length used. A specimen ready for test is shown in the photograph Fig 7.8.

The use of strain gauges is a rather expensive method of measuring small shear strains on specimens which are tested to destruction. However, if only a few specimens are involved this may not be important and their use does have the advantages of quick reading, and of indicating the magnitude of bending induced during a test.

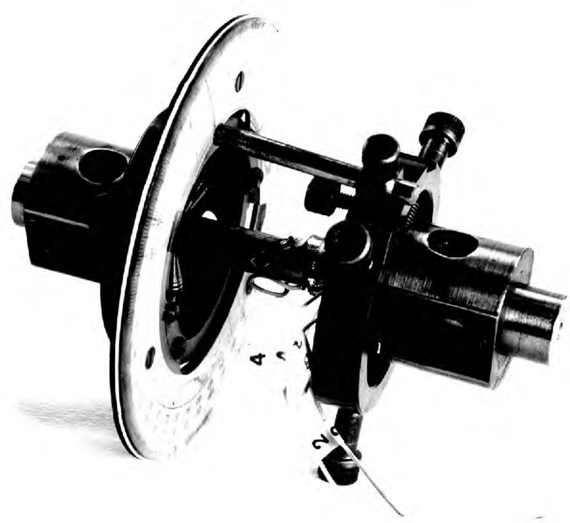

Fig. 7.8 Torsion Specimen Assembly.

CHAPTER 8.

ANCILLARY TEST RESULTS.

8.1 Hardness Tests.

The results of the hardness tests made at the two ends and the middle of bar No.1. are shown in Fig. 8.1. The points plotted are the average of hardness values measured along two diameters at right angles for each specimen. It can be seen by reference to the cutting up diagram Fig. 7.1 that the end specimens were taken from the part of the bar normally discarded. The plots in Fig. 8.1 thus represent the extreme variations of hardness which could be expected. One end of the bar is noticeably harder than the other probably as a result of being subjected to a more severe quench during the heat treatment. All parts of the bar exhibit softening in the centre although this is restricted to a region within 0.5 in (12.7 mm) radius of the centre. The region from 0.5 to 1 in (12.7 to 25.4 mm) radius of the centre, which would normally be used in a fatigue cylinder is of uniform hardness across the section and along the length of the bar providing the very ends are not used. This policy was adopted for the bars used in the test programme and the first and last 6 in (152 mm) were always discarded.

8.2 Tension Tests.

The results of tension tests carried out on large longitudinal specimens taken from the five test bars are shown in Table 8.1, and a typical autographic load/extension curve from a test is shown in Fig. 8.2. Specimens were cut from both ends and the centre of bar No.1., and it can be seen from the results table that the yield and ultimate stress values at the ends are some 4% higher than at the centre. The other bars were tested near the centre region and at one end and exhibited similar variation. The variation in tensile properties from bar to bar either at the end or away

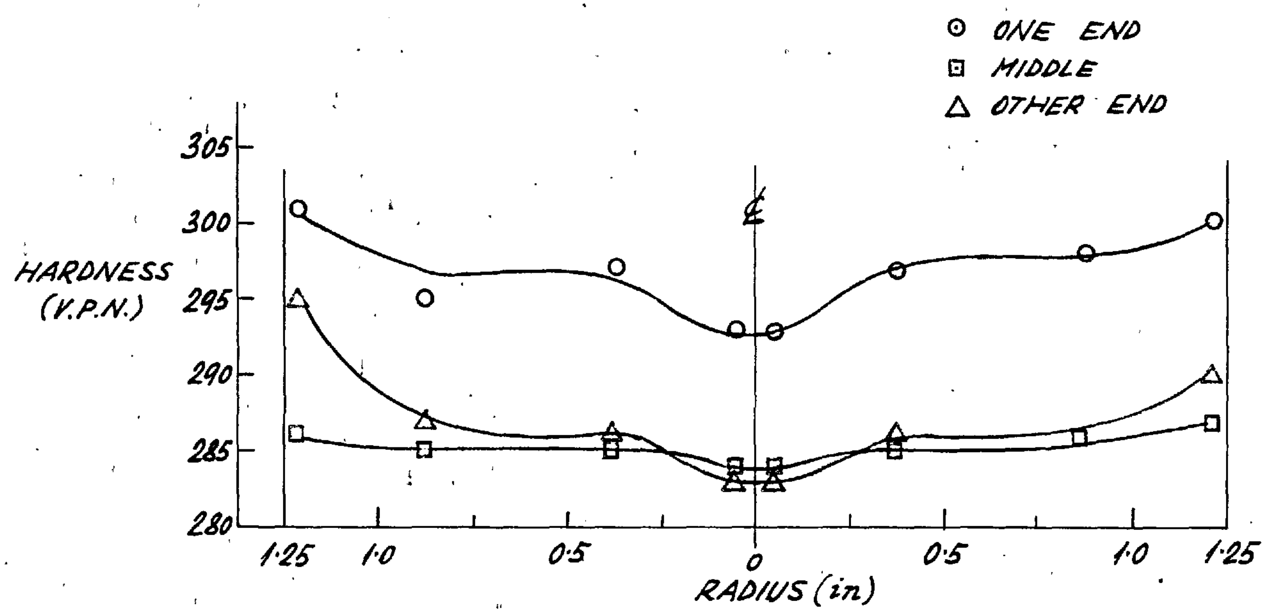

FIG. 8.1 HARDNESS DISTRIBUTION IN BAR No 1.

Table 8.1 Tension Tests on Large Longitudinal Specimens.

1. Detailed Results.

Bar No.	Specimen No.	Yield Stress. (Tonf/in^2).	Ultimate Stress. (Tonf/in^2)
1.	1.A. (i).	51.5.	59.0
	1.A. (ii).	51.8.	59.1.
	1.C. (i).	49.3.	57.4.
	1.C. (ii).	49.6.	57.8.
	1.E. (i).	51.2.	58.9.
	1.E. (ii).	51.0.	58.7.
2.	2.A. (i).	50.2.	58.7.
	2.A. (ii).	50.5.	58.7.
	2.C. (i).	48.5.	57.3.
	2.C. (ii).	48.6.	57.5.
3.	3.A. (i).	50.4.	58.6.
	3.A. (ii).	50.2.	58.5.
	3.D. (i).	48.2.	57.6.
	3.D. (ii).	48.2.	57.8.
4.	4.A. (i).	50.3.	58.5.
	4.A. (ii).	50.4.	58.7.
	4.D. (i).	47.8.	57.6.
	4.D. (ii).	47.8.	57.6.
5.	5.A. (i).	50.0.	58.8.
	5.A. (ii).	50.5.	58.6.
	5.C. (i).	49.1.	57.9.
	5.C. (ii).	48.7.	57.3.

2. Average properties away from the ends of the bars.

Lower Tensile yield stress	=	48.6 Tonf/in^2 (751 MN/m^2)
Ultimate Tensile stress	=	57.6 Tonf/in^2 (890 MN/m^2)
Reduction of area	=	60%.
Young's Modulus.	=	13,200 Tonf/in^2 (204 GN/m^2)

Fig 8.2

115

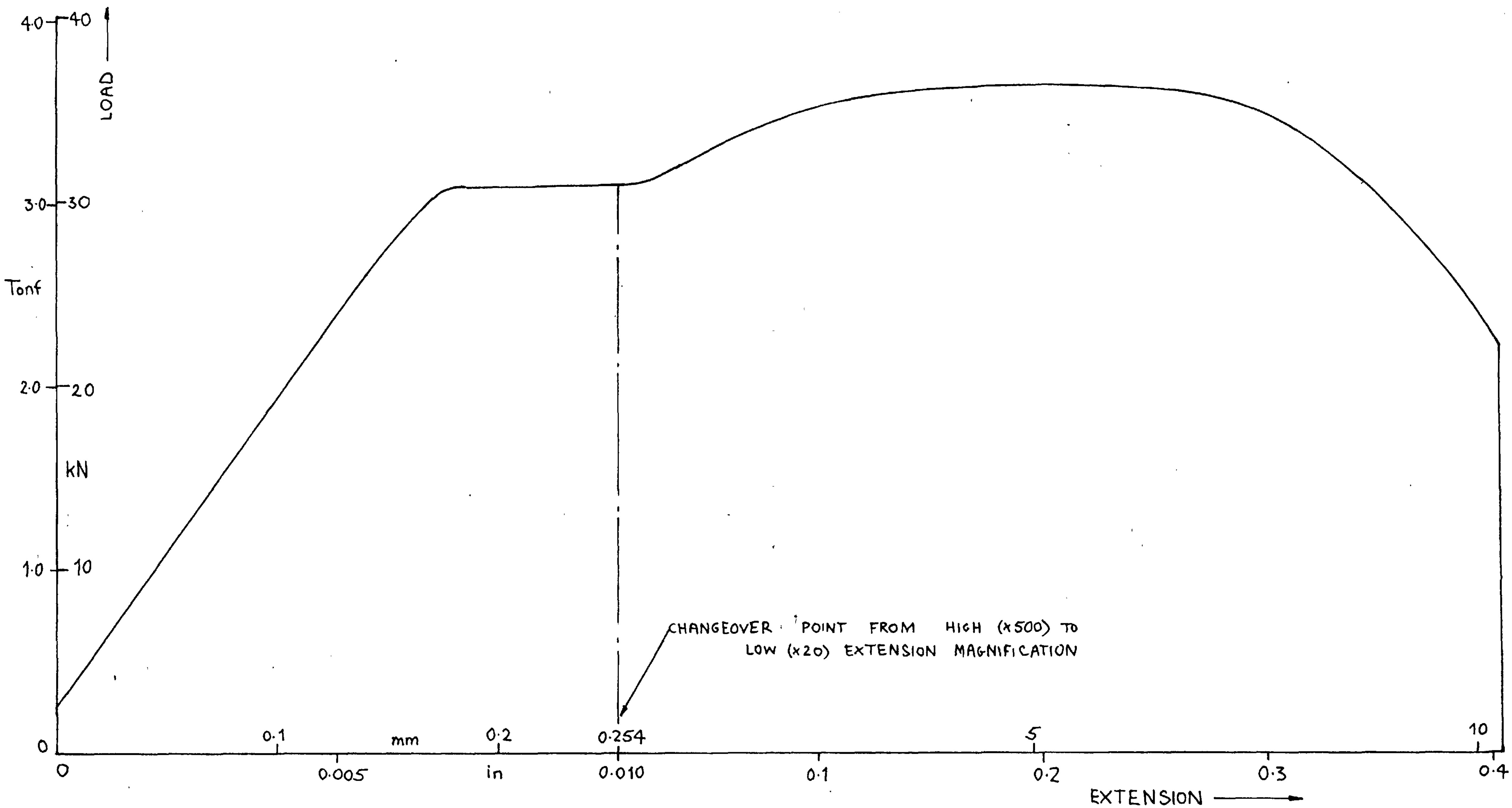

FIG. 8.2 TYPICAL AUTOGRAPHIC LOAD - EXTENSION CURVE FROM TEST ON LARGE TENSION SPECIMEN

Table 8.2. Results of tension tests on small longitudinal and transverse specimens.

Bar No.	Orientation.	Yield Stress. (Tonf/in^2).	Ultimate Stress. (Tonf/in^2)	% Reduction of Area.
3.	Longitudinal.	47.3.	57.5.	66.
	"	47.0.	57.7.	67.
	Transverse.	47.3.	57.7.	46.
	"	47.0.	57.5.	45.
5.	Lonitudinal.	48.7.	58.6.	66.
	"	48.8.	58.8.	65.
	Transverse.	48.7.	58.7.	45.
	"	48.7.	58.5.	43.

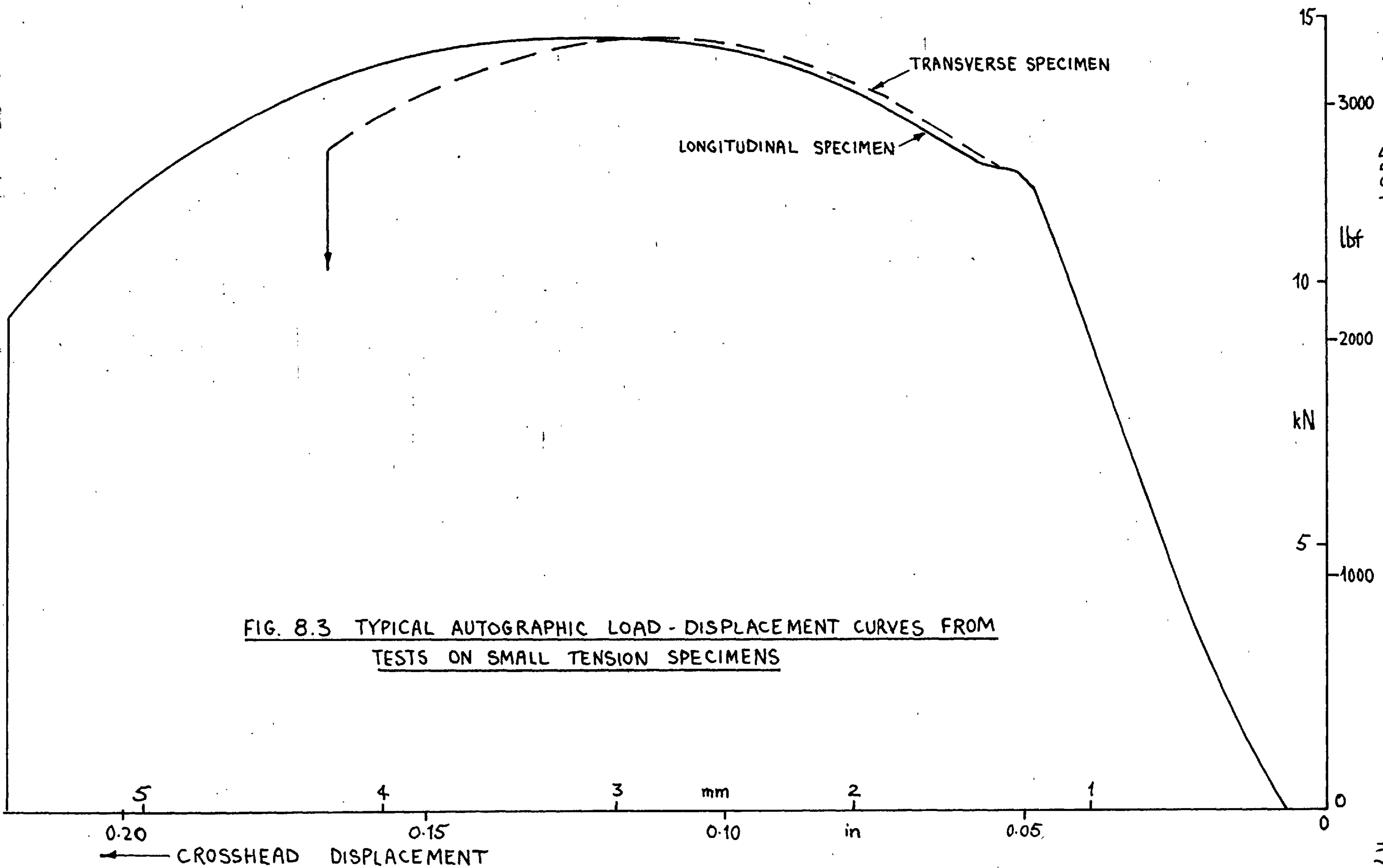

FIG. 8.3 TYPICAL AUTOGRAPHIC LOAD - DISPLACEMENT CURVES FROM TESTS ON SMALL TENSION SPECIMENS

from the end is also within 4% although the extreme overall variation is as much as 8%. However, in the case of bars Nos. 3 and 4 test pieces were taken at the beginning of the last 3.ft. (0.9 m) length of each bar and yet still exhibited the same 4% lower values than at the very ends. This indicates that the material with higher tensile properties is restricted to a fairly limited region at the ends of each bar. Table 8.1. also gives average properties away ffom the end of the bars. No significant variations were discovered in the values of either reduction in area or Young's Modulus.

The resultsof the smaller tension specimens cut in a transverse as well as longitudinal direction from bars Nos. 3. and 5 are shown in Table 8.2. and typical autographic plots are shown in Fig 8.3. The results indicate that there is no difference in yield and ultimate strength between the transverse and longitudinal directions, but that there is a marked difference in the reduction of area figure. This lower ductility in the case of transverse specimens is also manifested in the autographic plot by the reduced displacement at which the transverse specimen fails. Two of the four transverse specimens fractured in a 45° plane across the section instead of the classic cup and cone fracture obtained with all longitudinal specimens.

8.3. Torsion Tests.

The results of torsion tests on two large and two small specimens taken from bar No.5. are plotted on the basis of Tr/J against shear strain in Figs. 8.4 and 8.5. Fig 8.4 is drawn to a large shear strain scale to show in detail the elastic and elastic-plastic regions of shear strains appropriate to the expansion of moderately thick walled cylinders up to the collapse point. The experimental ~~points~~ curves in Fig 8.4. are largely from strain gauge readings. Fig. 8.5. shows the shear stress/strain curve at large plastic shear strains up to fracture, and in this case the experimental

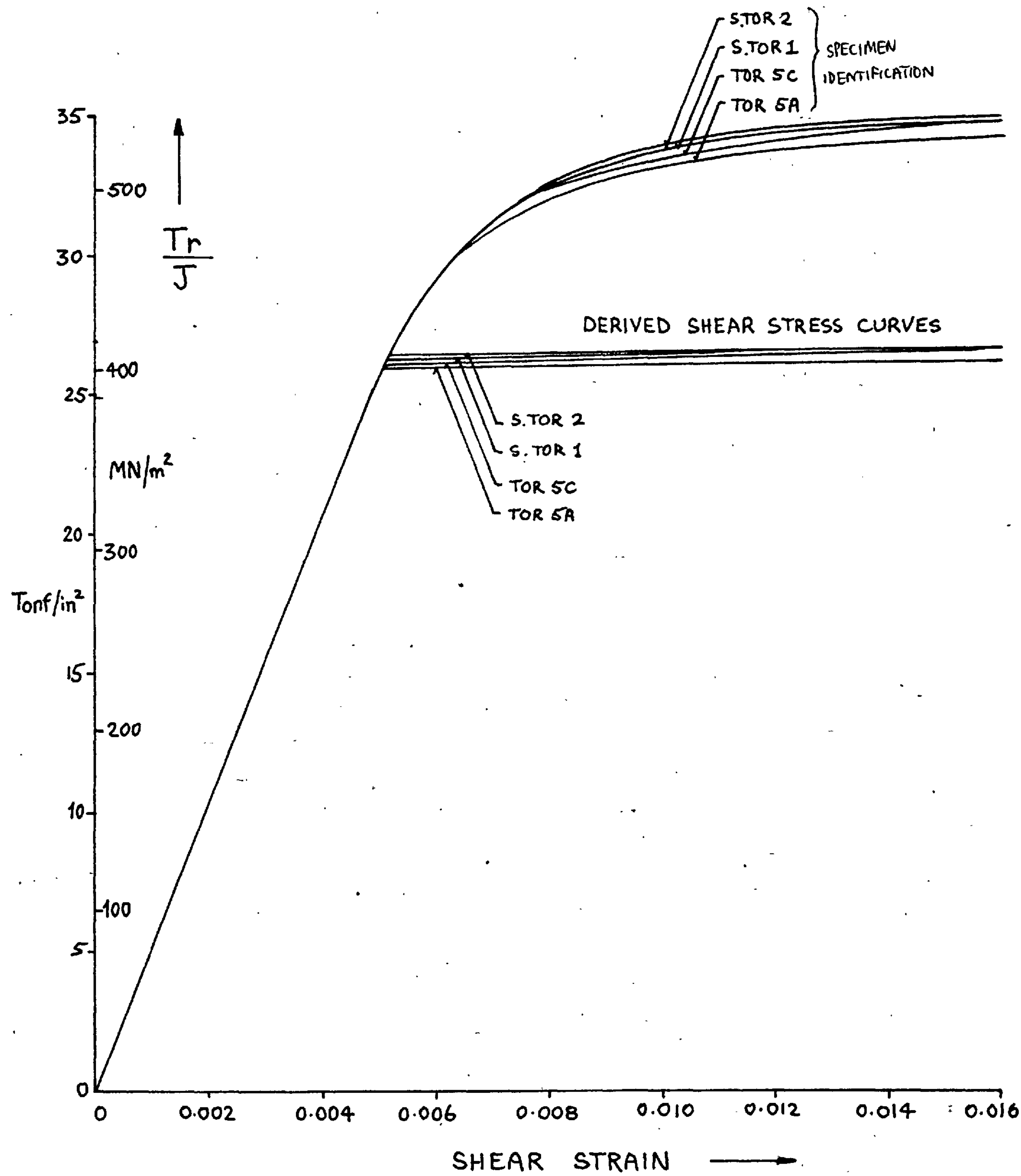

FIG 8.4 RESULTS OF TORSION TESTS AT SMALL STRAINS

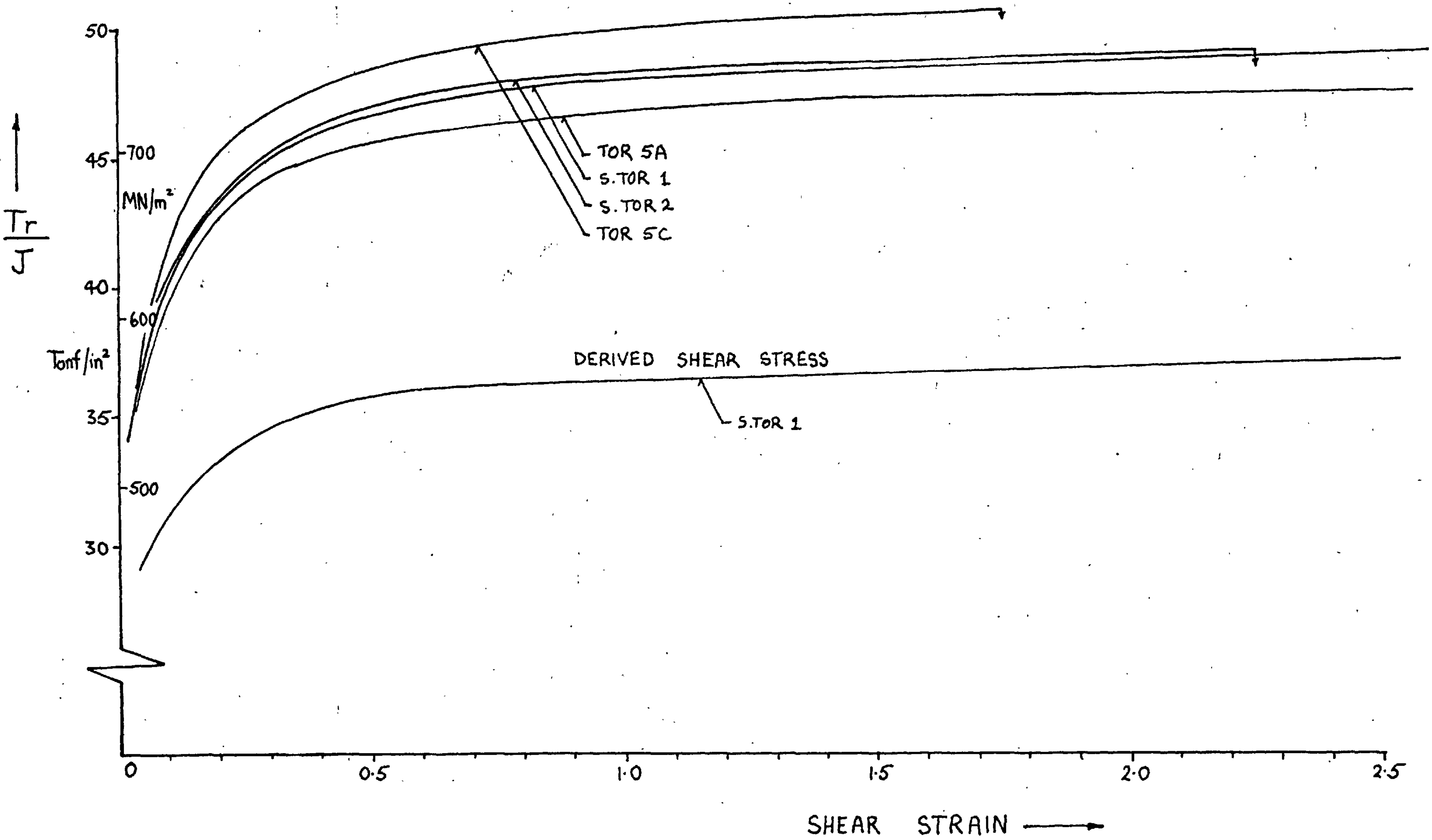

FIG. 8.5 RESULTS OF TORSION TESTS AT LARGE STRAINS

points were derived from angular torsiometer measurements.

In Fig. 8.4. the difference between the results of the four tests are very small although as would be expected the large specimens taken from the core of the test bar are slightly softer than the small specimens away from the core. The shear stress curves beyond yield were derived from the experimental curves by Nadai (52) construction, and exhibit virtually no hardening up to a shear strain of 0.015 or so. This behaviour is typical of En.25 steel and agrees well with results from a careful series of experiments on both solid and tubular torsion specimens by Franklin and Morrison (53). In Fig. 8.5. the Nadai construction has again been used to derive the shear stress/strain curve. The average properties of the material in torsion are given in Table 8.3., and these agree well with data on En.25 given by Morrison et al (24) Austin and Crossland (27), and Crossland and Burns (5).

Table 8.3. Results of Torsion Tests on Bar No.5.

Specimen Size.	Specimen No.	Shear Yield Stress. (Tonf/in^2).	Shear Modulus. (Tonf/in^2).
Large.	L.T.5.A.	26.0.	5,200.
Large.	L.T.5.C.	26.1.	5,200.
Small.	S.T.1.	26.5.	5,180.
Small.	S.T.2.	26.3.	5,210.

CHAPTER 9.

PRESSURE TESTS ON STRAIN GAUGED CYLINDERS.

9.1 Introduction.

Tests were carried out on two plain cylinder specimens to establish the pressure expansion and contraction curves under internal and external pressure conditions. In the case of the internally pressurised cylinder the effect of cycling beyond the yield pressure was investigated.

9.2 Test Procedure.

9.2.1. Internally Pressurised Cylinder.

A plain cylinder of 1.75 K. ratio was carefully marked out with guide-lines on the outside surface so that three axial and three circumferential resistance strain gauges could be accurately positioned. The gauges were installed alternately in the axial and circumferential directions as can be seen in the photograph Fig. 9.1. The gauges used were of 0.5 in (12.7 mm) gauge length and negligible transverse sensitivity.

The strain gauged specimen was installed in the test rig using static support rig components with the exception of the outer vessel. This was replaced by a large diameter thin walled tube with a hole in the wall through which the strain gauge leads could emerge. The leads from each strain gauge were individually connected to the terminals of a multi-way selector box, which itself was connected to a Budd Strain Indicating Bridge. In this way each of the six gauges could be selected in turn, the bridge balanced, and the strain recorded.

The internal pressure was generated with the usual sealed plunger arrangement, but in order to increase the pressure incrementally and to hold the pressure constant for each increment special measures were taken. The leads from the pressure switch to the electrical control cabinet of the press were disconnected so that the press could be used in 'Auto' without the ram reversing once the maximum pressure had been built up.

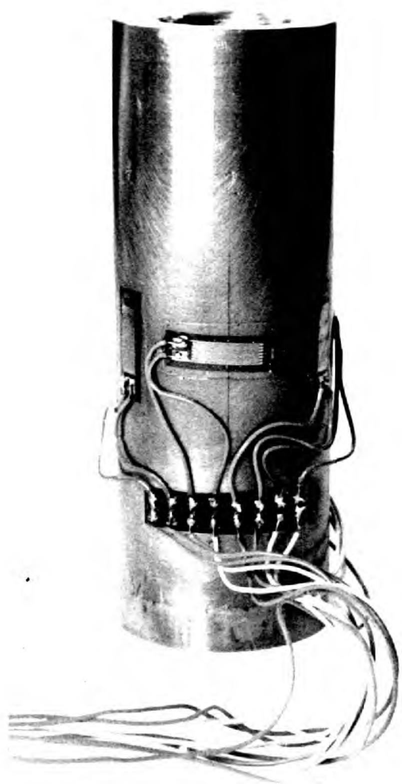

Fig. 9.1. Strain Gauged Cylinder.

Thus for any setting of the main relief valve a constant plunger pressure could be maintained, and by adjusting the relief valve the pressure could be gradually raised or lowered.

Initially a number of low pressure excursions were made to check and stabilise the performance of the strain gauges. The pressure was then raised to 25.4 $Tonf/in^2$ (392 MN/m^2) incrementally and back to zero, a full record being taken of all strain gauge readings. A few more such pressure excursions were made before restoring the pressure switch in the control circuit so that the press could be cycled normally. An X - Y plotter was connected up to the strain gauges at this stage in the hope of monitoring the pressure-strain characteristic as the test proceeded. However, the response of the plotter was insufficiently fast and the pen tended to overshoot making it difficult to get sensible results. A record was therefore kept of the strain gauge readings from the Budd bridge at minimum pressure at intervals throughout the test. A second stage of the test involved increasing the pressure cycles to a higher maximum pressure 27.3 $Tonf/in^2$ (422 MN/m^2) while still keeping a check on the strain gauge readings. The number of cycles achieved at this stage was roughly half the anticipated life, and the specimen was finally statically burst.

9.2.2. Externally Pressurised Cylinder.

Two axial and two circumferential strain gauges were installed in the bore of a plain cylinder specimen of 1.75 K ratio. It was necessary to use (0.25 in (6.4 mm) gauges in the circumferential direction although 0.5 in (12.7 mm) gauges were used axially. The 0.25 in (6.4 mm) gauges have a cross sensitivity factor of 0.4% but as the axial strains are only roughly 0.28 times the hoop strains the cross-sensitivity effect could be ignored. Each gauge with leads attached carefully was mounted face down on a long strip of sellotape, and Eastman 910 adhesive applied to the back of the gauge. The strip was then introduced in the bore of the specimen

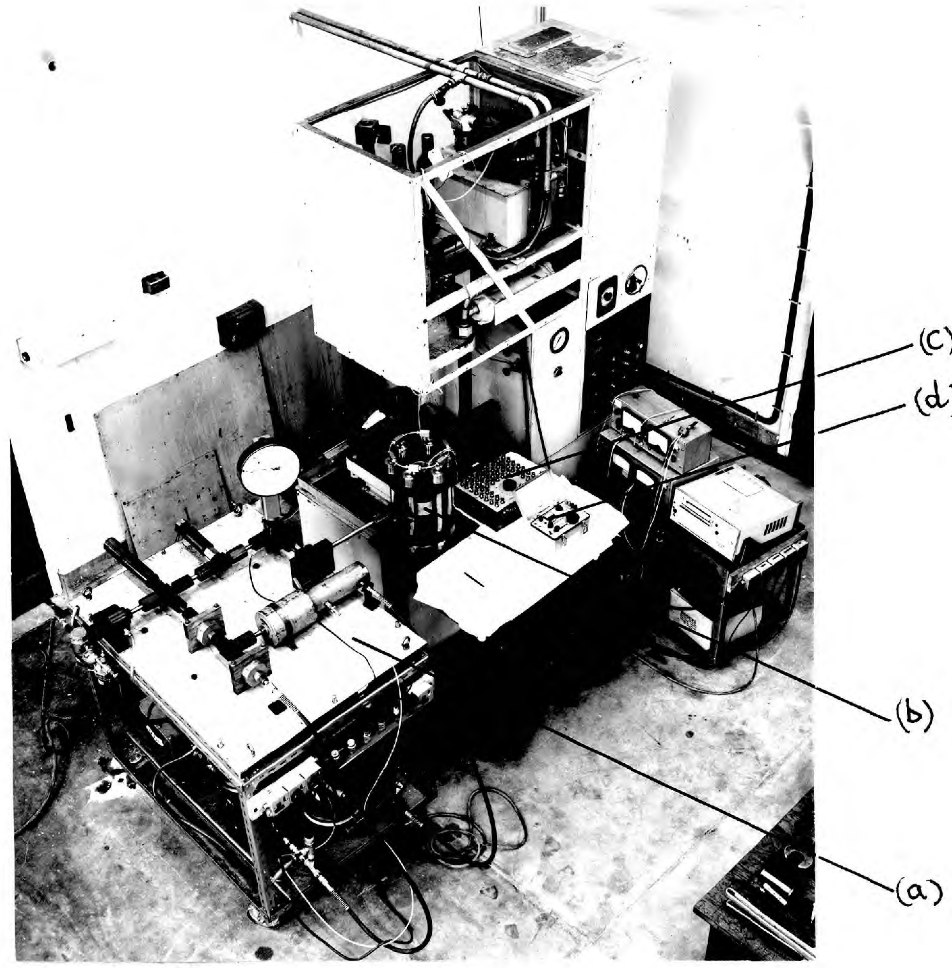

Fig. 9.2. Experimental Arrangement for External Pressurisation Test.

(a) High Pressure Pumping Rig.

(b) Static Support Rig.

(c) Selector Box.

(d) Strain Indicating Bridge.

and when aligned with pairs of guide-lines on the end faces pressed down to fix the gauge in position. The leads were soldered to a terminal strip and connections made to the selector box and bridge unit as before.

The specimen was installed in the static support rig but with modified end closures so that no component entered the bore of the specimen. External pressure was provided in the usual way from the static pumping rig and the phograph Fig. 9.2. shows a general view of the experimental set up. Strain gauge readings were made at increments of pressure up to a maximum of 29.2 tonf/in^2 (451 MN/m^2) and during the reduction of pressure to zero.

9.3. Test Results.

9.3.1. Internally Pressurised Cylinder.

The summarised strain gauge readings are given in Table 9.1. During the elastic portion of the first pressurisation the variation between the circumferential strain readings is within 1.5%. The first two cycles of pressure are plotted on the basis of hoop strain in Fig 9.3., and it can be seen that after the first application of pressure the departure from linear elastic behaviour is quite small. The elastic axial strains are plotted in Fig 9.4. for the first application of pressure and from this graph and Fig 9.3. the elastic constants were calculated and are again given in Table 9.3. The values of the elastic constants are within about 2% of the anticipated values from static tests.

The results of pressure cycling on the measured strains are plotted in Fig 9.5 on the basis of a function ($\epsilon_\theta + \nu \epsilon_z$), which is proportional to the shear strain at the outside of the specimen. This method of plotting is useful when using the Franklin and Morrison (53) method of predicting the pressure-expansion curve. Such a curve predicted from static shear data is shown on the graph for comparison. It can be

TABLE 9.1 (a)

Summarised Strain Gauge Results for Cylinder Subjected to 25.4 Tonf/in^2 (392 MN/m^2) Repeated Internal Pressure

Cycle No	Pressure (Tonf/in^2)	Strain (microstrain) Mean Hoop (ϵ_θ)	Mean Axial (ϵ_z)	$\epsilon_\theta + \nu\epsilon_z$
1	0	0	0	0
	3.57	250	-66	231
	7.87	556	-148	515
	10.1	724	-196	669
	12.4	895	-248	826
	15.6	1125	-307	1039
	17.95	1298	-355	1199
	19.3	1411	-386	1303
	20.4	1512	-400	1400
	21.5	1627	-441	1503
	22.7	1773	-478	1639
	23.8	1928	-513	1784
	25.4	2184	-576	2023
	21.5	1905	-528	1757
	16.5	1522	-418	1405
	12.2	1194	-320	1104
	7.45	835	-214	775
	5.25	662	-163	616
	0	255	-34	245
2	25.4	2224	-577	2062
	0	294	-38	283
3	25.4	2222	-574	2061
	0	308	-41	297

TABLE 9.1 (a) cont'd

Cycle No	Pressure (Tonf/in^2)	Strain (microstrain)		
		Mean Hoop (ϵ_θ)	Mean Axial (ϵ_z)	$\epsilon_\theta + \gamma\epsilon_z$
4	25·4	2232	-575	2071
	0	319	-41	308
5	25·4	2236	-577	2074
	0	326	-43	314
25	0	348	-46	335
575	0	387	-55	372
1,225	0	409	-35	399

TABLE 9.1 (b)

Summarised Strain Gauge Results for Cylinder Subjected to 27.3 Tonf/in^2 (422 MN/m^2) Repeated Internal Pressure

Cycle No.	Pressure (Tonf/in^2)	$\epsilon_\theta + \nu \epsilon_z$ (microstrain)
1	27.3	2288
	0	466
1000	27.3	2590
	0	783
2000	27.3	2649
	0	840
3000	27.3	2685
	0	873
4000	27.3	2712
	0	893

Fig 9.3

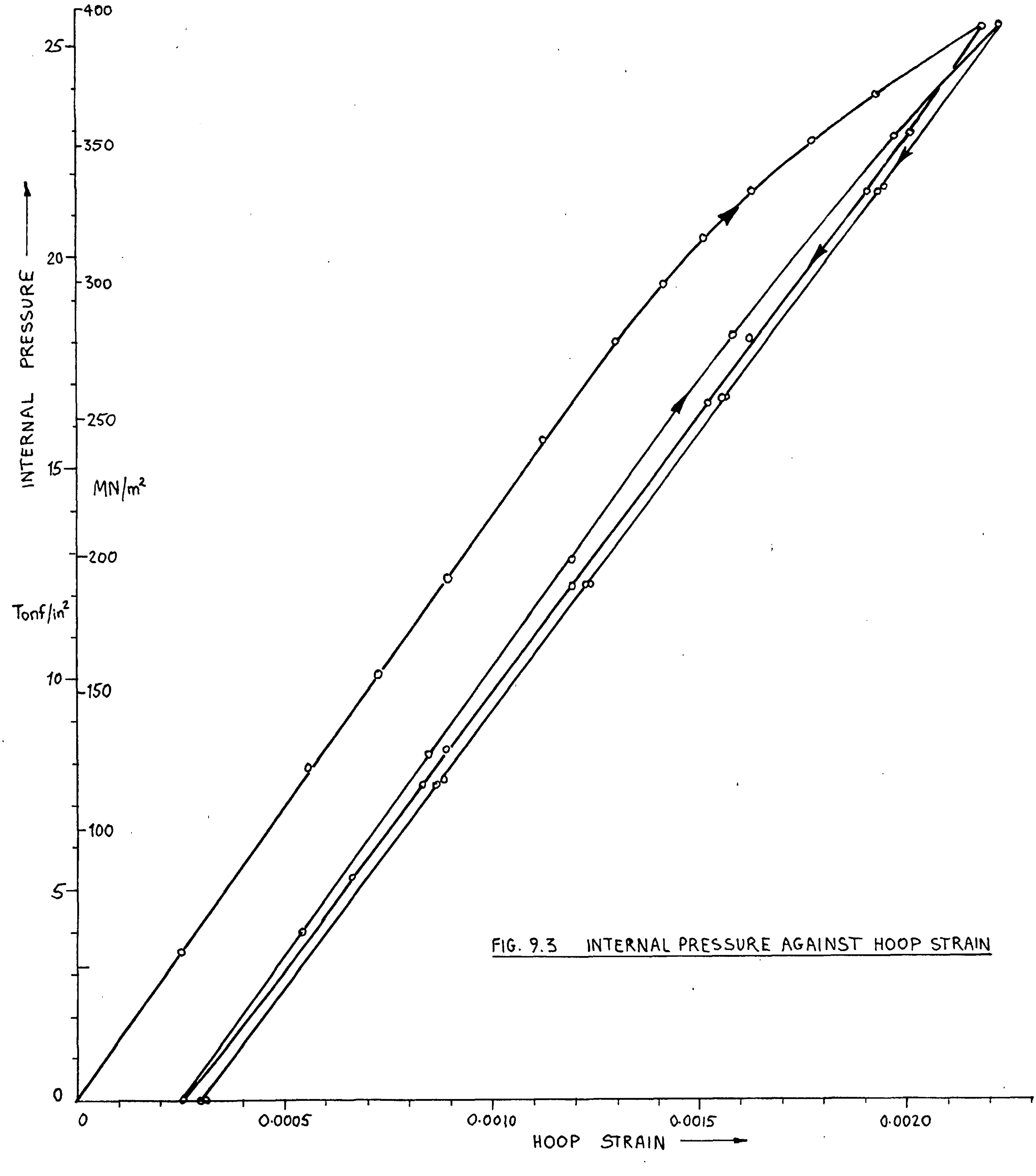

FIG. 9.3 INTERNAL PRESSURE AGAINST HOOP STRAIN

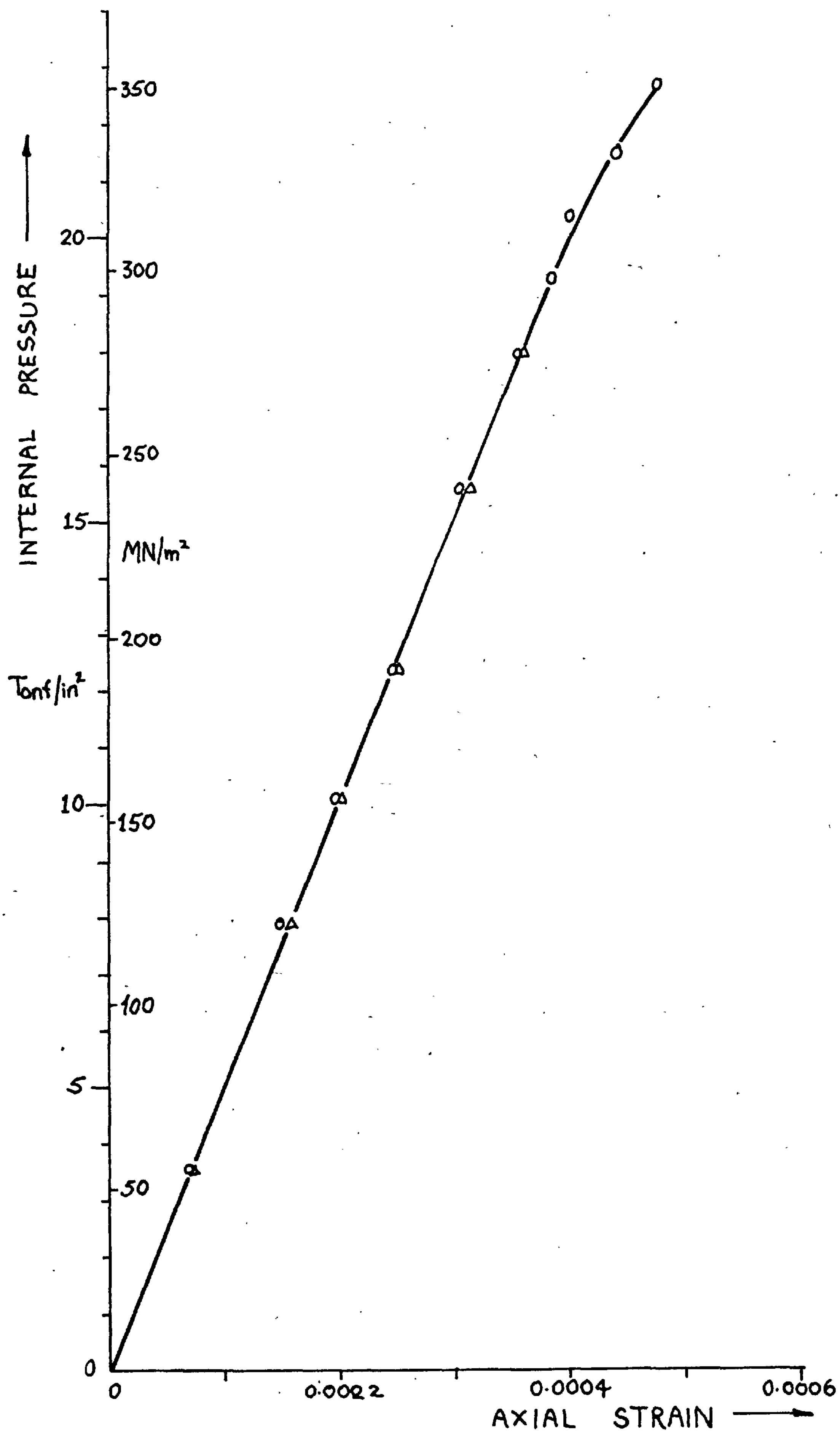

FIG. 9.4 INTERNAL PRESSURE AGAINST AXIAL STRAIN

Fig 9.5

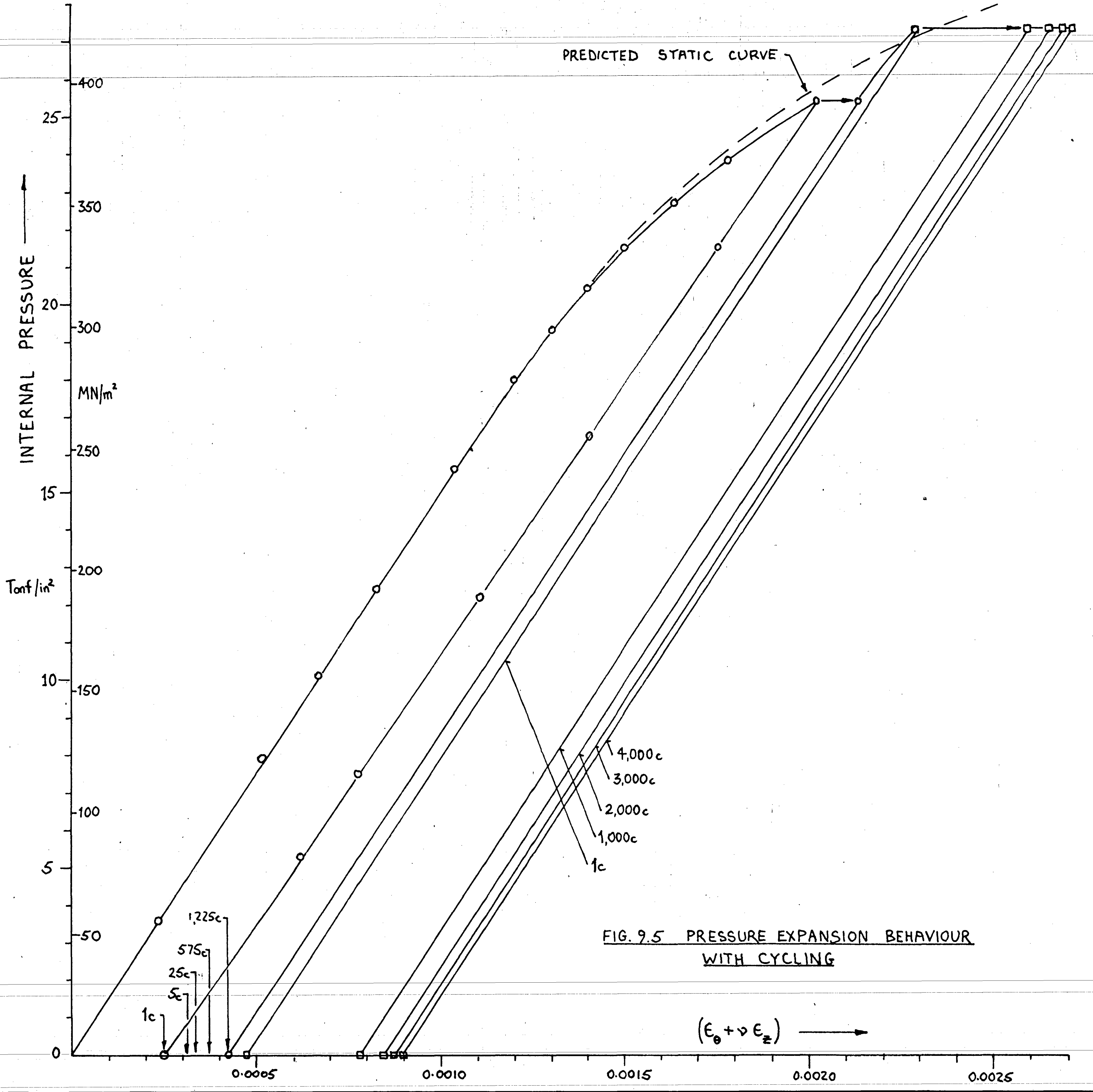

FIG. 9.5 PRESSURE EXPANSION BEHAVIOUR WITH CYCLING

seen from Fig. 9.5. that the effect of pressure cycling is quite marked in the early stages of the test but that as the number of cycles increases less softening takes place. The static yield pressure from Fig. 9.5. is given in Table 9.3. along with the final burst pressure.

9.3.2. Externally Pressurised Cylinder.

The strain gauge readings are given in Table 9.2. and it can be seen that up to yield approximately 18 $Tonf/in^2$ (280 MN/m^2) the variation in either axial or circumferential readings is within 1.5%. The elastic portion of the pressurisation is plotted in Fig. 9.6 for both axial and circumferential strains and from this information the elastic constants given in Table 9.3. were calculated. Beyond yield the agreement between the gauges was very poor as can be seen in Fig 9.7. This may have been due to local non uniform deformation but it is more likely due to poor adhesion and strain gauge performance at very large strains. Post yield strain gauges were not used in this test.

TABLE 9.2

Strain Gauge Results for Externally Pressurised Cylinder

Pressure (Tonf/in^2)	Strain (microstrain)			
	Gauge 1 Hoop	Gauge 2 Hoop	Gauge 3 Axial	Gauge 4 Axial
0	0	0	0	0
8.9	1951	1946	564	557
9.25	2043	2040	590	585
10.5	2295	2290	662	657
13.2	2896	2868	838	829
16.1	3521	3460	1018	1007
17.2	3803	3720	1096	1087
19.5	4429	4288	1263	1241
21.0	4961	4774	1394	1343
23.1	6266	6109	1618	1521
24.8	10988	-	-	-
25.4	11975	11760	3862	3507
26.5	17595	16072	5701	5493
28.5	26055	22300	7830	7040
29.2	32985	26506	8068	6737
21.0	31145	25046	7386	6117
12.5	29037	23450	6756	5533
5.25	26868	21824	6148	4985
0	24827	20296	5568	4467

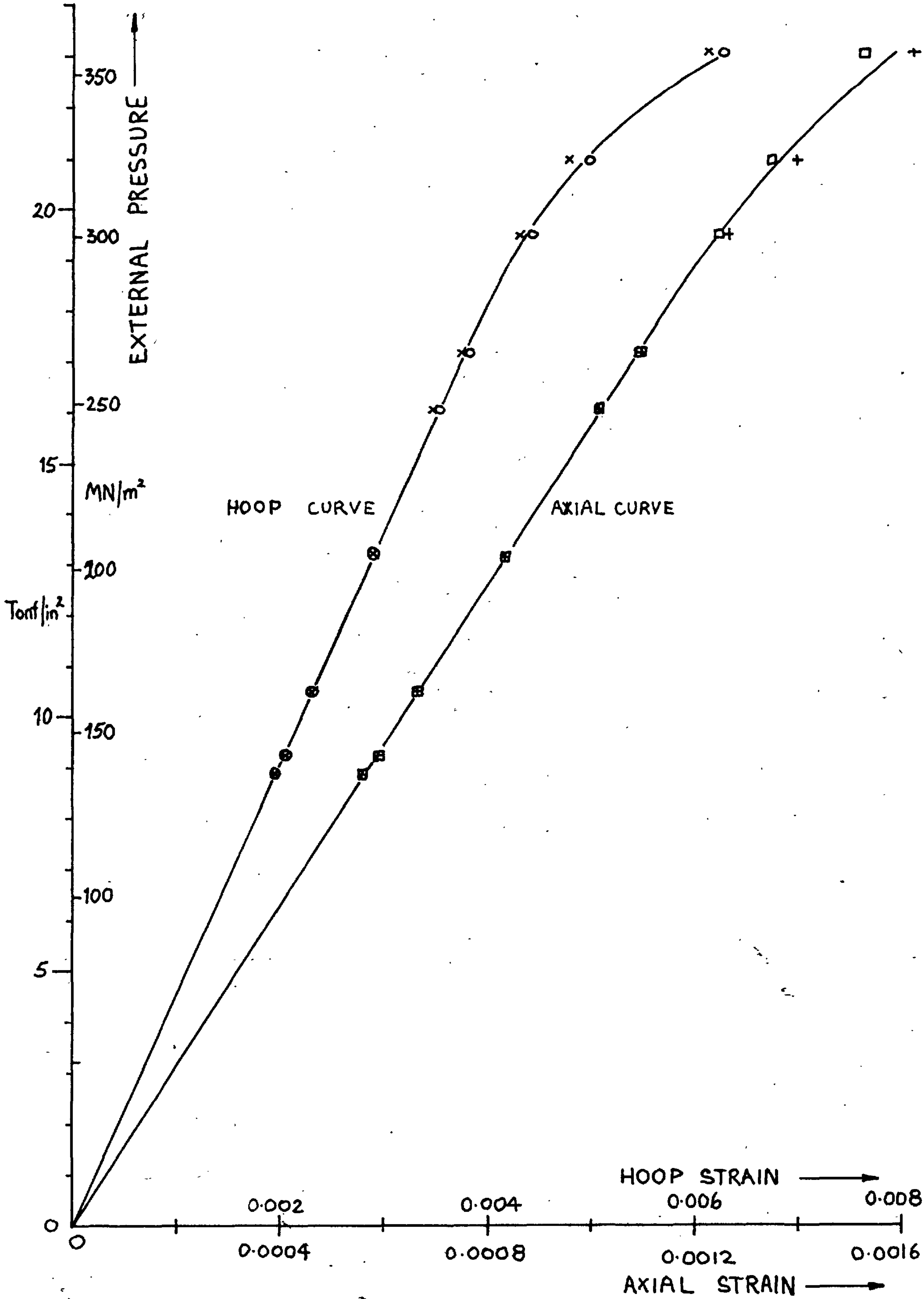

FIG. 9.6 EXTERNAL PRESSURE AGAINST HOOP AND AXIAL STRAIN AT THE BORE

Fig 9.7

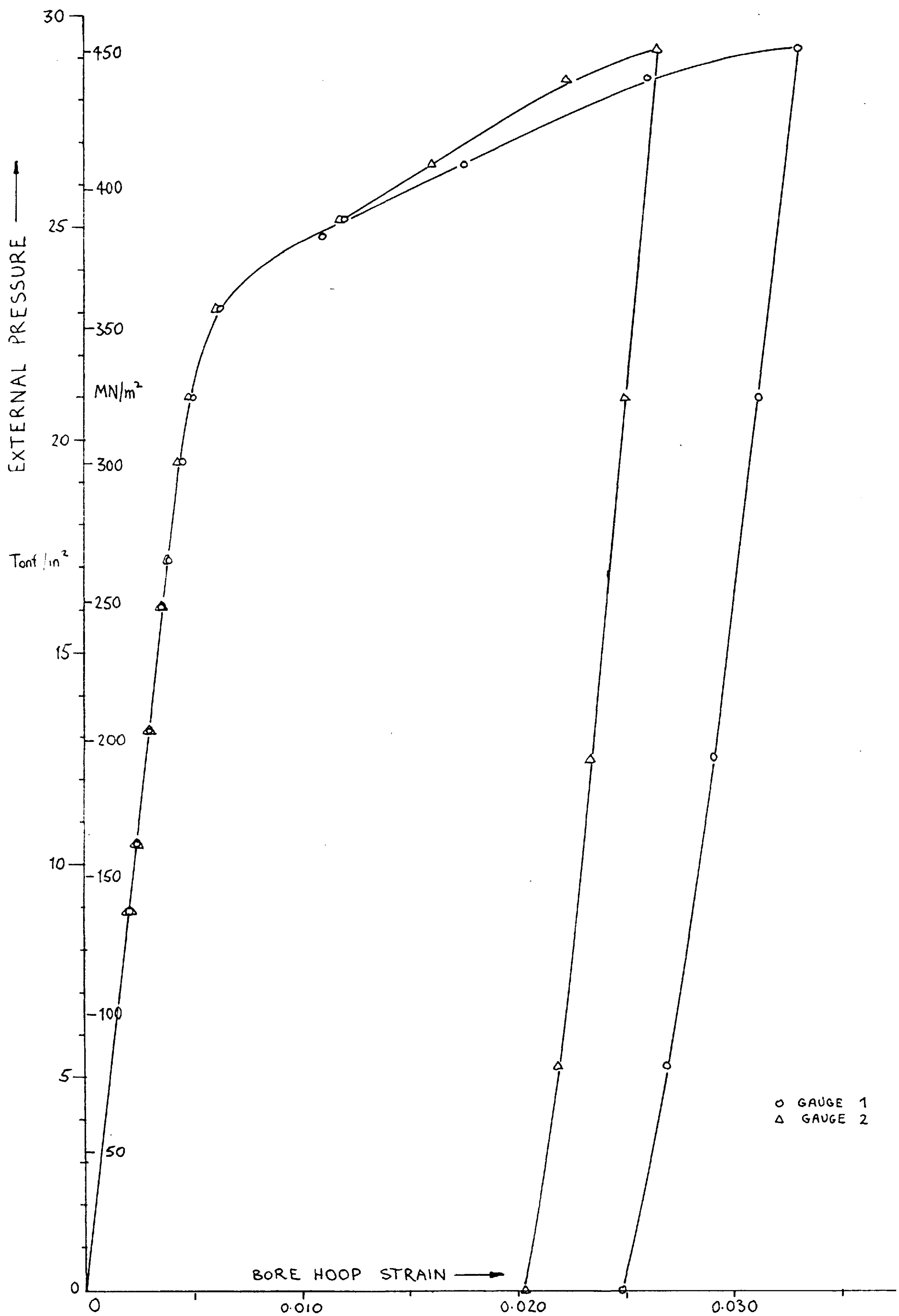

FIG. 9.7 EXTERNAL PRESSURE AGAINST BORE HOOP STRAIN

TABLE 9.3

Summarised Mechanical Properties from Strain Gauge Tests

	Internally Pressurised Cylinder	Externally Pressurised Cylinder
Young's Modulus	13,500 Tonf/in^2	13,500 Tonf/in^2
Poisson's Ratio	0.276	0.288
Yield Pressure	17.8 Tonf/in^2	17.8 Tonf/in^2
Shear Yield Stress	26.4 "	26.4 "
Burst Pressure	35.0 "	

CHAPTER 10.

STRESS AND STRAIN ANALYSIS OF FATIGUE SPECIMENS.

10.1 Introduction.

One of the chief problems in the design of a fatigue specimen is the choice of a shape which will ensure that fatigue failures occur consistently in a region of the specimen where the stress conditions are accurately known. In a cylinder this would hopefully be in a central region where Lamé conditions were known to apply. Although the specimen designs adopted in the present work are broadly similar to proven designs used by Morrison et al (24) and Austin and Crossland (27) the effects of entirely different sealing arrangements, external as well as internal pressurisation and open ended instead of closed ended conditions are unknown. It is particularly at seals where pressure discontinuities give rise to stress discontinuities that the stress conditions could be sufficiently severe to cause failure at Lamé stresses significantly less than the critical values. A detailed examination of elastic conditions is given in the following section, 10.2. For the analysis of fatigue behaviour of thick walled cylinders in the mortal region it is important to know the stress and strain conditions beyond yield. Elastic-plastic analysis is examined in section 10.3 for both static and dynamic pressurisation.

10.2 Elastic Analysis.

10.2.1. Previous Work and Methods of Analysis.

An analysis of the stresses in the necked static support specimen, Fig. 7.3 (a), could be achieved experimentally by strain gauge or photo-elastic methods. The use of strain gauges could prove difficult in the seal region in a fluid pressure environment, and problems would certainly arise if through the wall stresses were needed. Three dimensional photo-elasticity using either the stress-freezing or sandwich technique appears to be a better experimental technique although only very small model pressures would be needed, and under these conditions the viscoelastic behaviour of the rubber seal would not be representative. A theoretical analysis by Kudo and Matsubara (54) revealed that stress discontinuities in cold forging dies are greatly influenced by Poisson's ratio, This would cast doubt on the validity of the stress freezing photoelastic approach in this application. However, the sandwich technique has been successfully employed by El-Behery and Lamble (55) to determine the stress distribution in an extrustion container during extrusion.

A variety of methods are available for theoretical analysis of the discontinuity and steady stresses in a thick walled cylinder subjected to a band of pressure. One of the most exhaustive treatments of the subject is given in the "Thick Walled Cylinder Handbook"(56) where the Fourier integral method is used to calculate the stress discontribution in plain semi-infinite cylinders with internal pressure, internal shear, external shear loading. Similar results are reproduced by Timoshenko and Goodier (57) from the paper by Barton(58). In these analyses the pressure loading is assumed to reduce instantaneously to zero at the end of the pressure band, which probably represents a more severe situation than in practice with a rubber seal and mitre ring. The fact that analysis of semi-infinite cylinders does not take account of end effects in short cylinders is a further unrepresentative feature.

Kudo and Matsubara (54) used the successive over-relaxation method due to Southwell to calculate the stresses induced in a cylindrical die of finite length by a band of uniform internal pressure. The analysis shows that considerable constraint is provided by the pressure-free ends of the die so that hoop stresses less than the corresponding Lamé values are present in the pressurised portion of the die. The maximum constraint is provided when the pressure-free length is greater than 0.5 to 1.0 times the bore in diameter, in the case of a pressurised length equal to the bore diameter. Lamé hoop stresses are only achieved when the pressurised length is greater than three times the bore diameter for the case of a 5.0 K ratio and a pressure free length equal to the bore diameter. Although most of the analysis assumes a rectangular or step pressure distribution an example is given of a trapezoidal or ramp pressure distribution. This has the effect of significantly reducing the amplitude or severity of the stress discontinuities.

Thick shell analysis has been used by Mohaupt et al (59) to investigate stress distributions in a thick-walled vessel subject to equal internal and external pressure. The results of finite element analysis were also presented and provided a useful comparison. Two arrangements were considered, one an open ended cylinder with a ram seal half way down the bore, and the other an open ended cylinder with a rigidly constrained end and pressure over the whole length. The analysis shows that significant tensile stresses are induced in the bore of the cylinder on the ram side of the seal and that the magnitude and distribution of longtitudinal stress is unaffected by the nature of the pressure drop at the seal be it a step function, or ramp function over 0.2 in (5.1 mm). The latter conclusion contradicts the findings of Kudo and Matsubara (54) and seem intuitively unlikely. Furthermore, the finite-elementpredicted longitudinal stress distribution exhibits a sharper stress discontinuity than the thick-shell analysis although the peak values are in agreement. Tensile longitudinal stresses in the bore are also predicted near the end of the constrained cylinder. However, higher tensile stresses can be found in the same region on the outside of the component. It was agreed in the discussion on this paper that the loading case of zero internal pressure with external pressure could give rise to significant discontinuity stresses and should not be ignored.

The numerical method of boundary-point-least-squares (61) was used by Simonen et al (60) to examine discontinuity stresses in a plain cylinder of K = 2. No end effects were considered and a ramp function pressure drop over a length of 0.05 in (1.3 mm) was assumed. Internal and external pressure loadings were applied separately and the conclusion in both cases was that the most severe shear stresses were to be found in the pressurised portion of the cylinder away from the discontinuity.

The examples quoted in the previous paragraphs serve to show the importance of detailed analysis of stress discontinuities at seals in high pressure cylinders. The most significant feature of such discontinuities is the possibility of longitudinal tensile stresses. Both the longitudinal and hoop stress conditions are greatly influenced by factors such as the relative pressurised and unpressurised lengths of the cylinder, the K ratio, and the pressure drop function. A further complication not dealt with in previous analyses is the precaution usually taken with fatigue specimens of necking the cross section in the region of intended failure. It was decided to examine the plain and necked static support specimens, K = 1.75, for both internal and external pressure loadings. The finite element method seemed the best choice for analysis, and a programme was already available (62) for axi-symmetric solids of revolution.

<u>10.2.2 The Finite Element Method.</u>

The finite element method of stress analysis is to-day the major computer orientated stress analysis technique, and is rapidly gaining acceptance as an alternative to the traditional experimental techniques. The whole subject is treated at length by Zienkiewicz (63). The method involves the division of a structure or continuum into a number of small (finite) elements, commonly triangular in cross-section, interconnected at their corners. These connecting points are known as nodes, and external loading is applied to the body via the nodal points. In the case of plane stress or plain strain the elements are effectively triangular laminae, and in the axi-symmetric case are rings of triangular cross section. The first step in the analysis is to determine the stiffness matrix for each element, that is a matrix expressing the nodal forces corresponding to unit nodal displacements. The element stiffness matrix is built up using the equilibrium conditions, the stress strain relationship, and displacement conditions which ensure compatibility between adjacent elements. The stiffness of the whole structure is then obtained by summing, the effects of each nodal point of all the adjacent elements. Using the overall stiffness matrix the equations relating nodal forces and displacements for the whole structure can be defined and solved using the Gauss-Seidal iteration procedure. Element strains and stresses can then be evaluated from the calculated nodal point displacements. It is not particularly convenient to have <u>element</u> stresses, that is stresses acting at the centroid of each element, as boundary stresses are usually of greatest interest for analysis. Element stresses must therefore be used either in numerical averaging techniques or in graphical extrapolation to predict nodal point stresses at boundaries.

10.2.3. Finite Element Analysis of Test Specimens.

Two specimen geometries were analysed using an Imperial College (Mechanincal Engineering Department) axi-symmetric finite element programme on the College IBM 7094 computer. The programme has the facility for elastic-plastic analysis although only elastic analysis was performed. The necked and plain versions of the static support specimen were selected for analysis although the information gained about stress discontinuities at seals and the specimen length required to develop Lamé stress conditions would read across to other similar geometries such as the dynamic support specimen.

The finite element mesh was made as fine as possible within the limitations of the programme and the available computer core store.

The mesh was defined uniformly along the length of the specimen. This was considered preferable to the alternative of a coarser mesh away from stress concentrations and a finer mesh around the stress concentrations themselves, as the stress gradients are too severe in a thick-walled cylinder even in Lamé stress regions for a true representation of the total stiffness of the cylinder by a coarse mesh. The configuration used in the analysis is shown in Fig. 10.1 and it will be noticed that the mesh coarsens radially outwards from the bore. The radial heights of the elements were calculated to give the same hoop stress gradient radially across each element. The pitch of the elements axially is 0.1 in (2.54 mm). Because of geometrical symmetry about the centre sections of both the necked and plain specimens, it is sufficient to consider only half the total length of each specimen, as shown in Fig. 10.1 which is an illustration of the final version of the input data as drawn by the Calcomp plotter.

Two loading conditions were analysed for each specimen geometry. The first condition was unit internal pressure applied uniformly to a fixed length of the bore, and then a linear decrease to zero over one element length, that is 0.1 in (2.54 mm). The second condition was unit external pressure again decreasing linearly to zero over one element. The positions of these ramp function pressure drops correspond closely to the extreme positions of the mitre rings in the static support rig. The internal and external mitre rings wre 1/16 in and 3/64 in (1.2.mm) long respectively. Both upper and lower external seals were $\frac{3}{8}$ in diameter. The ram seal was 9/32 in (7.1 mm) long and the lower internal seal was 1/16 in (1.6 mm) diameter. Thus the assumption made in the finite element analysis loading was that the pressure drop occurred mainly in the mitre ring, and that the seals themselves transmitted pressure hydrostatically for a good proportion of their length. This assumption seems reasonable, although there is no direct evidence to support it. The loading conditions are shown diagramatically in Fig. 10.1.

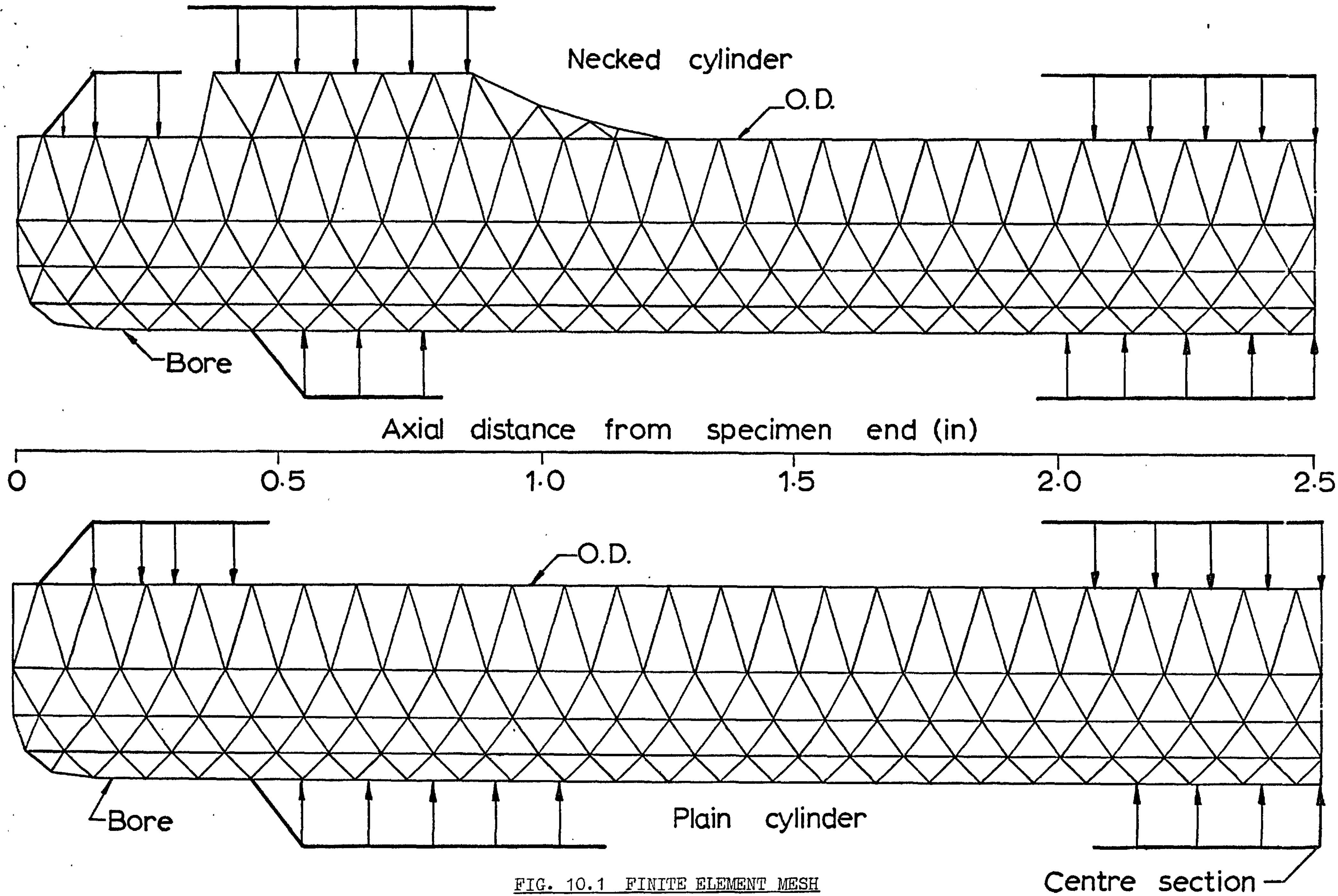

FIG. 10.1 FINITE ELEMENT MESH

The input of pressure loading to the finite element program involved the calculation of equivalent nodal point loads by the virtual displacement method. This method equates the work done by the applied pressure in deflecting the boundary by a certain amount, to the work done by an equivalent node load to give the same deflection. ~~The equivalent node load expressions derived for the analysis are given in Appendix~~ . The only specified boundary conditions were for the nodes at the very centre section of the specimens. As the specimens were cut in two for the analysis it was necessary to fix the z displacement of these central nodes.

10.2.4. Results of Analyses.

The results of finite element analysis on both the plain and necked static support specimen for internal and external pressure are summarised in Figs. 10.2 to 10.7. The vertical axes indicate stresses in any unit per unit pressure, if both stress and pressure are expressed in the same unit. Or, in other words, the stresses are given as a multiple of the pressure loading. The plots were obtained by first plotting the element stresses for elements closest to the inside and outside surfaces, which gave the general trend of the distributions. Boundary stress conditions were then evaluated by taking radial cross-plots at appropriate intervals and extrapolating to the boundaries. The somewhat laborious procedure is achieved numerically in more sophisticated finite element programmes. Nevertheless the cross-plots provide a useful check both on the accuracy of the finite element results, and on the degree of guesswork involved in extrapolation. Fig 10.2 shows a few hoop stress cross-plots for the plain cylinder with internal pressure. It can be seen that in the central region of the specimen the element stresses lie very close to the true Lamé stress distribution. In the seal region, however, the radial distributions are changing rapidly particularly near the bore. Extrapolation is more doubtful in this region and if greater

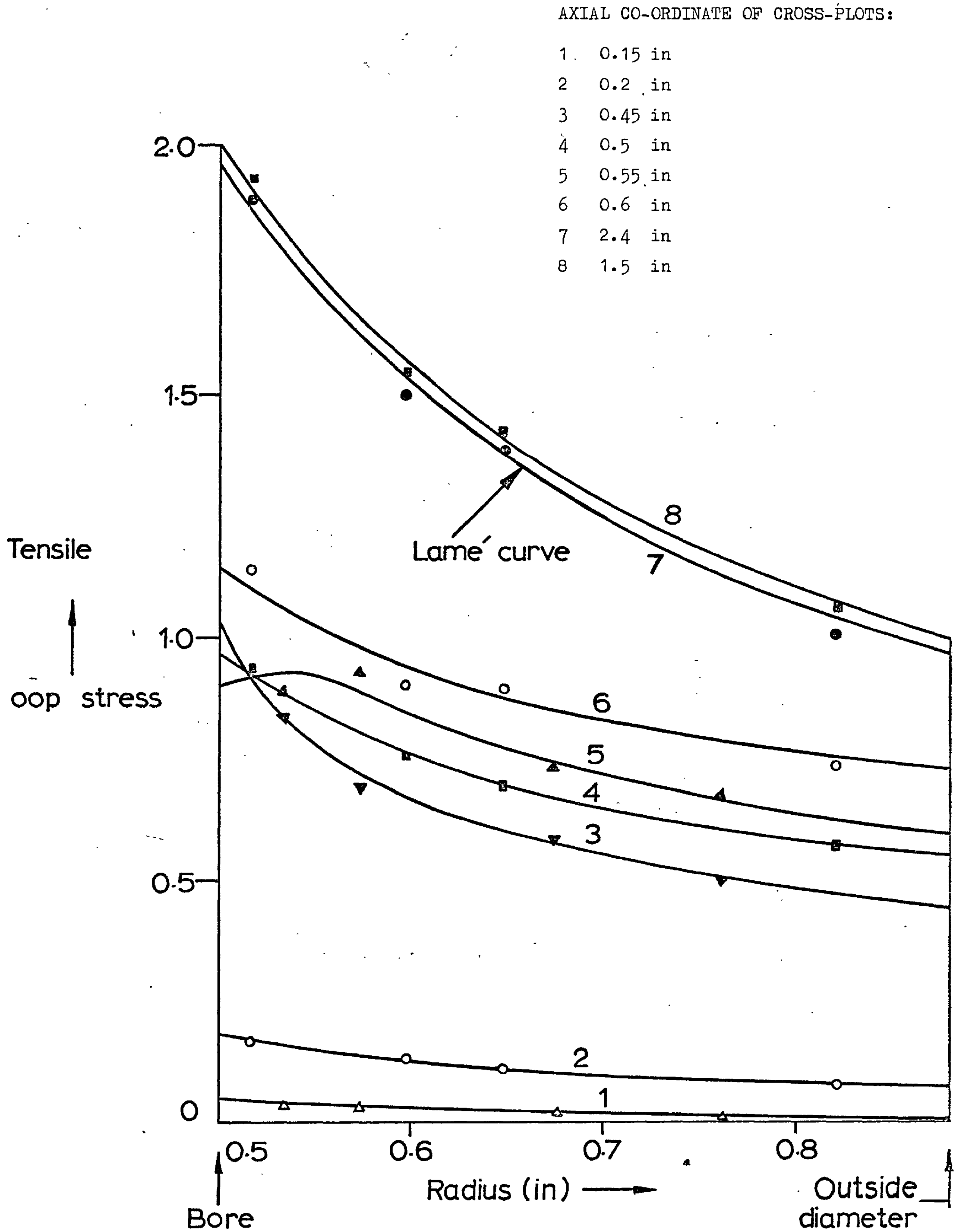

FIG. 10.2 RADIAL CROSS-PLOTS OF ELEMENT HOOP STRESSES

accuracy were required a much finer finite element mesh would be essential. The hoop stress cross-plots for the necked specimen with internal pressure, and the external pressure cases exhibited similar characteristics to Fig. 10.2. The axial stress cross-plots were also clearly defined except in the region very near to the seal where extrapolation was more doubtful. These local inaccuracies however are of only minor importance in the overall longitudinal stress distribution plots presented in Figs. 10.3 to 10.7.

10.2.4.1. Internal Pressure Loading.

Figures 10.3 and 10.4 deal respectively with the plain and necked specimens under unit bore pressure. The concept of the necked design is of course to minimise any undesirable stress conditions in the seal region and thereby ensure fatigue failures within the necked region only. The hoop stress distributions do show that the reduction of stress takes place more gradually over a longer distance in the necked specimen, but that this also has the effect of reducing the specimen length over which Lamé conditions apply. In the plain specimen the hoop stress distribution is within $1\frac{1}{2}$% of the Lamé values for a total length of 2 x $1\frac{1}{4}$ in = $2\frac{1}{2}$ in (63.5 mm) out of the 4 in (102 mm) length subjected to fluid pressure. The corresponding length for the necked specimen is about 2 in (51 mm). The magnitude of the bore hoop stress (σ_θ) discontinuity is 0.15 stress units per unit pressure, i.e. 15% of the bore pressure in both cases, although the discontinuity takes place at a slightly higher stress level in the plain cylinder. For pressure p and Poisson's ratio ν the discontinuity range for a step function pressure drop is $2\nu p$ (54), say 0.56 units in the case if p = 1. The ramp function pressure drop over 0.1 in (2.54 mm) applied in the finite element analysis is the reason for this difference. It has been shown (54) that a ramp function over 0.031 in (0.79 mm) causes

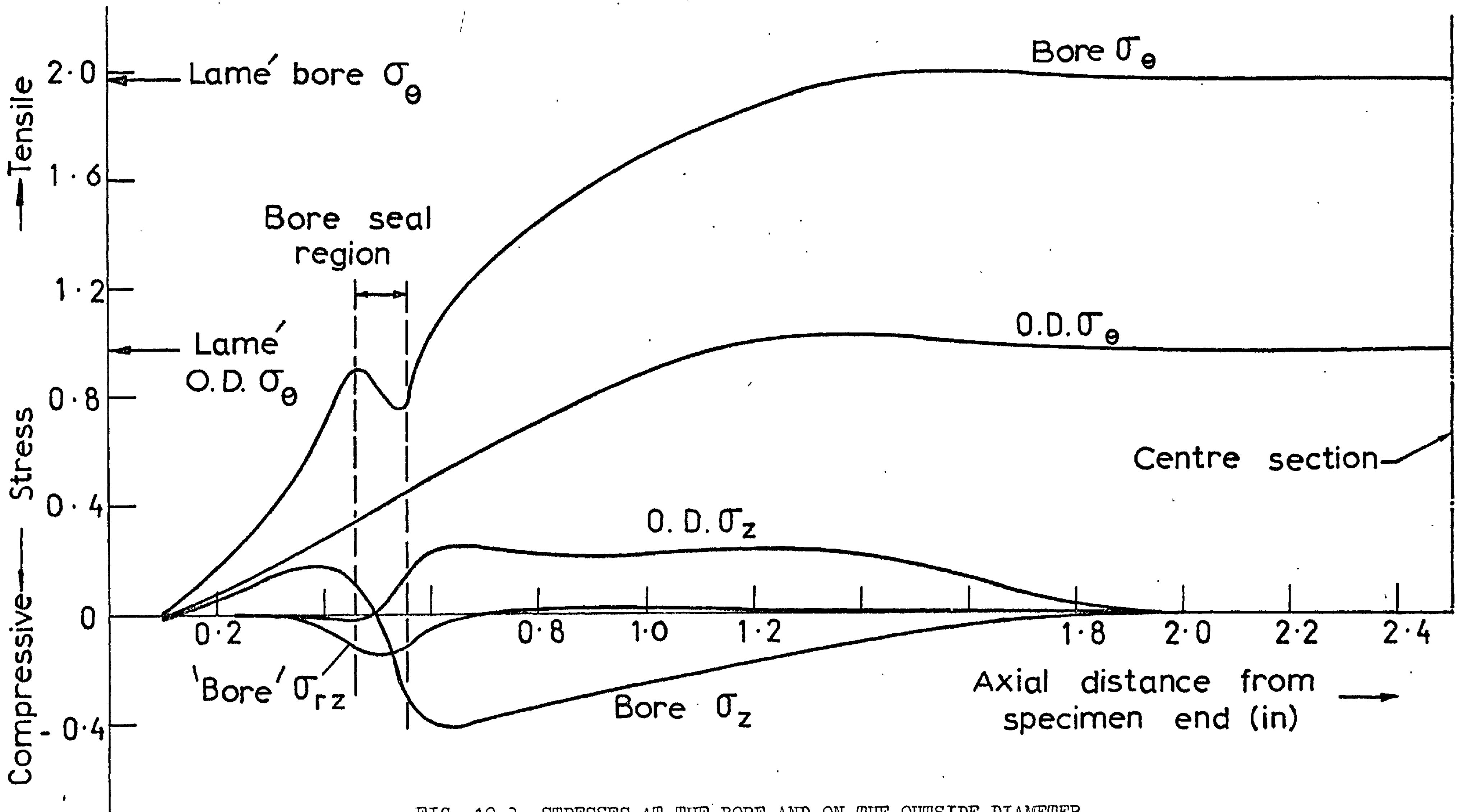

FIG. 10.3 STRESSES AT THE BORE AND ON THE OUTSIDE DIAMETER OF A PLAIN CYLINDER WITH UNIT BORE PRESSURE

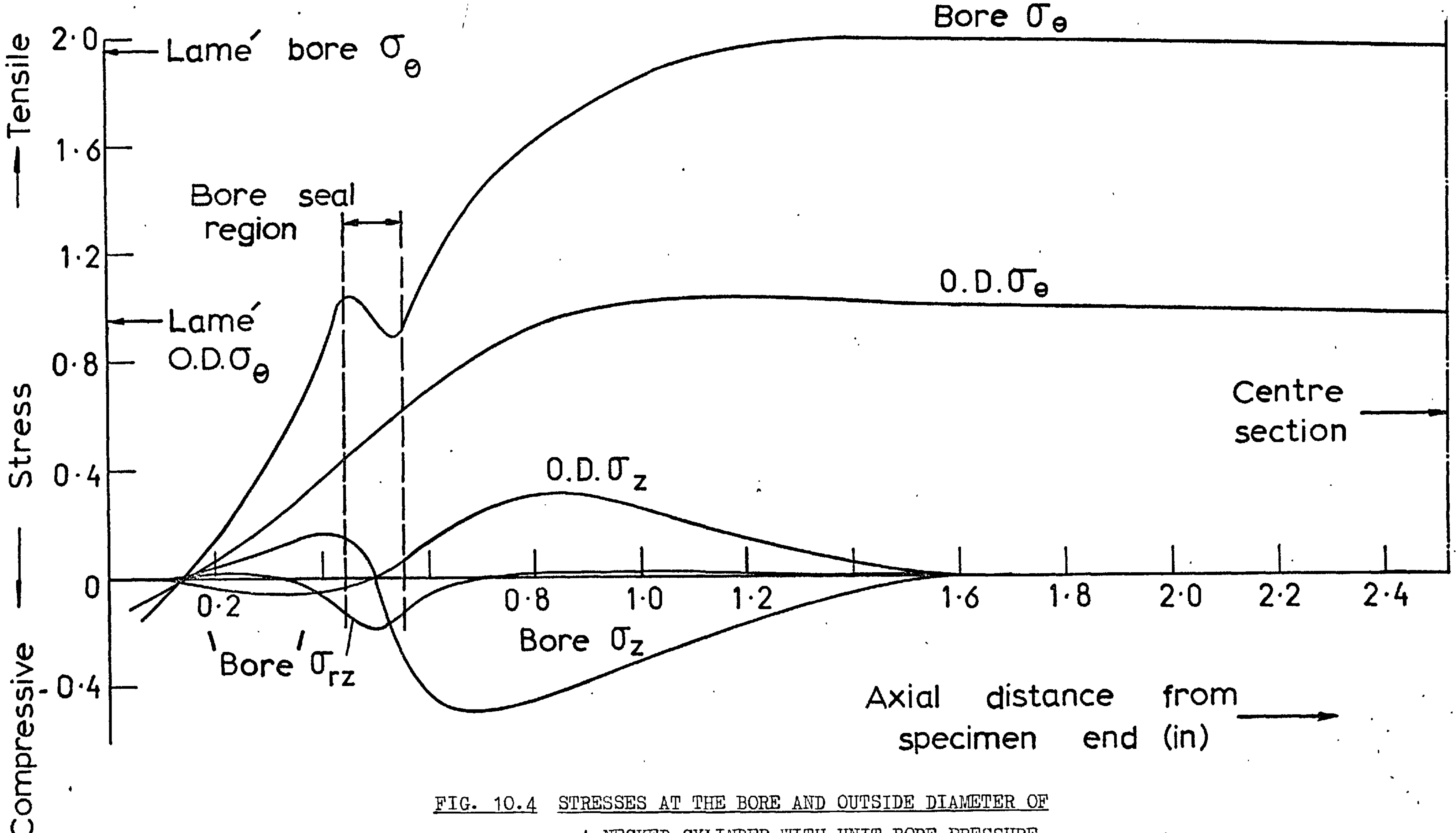

FIG. 10.4 STRESSES AT THE BORE AND OUTSIDE DIAMETER OF A NECKED CYLINDER WITH UNIT BORE PRESSURE

the discontinuity range to fall to about 0.42 units. If in the same way the step function discontinuity curve were terminated at points corresponding to a ramp function over 0.1 in (2.54 mm) the discontinuity range would fall to about 0.2 units per unit pressure.

The axial stress (σ_z) distributions at the bores of both plain and necked cylinders are very similar, slightly lower peak stresses occurring in the necked cylinder. At the pressure free ends of the cylinders tensile axial stresses are predicted, but only of about 0.18 units magnitude. On the other hand the peak compressive axial stress in the pressurised region is about 0.5 units giving a total discontinuity range of 0.68 units per unit pressure. The corresponding range for a step function pressure drop would be 1.0 unit, although this time the difference is not so directly related to the pressure drop function. It is more likely that the proximity of the seal to the end of the cylinder has reduced the magnitude of the tensile axial stress. Larger tensile axial stresses are in fact predicted on the outside diameter of the specimen although these would not normally be significant.

The shear stress (σ_{rz}) vanishes over the bore surface and thus the so called 'Bore' stress distribution refers to material just below the bore surface.

10.2.4.2. External Pressure Loading.

The stress distributions due to unit external pressure are shown in Figs. 10.5 and 10.6. The necked cylinder again exhibits a more gradual decay of bore and outside diameter hoop stress (σ_θ) than the plain cylinder but, as before, this is associated with a smaller length of the cylinder for which Lamé conditions apply. The plain cylinder hoop stress values, however, are within ~~with~~ 1% of the Lamé values for some 2 x 1½ = 3 in (76 mm) of the total 5 in (127 mm) length

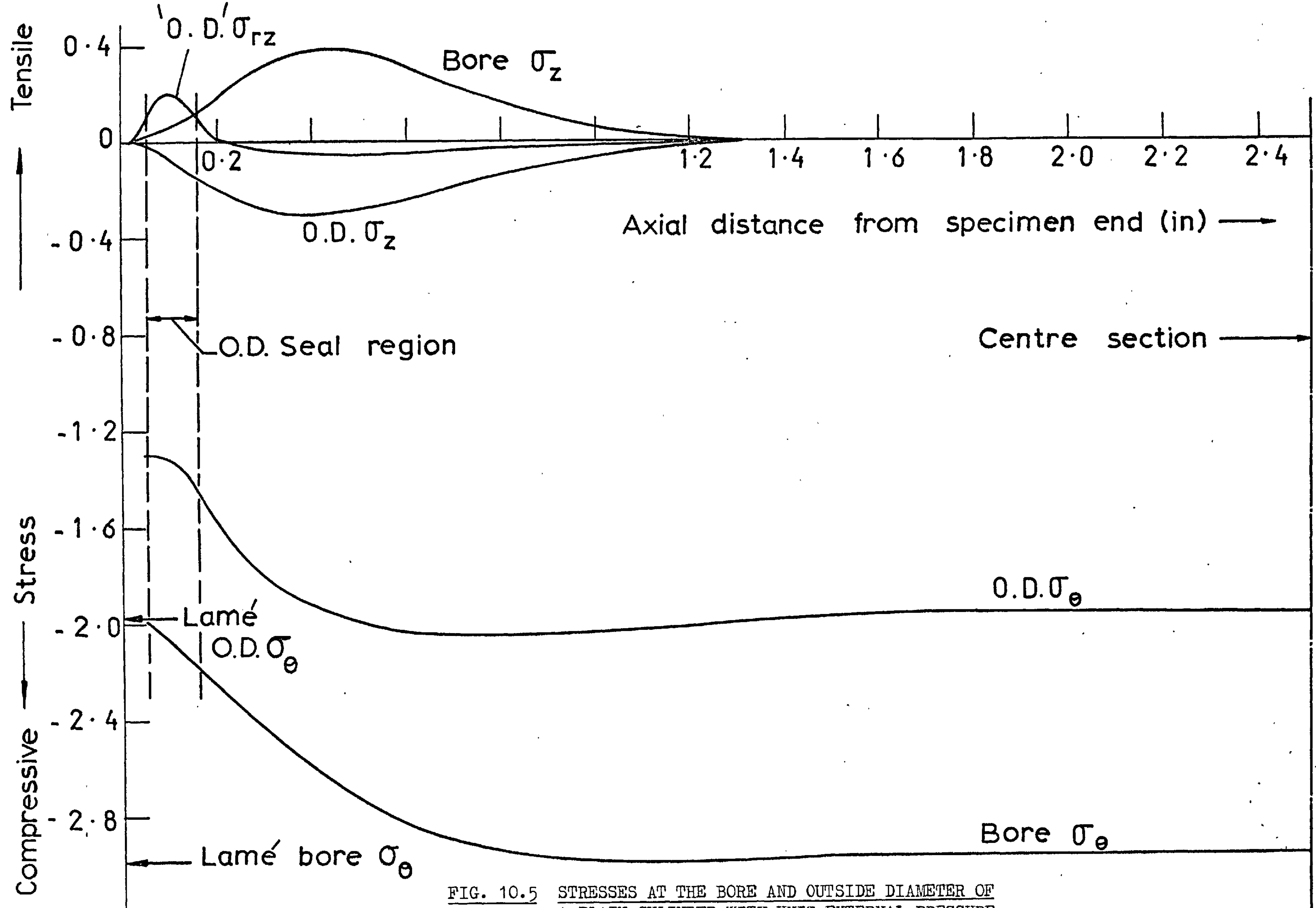

FIG. 10.5 STRESSES AT THE BORE AND OUTSIDE DIAMETER OF A PLAIN CYLINDER WITH UNIT EXTERNAL PRESSURE

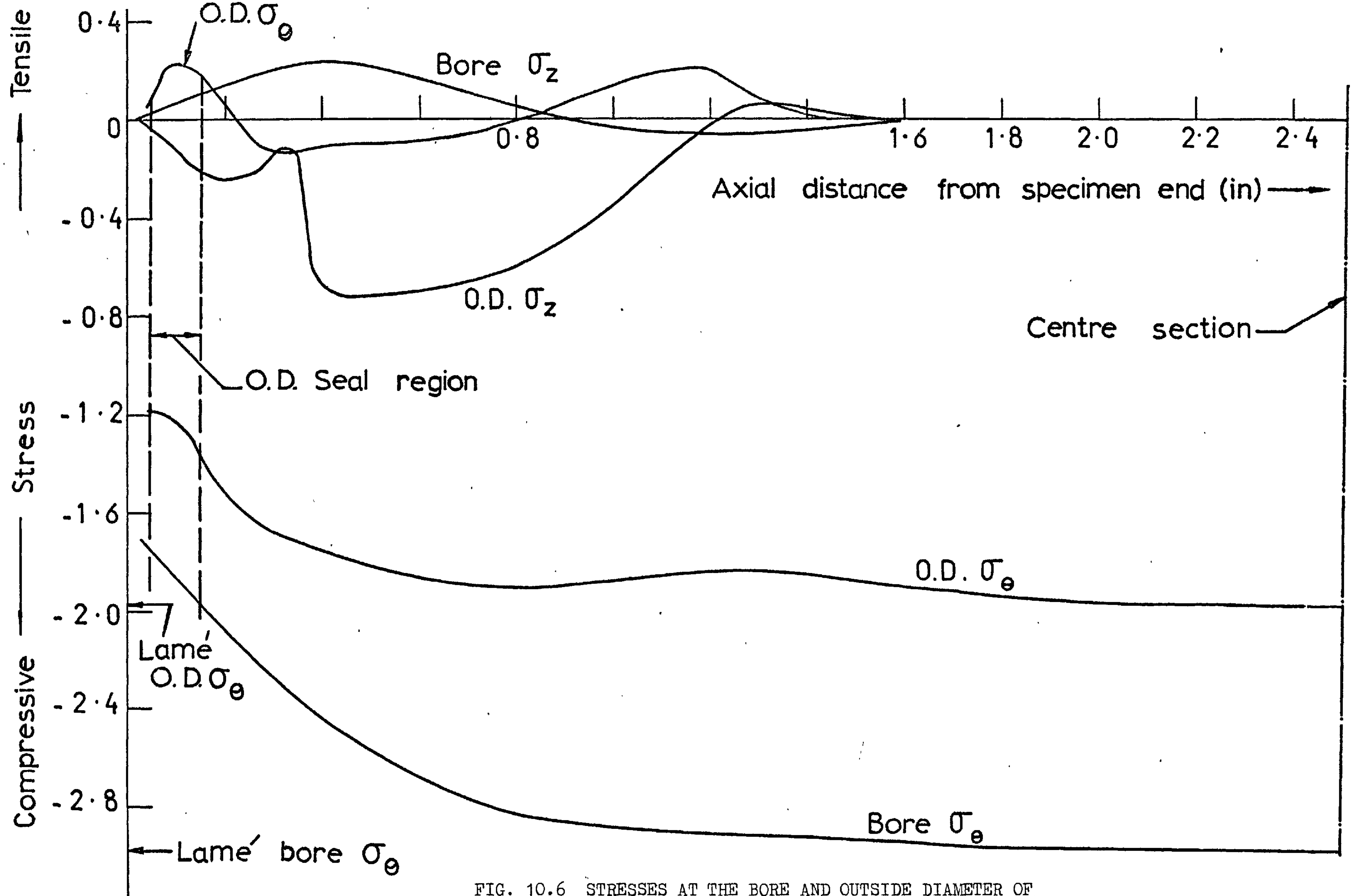

FIG. 10.6 STRESSES AT THE BORE AND OUTSIDE DIAMETER OF A NECKED CYLINDER WITH UNIT EXTERNAL PRESSURE

of the cylinder. As the external seal is very near to the end of the cylinder the hoop stress discontinuity which would be expected on the outside diameter has no oppotunity to develop.

Tensile axial stresses (σ_z) are generated at the bore in the pressurised region of peak magnitude 0.38 units per unit pressure in the plain cylinder, and 0.24 units in the necked cylinder. Corresponding compressive axial stresses can be observed on the outside diameter although the stresses inthe necked cylinder are increased considerably in the large diameter region because of the additional axial fluid pressure loading.

The shear stress just below the outside surface, and referred to as 'O.D.' σ_{rz} exhibits the characteristic peak in the region of the seal, and in the necked cylinder a second peak can be observed in the transition region between the radiused and parallel portions of the specimen.

10.2.5. Conclusions from Elastic Finite Element Analysis.

a. The difference between the stress distributions in necked and plain cylinders is so small that there is little advantage in using a necked specimen design. In fact, apart from manufacturing simplicity, the plain cylinder is more attractive because of the greater uniformity of stress conditions in the central region of the specimen.

b. The tensile axial stresses at the pressure free end of the bore of a cylinder with internal pressure are considerably less than the tensile hoop stresses in the same area, therefore, their effect is probably negligible in fatigue. The same argument applies to the tensile axial stresses predicted on the outside diameter in the pressurised region of the specimen. As the nominal bore hoop stress at the seal is about half of the Lamé value, fatigue failures due to repeated pressure should

should not occur at the seal unless fretting damage at the mitre ring becomes significant.

c. The case of external pressure loading is applicable to the situation in a static support fatigue test when the internal pressure is reduced to zero. In this case the axial tensile stress at the bore could be important particularly in a brittle material with low tensile strength. However, in a material such as EN25 the very large compressive hoop stresses would considerably retard if not prevent the development of a fatigue crack.

d. A most important condition is when both internal and external pressure loadings are present, such as in a static support or dynamic support fatigue test. In Fig. 10.7 the stress distributions have been plotted from Figs 10.3 and 10.5 for the case of a plain cylinder, when the external pressure is half the internal pressure and the latter has the value of unity. It can be seen that although a tensile Lamé hoop stress of 0.48 units is present at the bore in the central region of the specimen, in the seal and pressure-free regions the bore hoop stress is entirely compressive. However, the tensile axial stress at the bore in the seal region is augmented by the external pressure loading, achieving a peak of almost 0.4 units. This would not normally be serious in fatigue for a ductile material such as EN25, owing to the small range of the axial stress and the presence of local compressive hoop stresses. If the internal and external seals were opposite one another, rather than displaced as in the present case, then the axial stresses due to internal and external pressure loading would tend to cancel out and this would help to minimise tensile axial stresses. However, the displacement of the seals is an essential design feature of the necked specimen, and it was a matter of convenience to use the same arrangement for the plain specimen. An additional axial compressive stress would need to be provided even with opposite seals, if it were important to eliminate tensile stresses altogether.

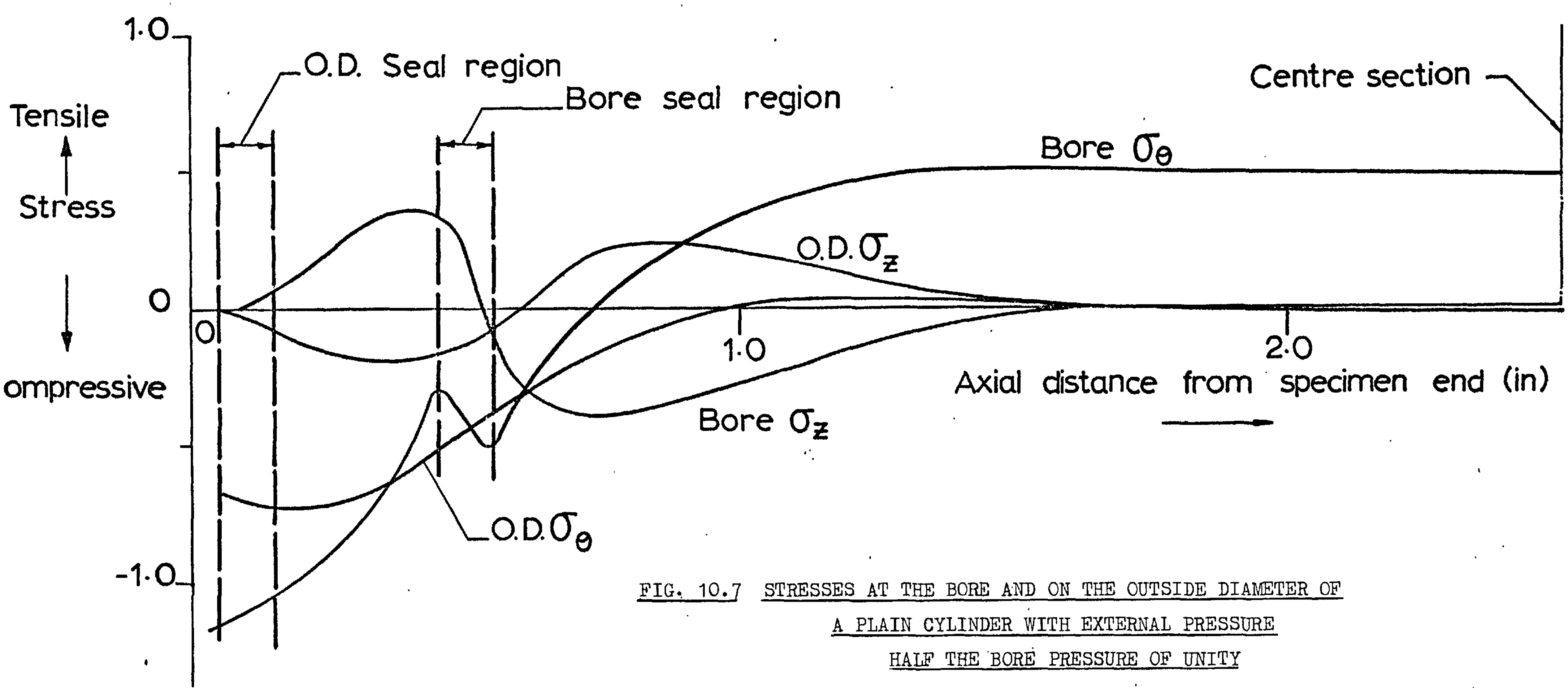

FIG. 10.7 STRESSES AT THE BORE AND ON THE OUTSIDE DIAMETER OF A PLAIN CYLINDER WITH EXTERNAL PRESSURE HALF THE BORE PRESSURE OF UNITY

e. The accuracy of the analysis of stress discontinuities at the seal is dependent not only on the fineness of the finite element mesh but also on the gross assumptions made about the normal and shear loadings at the seal. Knowledge of these loading conditions is needed if the design and positioning of high pressure seals is to be optimised.

10.3. Elastic - Plastic Analysis.

10.3.1 Methods of Analysis.

The analysis of the specimens could be carried out most exactly perhaps by application of elastic-plastic finite element analysis on the particular specimen geometries. However having established from elastic finite element analysis the fact that Lamé conditions held good over a large proportion of the specimen length, and that the stress conditions at the seal were less severe than elsewhere then the elastic-plastic analysis could be made general rather than specific to a particular specimen geometry. Elastic-plastic finite element analysis has the disadvantage of requiring large scale computing facilities and computing times an order of magnitude greater than the elastic case, and thus cannot be regarded as an economic design procedure if simpler alternatives exist. Fully plastic analysis of cylinders is not of interest in the present work because in fatigue fully plastic behaviour implies an unstable situation giving rise to ratcheting failures, which could not be regarded as a satisfactory design concept.

Theoretical analysies of the expansion of thick-walled cylinders under internal pressure are numerous. The various solutions differ in their basic assumptions with respect to plastic and elastic stress-strain relations, yield criterion, and axial end conditions. Useful summaries of previous work are given by Allen and Sopwith (64), Steele (65) and Crossland and Bones (66). The most rigorous solutions from a theoretical point of view are those which use both the Von Mises yield ~~interior~~ criterion and the Prandtl Reuss stress-strain relations, but the approach involves the numerical solution of a system of non-linear partial differential equations. A numerical solution is also required if the Prandtl Reuss relations are used in conjunction with the Tresca yield criterion. Simplification is achieved when the Prandtl Reuss relations are replaced by Hencky total deformation relations, and although this approach is not as rigorous it appears that the results are not seriously in error. Closed form solutions are possible but are again somewhat complex. A solution which has the virtues of both simplicity and rigour is that of Koiter (67), who obtained closed form solutions for all the important axial end conditions. The method involves the use of the Tresca yield criterion and the associated incremental stress-strain relations. It is assumed that the axial stress (σ_z) is the intermediate principal stress and then using the associated relations it follows that the plastic axial strain in zero. The total axial strain is therefore equal to the elastic axial strain, and by applying the particular end conditions the axial strain can be calculated. One of the points in Koiter's analysis is an examination of the validity of the assumption that the axial stress is always the intermediate stress for conditions of plane strain, open and closed ends. He concluded that for open ended cylinders with internal pressure the axial stress is intermediate for K ratios $\leqslant 6.19$. Koiters solution like many of the theoretical solutions assumes no work hardening of the cylinder material. However an analysis by Bland (68) which also uses the Tresca yield criterion with its associated flow rule does introduce work hardening and also includes the effect of external pressure.

An alternative approach advocated by authors such as Manning (69) Franklin and Morrison (53), and Crossland (70) involves the use of practical stress/strain data rather than mathematical models of the stress/strain curve. Franklin and Morrison in particular have carried out careful experimental work amply confirming the method, and it was decided to employ this approach initially to the present work.

10.3.2. Prediction of Pressure Expansion Curve.

The form of material data recommended by Franklin and Morrison is shear stress/shear strain from torsion tests. The reason being that the stress system in a closed ended cylinder at yield may be reduced to a uniform volumetric tensile stress plus a simple shear stress. By assuming that volumetric tension has the same insignificant effect as volumetric compression on the yield behaviour of a ductile material then it can be concluded that yield in a thick-walled cylinder is solely a function of the shear stress. If the shear yield stress is derived from torsion data then a criterion of yield does not enter the analysis. The analogy with a torsion test is continued in the elastic-plastic expansion of a cylinder by assuming that the behaviour of the cylinder material is exactly described by the shear stress-strain properties of the material in pure torsion. In addition it is assumed that the shear strain distribution across the wall of the cylinder is inversely proportional to the square of the cylinder radius. By employing these two basic assumptions Franklin and Morrison were able to make extremely accurate predictions of the pressure expansion curves under both increasing pressure, and pressure release conditions. An outline of the theoretical basis to Franklin and Morrison method is given in Appendix 1.3.2.

The Franklin and Morrison method was used in conjunction with the experimental results from torsion tests reported in Section 8.3 to predict the pressure expansion curve drawn in Fig. 9.5 for comparison with experimental results. It was found that over the range of strains corresponding to expansion of the 1.75 K ratio cylinder to just short of collapse the shear yield stress of En.25 was virtually constant. As may be seen from the tests on small torsion specimens in Fig 8.4 the shear yield stress varies from an initial value of 26.4 Tonf/in^2 (408 MN/m^2) to a value of 26.8 Tonf/in^2 (414 MN/m^2) at a shear strain of 0.017 which is the bore strain just short of collapse. This means that very little difference can be detected in the pressure expansion curve whether real shear stress values corresponding to particular strains are used in the evaluation of $\int \frac{\tau_y}{r}$ by a numerical method, or alternatively if the definite integral $\tau_y \int \frac{1}{r} dr = \tau_y \ln r$ is used with an initial or average value of τ_y. The former approach is of course essential if accurate residual stress conditions are required with due allowance for the Bauschinger effect, but the strain gauge tests reported in Chapter 9 established that after a few cycles the cyclic behaviour is purely elastic.

It is apparent from Fig 9.5 that although the static pressure expansion curve can be predicted accurately it is necessary in addition to investigate the steady state cyclic pressure expansion curve. For a particular repeated pressure the cylinder strains will increase and eventually settle down to an identical pattern every cycle. It is these steady state strain conditions which need to be known in order to define the mean strain for fatigue analysis. As the cyclic expansion of a cylinder in the early stages of life is the result of cyclic softening of the En.25 material it is possible that the cyclic shear stress/shear strain curve for En.25 could be used as basic data in the Franklin and Morrison method rather than static stress/strain data. Cyclic shear stress/shear strain information from reversed torsion tests, by Mackenzie, Burns and Benham (71) on En 25 in a similar condition to the present test material was used with the Franklin and Morrison method to produce the cyclic pressure expansion curve in Fig. 10.8. It can be seen that the use of cyclic shear stress/shear strain data considerably overestimates the amount of cyclic expansion when compared with the experimental strain gauge results.

In fact the static pressure expansion curve is much closer to the experimental curve. The main reason for the poor prediction from cyclic shear stress/shear strain data must lie in the fact that reversed strain cycling is not reprentative of the cyclic conditions at any part of the wall of a thick-walled cylinder.

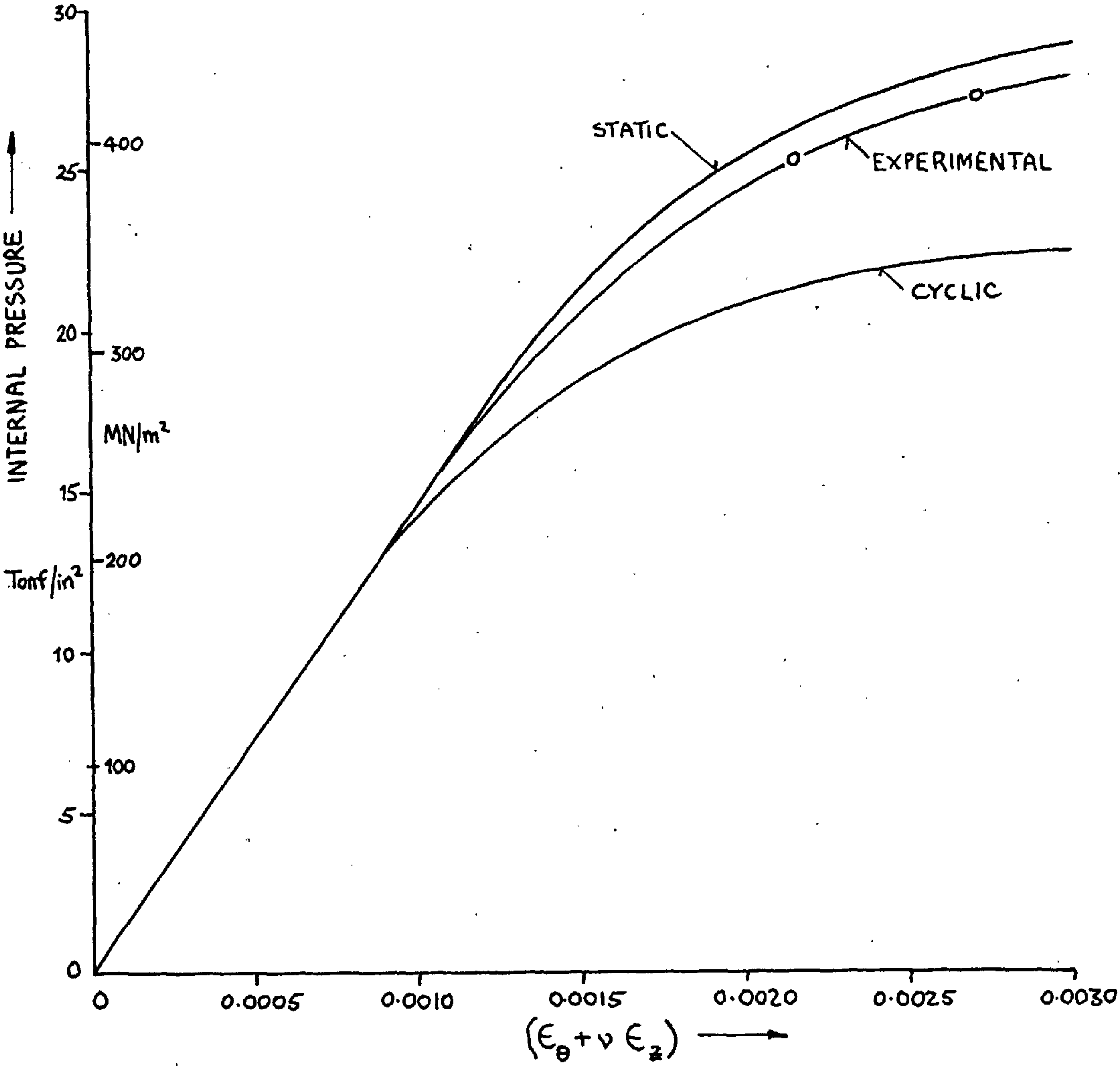

FIG. 10.8 STATIC AND CYCLIC PRESSURE EXPANSION CURVES

So far discussion has centred on the case of repeated internal pressure only, but in the present work the case of combined internal and external pressure is equally important. Under these circumstances the mean strain conditions will be different and the cyclic pressure expansion behaviour will change. Experimental strain gauge data would be difficult to acquire under conditions of both internal and external pressure and it is proposed to accept the static pressure expansion curve in spite of the inaccuracy in the mean strain prediction. The cyclic strain range is of course known from elastic considerations.

The pressure expansion information presented in Fig. 10.8 refers to conditions on the outside diameter of the cylinder but for fatigue analysis of thick-walled cylinders at the bore are needed. The Franklin and Morrison approach involves the assumption that the shear strain at any radius in the cylinder is in inverse proportion to the square of that radius. That this assumption is in error is unimportant for the purposes of defining the pressure expansion curve as the shear stress is almost independent of shear strain in the region of interest. However if the calculation of bore shear strains is the purpose then the assumption may be unacceptable. There is the further problem if the cylinder is subjected to external pressure that the axial stress may no longer remain the intermediate principal stress. These points were investigated in the present work by the application of the Tresca yield criterion with its associated flow rule to the general case of a cylinder with internal and external pressure.

It was shown earlier that for cylinders of moderate K ratio in En25 material the assumption of no work hardening is completely valid. The general equation for the internal pressure which corresponds to a particular position of the elastic-plastic interface radius can be stated as (Appendix 1)

$$p_i = 2\tau_y \ln\frac{c}{a} + \tau_y\left[1 - \left(\frac{c}{b}\right)^2\right] + p_o \qquad (10.1).$$

By the application of the associated flow rule it can be shown that in the plastic region:

$$u_r = \frac{1-2\nu}{G}\tau_y r\left[\ln\frac{r}{c} + \frac{1}{2}\left(\left(\frac{c}{b}\right)^2 - 1 - \frac{p_o}{\tau_y}\right)\right] - \nu\epsilon_z r + \frac{1-\nu}{G}\tau_y\frac{c^2}{r} \quad (10.2).$$

The shear strain in the plastic region is given by

$$\gamma = \epsilon_\theta - \epsilon_r = \frac{u}{r} - \frac{\partial u}{\partial r} \quad (10.3).$$

Substituting (10.2) in (10.3) gives

$$\gamma = 2(1-\nu)\frac{\tau_y}{G}\left(\frac{c}{r}\right)^2 - (1-2\nu)\frac{\tau_y}{G} \quad (10.4).$$

Equations (10.1) and (10.4) can now be combined, graphically to produce a pressure expansion curve in terms of bore shear strain. This curve is plotted for the case of 1.75 K ratio in Fig. 10.9. The curve predicted by the Franklin and Morrison is shown for comparison and it can be seen that this method significantly underestimates the magnitude of the bore shear strain. The validity of the assumption that the axial stress is always the intermediate principal stress is examined in Appendix 1.3.4, and depends upon the cylinder K ratio and the ratio external pressure / shear yield stress. It is shown that the validity criterion is not violated anywhere in the application of Koiter's approach to the analysis of the present work.

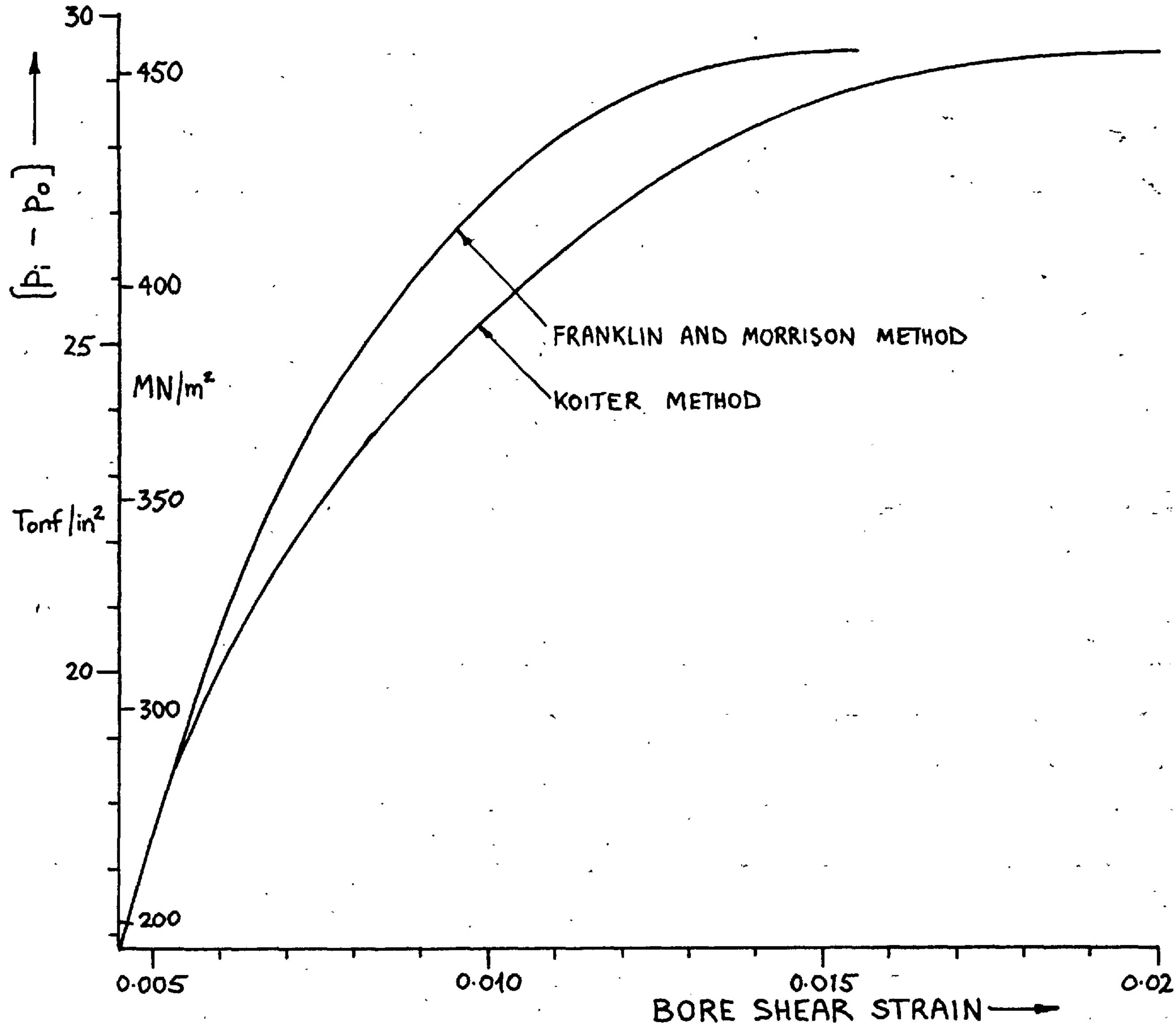

FIG. 10.9 DIFFERENCE BETWEEN INTERNAL AND EXTERNAL PRESSURE $[p_i - p_o]$ AGAINST BORE SHEAR STRAIN

CHAPTER 11.

FATIGUE TEST RESULTS.

11.1 Introduction.

The basic quantitative results of the fatigue test prgramme are the details of the specimen endurances and fatigue loadings. These are presented in this chapter along with the details of the observed fatigue fractures and also data and experiences relating to the performance of the fatigue press and test rigs.

11.2. Tests with Pulsating Internal Pressure.

Two series of tests were conducted, one with an internal base pressure equal to the 250 lbf/in^2 (1.7 MN/m^2) replenishing supply pressure, and the other with a much higher base pressure provided by the static pumping rig.

In the first series with nominally zero base pressure specimens with K ratios of 1.4, 1.8 and 1.75 were tested. The 1.4 and 1.8 K ratio specimens were manufactured to the dynamic support specimen geometry, Fig. 7.2, and were fatigued early in the experimental program on a small subpress during commissioning of the fatigue press. The later 1.75 K specimens were manufactured to either the necked or plain static support specimen geometries, Fig. 7.3, and were tested in the static support rig, Fig. 5.4. A simple thin walled spacing tube which also acted as a safety screen replaced the outer vessel. The results of the zero base pressure tests are summarised in Table 11.1 and are plotted on the graphs Fig. 11.1 and Fig. 11.5.

The elevated base pressure tests were also performed in the static support rig by using an adaptor to connect the static pumping rig to the replenishing supply tapping. The specimens were all of 1.75 K ratio and the plain static support design. A single

TABLE 11.1

Results of Tests for Pulsating Internal Pressure with a Zero Base Pressure

K ratio	Test No.	Specimen No.	Maximum Cyclic Pressure ($Tonf/in^2$)	Maximum Cyclic Pressure (MN/m^2)	Life (cycles)
1.75	3	2	27.3	422	14,092
	30	33P	23.6	364	19,038
	37	37P	21.7	335	32,279
	29	32P	21.3	329	56,792
	28	25	18.4	284	59,778
	27	29P	18.0	278	129,620
	31	30P	14.9	230	94,000
	32	31P	13.5	208	160,000
1.4	11'	13D	15.3	236	33,200
	6'	8D	15.3	236	33,651
1.8	7'	5D	23.5	363	26,678
	9'	7D	23.6	364	26,964

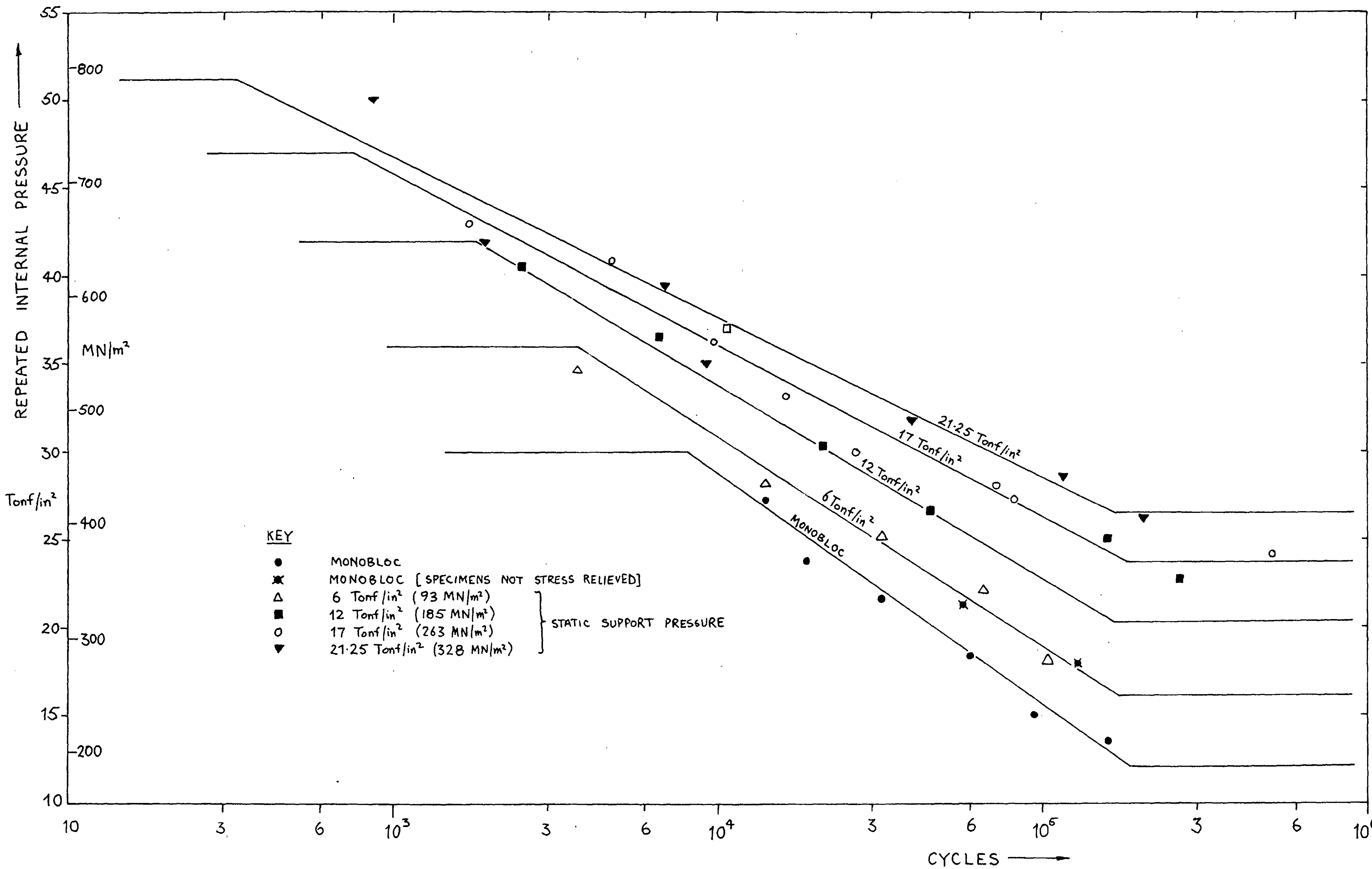

FIG. 11.1 RESULTS OF STATIC SUPPORT AND MONOBLOC FATIGUE TESTS ON 1.75 K RATIO CYLINDERS

base pressure level of 5.5 Tonf/in^2 (85 MN/m^2) was used in all the elevated base pressure tests. This is a convenient working pressure for the pumping rig when operating without intensification. The results of the elevated base pressure tests are summarised in Table 11.2 and plotted in Fig 11.2.

The point of failure, determined by the first leakage of fluid through the specimen wall, was easy to detect in the tests without external fluid support. On the occasions when failure occurred in the author's presence there was often at higher pressures a sharp cracking sound but normally the only indication of failure was an atomised mist of oil issuing from the specimen and out of the spacing tube hole. The evidence of the ultra-violet traces makes it possible to state with confidence that the press was brought to a halt immediately in every test at failure. This means that the test room is not likely to fill with oil mist before the press switches off creating considerable risk of fire.

Although a few tests proved irksome because of check valve leakage or accidental manganin gauge damage the majority were trouble-free. The performance of the fatigue press was if anything improved during the elevated base pressure tests. This was due to the fact that the minimum hydraulic system pressure in the cycle, about 275 lbf/in^2 (1.9 MN/m^2), was higher than the unrestricted decompression pressure in the main control valve. Thus the occasional irregular travel of the ram at the end of its upstroke mentioned in Section 2.6 was avoided. An ultra-violet trace from a high base pressure test, No.44, is shown in Fig 11.3. It can be seen that the internal pressure reduces steadily from the peak value. This is in contrast to the sudden release of pressure which can be seen at the end of the pressure reduction in Fig.11.4. This is a trace from a static support test where the base pressure was nominally zero.

TABLE 11.2

Results of Tests for Pulsating Internal Pressure with a Base Pressure = 5.5 Tonf/in^2 (85 MN/m^2)

K ratio	Test No.	Specimen No.	Maximum Cyclic Pressure		Life
			(Tonf/in^2)	(MN/m^2)	(cycles)
1.75	46	47P	29.1	449	8,919
	45	46P	26.7	412	31,691
	43	45P	24.2	374	31,500
	47	49P	22.5	347	38,413
	44	44P	20.3	314	111,857

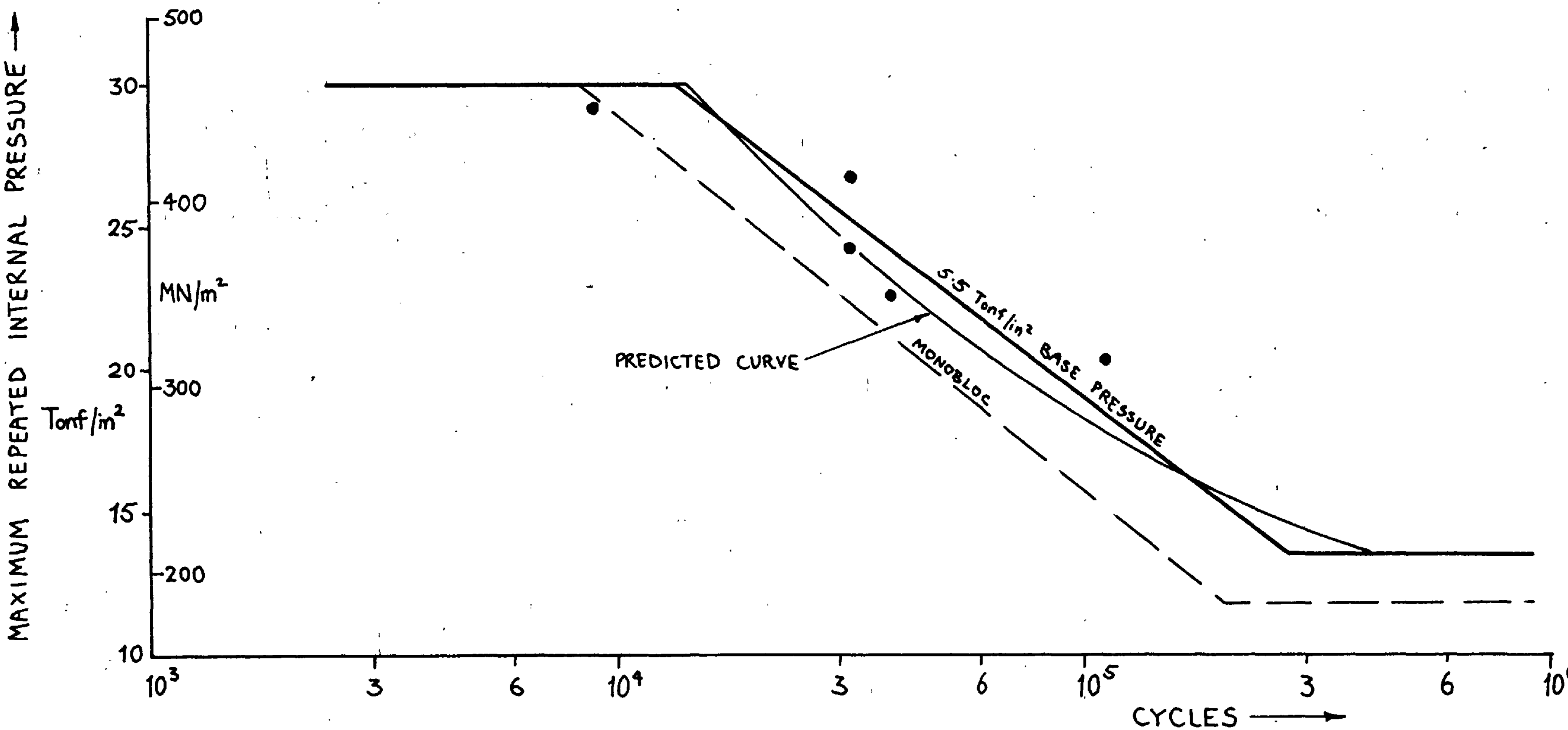

FIG. 11.2 RESULTS OF FATIGUE TESTS ON 1·75 K RATIO CYLINDERS WITH 5·5 Tonf/in² (85 MN/m²) BASE PRESSURE

Virtually no demands were made of the static pumping rig as the amount of replenishment was so small, a ml, or so per hour. Consequently the base pressure was maintained to within 2% of the nominal value. The high pressure Budenberg gauge was used to switch off the pumping rig at failure.

11.3. Tests with Pulsating Internal Pressure and Static External Pressure.

11.3.1. Experimental Results.

The static supported tests were carried out on 1.75 K ratio specimens with four different levels of external pressure 6, 12, 17 and 21.25 Tonf/in^2 (93,185,263 and 328 MN/m^2). Usually eight specimens were tested at each pressure level. The results are presented in Table 11.3 and it can be seen from the test identification numbers that at any one external pressure the tests were generally performed sequentially. The occasional high test number refers to a test which was performed later in the test programme to confirm a trend or fill a gap in the data. The specimen geometries are mixed to a limited extent between the plain and the necked designs as can be seen from the table. The results are plotted in Fig. 11.1.

The test series was performed using the complete static support rig as described in Chapter 5. In the case of 6.0 Tonf/in^2 (93 MN/m^2) tests the intensifier was bypassed and the system was fed directly from the Olinair drive pump. The detection of the point of failure in the static supported tests was not always reliable. As in all the fatigue tests on pressurised cylinders the point of failure is defined as that moment when the fatigue crack finally penetrates the outside surface of the specimen. If the specimen is surrounded by a pressurised fluid then clearly leakage from inside to outside will be retarded particularly if the pressure difference is small. Now in order to stop the test at failure one or both of two control features must be tripped. Either the static pressure gauge pointer must rise sharply by at least 1.0 Tonf/in^2 (15 MN/m^2) to operate the reed switch control, or the pressurising plunger

TABLE 11.3

Results of Tests for Pulsating Internal Pressure with a Zero Base Pressure and Static External Pressure

K ratio = 1.75 throughout

Test No.	Specimen No.	Maximum Cyclic Pressure		Static External Pressure		Life
		($Tonf/in^2$)	(MN/m^2)	($Tonf/in^2$)	(MN/m^2)	(cycles)
42	43P	34.6	534			3,684
33	34P	28.0	432			13,954
36	38P	25.1	388	6.0	93	32,276
35	36P	22.25	343			66,073
34	35P	17.9	276			104,000
22	26P	45.2	698			650
26	28P	40.5	625			2,468
21	21	37.0	571			10,771
41	42P	36.6	565			6,612
25	24	30.3	468	12.0	185	21,117
20	20	26.6	411			45,163
23	22	25.0	386			159,336
24	23	22.7	351			265,978

Cont'd overleaf

TABLE 11.3 cont'd

Test No.	Specimen No.	Maximum Cyclic Pressure (Tonf/in^2)	Maximum Cyclic Pressure (MN/m^2)	Static External Pressure (Tonf/in^2)	Static External Pressure (MN/m^2)	Life (cycles)
11	11	49.4	763			825
39	41P	42.9	663			1,701
9	12	40.8	630			4,717
10	10	36.2	559			9,700
5	19	33.1	511	17.0	263	16,235
6	13	29.85	461			26,819
8	8	28.0	432			73,200
1	1	27.3	422			82,000
7	14	24.1	372			514,000
17	18	49.9	771			860
40	39P	41.8	646			1,897
15	16	39.5	610			6,900
14	15	34.9	539	21.25	328	9,260
12	7	31.7	490			39,950
13	9	28.5	440			117,300
16	17	26.2	405			206,000

must overstroke by at least $\frac{1}{4}$" (6.4 mm). In the majority of static external pressure tests these conditions were met and the press was halted immediately, but in tests where the difference between the static external and maximum internal pressures was less than about 10 Tonf/in^2 ((154 MN/m^2) the precise point of failure was often missed. Fortunately the ultra-violet trace always provided a true record of what had happened. The pulsating internal pressure trace shows no hint of failure but the external pressure trace rises steadily from the point of failure to a point where the pressure gauge contacts eventually switch the press off. During this period the fatigue crack acts as a check valve permitting a small leakage of internal pressure on the downstroke of the plunger, and preventing leakage of the external pressure on the upstroke. The effects of the small leakage of internal pressure are twofold. Firstly the plunger stroke is increased only slightly so that the overstroke limit switch does not detect this fact and the replenishing supply is well able to make up the loss of fluid, and secondly the volume of external fluid is very large in comparison with the leakage volume per stroke so that the external pressure is increased quite slowly. It is possible for the maximum pulsating internal pressure to be maintained under these conditions only because a significant pressure drop exists radially outwards along the fatigue crack due to the very small orifice which it presents. Evidence for this effect was provided by one of the unsupported tests, No.28, when it was possible to gradually increase the internal pressure of the failed specimen to about 9 Tonf/in^2 (139 MN/m^2), the maximum fatigue test pressure was 18.4 Tonf/in^2 (284 MN/m^2), before oil mist issued from the crack. In another test, No.33 with 6.0 Tonf/in^2 (93 MN/m^2) static external pressure it was possible to hold about 10 Tonf/in^2 (154 MN/m^2) internal pressure after failure of the specimen before an increase in the static external pressure could be detected.

An extreme example of a test in which the press continued to cycle after failure is that of Test No.16 where 34,000 cycles were executed with a failed specimen. A slight leakage in pumping rig system was just counterbalanced by the leakage of internal pressure from the specimen so that instead of the external pressure increasing after failure it merely stabilised the previous rise and fall about the nominal pressure. Other tests have continued for much shorter periods, but the evidence points to the inherent safety of the static support system, and at the same time the necessity for reliable pressure monitoring for fatigue work. Without the complete ultra violet trace record it would have been impossible to determine the true life of the specimen.

Another area where instrumentation has proved important in the assessing of the performance of the static pumping rig in maintaining a constant pressure within close limits. There are two chief factors which limit this performance. Firstly there is seal leakage particularly at the specimen itself, but also within the static pumping rig. The latter was usually negligible but specimen seal leakage was never entirely cured which meant that the static pumping rig had to make good the lost fluid. The effect was a slow loss of pressure between strokes of the Olinair Drive Pump. Normally this pressure loss would not exceed 5% of the nominal static pressure and the Drive Pump would stroke every 30 minutes or so. Under these circumstances the intensifier piston would reach the end of its stroke and the system would recharge itself every 3 or 4 hours. Occasionally and for no observable reason the external specimen seal leakage increased with the result that the pumping rig stroked more frequently and the pressure loss rose to between 5 and 10% of the nominal value.

A second factor which influences the accuracy of the static pressure is a pressure ripple at the test frequency due to the elastic displacement of the specimen under fluctuating internal pressure. In fact the persistent leakage from the external specimen seals could be partly attributed to this cyclic movement of the specimen as no leakage ever occurred when internal pressurisation of the specimen was stopped. At a typical test frequency of 50 or 60 cycles per minute the high pressure Budenberg gauge pointer was unable to respond accurately to the pressure ripple and thereby the misleading impression of a steady pressure was given. The true situation is shown on the ultra-violet trace from Test 7 in Fig. 11.4. The amplitude of the pressure fluctuation is about $\pm$ 2.5%, which is a figure typical of the variation obtained after the installation of the high pressure reservoir in the pumping system. The reservoir more than doubled the working volume of high pressure fluid from about 3.6 in^3 (59 ml) to 8.0 in^3 (130 ml) and roughly halved the amplitude of the pressure ripple.

The accuracy with which the manganin gauge signal indicates the static pressure variations is very dependent upon the high pressure fluid. The fluid used for the trace in Fig. 11.4 was Univis P.38, but with exactly the same experimental conditions and Tellus 27 as fluid the pressure ripple lagged the internal pressure cycle and the amplitude was only $\pm$ 0.5%. The remote position of the manganin cell from the test rig had resulted in the damping of the pressure fluctuations by the more viscous Tellus 27 although the compressibilities of Tellus and Univis are very similar.

The figures quoted for the static pressure levels in Table 11.3 represent the mean of the combined long term variations due to leakage and short term variations due to specimen displacement. It

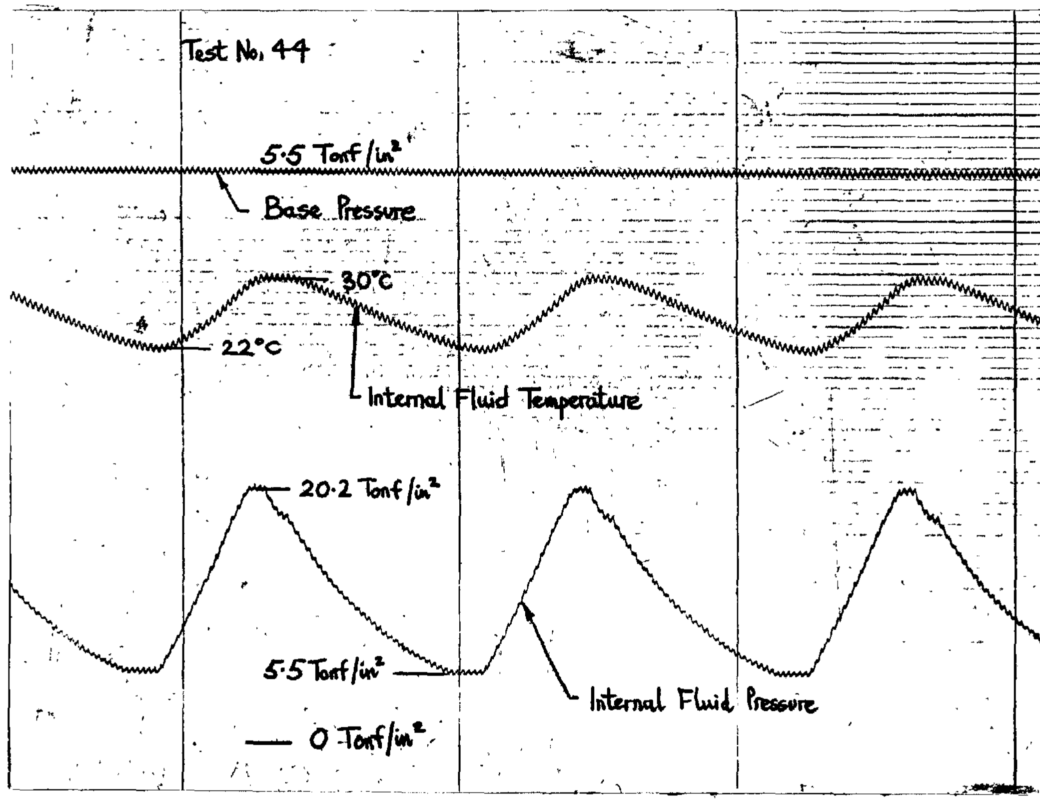

Fig. 11.3. Ultra-Violet Trace of High Base Pressure Test.

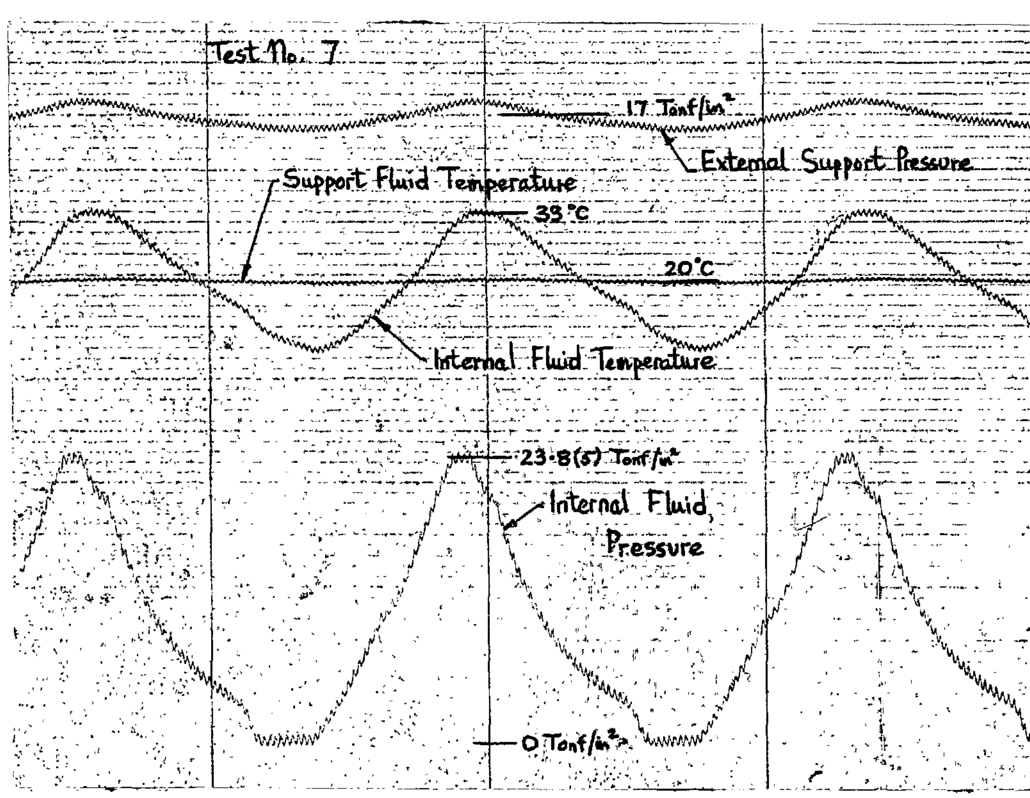

Fig. 11.4 Ultra-Violet Trace of Static Support Test.

is not possible to put a single percentage variation figure about the mean value as the pressure ripple contribution was chiefly dependent upon the magnitude of the internal pressure range, but in general the total variation about the nominal static pressure was between $\pm$ 3 and $\pm$ 6%.

11.3.2. Predictions of Static Pressure Fluctuation.

In a hydrostatic extrusion system the pressures would be higher than in the present work and it might be impracticable to provide a large enough high pressure reservoir with the result that the fluctuations in static external pressure caused by elastic displacements could be a significant factor. For example the outer vessel could no longer be designed from purely static considerations. It is therefore important to be able to predict the fluctuations in static pressure which arise from the cyclic displacements of the liner wall.

For accurate prediction it is necessary to know the pressure / compressibility characteristic for the working fluid. Two different characteristics are usually presented , the isothermal and the isentropic , because the compressibility is temperature dependent. In the case of the pumping rig the true situation lies somewhere between the two cases, probably nearer to the isothermal. However compressibility data of any sort at high pressures is relatively scarce and particularly for oils such as Tellus 27 and Univis. Some room temperature (20°C) isothermal compressibility curves from different sources are presented in Fig. A 4.1 Evaluation of the volume of working fluid is also difficult and although the elasticity of containing vessels can be approximated doubt remains about the compressibility of seals. It is possible to draw up an expression for the net reduction in fluid volume in terms of the internal pressure and the amplitude of the fluctuating external pressure, Δp_0. Using the compressibility characteristic the reduction in fluid volume, d V, corresponding to an increase in external pressure also can be found.

The correct Δ_{p_o} gives the same compressibility from both considerations and must be found by trial and error. However, for simplicity the elastic distortion due to the extra external pressure may be neglected and the dV found solely from the maximum internal pressure and the K ratio. This is quite reasonable in view of the lack of precision in the compressibility characteristic and the large external fluid volume. It also gives an upper limit to the fluctuation figure. The analysis is detailed in Appendix 4 It can be seen that for Test 7 the predicted variation in static pressure is 17.0 ± 0.5 Tonf/in^2 (263 ± 8 MN/m^2) whereas the actual variation shown in Fig. 11.4 is 17.0 ± 0.4 Tonf/in^2 (263 ± 6 MN/m^2).

11.4 Tests with Pulsating Internal Pressure and Simultaneous Pulsating External Pressure.

The dynamic supported tests were carried out on five specimens of different K ratios as listed in Table 11.4. The results are also given in Table 11.4 and are plotted in Fig. 11.5. The 1.4, 1.8, and 2.0 K ratio specimens were manufactured to the design shown in Fig 7.2. these K ratios having been chosen for comparison with the results of other workers. The 1.75 K ratio specimen was chosen for comparison with the static supported specimens. Although the number of specimens tested successfully is limited, other specimens were in fact cycled during the development of the technique.

Many of the problems with the rig have been detailed already and it is more appropriate here to describe the practical results of the tests. The detection of the point of failure in dynamic support tests was always immediate. This is not surprising as the pressure differential between inside and outside pressures

TABLE 11.4

Results of Tests for Pulsating Internal Pressure with Simultaneous Pulsating External Pressure

K ratio	Test No.	Specimen No.	Maximum Internal Cyclic Pressure		Maximum External Cyclic Pressure		Life
			($Tonf/in^2$)	(MN/m^2)	($Tonf/in^2$)	(MN/m^2)	(cycles)
1.4	2'	2D	20.55	317	6.8	105	64,200
1.75	6'	12D	29.0	448	9.0	139	42,000
1.8	4'	10D	28.5	440	9.4	145	84,900
2.0	3'	4D	29.3	453	9.7	150	102,800
	5'	6D	30.8	476	10.2	158	65,400

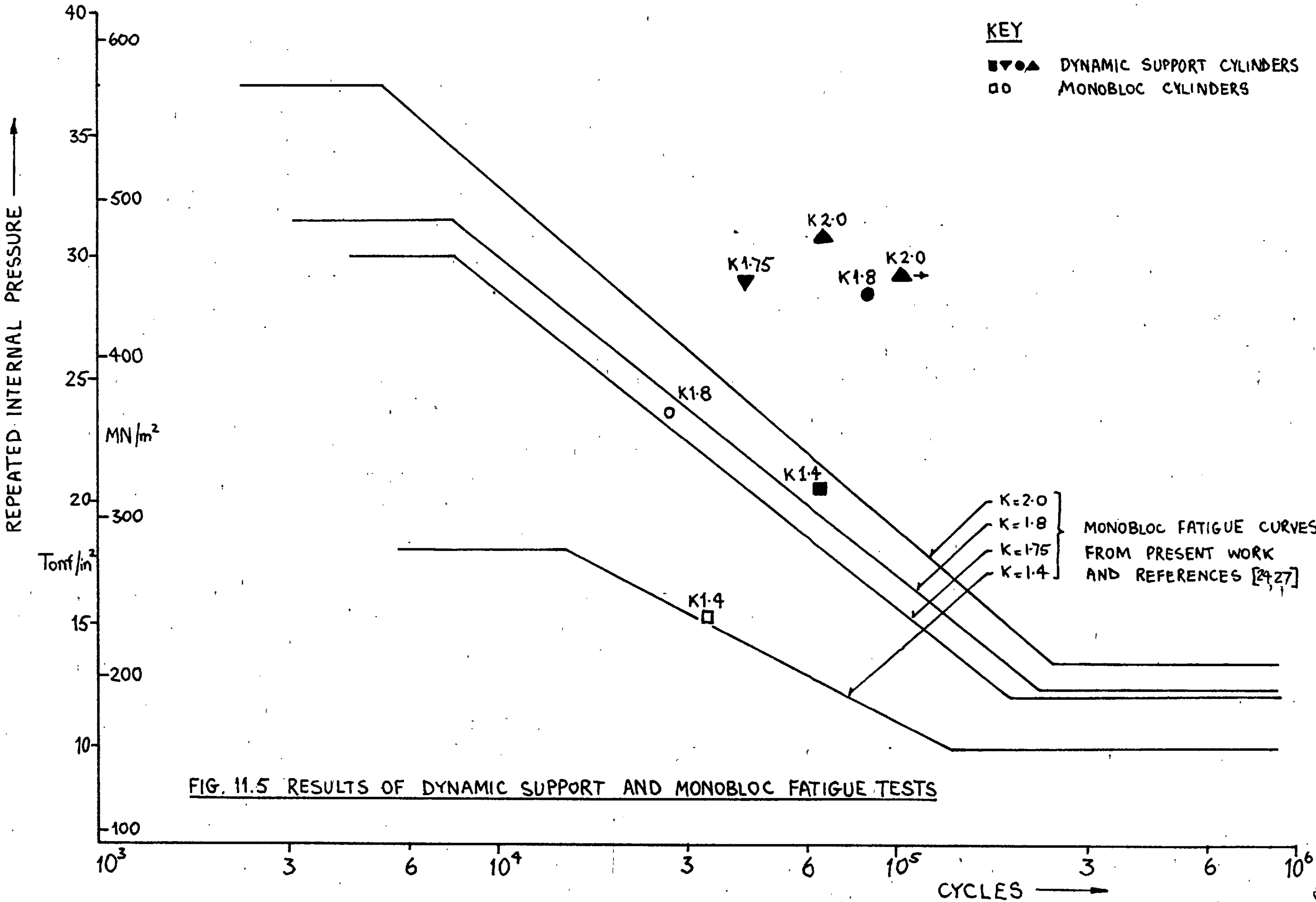

FIG. 11.5 RESULTS OF DYNAMIC SUPPORT AND MONOBLOC FATIGUE TESTS

was large, and as soon as inside pressure was able to leak the specimen assembly could no longer operate dynamically. However on some occasions the press had stopped automatically and one was unsure whether the specimen had failed. If the press were then restarted, the outer chamber became pressurised via the crack and this pressure was held on return of the ram. In the same way as in the static support tests the specimen was acting as a non-return valve, but with an important difference that in the dynamic support rig there is no provision for letting down this external pressure. This led on two occasions to extreme difficulty in dismantling the rig. With the extra load on the end plates it was not possible to pressurise the hydraulic tie rod nuts sufficiently to remove the shims. It was then necessary to use a testing machine to pre-compress the end plates while unfastening the nuts. It would of course be possible to incorporate a high pressure let down valve in the external pressure end closure but this would complicate the component and could give rise to fatigue problems.

The specimens were all tested at one external pressure/internal pressure ratio although the rig can accommodate a range of such ratios. It is important to examine how the pressure generating performance predicted from simple area ratio considerations differs from that obtained in practice.Fig. 11.6 shows the external pressure plotted against internal pressure. The static curve was obtained by gradually increasing the internal pressure without cycling the pressure. The second curve shows the dynamic pressure ratios achieved in the tests. It can be seen that the measure of disagreement between these curves and the ideal frictionless curve is significant. There are two main reasons for this difference, firstly the effect of rig seal friction, and secondly geometric changes due to elastic displacements under pressure. The latter effect can normally be ignored. For example, with

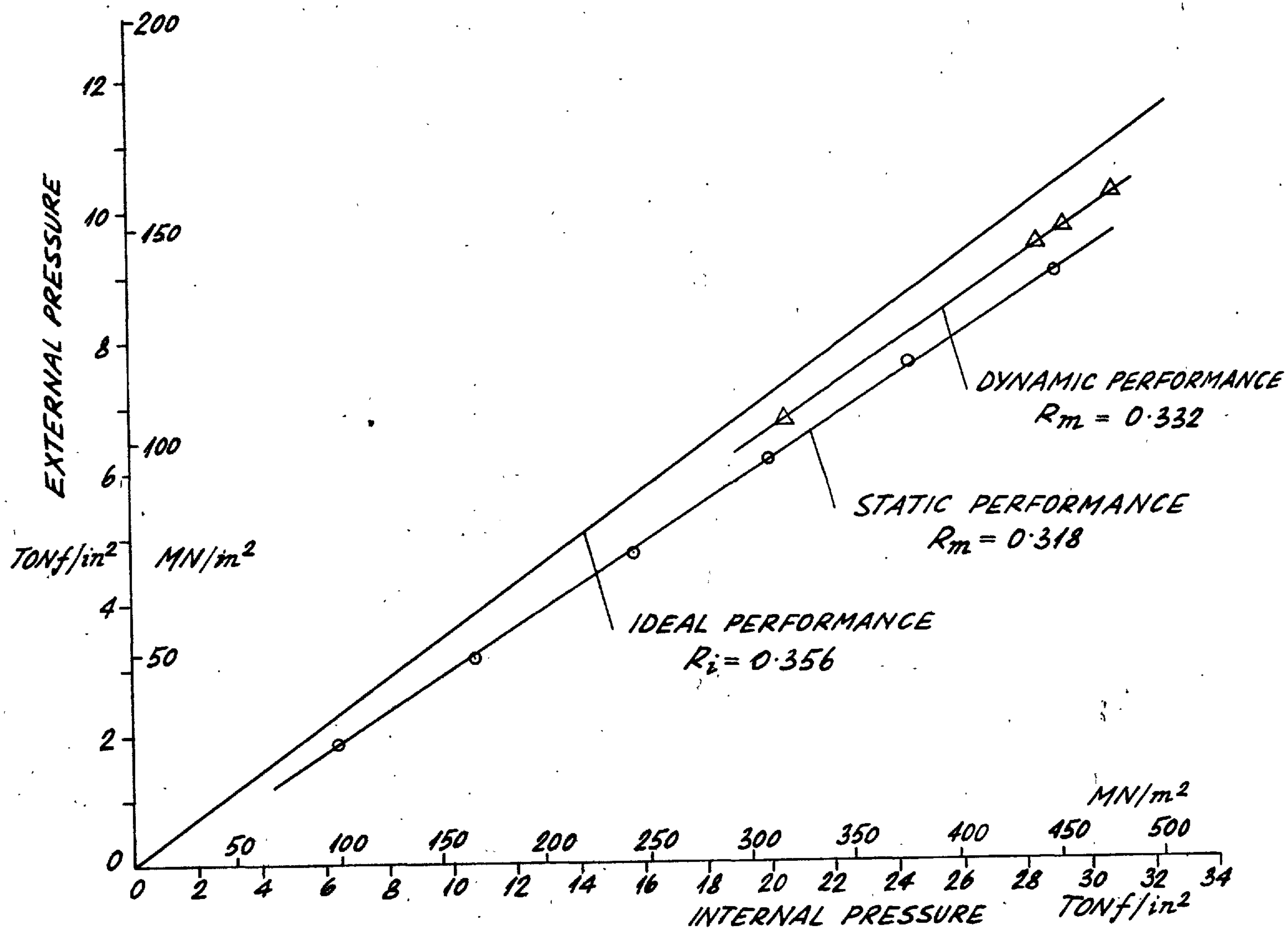

FIG. 11.6 PERFORMANCE OF DYNAMIC SUPPORT RIG.

an internal pressure of 30 $Tonf/in^2$ (463 MN/m^2) and an external pressure of 10.7 $Tonf/in^2$ (165 MN/m^2) the pressure ratio taking into account elastic distortion and manufacturing tolerances is about 0.358 as against 0.356 ideally, . The difference is negligible, but if the modified pressure ratio were used it would give rise to higher not lower external pressures for a given internal pressure. Thus seal friction losses must account entirely for the reduced performance exhibited in Fig.11.6.

It is assumed that the total frictional resistance of the three 'moving' seals acting on the specimen assembly is given by frictional loss factor, k, calculated from the expression

$$k = \frac{R_i - R_m}{R_i}$$

where R_i and R_m refer respectively to the ideal and measured pressure ratios. Referring to Fig. 11.6 the gradient of the dynamic line is $R_m = 0.332$, and for the ideal line $R_i = 0.356$ thus using the above formula $k = 0.067$, or 6.7%. The gradient of the quasi-static line $R_m = 0.318$ and $k = 0.107$ or 10.7% for the three seals. However if the quasi-static line were extrapolated it would not pass through the origin, which would suggest a small static component of friction should be included. The frictional losses which this simplified analysis predicts are low and would indicate that the seal behaviour must be partially hydrodynamic. This perhaps explains why under such arduous high pressure conditions, compared with normal hydraulic practices, satisfactory seal lives have been obtained with commercial hydraulic seals in both static and dynamic support test rigs.

11.5 Fatigue Fractures.

11.5.1 Introduction.

The 'classic' fatigue failure of a thick-walled cylinder subjected to repeated internal pressure starts at the bore and propagates radially through the wall until the outside surface is reached. Typically there is only one crack about twice the wall thickness in length situated axially in the bore. At the outside surface the only evidence of the crack is two faint surface markings similar to thumbnail impressions. If the cylinder were split open longitudinally in the plane of the crack a fracture surface roughly semi circular in shape would be revealed as shown in Fig 11.7. Almost all the fatigue tests in the present series were taken to failure so that a large collection of fractures over a wide range of conditions were obtained. In relatively few cases did the cracks exhibit all the features described above. Inspection of both internal and external cracks was by eye with the help of magnetic crack detection techniques, where necessary, and thus only macroscopic or 'engineering' cracks will be discussed.

11.5.2. External Cracks.

The symmetric thumb nail crack is illustrated in Fig. 11.8 (a). Only the central region is actually fractured and this type of crack is typical of specimens tested without support pressure, or with low levels of static or dynamic support pressure. The axial extent of the thumb nail impression is roughly proportional to the maximum repeated internal pressure so that for long lives at low pressures the length is roughly 3/16 in (4.8 mm) and for short lives at higher pressures ¾ in (19 mm) or more long. At pressures close to the collapse pressure the crack also tends to open out and to exhibit irregularities typical of a burst fracture. The external cracks observed on specimens subjected to higher levels of support pressure showed considerable variety in appearance. It was noticeable

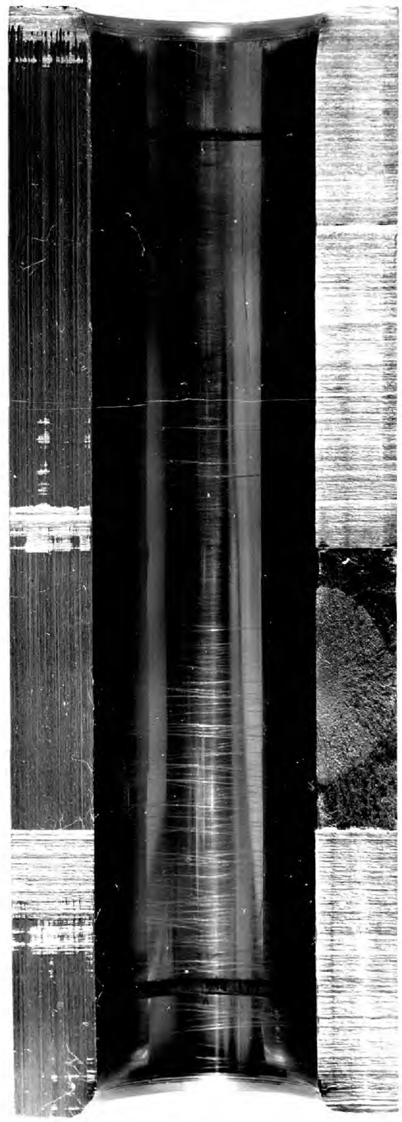

Fig. 11.7. Typical Fracture in Plain Specimen.

TYPE (a)

TYPE (b)

TYPE (c)

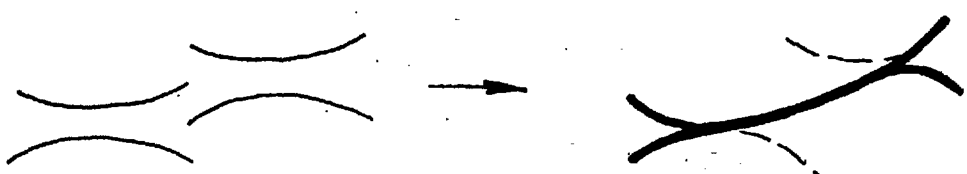

TYPE (d)

FIG. 11.8 TYPES OF EXTERNAL 'THUMB NAIL' CRACKS.

that the type (a) crack of Fig. 11.8 could be found in specimens with high repeated internal pressures and substantial support pressure rather than the open burst like fractures mentioned earlier. At lower pressures a crack of the type illustrated in Fig. 11.8 (b) was typical. The whole of one of the thumb nail impressions had become fractured. An extension of this type is shown in Fig. 11.8 (c) where the crack has propogated axially beyond the thumb nail boundary. However the type (c) crack appeared to be characteristic of tests at high support pressures which had continued to cycle after failure, and this may account for the extensions. Fig. 11.9 shows two views of specimen No.16. The characteristic thumb nail fracture can be seen in view (a), but in addition a more widely spaced thumb nail impression can be seen nearby. When the specimen was sectioned a fatigue crack was revealed which had grown to about 1/16 in (1.6 mm) short of the outside surface. In view (b) of Fig. 11.9 a third faint thumb nail impression can be seen. If two cracks propogate in close proximity as in Fig. 11.9 (a) they may well merge, at the outside surface as shown in Fig. 11.8 (d) and the resulting fracture is skew with respect to the axis of the specimen. This type fracture was in fact observed on a number of specimens.

11.5.3. Bore Cracks.

The classical single axial bore crack was found on almost all specimens with endurances over 100,000 cycles. At somewhat higher loading conditions the failure crack was still a straight axial crack although a number of shorter cracks could be seen in addition. Perhaps the most common type of crack found in the static support specimens was a chain of axial cracks which had linked up to form an exceptionally long irregular but basically axial fracture.

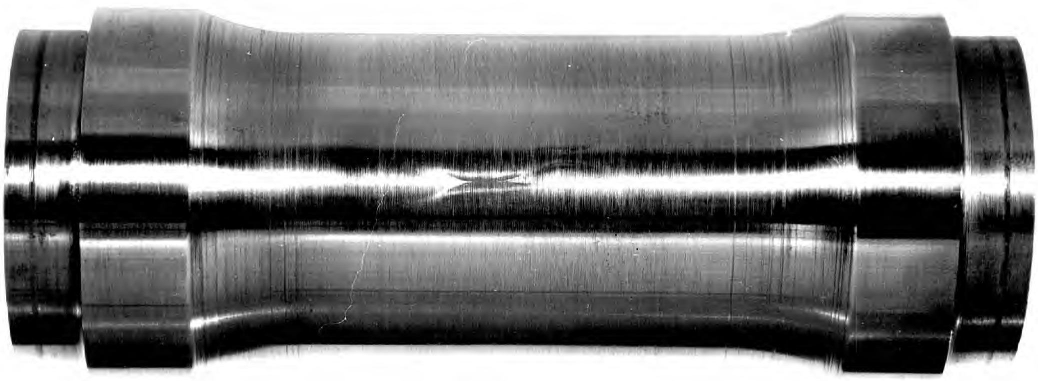

Fig. 11.9. (a) External Cracks on One Side of Specimen No.16.

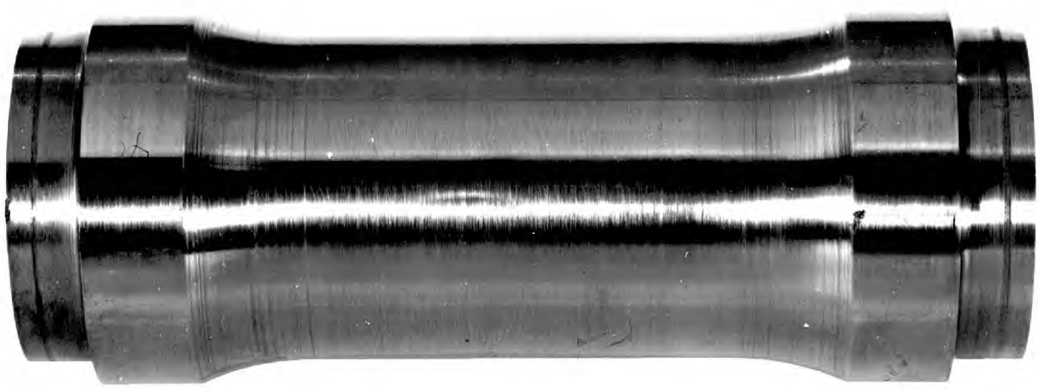

Fig. 11.9. (b) External Cracks on the Opposite Side of Specimen No.16.

This is shown in Fig. ~~11.9~~ 11.10(a) for specimen No.16 where fluoresecent magnetic ink has been used to emphasise the cracks. It is interesting to note the complete absence of cracks outside the parallel gauge length of the specimen. The main crack was not the failure crack in spite of its length. In fact it appears that the linking up of a number of cracks retards the radial growth of the main crack in preference to axial growth. The failure crack (not shown) in specimen No.16 was fairly short with only one link up. The multiplicity of short cracks sometimes as many as 30, always accompanied this type of failure.

11.5.4. Crack Propagation.

Information was gained on two aspects of crack growth in a thick walled cylinder during the test programme. The two aspects are, the stage in the life of the specimen when a bore crack can first be observed, and the direction in which the crack propagates through the cylinder wall.

During the test programme a number of tests were interrupted prematurely through some failure of the rig or instrumentation. Usually the rig was stripped down to repair the fault, and the opportunity was taken to inspect the specimen. A record was kept on these occasions of whether bore cracks could be detected by eye with or without the help of magnetic crack detection. The results of these intermediate inspections are summarised in Table 11.5. It can be seen from the Table that no cracks could be detected as late as 71% of the life of one specimen, and that the earliest cracks were detected at 81% of the life of another specimen. The results cover a range of endurances from about 2,000 cycles to over 100,000 cycles, and in spite of the unsystematic way in which results

TABLE 11.5

Tests with Intermediate Inspection for Cracks

Test No.	Total life (N_t cycles)	Life when inspected (N_i cycles)	$\frac{N_i}{N_t}$ %	Comments
7	514,000	227,741	44%	No cracks
13	117,300	51,572	44%	No cracks
		103,931	89%	6 bore cracks
		107,598	92%	Same 6 bore cracks slightly longer
27	129,620	125,081	97%	1 bore crack about $\frac{1}{4}$ in. (6.4 mm) long - same crack at failure about $\frac{3}{4}$ in. (19 mm) long.
30	19,038	11,130	58%	No cracks
		13,521	71%	No cracks
36	32,276	18,117	56%	No cracks
37	32,279	15,000	46%	No cracks
40	1,897	1,532	81%	Large number of short bore cracks longest about $\frac{1}{4}$ in. (6.4 mm)
46	8,919	5,506	62%	No cracks

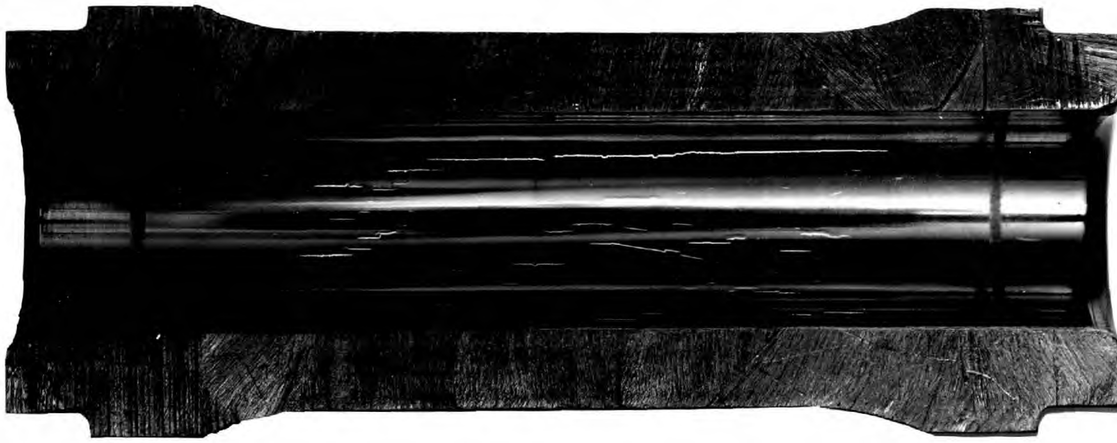

Fig. 11.10. (a) Bore Cracks in Specimen No.16.

Fig. 11.10 (b) Radial Slice showing Crack Propogation in Specimen No.16.

were acquired it does appear that as little as the last 20% of life is spent in macro-crack propagation.

An inspection procedure was carried out on all failed specimens to establish whether the bore failure crack was radially in line with the external crack. Only a few specimens departed from the purely radial propagation, and two of these were sectioned for detailed examination. The photograph Fig. 11.10(b) shows a typical example from specimen No.16. The deviation from a radial line is about 12°.

11.6. Experience with Seals during the Fatigue Tests.

11.6.1. Plunger Seals.

Throughout the test programme only one type of plunger seal was used, $\frac{7}{8}$ in x 1 in x 9/32 in (16 mm x 25 mm x 7 mm) Hallprene seal. The Hallprene hydraulic seal is basically a combination of an 'O' ring with a 'U' ring. The 'U' ring consists of multi-ply cotton weave impregnated with nitrile rubber, and the softer header (or 'O') ring is of nitrile rubber (70 - 75° Shore hardness), and the two are bonded together to form the standard Hallprene seal. The soft header ring ensures that the 'U' ring sealing lips are constantly loaded even though the seal may be worn. It was the practice to use a new seal in each test and this seal invariably lasted out the test. For example a plunger seal endured 266,000 cycles at a repeated pressure of 22.7 Tonf/in^2 (351 MN/m^2) and at the other end of the scale another seal withstood a repeated internal pressure of 49.9 Tonf/in^2 (771 MN/m^2) for 860 cycles. The seal in the latter case certainly looked good for another 1,000 cycles at the same maximum pressure. The seal used in the former case is shown alongside a virgin Hallprene seal in Fig. 11.11 and the worn inner mitre ring is also shown for comparison with an unused

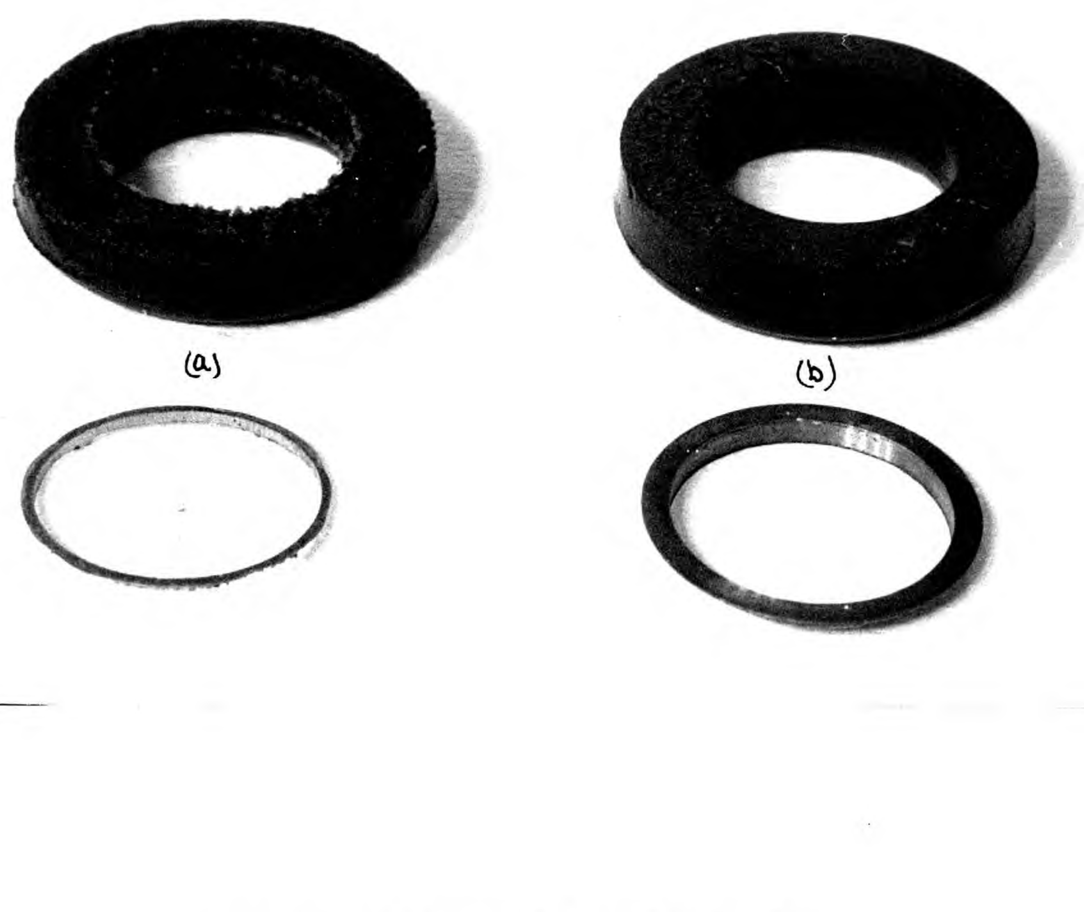

Fig. 11.11. Hallprene Seal and Mitre Ring.

(a) After Use.

(b) Before Use.

one. The wear of the phosphor bronze mitre ring after 266,000 cycles is very much more severe than of the seal itself. The seal, which is shown pressure side down, in fact has worn at the heel so that the fabric of the 'U' ring has become exposed but the sealing lip and soft header ring are still in good condition. Severe wear of the mitre ring was a feature of long life (>100,000 cycles) tests and appeared to be unrelated to the magnitude of the repeated pressure. The mitre ring is self centering and so wear is usually even as in Fig. 11.11. The material which is removed from the mitre ring during normal wear becomes deposited in the bore of the seal and in the course of a long test builds up into thin slivers which possibly give the seal added protection. Very fine particles of phosphor bronze also sink to the bottom of the specimen or get drawn out with the plunger on the upstroke. The accumulation of fine particles at the bottom of the specimen gave rise to short circuiting of the manganin coil terminal on occasion. It was thought that the wear or pick-up, between the plunger and the mitre ring could be minimised by hard plating and polishing the plunger. However within a short time the plated plunger picked up and became as scored as the original one.

Pick-up between the outer mitre ring of the plunger seal and the bore of the test specimen took place in every test. The outer mitre ring was never seriously worn and could be used for a number of tests. However the axial scoring and pick-up on the specimen bore was disturbing and it can only be due to the favourable stress conditions at the seal that fatigue cracks were not initiated in this region. The extent of the damage can be seen in Fig. ~~11.9~~ 11.10(a) at both ends of the specimen. The mitre ring at the bottom end of the specimen of course acts in the same way as the one at the top. In the dynamic support test the specimen slides relative to the outer mitre ring and the pick-up damage is consequently spread over a much longer axial length about $\frac{3}{8}$ in (9.5 mm) but fatigue cracks have never been initiated in this region.

In view of the wear process between the plunger and the seal it is of interest to examine the frictional losses occurring. A record was kept during the test programme of both the maximum repeated internal pressure in the specimen as measured by the manganin gauge, and the maximum pressure in the fatigue press hydraulic circuit measured by the pressure gauge on the control panel. A graph of these pressures for fourteen representative tests is shown in Fig. 11.12 and this gave rise to a useful but fortuitous rule of thumb. If the hydraulic pressure is divided by 50 the quotient gives the internal pressure generated in the specimen. An overall frictional loss factor, k, may be calculated from the equation

$$k = 1 - \frac{p_i \; A_i}{p_h \; A_h}$$

where p_i and p_h are the internal specimen pressure, and the hydraulic pressure. A_i and A_h are the plunger and annular piston areas. Using the information from Fig. 11.12 the overall loss factor is 6.5%. As the frictional loss at a conventional hydraulic piston seal could not be less than about 3% then the plunger seal loss also can only be about 3%. This low value agrees with the figures obtained in Section 11.4 for the dynamic support rig.

11.6.2. Seals in the Dynamic Support Rig.

The dynamic support rig involves two seals against which the specimen assembly reciprocates. The top seal is merely a sealed up version of the plunger seal arrangement and Hallprene seals were again used. An attempt was made to use a pair of 'O' rings for the bottom seal around the assembly end extension but within a few cycles

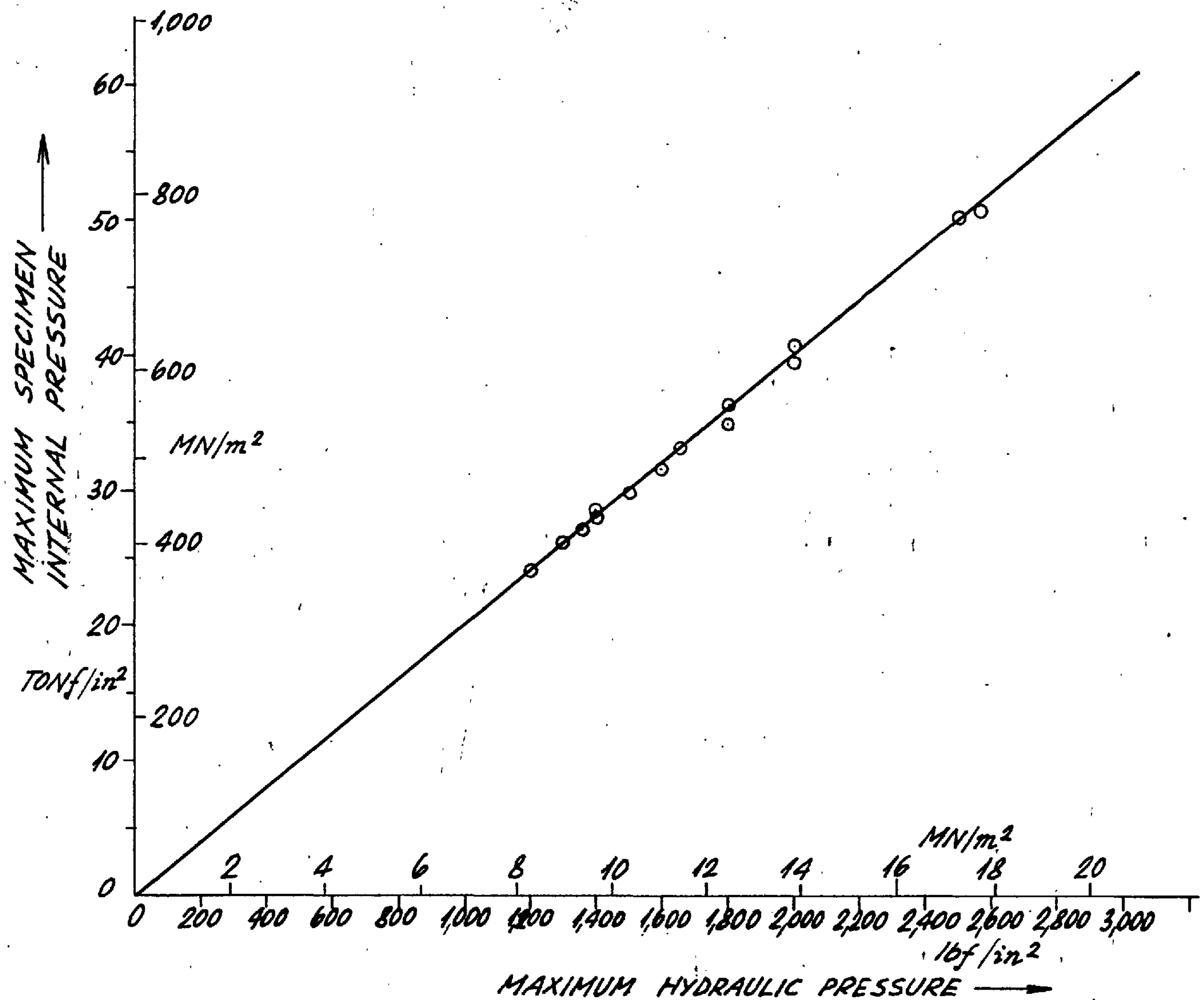

FIG. 11.12. RELATION BETWEEN GENERATED INTERNAL PRESSURE AND HYDRAULIC SYSTEM PRESSURE.

these were twisted and knotted beyond recognition, and from then on Hallprene seals were used.

11.6.3. Static Seals.

'O' rings were used exclusively for static seals and with the exception of one specific case were absolutely reliable and trouble-free. The 'O' rings could generally be used for test after test, although eventually a wear mark could be detected on the outside circumference. This wear was presumably due to the small repeated elastic displacements of the specimen bore during the fatigue test. 'O' ring sealing problems were encountered in sealing the outside pressure during the static support tests. In fact while static pressure alone was applied the sealing was entirely satisfactory, but as soon as the inside pressure was cycled then leakage occurred. The leakage was never very severe and the static pumping rig could always maintain the required pressure, but nevertheless it was an irritating defect. Various remedies were tried, larger and smaller mitre rings, two seals instead of one, but without success. A particular feature of these external pressure seals is that two independent mitre rings are involved in sealing two independent surfaces, whereas in other static seals only one mitre ring is wedged against both surfaces. A design modification on these lines could perhaps solve the problem.

11.7 Temperature Rise due to Cyclic Pressure.

The indications are that plunger seal life is largely dependent upon mitre ring wear within the range of conditions encountered in the test programme. However a factor which could affect seal life at higher cyclic pressures is the temperature rise in pressurisation. The temperature rise is due to the work done on the fluid in raising its pressure from a lower to a higher level and is therefore dependent largely on the compressibility of the fluid. The temperature rises from 23 static

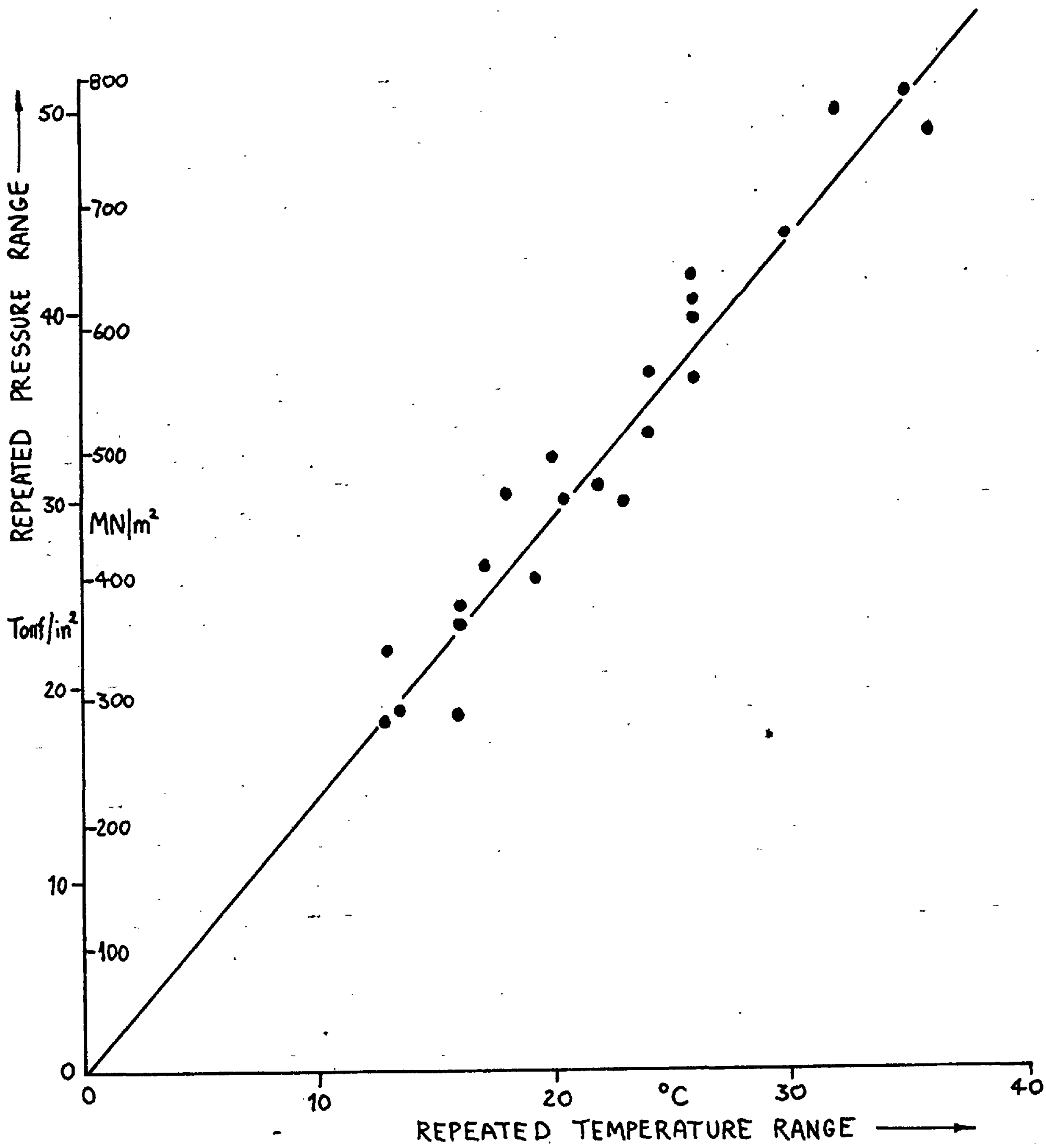

FIG. 11.13 TEMPERATURE RISE DUE TO PRESSURISATION

support fatigue tests are plotted in Fig. 11.13. The scatter of results is due to the different cycle speeds, fluid volumes, and heat transfer condition in each test. A linear relationship between pressure and temperature rise would not normally be expected because of the non linear pressure dependence of factors such as compressibility and specific heat, but a rough figure of 0.7°C per Tonf/in^2 (0.045°C per MN/m^2) can be extracted from the graph. Thus for a repeated pressure of 50 Tonf/in^2 (772 MN/m^2) the temperature range would be 35°C. At the start of a fatigue test the temperature could be 23°C say and thus a peak of 68°C would be reached at a maximum pressure of 50 Tonf/in^2 (772 MN/m^2). As the test proceeded the base temperature would rise until a stable thermal equilibrium condition was reached, and with a repeated test pressure of 50 Tonf/in^2 (772 MN/m^2) this base temperature could be as much as 60 or 70°C. Thus the resulting temperatures are in the 130°C region.

The normal maximum operating temperature for hydraulic seals is 120°C, and this can be extended by the use of materials such as Du Pont Viton rubber. However, if repeated pressures of 100 Tonf/in^2 (1544 MN/m^2) and more are envisaged at the present cycle rate in the fatigue tests, then clearly excessive temperatures will be involved which could limit seal life. The problem may be minimised by using a fluid of low compressibility, or cycling the pressure at a slower rate, or by cooling the pressure vessel.

One benefit in the present work derived from the temperature rise was the ability to use Tellus 27 as a working fluid, which under static conditions would freeze at well below the applied maximum pressure.

CHAPTER 12.

DISCUSSION OF RESULTS.

12.1 Introduction.

The basic fatigue results are plotted on the basis of pressure against life in Figs 11.1, 11.2 and 11.5 of the previous chapter. A number of general observations can be made of these graphs before undertaking more detailed analysis. The static support and monobloc test results presented in Fig. 11.1 were all carried out on cylinders of 1.75 K ratio and straight lines have been drawn to fit the experimental points for each external pressure condition. The graph clearly shows how the application of static external pressure enables a higher cyclic internal pressure to be resisted. The maximum benefit occurs at longer endurances. At low endurances the fatigue curves are bounded by the estimated collapse pressures calculated from the following formula (see Appendix 1.4)

$$p\ \text{collapse} = 2\tau_y \ln K + p_o \qquad (12.1).$$

The curves are terminated in the long life region by endurance pressures predicted by a method discussed in Section 12.3.1 of this chapter.

The high base pressure tests in Fig. 11.2 have been shown for comparison against the simple monobloc fatigue curve from Fig. 11.1. In view of the scatter of the results a rather doubtful straight line has been drawn to represent the high base pressure results. The results show that a higher maximum cyclic pressure can be withstood when the pressure does not return to zero. However at low endurances the fatigue curve must be bounded by the collapse pressure for a monobloc cylinder. The curve is terminated in the long life region by an endurance pressure predicted by the method discussed later in Section 12.3.3.

The dynamic support test results are presented in Fig. 11.5 along with monobloc fatigue curves for 1.4,1.75, 1.8, and 2.0 K ratios cylinders. The 1.4 and 1.8 K ratio curves were taken from Austin and Crosslands' (27) work and the few monobloc tests which were carried out with these K ratios are in good agreement with their curves. The 1.75 K ratio fatigue curve was taken from Fig. 11.1 and again is in good agreement with Austin and Crossland. This agreement is reassuring as the En.25 Steel came from different sources with different histories, and the end conditions of the test cylinders were different in the two cases. Austin and Crosslands' cylinders were closed-ended as against open-ended in the present work. The dynamic support results plotted in Fig. 11.5 demonstrate clearly the benefits of external dynamic support pressure. The maximum cyclic internal pressures sustained are typically 50% higher than those sustained by monobloc cylinders for the same fatigue life.

It is important in assessing the results of the tests to seek a satisfactory criterion of failure which will link the fatigue behaviour of cylinders under a wide variety of conditions, and at the same time relate to basic fatigue data for the material. One of the most favoured criteria in previous work has been bore shear stress range with mean bore shear stress as a secondary parameter. It is therefore appropriate to examine these factors in the light of the present work.

12.2 The Significance of Shear Stress Range and Mean Shear Stress.

The results of the monobloc static supported and high base pressure tests have been plotted on the basis of shear stress range, against mean shear stress at the bore in 12.1 for a series of lives. The points on the graph were calculated from the pressure conditions indicated for the particular lives on each of the constant external pressure lines in Fig. 11.1. The diagram is bounded by the static yield lines which has meant the exclusion of a considerable amount of information. If these

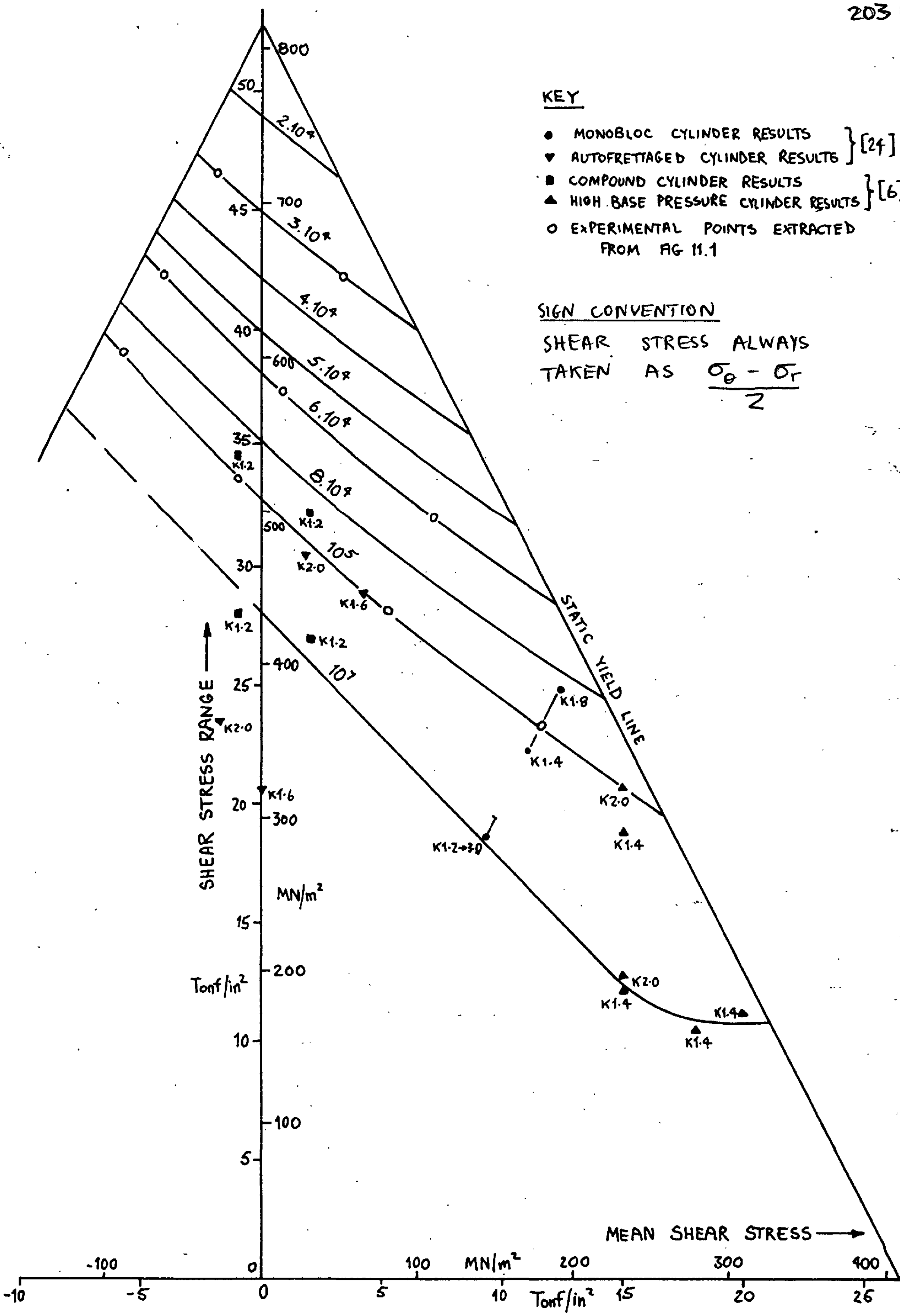

FIG 12.1 CONSTANT LIFE CURVES OF SHEAR STRESS RANGE AGAINST MEAN SHEAR STRESS AT THE BORE

data were plotted the points would fall along the static yield lines and be meaningless. The curves show the great importance of mean shear stress in pulsating pressure fatigue. The results of other work on autofrettaged, compound, and monobloc cylinders due to Morrison et Al. (Ref. 24), Austin and Crossland (27), and Burns and Parry (6) have been included for comparison with the present work. The trend set by the 10^7 endurance line is reproduced by the present results for endurances from 10^5 to 3.10^4, and the results from other sources are in good agreement with the 10^5 endurance line. The agreement is particularly significant as a wide range of K ratios from 1.2 to 2.0 were involved. One of the anomolies of the 10^7 endurance line is the autofrettage test results which lie well below the line. This was noted by Burns and Parry (6) who suggested that the residual stresses in autofrettaged cylinders are significantly altered by cyclic loading. However it can be seen that at 10^5 cycles the autofrettage cylinder results agree well with the static support results. The compound cylinder results for 10^5 cycles involved assumptions about the mean shear stresses. It was assumed that the cylinders which were designed to exhibit zero mean shear stress in fact gave a mean shear stress of - 1.0 Tonf/in^2, and that the cylinders designed for 4 Tonf/in^2 gave 2 Tonf/in^2. These figures have been deduced from the values published by Burns and Parry (6) for the few cylinders which were strain gauged, and cannot be regarded as exact. Nevertheless the points lie close to the 10^5 endurance line. The monobloc results from Austin and Crossland (27) emphasize the point that at lives less than 10^7 cycles significant differences are obtained in the shear stress conditions for cylinders of different K ratio. The elevated base pressure tests exhibit a similar difference between the 2.0 K ratio and 1.4 K ratio results. However the flattening out of the 10^7 life curve, as it approaches the static yield line is not reproduced on the curves for shorter lives. The behaviour of the 10^7 life curve was attributed to cyclic softening of the cylinder material. Cyclic softening must certainly have taken place in the results at shorter lives but the effect may have been masked by the general trend of the curves.

Previous attempts to relate the fatigue behaviour of thick walled cylinders to the results of standard fatigue tests have considered plots of the maximum range of shear stress against the mean shear stress, or against the maximum tensile stress, or against the maximum normal stress acting on planes of maximum shear stress (31). The maximum range of shear stress was found to be particularly successful in correlating the fatigue limit results of monobloc cylinder tests of various K ratios (24) and has therefore always been regarded as an important parameter. It also proved to be reasonably good in the mortal region, whereas a maximum tensile stress criterion places the smaller K ratio cylinders at longer lives than the higher K ratio cylinders (27). Criteria involving the maximum tensile stress or the maximum normal stress on planes of maximum shear stress in conjunction with the shear stress range suffer from the problem that monobloc cylinder results of different K ratios give a series of separate points at virtually constant shear stress range. The mean shear stress/shear stress range plot however, is perfectly acceptable in this respect. Burns and Parry (6) have shown already that basic fatigue data from push-pull or torsion tests can not be related in any simple way to the fatigue results from pressurised cylinders, and Fig. 12.1 does not clarify the situation any further. The graph does however provide constant life fatigue curves over a very wide range of both shear stress range and mean shear stress which may be used as basic design information for En.25.

So far no mention has been made of dynamic support cylinders in relation to either shear stress range or mean shear stress performance.

The dynamic support results have been plotted on the basis of bore shear stress range in Fig. 12.2 along with a band of results for monobloc cylinders of K ratios from 1.4 to 2.0 (24). The experimental dynamic support results lie within or very close to this band indicating the importance of bore shear stress range as a fatigue parameter. There is no gain plotting the dynamic support results on the mean shear stress / shear stress range graph as the mean shear stress is always half the maximum shear stress as in a monobloc cylinder. Thus dynamic support results should be exactly comparable with monobloc results on a shear stress basis. However one of the important effects of external support pressure is the reduction in maximum tensile hoop stress. It appears therefore that either the maximum tensile hoop stress has no influence in cylinder fatigue, or that the benefits of reduced hoop stress are cancelled out by the effects of higher cyclic internal pressures. These two alternatives are both somewhat unlikely but further conclusions can hardly be drawn from the limited experimental evidence. Whatever the explanation it appears that the best method of predicting the lives of dynamic support cylinders is on the basis of bore shear stress range data from monobloc cylinder tests, For a given K ratio and fatigue life this simply means that a dynamic support cylinder will withstand a cyclic internal pressure equal to the sum of the cyclic pressure withstood by a monobloc cylinder at the given life, and the maximum cyclic external pressure applied. That is for,

$$\tau_{range_d} = \tau_{range_m} \qquad \text{where d = dynamic support, m = monobloc.}$$

then $$\frac{K^2}{K^2-1} \cdot (p_{i\,max.} - p_{o\,max.})_d = \frac{K^2}{K^2-1}(p_{i\,max})_m$$

giving $$p_{i\,max.d} = p_{i\,max.m} + p_{o\,max.d.} \qquad (12.2)$$

if pressure ratio $\left(\frac{p_o}{p_i}\right)_d = r$

THEN $$p_{i\,max\,d} = \frac{p_{i\,max.m}}{1 - r.} \qquad (12.3)$$

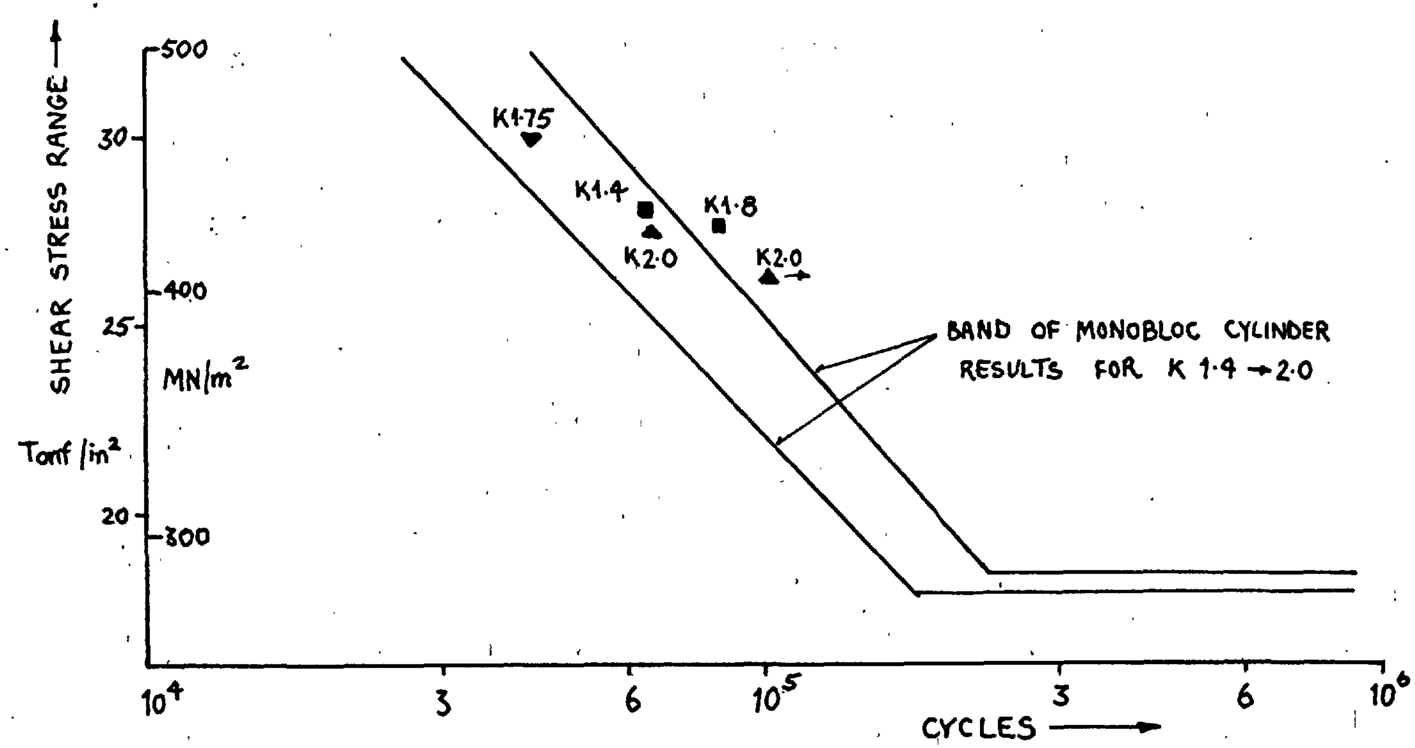

FIG. 12.2 BORE SHEAR STRESS RANGE AGAINST LIFE FOR DYNAMIC SUPPORT RESULTS

12.3.1 The 'Oil Effect' and Prediction of Fatigue Limit for Monobloc Cylinders.

The chief difficulty in predicting thick cylinder results lies not so much in reproducing or assessing the effect of the stress conditions in the cylinder but in reproducing and assessing the effect of the pressurised oil on the stress conditions. It is well known that a cylinder whose bore is protected from the direct effect of the oil pressure lives much longer than an unprotected cylinder. However bore protection still does not raise the fatigue strength of a cylinder to the value predicted by the torsional fatigue strength. Tests have been carried out by Frost and Burns (31) on thick cylinders with static and dynamic shear stresses in a pressure vessel. The results showed that the fatigue strength was unaffected by either Tellus 15 oil or mercury at high pressures and that there was still no correlation with thick cylinder results. It was suggested that the discrepancy might be attributed to some mechanical effect due to the repeated penetration of oil into the bore suface.

The complete lack of success of previous workers to relate thick cylinder results to other fatigue tests has resulted in more attention being given to the quantifying of the oil effect. Frost (72) first suggested that if fluid pressure penetrated microcracks in the bore of a cylinder then the Lame hoop stress would be augmented by the fluid pressure resulting in a nominal crack opening stress of 2 times the bore shear stress. Similar reasoning was put forward by Jones and Tomkins (34) in explanation of the effect of hydrostatic pressure on both the fatigue limit in torsion and thick cylinder fatigue. The effect of oil penetration was assessed for both the maximum shear stress and the stress normal to the maximum shear stress plane.

For an unprotected cylinder,

omitting the oil effect $\sigma_n = \dfrac{p}{K^2 - 1}$ and $\tau = \dfrac{K^2 p}{K^2 - 1}$ (12.4).

when the effect is included $\sigma_n = \dfrac{p}{K^2 - 1} + \dfrac{p}{2}$ and $\tau = \dfrac{K^2 p}{K^2 - 1} + \dfrac{p}{2}$ (12.5).

Jones and Tomkins showed that using the pressure modified stress expressions that cylinder and other fatigue results plotted on the basis of maximum range of shear stress against maximum normal stress on the plane of maximum shear stress were more consistent. An additional refinement of presenting the mean shear stress as a third parameter was suggested by Frost and Burns,(31) and served as a partial explanation of the scatter band. Thus the inclusion of an oil effect had helped to rationalise the mass of fatigue data but no simple relationship between cylinder fatigue and conventional tests had yet emerged.

Haslam (36) considered the problem as one of combined stress fatigue. It was known that cylinder fatigue results were independant of the intermediate principal stress (30) and thus a biaxial fatigue criterion would suffice. Gough's (15) elliptical equation was expressed in principal stress form and further simplification made by eliminating the torsional fatigue limit term. The simplified criterion is, $\sigma_1^2 + \sigma_3^2 = b^2$

where $\sigma_1 = \sigma_e$, $\sigma_3 = - p$, and b = uniaxial repeated transverse limit (12.6).

By substituting Lamé values in the equation we obtain

$$p = b\left\{\left\{\frac{K^2 + 1}{K^2 - 1}\right\} + 1\right\}^{-\frac{1}{2}} \qquad (12.7)$$

Haslam found that the fatigue limit of protected bore cylinders was accurately predicted by the equation, but that unprotected specimens had a much lower fatigue limit pressure. The oil effect was included as a term (n p) added to the Lamé hoop stress, and the value of n evaluated by the analysis of a wide range of cylinder fatigue data. Haslam found that the oil effect function n could be defined by the empirical equation,

$$n = \frac{5}{K + 1} \qquad (12.8).$$

and thus the effective hoop stress including the oil effect is given by,

$$\sigma_{\theta_{effective}} = \sigma_{\theta_{Lamé}} + \frac{5}{K + 1} p = \left\{ \frac{K^2 + 1}{K^2 - 1} + \frac{5}{K+1} \right\} p \qquad (12.9).$$

Substituting in equation (12.6) we obtain the fatigue limit of a cylinder subjected to repeated internal pressure as,

$$p = b \left[\left\{ \frac{K^2 + 1}{K^2 - 1} + \frac{5}{K + 1} \right\}^2 + 1 \right]^{-\frac{1}{2}} \qquad (12.10)$$

Although the equation is purely empirical and has no direct physical explanation in terms of the oil pressure effect it nevertheless works extremely well for a wide variety of materials and cylinder K ratios.

12.3.2 Prediction of Fatigue Limit for Static Support Cylinders.

In the context of the present work on fluid supported cylinders it is necessary to evaluate the usefulness of Haslam's approach. The effect of oil pressure on the bore Lame hoop stress should be the same whether or not the cylinder has external pressure. Thus using equation (12.9) we have,

$$\sigma_{\theta_{effective_{max.}}} = \left\{ \frac{K^2 + 1}{K^2 - 1} + \frac{5}{K + 1} \right\} p_{i_{max}} - \frac{2K^2}{K^2 - 1} po \qquad (12.11)$$

When the internal pressure is reduced to zero the oil pressure effect does not exist and the bore hoop stress is compressive. It is assumed that the compressive part of the cycle has no influence on the fatigue behaviour and may therefore be ignored. If the conventional maximum Lamé hoop stress itself is zero or compressive then the pressure effect alone will contribute to the effective tensile hoop stress value.

Substituting (12.11) in Gough's simplified principal stress criterion given in equation (12.6) we obtain,

$$\left[\left(\frac{K^2+1}{K^2-1}+\frac{5}{K+1}\right)^2+1\right]p_i^2-2\left(\frac{K^2+1}{K^2-1}+\frac{5}{K+1}\right)\left(\frac{2K^2\,p_o}{K^2-1}\right)p_i$$

$$+\left(\frac{2K^2}{K^2-1}\,p_o\right)^2-b^2=0 \qquad (12.12)$$

The solution to this equation may be expressed as,

$$p_i=\frac{AB}{A^2+1}\,p_o+\frac{\sqrt{b^2(A^2+1)-B^2p_o^{\,2}}}{A^2+1} \qquad (12.13)$$

where

$$A=\left(\frac{K^2+1}{K^2-1}+\frac{5}{K+1}\right) \quad \text{and} \quad B=\frac{2K^2}{K^2-1}$$

The endurance pressure in the bore of a cylinder of given K ratio, material, and static external support pressure can now be calculated. Three K ratios have been selected to test the method, two extremes K = 1.2 and K = 3.0, and the 1.75 K ratio used in the static support tests. The values of p_o used for the 1.75 K ratio case correspond to the experimental values used in the present work, whereas the p_o values used for the other K ratios were chosen merely for convenience. The value of b was calculated as 46.2 tonf/in^2 (714 MN/m^2) from the transverse rotating bending fatigue limit using the Gerber relationship. The predicted fatigue limit pressures are given in Table 12.1. The shear stress range (τ_{range}) and the mean shear stress (τ_{mean}) have also been calculated and are plotted in Fig. 12.3 for comparison with Burns and Parry's[4] experimental curve.

Fig 12.3 shows the predicted endurance lines for static support conditions above the repeated stress line, and for high base pressure conditions below the repeated stress line. It can be seen that the K = 1.75 curve for static support conditions follows the experimental curve closely, and that the K = 3.0 curve is quite good. The K = 1.2 curve however is less satisfactory. The linearity of the curves is surprising in view of the quadratic form of equation (12.13), and arises because $B^2 p_o^2$ is usually much smaller than $b^2 (A^2 + 1)$. Thus equation (12.13) may be simplified to a linear form

$$p_i = \frac{A\,B\,p_o}{A^2 + 1} + \frac{b}{(A^2 + 1)^{\frac{1}{2}}} \qquad (12.14).$$

The $\dfrac{b}{(A^2 + 1)^{\frac{1}{2}}}$ term is simply the endurance pressure of a monobloc cylinder without external pressure as given by equation (12.10). The gradient of equation (12.14) $\alpha = \dfrac{A\,B}{A^2 + 1}$ is dependent upon the cylinder K ratio as may be seen in Fig. 12.4. To assess the effect of the gradient variation on the shear stress range mean shear stress plot it is necessary to express equation (12.14) in terms of shear stress and mean shear stress.

TABLE 12.1

Predicted Fatigue Limit Pressures for Static Support Cylinders

K ratio	Static External Pressure		Predicted Cyclic Internal Pressure		Shear Stress Range		Mean Shear Stress	
	$Tonf/in^2$	MN/m^2	$Tonf/in^2$	MN/m^2	$Tonf/in^2$	MN/m^2	$Tonf/in^2$	MN/m^2
1.75	0	0	11.8	182	17.5	270	8.75	135
	6	93	16.1	249	15.0	232	3.05	47
	12	185	20.3	314	12.3	190	-2.8	-43
	17	263	23.7	366	9.95	154	-7.65	-118
	21.25	328	26.5	409	7.8	120	-9.3	-144
1.2	0	0	5.9	91	19.2	297	9.6	148
	4	62	9.2	142	30.0	463	2.0	31
	8	124	12.4	192	40.7	629	-5.75	-89
3.0	0	0	17.1	264	19.2	297	9.6	148
	12	185	26.0	402	29.2	451	1.15	18
	23	355	33.4	516	37.6	581	-7.1	-110

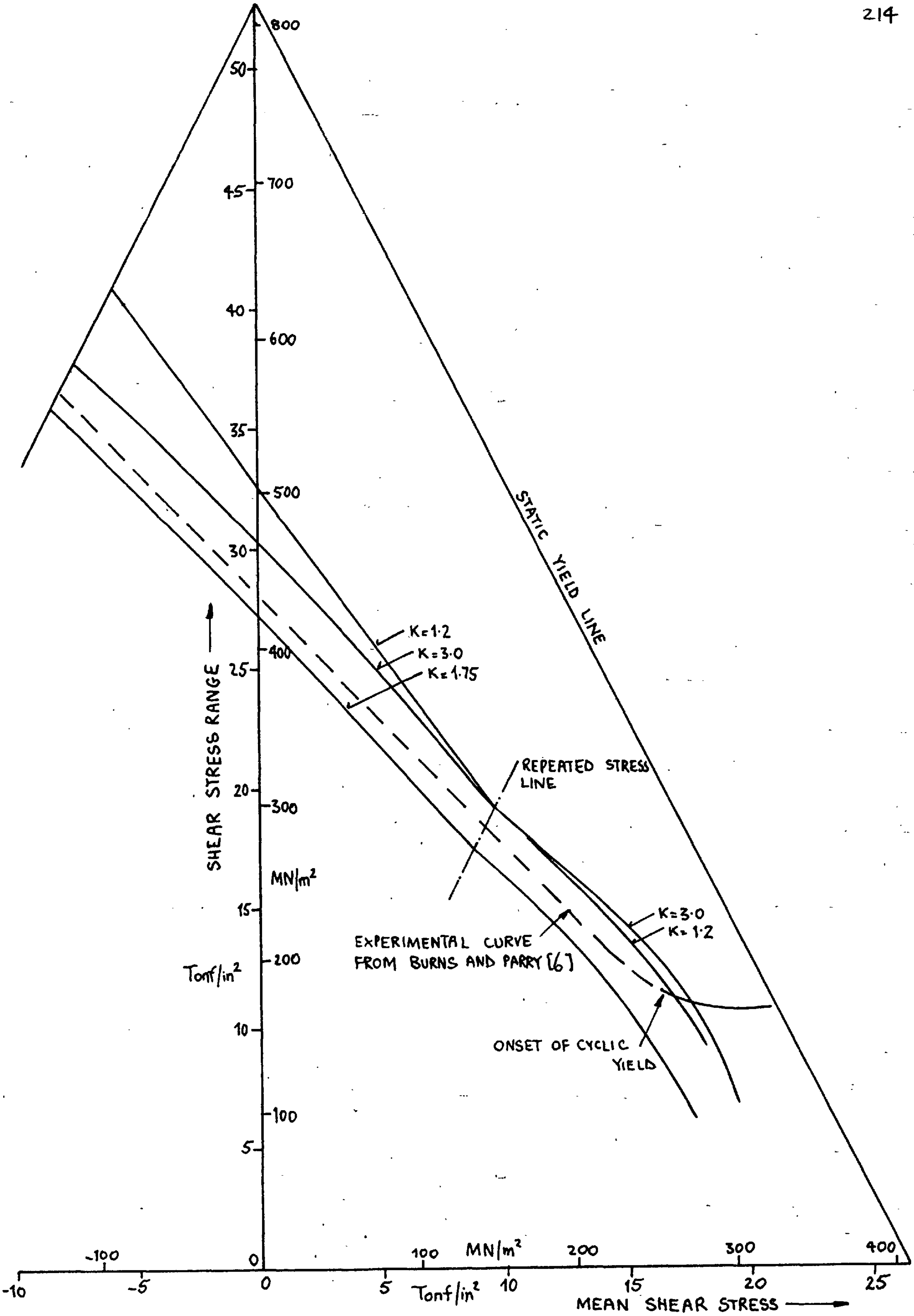

FIG. 12.3 PREDICTED FATIGUE LIMIT CURVES OF SHEAR STRESS RANGE AGAINST MEAN SHEAR STRESS AT THE BORE

From (12.14),

$$p_i = \alpha\, p_o + p_e \tag{12.15}$$

$$\tau_{range} = \frac{K^2}{K^2-1}\, p_i = \frac{K^2}{K^2-1}\,(\alpha\, p_o + p_e) \tag{12.16}$$

$$\tau_{mean} = \frac{K^2}{K^2-1}\left(\frac{p_i - 2p_o}{2}\right) = \frac{K^2}{K^2-1}\;\frac{(\alpha-2)\,p_o + p_e}{2} \tag{12.17}$$

Eliminating p_o from equations (12.16) and (12.17)

$$\tau_{range} = -\frac{2\alpha}{2-\alpha}\,\tau_{mean} + \frac{2}{2-\alpha}\cdot\frac{K^2}{K^2-1}\,p_e \tag{12.18}$$

Thus the gradient of the τ_{range}/τ_{mean} line is still a function of α, and the divergence of the K = 1.2 line on Fig. 12.3 is explained by the high value indicated in Fig. 12.4. It should be remembered that equation (12.18) has been derived from the simplified form of equation (12.13) and the reason that the K = 3.0 curve is not more divergent is that the $B^2\,p_o^{\,2}$ term is not negligible at the top end of the curve. A significant feature of Fig. 12.4 is the wide range of practical K ratios, from about K = 1.4 to K = 2.8, for which α varies only from 0.734 to 0.768 a total variation of less than 5%. It should also be noticed that $\frac{K^2}{K^2-1}\,p_e$ is the bore shear stress at the fatigue limit, which is known to be virtually independent of K ratio. Thus equation (12.18) predicts a τ_{range}/τ_{mean} relationship substantially independent of K ratio and of constant slope, which is confirmed by the limited experimental evidence available.

The high endurance region of Fig. 11.1 was defined from the 1.75 K ratio cylinder predictions given in Table 12.1.

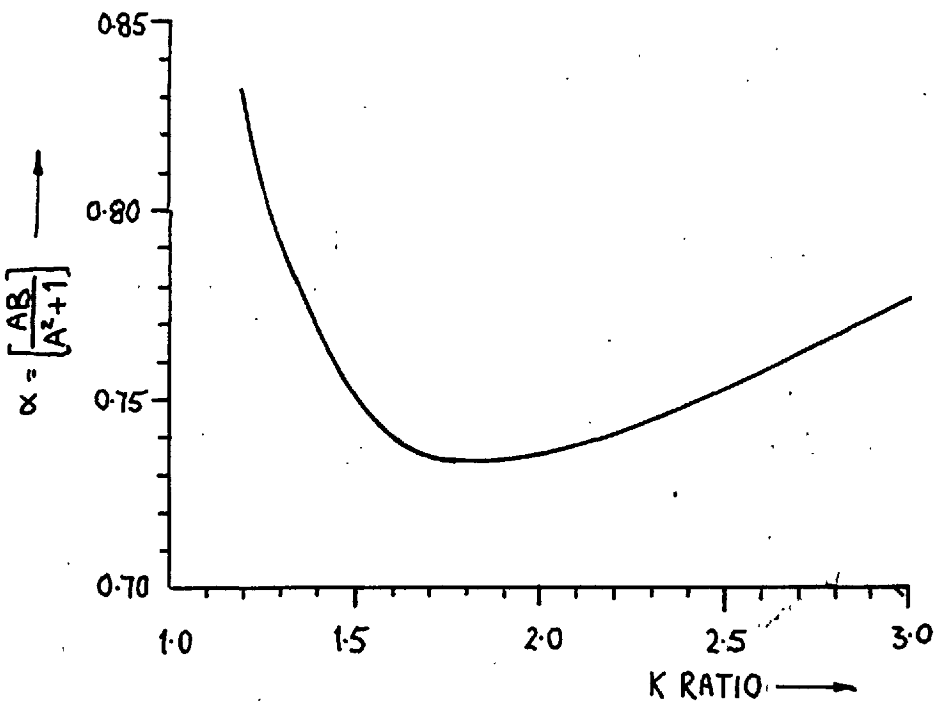

FIG. 12.4 PLOT OF $\alpha = \left[\frac{AB}{A^2+1}\right]$ AGAINST K RATIO

12.3.3 Prediction of Fatigue Limit for Cylinders with High Base Pressure

When a cylinder is subjected to cyclic internal pressures varying from a non zero minimum to a maximum the mean shear stress is raised, and the permissible range of shear stress is reduced. The 10^7 curve in Fig. 12.1 suggests that the linear τ_{range}/τ_{mean} relationship is continued until the onset of cyclic yielding. In the same way it could be argued that the curves obtained for static support conditions in Fig. 12.3 could be extrapolated beyond the repeated stress condition. However doing this would ignore the fact that when the base pressure is not zero the maximum hoop stress no longer reflects the range of stress. It is therefore necessary to introduce the minimum conditions of the fatigue cycle. The following analysis attempts to do this by an extension of Haslam's method for monobloc cylinders. Starting with the simplified Gough criterion in terms of principal stresses equation (12.6) it is proposed that the maximum conditions of the fatigue cycle are given by

$$\sigma_{1}{}^{2}_{max} + \sigma_{3}{}^{2}_{max} = b^{2}_{max} \qquad (12.19)$$

and the minimum conditions by,

$$\sigma_{1}{}^{2}_{min} + \sigma_{3}{}^{2}_{min} = b^{2}_{min} \qquad (12.20)$$

where

$$\sigma_{1_{max}} = \sigma_{\theta_{effective}} \qquad \text{when } p = p_{i_{max}},$$

that is

$$\sigma_{1_{max}} = \left(\frac{K^2+1}{K^2-1} + \frac{5}{K+1} \right) p_{i_{max}}$$

similarly

$$\sigma_{1_{min}} = \left(\frac{K^2+1}{K^2-1} + \frac{5}{K+1} \right) p_{i_{min}}$$

$$\sigma_{3_{max}} = -p_{i_{max}} \quad \text{and} \quad \sigma_{3_{min}} = -p_{i_{min}}$$

Substituting in (12.19 and (12.20) gives

$$b_{max} = p_{i_{max}} \sqrt{\left(\frac{K^2+1}{K^2-1} + \frac{5}{K+1} \right)^2 + 1} \qquad (1221)$$

$$b_{min} = p_{i_{min}} \sqrt{\left(\frac{K^2+1}{K^2-1} + \frac{5}{K+1} \right)^2 + 1} \qquad (12.22)$$

The fatigue conditions for b can now be defined as

$$b_{alternating} = \pm \frac{p_{i_{max}} - p_{i_{min}}}{2} \sqrt{\left(\frac{K^2+1}{K^2-1} + \frac{5}{K+1} \right)^2 + 1} \qquad (12.23)$$

$$b_{mean} = \frac{p_{i_{max}} + p_{i_{min}}}{2} \sqrt{\left(\frac{K^2+1}{K^2-1} + \frac{5}{K+1} \right)^2 + 1} \qquad (12.24)$$

The expressions may now be linked to the transverse alternating fatigue limit b_{a_o} by the Gerber relationship,

$$\sigma_{a_m} = \sigma_{a_o} \left[1 - \left(\frac{\sigma_m}{\sigma_u} \right)^2 \right] \qquad (12.25)$$

where

σ_{a_m} = alternating stress at mean stress σ_m,

σ_{a_o} = alternating stress at zero mean stress,

σ_u = ultimate tensile stress.

Substituting from equations (12.23) and (12.24) in (12.25) gives,

$$\frac{p_{i_{max}} - p_{i_{min}}}{2} \sqrt{A^2+1} = b_{a_o} \left[1 - \left\{ \frac{p_{i_{max}} + p_{i_{min}}}{2} \sqrt{A^2+1} \right\}^2_u \right] \qquad (12.26)$$

where $A = \sqrt{\left(\frac{K^2+1}{K^2-1} + \frac{5}{K+1} \right)^2 + 1}$

Equation (12.26) has been used to predict the maximum internal pressures at the fatigue limit for K ratios of 1.2, 1.75, and 3.0, and for various base pressure conditions. The pressures and corresponding shear stresses are listed in Table 12.2 and plotted in Fig. 12.3.

TABLE 12.2

Predicted Fatigue Limit Conditions with Elevated Base Pressure

K ratio	Base Pressure		Predicted Max Cyclic Pressure		Shear Stress Range		Mean Shear Stress	
	Tonf/in^2	MN/m^2	Tonf/in^2	MN/m^2	Tonf/in^2	MN/m^2	Tonf/in^2	MN/m^2
1.75	5.5	85	13.5	208	11.9	184	14.15	218
	10.0	154	14.05	217	6.0	93	17.8	275
1.2	2.0	31	6.55	101	14.9	230	13.9	215
	4.0	62	6.95	107	9.8	151	17.9	276
3.0	5.0	77	18.8	290	15.5	239	13.4	207
	10.0	154	20.5	316	11.8	182	17.2	266
	14.0	216	20.5	316	7.3	113	19.4	300

Fig. 12.3 shows that up to the point of cyclic yield the predicted curves follow the trend of the experimental curve faithfully. The agreement is better than that which would result from extrapolation of the static support curves. Beyond a mean shear stress of about 16 Tonf/in^2 (247 MN/m^2) the predictions should be ignored.

12.3.4 Prediction of Fatigue Limit for Dynamic Support Cylinders.

It was shown in Section 12.2 that in the mortal region the lives of dynamic support cylinders can be correlated simply on the basis of shear stress range. If in the absence of experimental results we assume that bore shear stress range is also the governing factor at the fatigue limit then the opportunity arises to assess the oil effect factor directly. The effective hoop stress in a dynamic support cylinder may be expressed as,

$$\sigma_{\theta_{effective}} = \left\{ \frac{K^2+1}{K^2-1} + n \right\} p_{i_d} - \frac{2K^2}{K^2-1}. \; p_{o_d} \qquad (12.27).$$

where n = oil effect factor.

Similarly in a monobloc cylinder,

$$\sigma_{\theta_{effective}} = \left\{ \frac{K^2+1}{K^2-1} + n \right\} p_{i_m} \qquad (12.28)$$

Substituting from (12.2) and equating (12.27) and (12.28) gives

$$\left\{ \frac{K^2+1}{K^2-1} + n \right\} p_{i_d} - \frac{2K^2}{K^2-1} \; p_{o_d} = \left\{ \frac{K^2+1}{K^2-1} + n \right\} \left\{ p_{i_d} - p_{o_d} \right\}$$

$$\text{hence } n = \frac{2K^2}{K^2-1} - \frac{K^2+1}{K^2-1} = 1$$

This is the oil effect factor suggested first by Frost (72) and subsequently by Jones and Tompkins (34), to account in a simple way for the effect of pressure in microcracks. However Haslam (37) has shown that in order to predict the fatigue behaviour of monobloc cylinders using Gough's combined stress criterion it is necessary to employ an oil effect factor of $\frac{5}{K + 1}$ p_i. If Haslam's factor were used to predict the endurance conditions of a dynamic support cylinder then the analysis would be identical to that detailed in Section 12.3.2 on static support cylinders. There would be no difference in the predicted cyclic internal pressure at the fatigue limit between a cylinder with static external pressure, and a cylinder with cyclic external pressure having the same maximum cyclic external pressure as the static external pressure. However the experimental evidence indicates that certainly in the mortal range dynamic support cylinders have greater fatigue resistance than corresponding static support cylinders. For example a 1.75 K ratio cylinder with 9 Tonf/in^2 (139 MN/m^2) static external pressure can withstand a cyclic internal pressure of about 25 Tonf/in^2 (386 MN/m^2) for 42,000 cycles, compared with 29 Tonf/in^2 (448 MN/m^2) when the external pressure cycles between o and 9 Tonf/in^2 (139 MN/m^2).

The fatigue limit of dynamic support cylinders is probably best estimated on a shear stress range basis by using equation (12.2) in conjunction with the monombloc fatigue limit pressure for identical material and K ratio. The monobloc fatigue limit may of course be predicted by Haslam's approach described in Section 12.3.1. However, the estimation of dynamic support fatigue limit conditions is essentially speculative until experimental results becombe available for this regime.

12.4 Fatigue Behaviour in the Mortal Region.

12.4.1. Introduction.

The work so far in this chapter has been concerned with the fatigue behaviour of cylinders at high endurances over a wide range of loading conditions. The analysis of fatigue limits has provided a datum from which the prediction of fatigue lives in the mortal region can now be built. The success of the predictions in the mortal region can be judged against the experimental data gained from the present work.

The analysis may be approached either by relating the elastic-plastic conditions in a cylinder to low endurance fatigue data by the Coffin-Manson Law, or by employing fracture mechanics to relate the cylinder conditions to crack propogation in simple specimens. The fracture mechanics analysis will be examined first.

12.4.2. Fracture Mechanics Analysis of Fatigue Behaviour.

The fracture mechanics approach makes use of the concept of the stress intensity factor K_1, which represents the stress field at a crack tip. It has been shown (14) that in fatigue the rate of fatigue growth is related to the range of stress intensity factor by the expression,

$$\frac{da}{dN} = B.(\Delta K)^m \qquad (12.29).$$

where a = crack length (for an edge crack),

N = number of cycles,

B = material constant.

ΔK = range of stress intensity factor,

and m = material constant.

Equation (12.29) applies only to an elastic situation. However it has already been demonstrated that the fatigue behaviour of a thick-walled cylinder beyond yield is essentially elastic after a few cycles, and thus the use of linear elastic fracture mechanics is justified. The attraction of linear elastic fracture mechanics in fatigue lies in the fact that once a master curve for a particular material relating fatigue crack growth rate and range of stress intensity factor is available then the growth rate in any cracked body configuration can be predicted.

Stress intensity factors are now known for a wide range of cracked configurations, and often more complex geometries can be successfully represented by simpler known solutions.

Haslam (38) has applied fracture mechanics to the analysis of a monobloc cylinder by using a compromise stress intensity factor K_1 given by,

$$K_1 = \sigma(\pi a)^{\frac{1}{2}} \qquad (12.30)$$

This expression lies between the respective standard equations for a straight-fronted, and a semi-circular fronted edge crack in a semi-infinite plate subjected to a gross stress, σ.

Substituting (12.30) in (12.29) and integrating over the whole fatigue life span from an initial crack length (a_o) to a final crack length (a_c) equal to the cylinder wall thickness gives,

$$N = \frac{2}{2 - m} \quad \frac{1}{B\,\sigma^m\,\pi^{\frac{m}{2}}} \quad \left[a^{\frac{2-m}{2}} \right]_{a_o}^{a_c} \text{cycles.} \qquad (12.31)$$

Values for the constants in the above equation may be obtained from the work of Frost, Pook and Denton (20) and equation (12.29). Substitution of the appropriate constants for steel in (12.31) gives

$$N = \frac{110}{\sigma^3} \left[\frac{1}{\sqrt{a_o}} - \frac{1}{\sqrt{a_c}} \right] 10^6 \text{ cycles.}$$

but as the initial crack length is very much smaller than the cylinder wall thickness the above equation reduces to

$$N = \frac{110}{\sigma^3} \quad \frac{1}{\sqrt{a_o}} . \ 10^6 \text{ cycles} \qquad (12.32).$$

This equation is in Imperial Units and σ must be expressed as $Tonf/in^2$, and a_o in inches.

The initial crack length is taken as the length of crack which will just fail to propagate at the fatigue limit, and may be calculated from,

$$a_o = \frac{c}{\left(\frac{1}{2}\,\sigma_{effective}\right)^3} \qquad (12.33).$$

where c is a material constant given for a range of conditions by Frost and Greenan (73), and $\sigma_{effective}$ is the effective hoop stress at the fatigue limit of the cylinder.

From (12.10) endurance pressure $p = b\left\{\left(\frac{K^2+1}{K^2-1} + \frac{5}{K+1}\right)^2 + 1\right\}^{-\frac{1}{2}}$

Substituting in (12.9)

$$\sigma_{\theta\,effective} \text{ at endurance} = \frac{b}{\sqrt{1 + \left\{\dfrac{1}{\dfrac{K^2+1}{K^2-1} + \dfrac{5}{K+1}}\right\}^2}} \qquad (12.34)$$

The σ term in equation (12.32) is the local effective repeated tensile hoop stress as given by (12.9) that is,

$$\sigma = \left\{\frac{K^2+1}{K^2-1} + \frac{5}{K+1}\right\} p_i$$

Thus by substituting for a_o and σ in equation (12.32) Haslam was able to obtain relationships between N and p_i for particular materials and K ratios. The agreement between the predicted curves and experimental results was quite satisfactory for ferrous materials.

It is now appropriate to examine how the fracture mechanics approach may be employed to predict the experimental results obtained in the present work. Considering first the static support condition along with the simple unsupported case, the endurance pressures have already been calculated and are listed in Table 12.1. It is reasonable (74) to calculate the range of intensity factor K on the assumption that the crack is completely closed on the compressive part of the cycle, and that the effective cycle is from zero to the maximum tensile condition.

Thus the value of σ in equation (12.32) may be taken from equation (12.11)

$$\sigma = \left[\frac{K^2+1}{K^2-1} + \frac{5}{K+1}\right]p_i - \frac{2K^2}{K^2-1}\ p_o$$

Similarly equation (12.11) may be used to calculate $\sigma_{effective}$ by substituting the endurance pressure from Table 12.1 along with the corresponding external pressure value. For repeated stress conditions in steels the value of c in equation (12.33) is 0.7 $(\text{Tonf/in}^2)^3$ in (73).

For a K ratio of 1.75 in En 25 steel and taking b = 46.2 Tonf/in^2 the following equations are predicted from equation (12.32) for particular external pressures.

$$\left.\begin{aligned}
p_o &= 0, & N &= \frac{254}{p_i^3} \cdot 10^6 \text{ cycles.}\\
p_o &= 6 \text{ Tonf/in}^2, & N &= \frac{131}{(3.79p_i - 17.8)^3} \cdot 10^8 \text{ cycles.}\\
p_o &= 12 \text{ Tonf/in}^2, & N &= \frac{124}{(3.79p_i - 35.6)^3} \cdot 10^8 \text{ cycles.}\\
p_o &= 17 \text{ Tonf/in}^2, & N &= \frac{114}{(3.79p_i - 50.5)^3} \cdot 10^8 \text{ cycles.}\\
p_o &= 21.25 \text{ Tonf/in}^2, & N &= \frac{106}{(3.79p_i - 63.1)^3} \cdot 10^8 \text{ cycles.}
\end{aligned}\right\} \quad (12.35).$$

The curves for equations (12.35) have been plotted individually against the experimental data in Figs. 12.5 to 12.9. The curves have been terminated at high pressures by the collapse pressures given in Appendix 1.4 and at low pressures by the endurance pressures listed in Table 12.1. The predicted curve for the unsupported case Fig. 12.5 is in good agreement with the experimental results and gives a slightly conservative prediction.

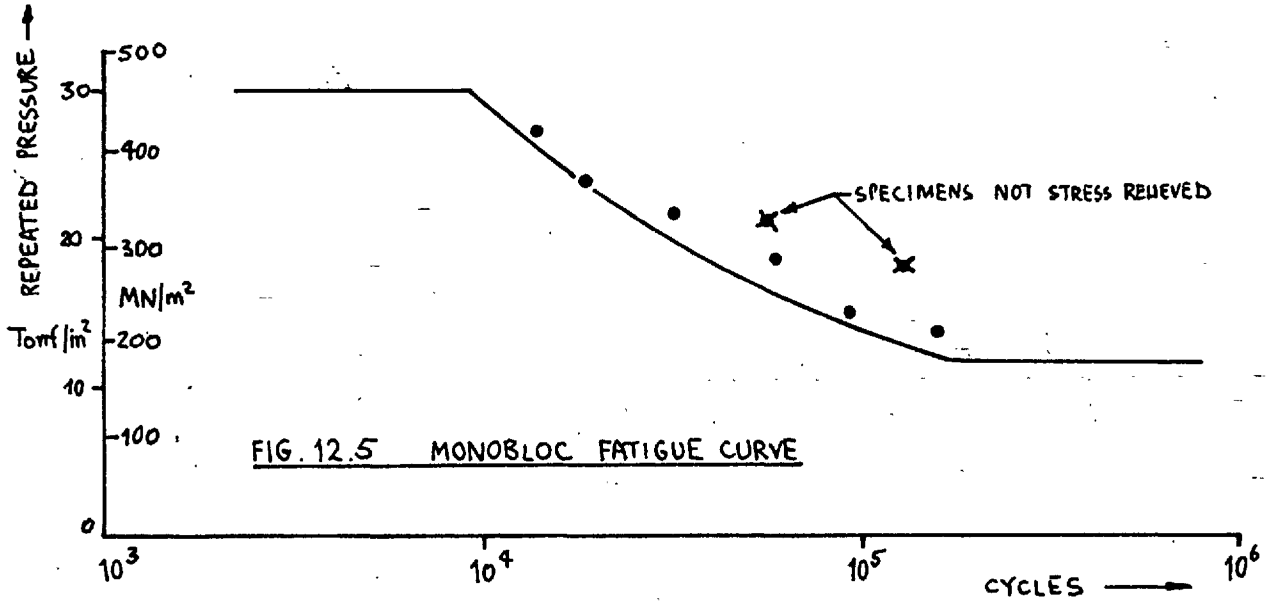

FIG. 12.5 MONOBLOC FATIGUE CURVE

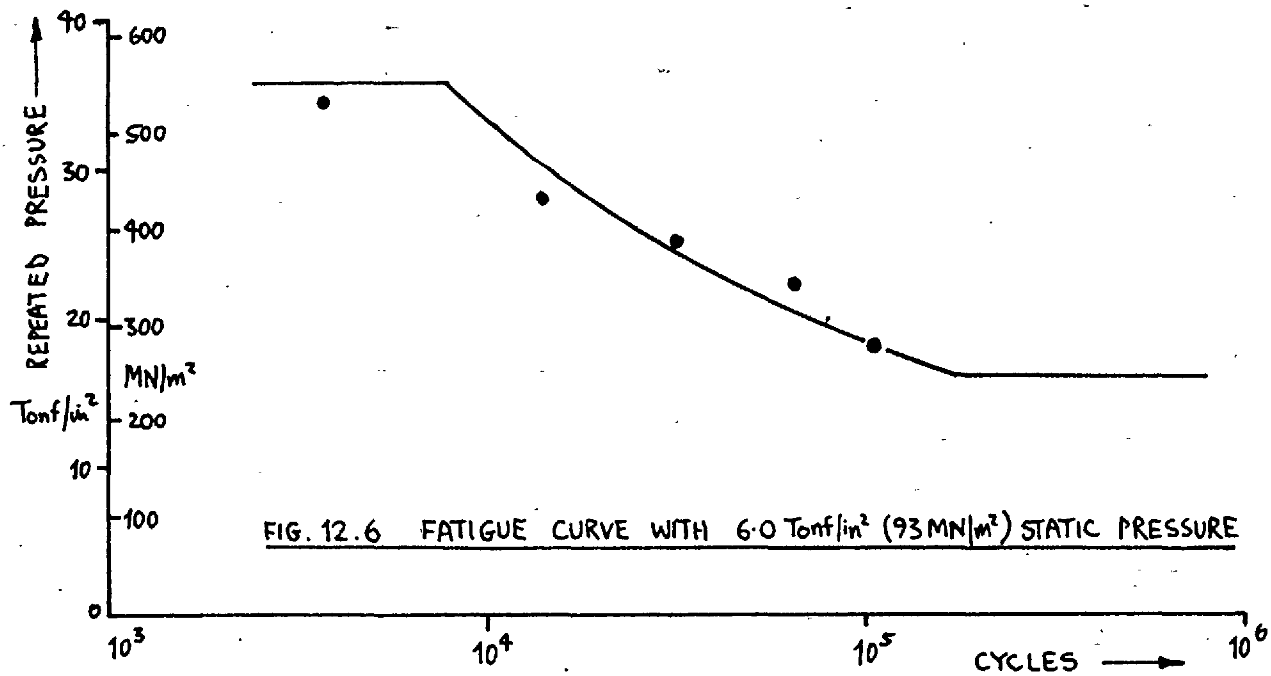

FIG. 12.6 FATIGUE CURVE WITH 6·0 Tonf/in² (93 MN/m²) STATIC PRESSURE

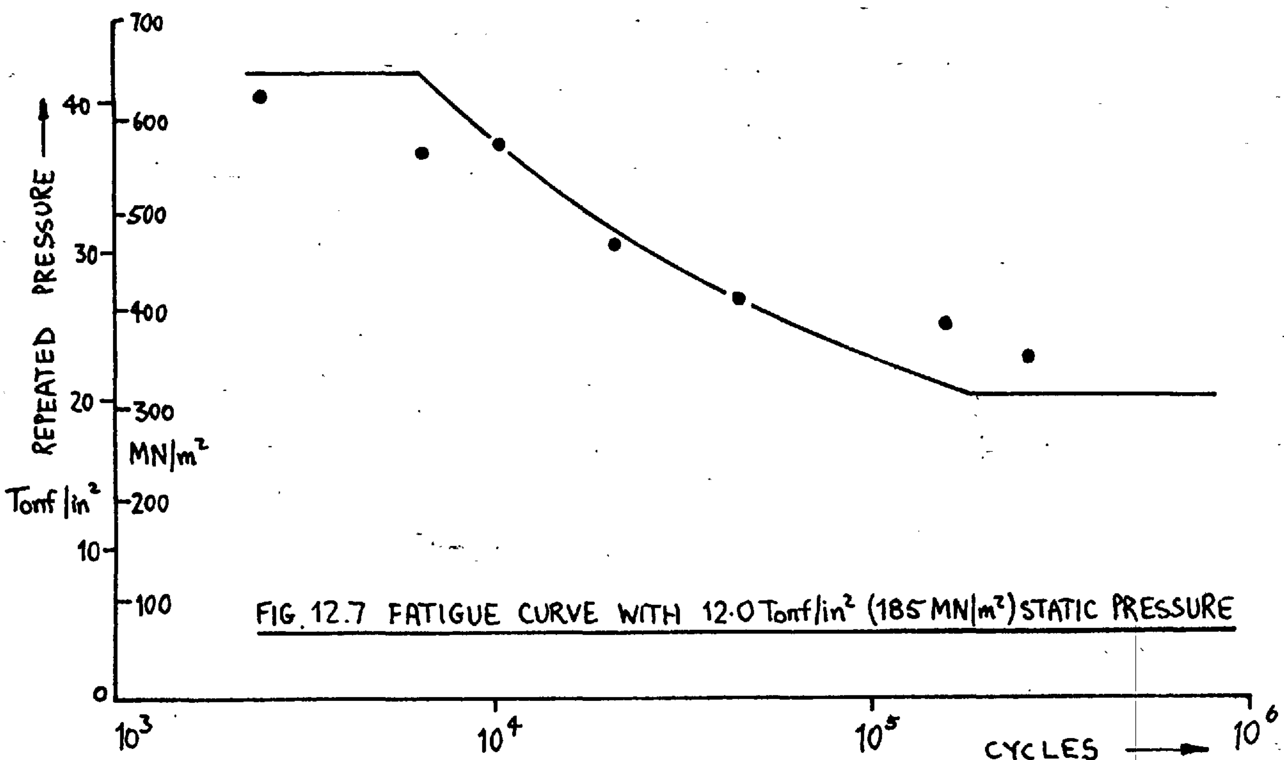

FIG. 12.7 FATIGUE CURVE WITH 12·0 Tonf/in² (185 MN/m²) STATIC PRESSURE

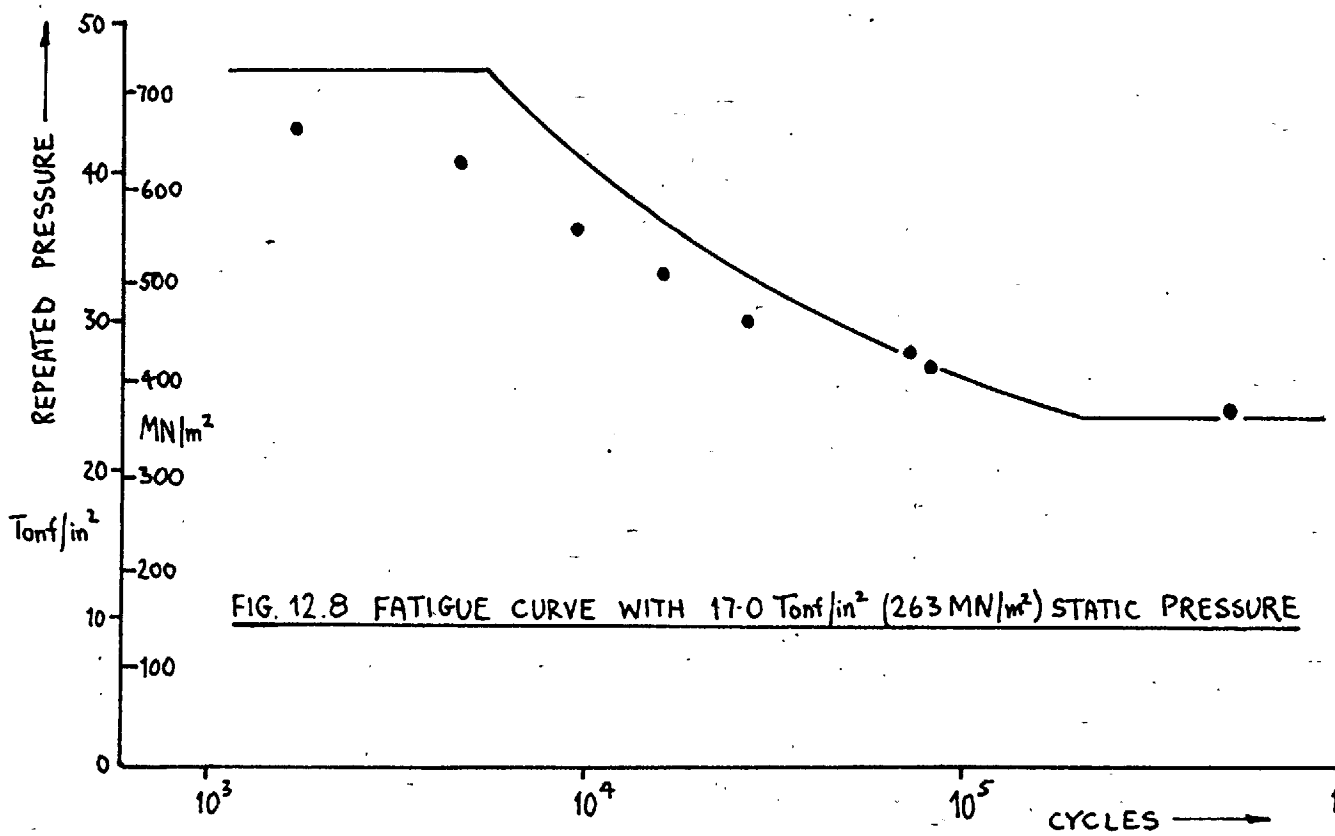

FIG. 12.8 FATIGUE CURVE WITH 17·0 Tonf/in² (263 MN/m²) STATIC PRESSURE

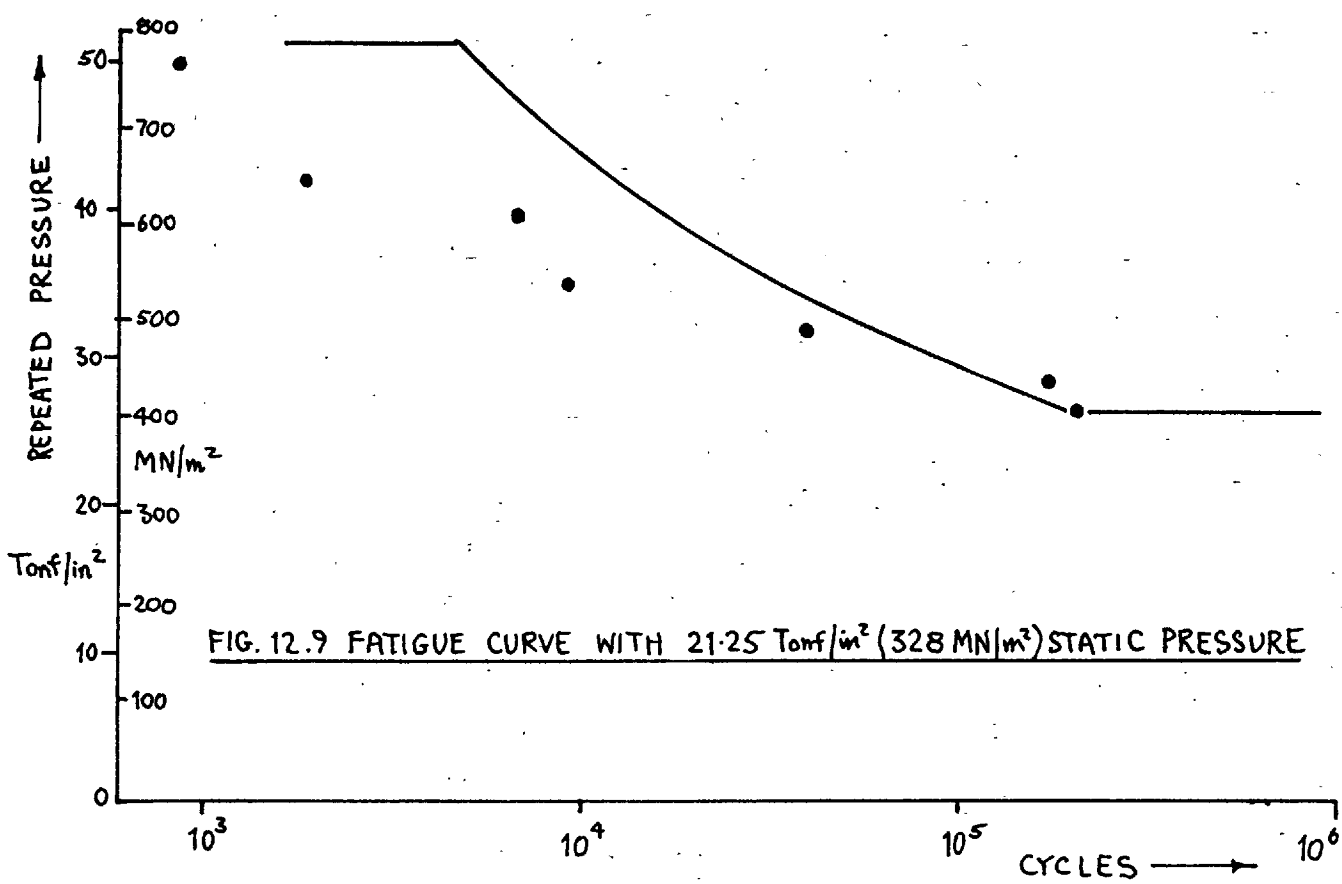

FIG. 12.9 FATIGUE CURVE WITH 21·25 Tonf/in² (328 MN/m²) STATIC PRESSURE

The same effect occurred in Haslam's (38) prediction of 1.8 K ratio cylinder behaviour. The predicted curves for static external pressures of 6 and 12 Tonf/in^2 (93 and 185 MN/m^2) Figs. 12.6 and 12.7 are in very good agreement with the experimental results, although in the region of the collapse pressure it is clearly unrealistic to suggest as the curve does that the transition between fatigue and collapse is sudden In the case of ~~Figs. 12.8 and 12.9~~ the 17 and 21.25 Tonf/in^2 (263 and 328 MN/m^2) external pressure results Figs 12.8 and 12.9 the predicted curves lie on the optimistic or dangerous side of the experimental results. The reason for this discrepancy may probably be attributed to the high external pressures giving rise to plasticity effects at the crack tip which are no longer dealt with by simple linear elastic fracture mechanics. The predicted curves have been summarised for comparison in Fig. 12.10.

The analysis of the high base pressure results once again requires special consideration because of the non zero minimum conditions of the fatigue cycle. The first task is to calculate a_o in equation (12.33). The experimental results were obtained for a constant minimum pressure of 5.5 Tonf/in^2 (85 MN/m^2) and for an En25 cylinder of 1.75 K ratio the maximum internal pressure at the fatigue limit has been calculated as 13.5 Tonf/in^2 (208 MN/m^2). The effective hoop stress at the fatigue limit may be expressed in terms of mean and alternating components as follows:

$$\text{mean } \sigma_{\theta\,\text{effective}} = \left\{\frac{K^2+1}{K^2-1} + \frac{5}{K+1}\right\}\left\{\frac{p_{i\,max} + p_{i\,min}}{2}\right\} \quad (12.36)$$

$$\text{alternating } \sigma_{\theta\,\text{effective}} = \pm\left\{\frac{K^2+1}{K^2-1} + \frac{5}{K+1}\right\}\left\{\frac{p_{i\,max} - p_{i\,min}}{2}\right\} \quad (12.37)$$

and the ratio

$$\frac{\text{mean } \sigma_{\theta\,\text{effective}}}{\text{alternating } \sigma_{\theta\,\text{effective}}} = \frac{p_{i\,max} + p_{i\,min}}{p_{i\,max} - p_{i\,min}}. \quad (12.38).$$

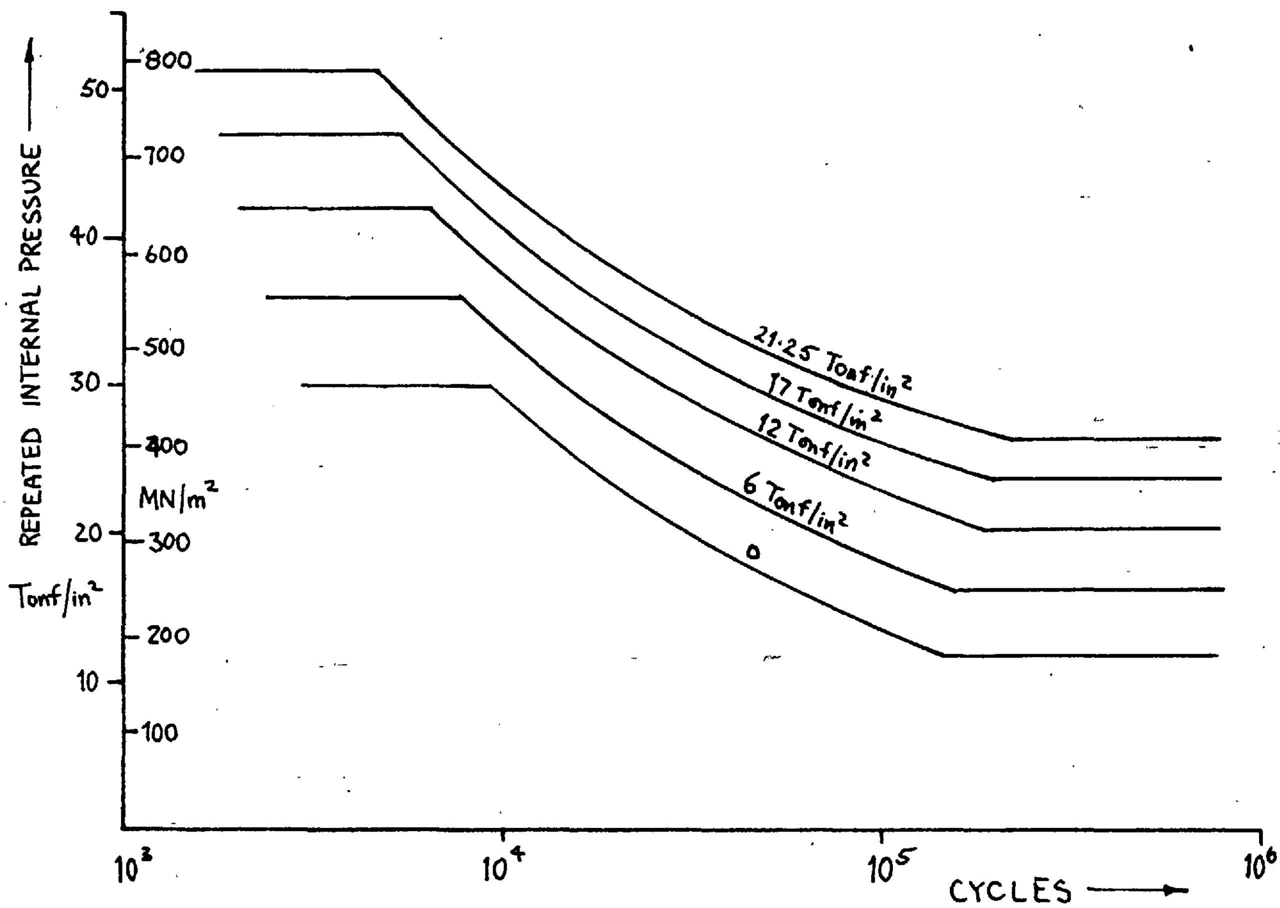

FIG. 12.10 COMBINED STATIC SUPPORT AND MONOBLOC FATIGUE CURVES

The ratio in equation (12.38) is necessary for the selection of the appropriate value of the constant c in equation(12.33) from the work of Frost and Greenan (73). In the case of $p_{i\ max} = 13.5$ Tonf/in^2 and $p_{imin} = 5.5$ Tonf/in^2, c is given as 0.33 (Tonf/in^2)^{3}in. As equation (12.37) gives the alternating component (σ_a) equation (12.33) becomes simply

$$a_o = \frac{c}{\sigma_a^{3}}$$

Substitution for c and σ_a gives $a_o = 0.94 \cdot 10^{-4}$in (2.4μm).
The tensile hoop stress range σ which determines the range of stress intensity factor is given by

$$\sigma = \left\{ \frac{K^2+1}{K^2-1} + \frac{5}{K+1} \right\} \left\{ p_{i\ max} - p_{i\ min} \right\} \qquad (12.39)$$

In spite of the higher mean stress conditions present in higher base pressure tests it is legitimate to use the same material constants B and m in equation (12.29) so that the governing equation (12.32) may still be used. The justification for this statement lies in the work of Frost, Pook and Denton (20). It was found that for steel, the range of stress intensity factor / crack growth rate data fall into a narrow band irrespective of the value of R, the ratio minimum stress / maximum stress. This implies that the material is insensitive to mean stress.

It is now possible to substitute the various conditions in equation (12.32) and obtain the following general fatigue equation for the case of $p_{i\ min} = 5.5$ Tonf/in^2,

$$N = \frac{113.5}{\left\{3.79\ (p_{i\ max.} - 5.5)\right\}^2}\ 10^8 \qquad (12.40)$$

The curve is plotted for comparison against the experimental results in Fig. 11.2. Although the experimental results are rather scattered the curve is in good agreement with the general trend.

If the fracture mechanics approach were employed to analyse the fatigue behaviour of dynamic support cylinders in the mortal region then the analysis would duplicate the static support analysis. The duplication arises because having neglected the part of the static support cycle where the effective hoop stress is compressive the static and dynamic cycles are identical. The fracture mechanics approach may however be used to establish the basis monobloc fatigue curve in the mortal region and then dynamic support behaviour can be predicted on the basis of shear stress range by equation (12.2)

12.4.3. Fracture Mechanics Analysis of Crack Propagation.

The fracture mechanics approach may be used to predict the propagations of a crack throughout the life of a component, or at least until the onset of fast fracture. In view of the experimental evidence for the presence or absence of cracks at various stages of cylinder life presented in Section 11.5.4 of the previous chapter it is interesting to predict the stage at which a visible crack should appear. From equations (12.29) and (12.31) and after substituting the appropriate constants for steel the following general equation may be derived,

$$N_r = \frac{110}{\sigma^3} \left\{ \frac{1}{\sqrt{a_o}} - \frac{1}{\sqrt{a_r}} \right\} \cdot 10^6 \qquad (12.41)$$

where a_r is the crack length after N_r cycles have elapsed.

The total life to failure (N_t) is given by equation (12.32) that is

$$N_t = \frac{110}{\sigma^3} \frac{1}{\sqrt{a_o}} 10^6$$

If equation (12.41) is divided by equation (12.32) then,

$$\frac{N_r}{N_t} = 1 - \left\{ \frac{a_r}{a_o} \right\}^{-\frac{1}{2}} \qquad (12.42)$$

This expression is plotted in Fig. 12.11 and it can be seen that roughly 70% of the total life is spent in propagating an initial crack to ten times its original length. As an example consider an En 25 monobloc cylinder of 1.75 K ratio. The initial crack length (a_o) can be calculated from equations (12.33) and (12.34) as approximately $0.6.10^{-4}$in (1.5μm). If we assume that an axial crack about 3.10^{-3}in (0.076 mm) is the minimum length which could be detected by eye then $a_r = \frac{1}{2}.\ 3.10^{-3}\text{in} = 1.5.10^{-3}$in assuming a semi-circular crack surface.

$$\text{Thus } \frac{a_r}{a_o} = 25.$$

From Fig 12.11 it can be seen that this condition is satisfied only when 80% of the total life has been spent. The analysis does therefore confirm the experimental observation that cracks can be detected only very late in the specimen life.

12.5. Low Cycle Fatigue Analysis.

The previous section has shown that the technique of fracture mechanics can be successfully applied to the fatigue behaviour of thick-walled cylinders. It is proposed in this section to examine whether low cycle fatigue analysis, often referred to as the Manson - Coffin approach, can more easily or successfully be applied to thick-walled cylinder fatigue behaviour. The objective is to relate the cylinder fatigue results to basic low cycle fatigue information which is generally available, or can be easily deduced, for a wide range of materials. In this way the results of the test programme become more widely applicable and are not restricted to the cylinder geometry and material used.

Low cycle fatigue analysis is generally related to fatigue data from push-pull strain cycling although reversed torsion data is also used.

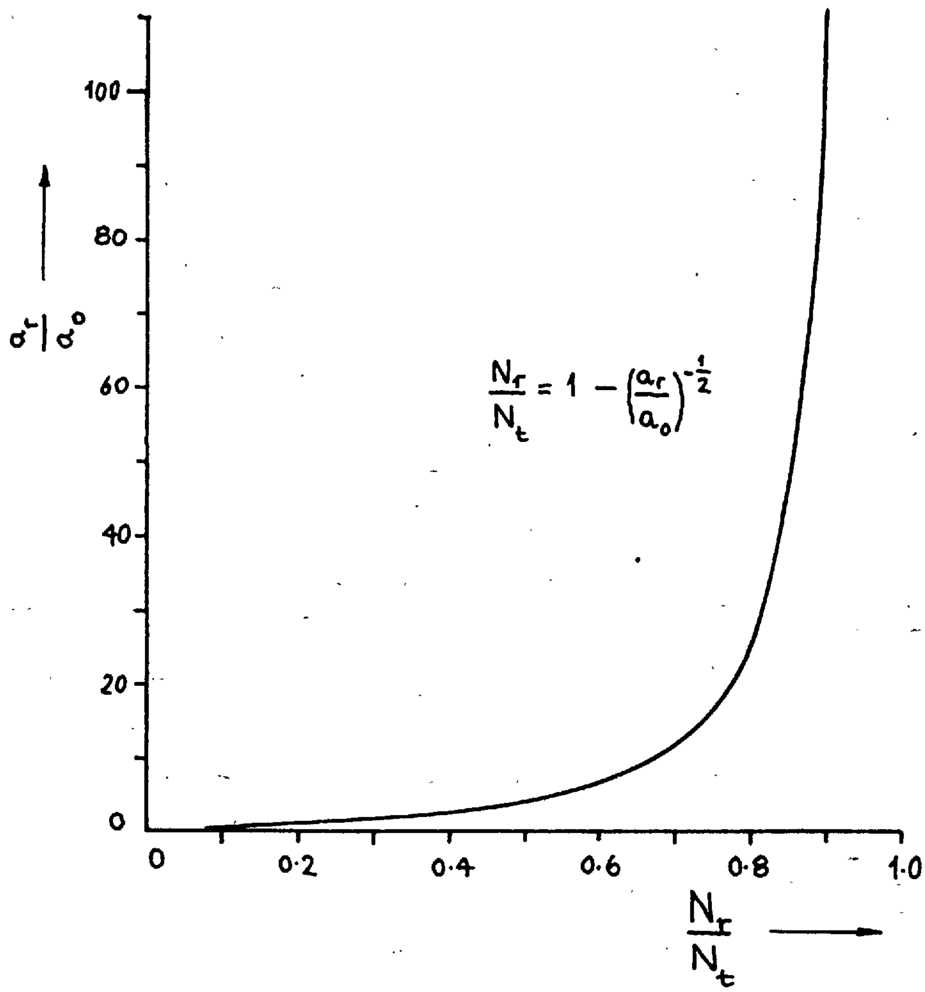

FIG. 12.11 CRACK PROPAGATION ANALYSIS

Push-pull testing is relatively simple and the nature of the test avoids the complications which would be introduced by the presence of a mean strain. Since the stress strain characteristics of most materials are altered by progressive cyclic straining the cyclic stress range may either increase or decrease depending on whether the material cycically strain hardens or strain softens. It was recorded in Section 10.3.2 that En 25 falls into the latter category. After relatively few cycles the stress range settles down to a fairly constant value known as the asymptotic stress range. Normally a standardised asymptotic stress range is assumed to occur at half the life to failure. The asymptotic cyclic stress strain characteristic is defined as a result of a number of tests at different strain ranges.

Manson (14) found that the plastic strain per cycle (ϵ_p) was related to the cyclic life (N_f) by a power law of the form,

$$\epsilon_p = M N_f^{z} \qquad (12.43).$$

where M and z are constants.

Coffin (75) suggested that $z = -\frac{1}{2}$ was universally applicable to all materials, and equation (12.43) is normally known as the Manson - Coffin Law.

If the asymptotic stress range ($\Delta\sigma$) is divided by the elastic modulus (E) the quotient can be regarded as the elastic strain range (ϵ_{el}) associated with the cyclic life of (N_f). It was found for many materials a power law was also justified of the form,

$$\frac{\Delta\sigma}{E} = \epsilon_{el} = \frac{G}{E} N_f^{\gamma} \qquad (12.44).$$

where G and γ are constants.

Fig. 12.12 shows the asymptotic stress range curve for En 25 in the same condition as the present test material from the work of Mackenzie and Benham (76) and White et al (77).

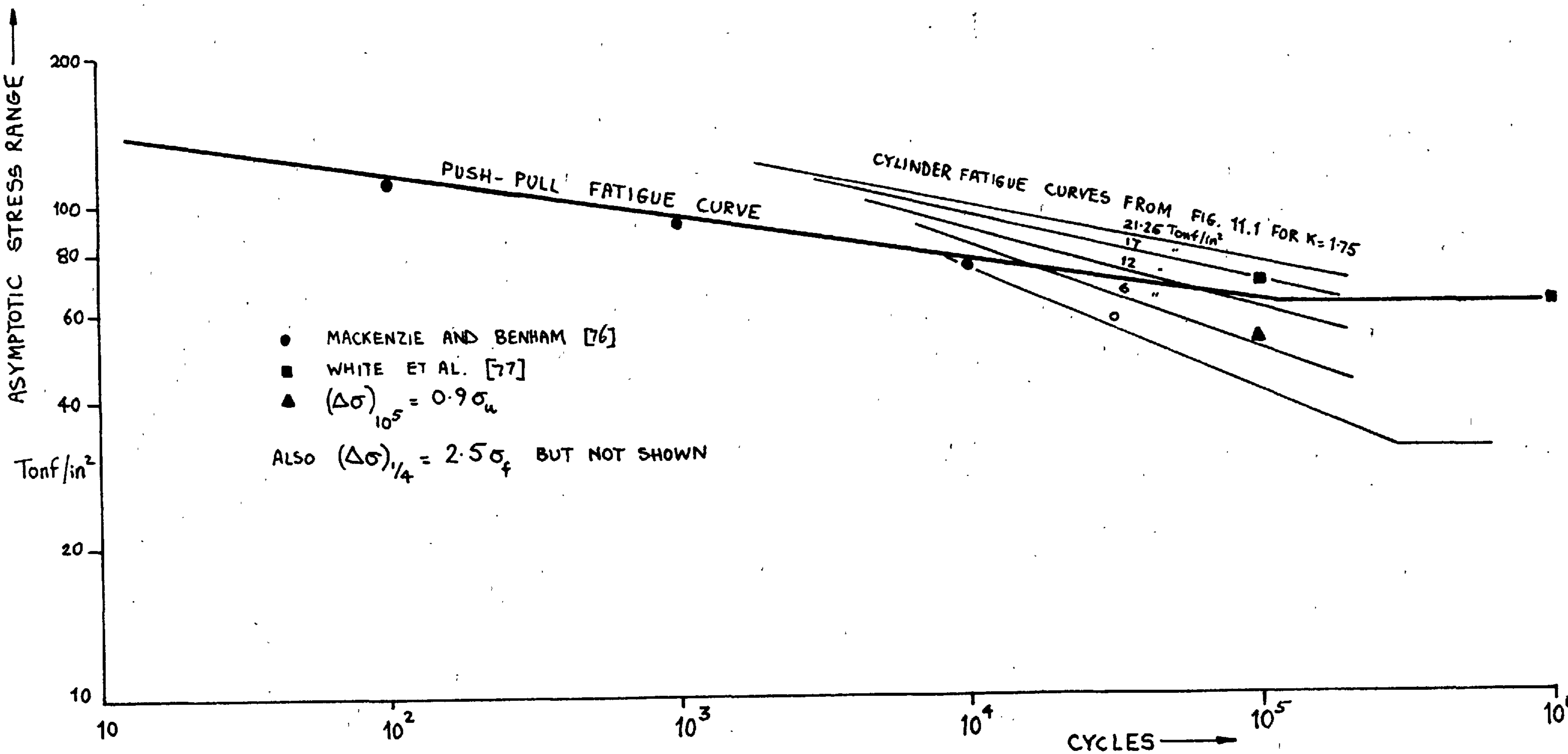

FIG. 12.12 PUSH-PULL AND CYLINDER FATIGUE RESULTS FOR EN 25 STEEL

The total strain range ($\Delta\epsilon$) is obtained by combining the plastic and elastic components from equations 12.43 and (12.44) to give,

$$\Delta\epsilon = M N_f^{z} + \frac{G}{E} N_f^{\gamma} \qquad (12.45).$$

A major attraction of the Manson - Coffin approach lies in a number of empirical relationships by which the constants in equations (12.43) and (12.44) may be calculated quite accurately from static strength data. Two examples of these relationships are given in Fig. 12.12.

Relating the fatigue behaviour of a thick walled cylinder to basic low cycle fatigue data raises a number of problems. The main difficulties may be listed as follows,

(i) thick-walled cylinders with cyclic internal pressure are subjected to a load cycle not a strain cycle.

(ii) the strain conditions are multiaxial not uniaxial.

(iii) the mean strain components are non zero and are again multiaxial.

(iv) the fatigue conditions are modified by the pressurised oil in contact with the bore.

All these factors must be considered and if significant included in the analysis,

The difference between load and strain cycling behaviour is not great in low cycle fatigue as far as the cyclic life is concerned. Coffin and Tavernelli (78) have shown that the cyclic stress-strain relation developed after a large number of cycles is substantially constant irrespective of prior strain history. Thus it is reasonable to assume that the strain range changes which take place during the early cycles of load or stress cycling have relatively little effect on the final cyclic stress - strain relation. Experimental evidence for the good agreement between load and strain cycling fatigue curves for En 25 is given by Mackenzie and Benham (76).

Multiaxial stresses and strains must be reduced to single equivalent values in order to apply the Manson - Coffin approach. The expressions used are analogous to the von Mises equivalent stress and strain relations,

Equivalent stress range,

$$\Delta\sigma_{eq} = \frac{1}{\sqrt{2}}\left\{ \left[\Delta(\sigma_1-\sigma_2)\right]^2 + \left[\Delta(\sigma_2-\sigma_3)\right]^2 + \left[\Delta(\sigma_3-\sigma_1)\right]^2 \right\}^{\frac{1}{2}} \qquad (12.46)$$

Equivalent strain range,

$$\Delta\epsilon_{eq} = \frac{\sqrt{2}}{3}\left\{ \left[\Delta(\epsilon_1-\epsilon_2)\right]^2 + \left[\Delta(\epsilon_2-\epsilon_3)\right]^2 + \left[\Delta(\epsilon_3-\epsilon_1)\right]^2 \right\}^{\frac{1}{2}} \qquad (12.47)$$

An alternative approach which eliminates the need for an equivalent stress or strain is to employ shear stress - strain analysis in conjunction with shear fatigue data from a torsion test say. From past experience this approach should be very suitable. For example the endurance limits of a wide range of cylinder K ratios have been shown to correlate well on the basis of shear stress, and the elastic plastic expansion of a thick-walled cylinder can be accurately predicted from shear stress - strain information from a torsion test.

The effect of a mean stress or strain in low cycle fatigue may give rise to continually changing stresses and strains with every cycle. However unstable conditions such as these will only occur in a pressure vessel very near to collapse which is not an aspect of vessel behaviour of interest for normal safe working. Of more practical importance is the case where after a few cycles the stress and strain behaviour settles down to an asymptotic repetitive condition. Manson (11) suggests that a cyclically loaded part either settles down to a repetitive plastic flow per cycle in which case it cannot support a mean load, or it settles down to a repetitive elastic straining with zero plastic strain in which case a mean load can be supported. In practice conditions may arise somewhere between these two extremes. The strain gauge tests described in Chapter 9 showed that a thick-walled cylinder of moderate K ratio with repeated internal pressure settles down to a repetitive elastic cycle with negligible cyclic plasticity. Thus the stress and strain ranges associated with a particular repeated pressure may be calculated purely from elastic considerations, whether or not the static or cyclic yield condition has been exceeded. Furthermore in relating the cylinder behaviour to basic fatigue data only the elastic strain range or asympotic stress range component given by equation (12.44) need be considered. The equivalent stress range may be calculated from equation (12.46) and it may be assumed that conditions at the bore dictate the fatigue life. This is reasonable in view of the experimental and theoretical evidence presented in Sections 11.5.4 and 12.4.3 for the fact that crack propagation through cylinder wall occupies a relatively small fraction of the total life. For an open ended cylinder with or without static external pressure the elastic stress ranges are as follows,

$$\Delta(\sigma_1 - \sigma_2) = \frac{K^2 + 1}{K^2 - 1}\, p_i, \quad \Delta(\sigma_2 - \sigma_3) = p_i, \quad \Delta(\sigma_3 - \sigma_1) = \frac{-2K^2}{K^2 - 1}\, p_i$$

and substitution in equation (12.46) gives,

$$\Delta\sigma_{eq} = \frac{\sqrt{3K^4 + 1}}{K^2 - 1}\, p_i \qquad (12.48)$$

for K = 1.75 $\Delta\sigma_{eq} = 2.62\, p_i$

The corresponding equation for a closed ended cylinder is given by

$$\Delta\sigma_{eq} = \frac{\sqrt{3K^4}}{K^2 - 1}\, p_i \qquad (12.49)$$

which is virtually identical to equation (12.48). Thus the equivalent stress relation does not contradict the experimental observation that the fatigue lives of open and closed ended cylinders are the same.

The fatigue results from the present work on 1.75 K ratio cylinders, which were presented earlier in Fig. 11.1, have been converted to equivalent stress ranges and are plotted in Fig. 12.12 for comparison with the basic asymptotic stress range / life curve. It is interesting that the curve for a monobloc cylinder without external support pressure approaches the basic fatigue curve at the short life end. This could point to the fact that at low endurances the oil effect is insignificant in comparison with the stress range. However as the fluid pressure is highest at low endurances it is difficult to imagine how the oil effect is reduced. The static supported fatigue curves generally lie above the basic fatigue line and thus the inclusion of an oil effect would produce even wider divergence from the basic fatigue line. To a certain extent the discrepancy may be explained by the influence of the mean load in the fatigue cycle.

There are two main problems in including the effect of mean conditions. One is to convert basic fatigue information obtained with zero mean strain to corresponding fatigue strain ranges for non zero mean strains. The second is to predict the steady state mean strain conditions in a cylinder after cyclic softening has taken place. The first problem may be dealt with simply by the use of a modified Goodman diagram as the cyclic conditions are predominantly elastic. The problem of accurately predicting the steady state conditions was illustrated in Chapter 10. It was found that the cyclic stress - strain information overestimated the steady state expansion of the cylinder, and that although a static approach underestimated the expansion it came nearer to the measured strain gauge values. Thus the mean components could be defined approximately by elastic-plastic analysis. It is suggested by Manson that these multiaxial components may be resolved into a single equivalent value by expressions of the form given in equations (12.46) and (12.47). However the sign of the individual components then becomes lost as a result of squaring and the mean component itself can have no meaningful sign. It does appear from these problems and the lack of agreement exhibited in Fig. 12.12 that the fatigue behaviour of thick-walled cylinders can not satisfactorily be explained by the use of equivalent stresses or strains and low cycle fatigue data from push-pull tests. It was mentioned earlier than a shear stress - strain approach has certain advantages in connection with cylinder behaviour and this aspect will now be given further consideration.

The shear strain range ($\Delta\gamma$) can be calculated simply from elastic considerations as

$$\Delta\gamma = \frac{1}{G} \left\{ \frac{K^2}{K^2 - 1} \right\} p_i \qquad (12.50).$$

whether or not static external pressure is present. It is more convenient in this case to deal throughout in shear strains rather than shear stresses.

The pressure / bore shear strain curve Fig. 10.9 can be used to determine the maximum bore shear strain which would occur under a particular combination of internal and external pressures. Under cyclic conditions the steady state maximum shear strain would be larger and the value obtained can only be regarded as approximate. The mean shear strain can be obtained by subtracting half the strain range from the maximum. These calculations have been performed for all the tests on 1.75 K ratio specimens and are presented in the form of shear strain range against mean shear strain in Fig. 12.13. Included on the graph are also the results of other workers at high endurances. The trend of the constant life curves is generally what would be expected say of torsional fatigue tests but with the important feature

Fig12.13

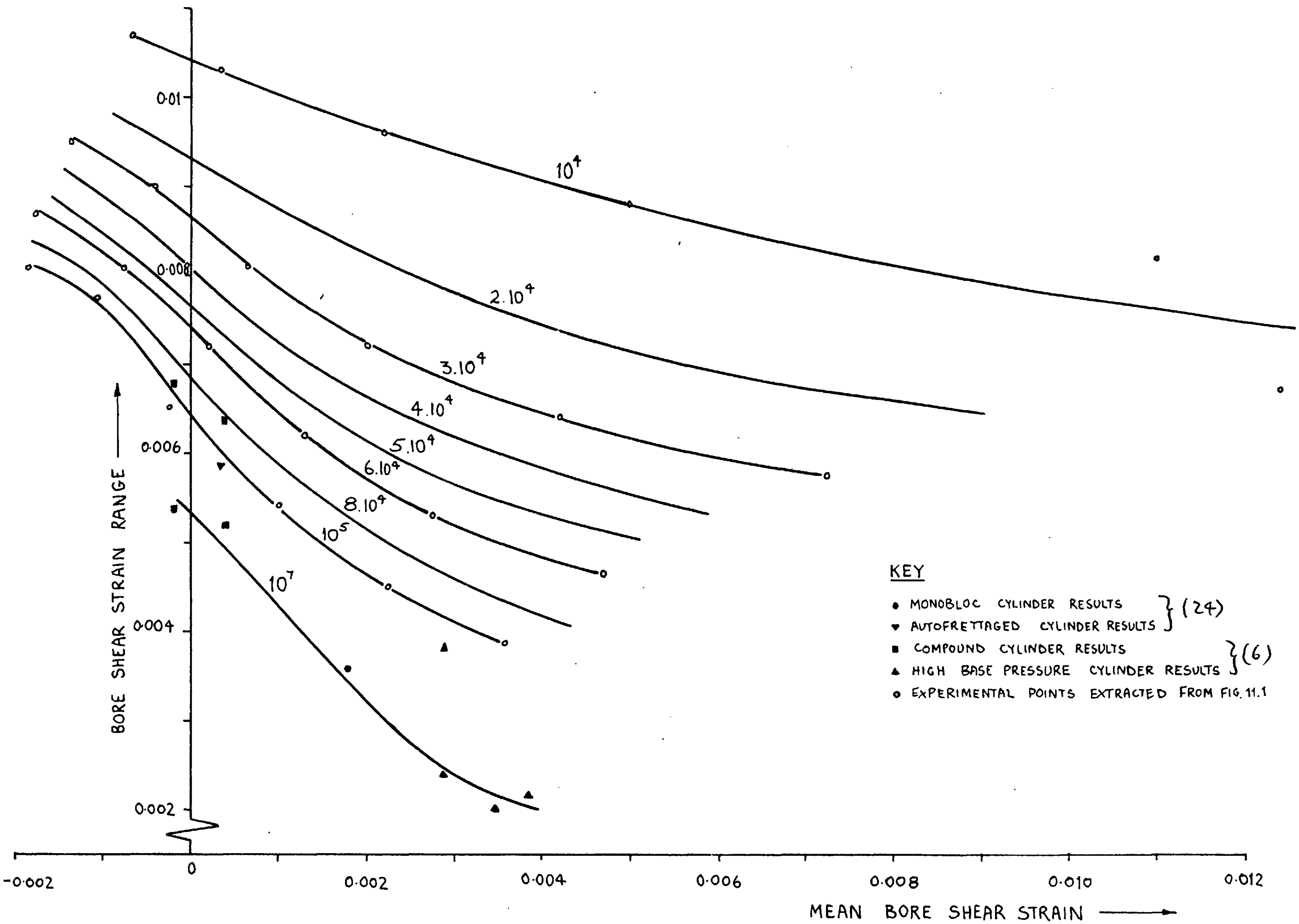

FIG. 12.13 CONSTANT LIFE CURVES OF SHEAR STRAIN RANGE AGAINST MEAN SHEAR STRAIN AT THE BORE

that higher strain ranges can be tolerated even when the mean shear strain changes sign. A series of strain ranges for zero mean strain can be extracted from the graph for comparison with basic fatigue data. Fig. 12.14 shows the total, plastic, and elastic shear strain range curves from the work of Mackenzie et al (71) for En25 in a similar condition to the present test material. The curves were obtained from reversed torsion tests on thin walled tubes with zero mean shear strain. Also potted on Fig. 12.14 are the basic cylinder fatigue curves of Fig. 11.1 expressed simply in terms of shear strain range without regard to mean shear strain values. Points which have been extracted from Fig. 12.13 for zero mean shear strain are also plotted and a straight line drawn between them.

There are a number of points which are highlighted in Fig. 12.14. At the high endurance end of the graph the well known discrepancy between cylinder fatigue results and reversed shear results is exhibited. The zero mean strain line however goes about half-way to accounting for the discrepancy at 10^6 cycles and at fatigue lives around 10^5 cycles actually coincides with the basic elastic line. At lives less than 10^5 cycles the divergehce of the zero mean strain line from the basic elastic line again increases although now the cylinders are able to withstand a higher shear strain range for a given life. This divergence must be due to the combination of other stress or strain components whose beneficial influence is inadequately represented by the shear components and the oil pressure effect. However as the basic fatigue information in Fig. 12.14 was not obtained with the cylinder material itself it is important to remember that some portion of the discrepancy may have arisen as a result of this. The cylinder fatigue curves which have been expressed in terms of shear strain range show no better agreement with the basic fatigue curves than the corresponding cylinder results in Fig. 12.12, and no meaningful conclusions can be drawn.

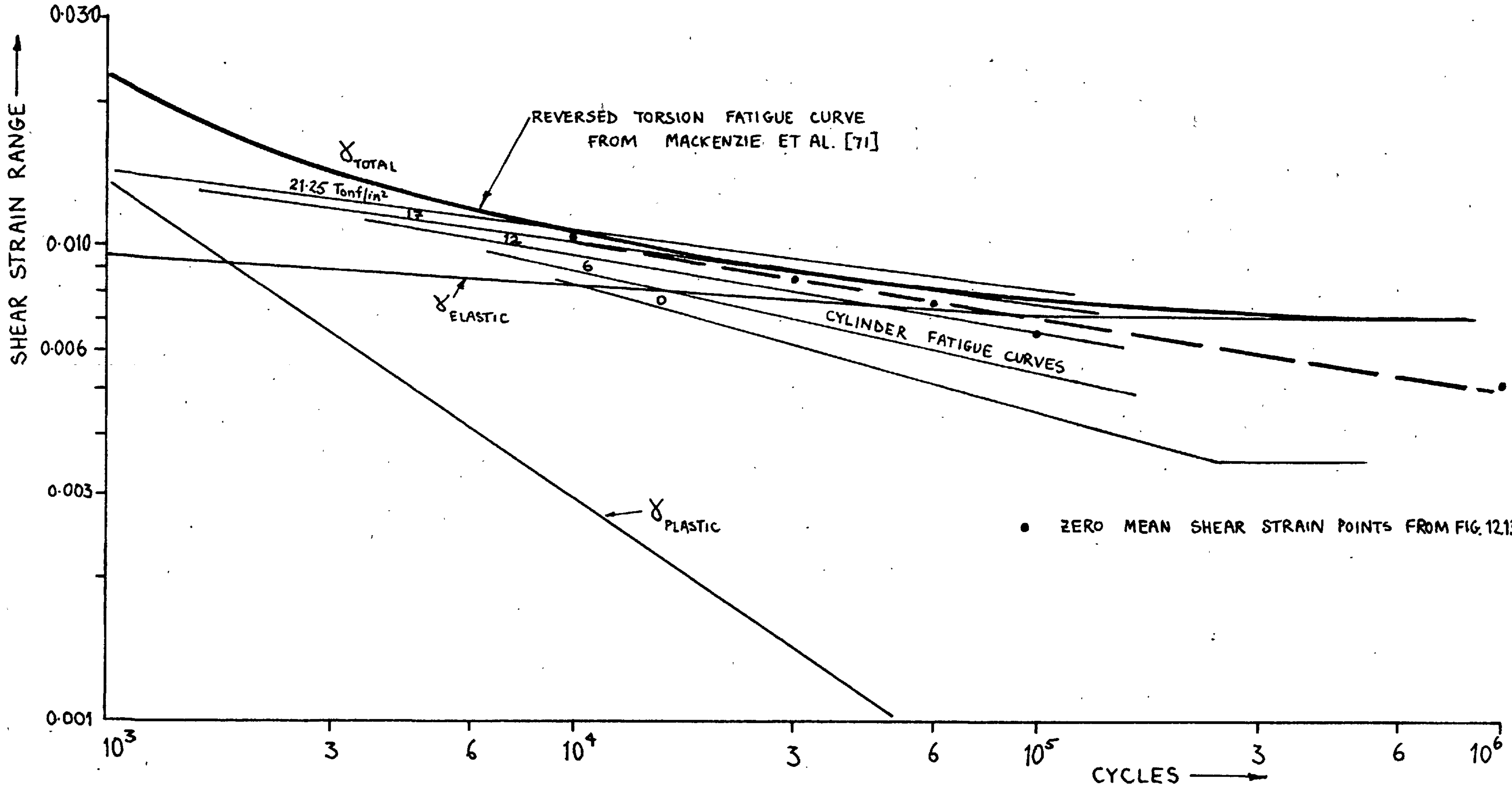

FIG. 12.14 REVERSED TORSION AND CYLINDER FATIGUE RESULTS IN EN 25 STEEL

12.6 Summary of Design Approaches and Worked Example

It was mentioned in the Introduction that an important aspect of the fatigue testing of fluid supported vessels would be the application of the results not only in the design of further fluid supported vessels but also in the design of more traditional vessels. However no single design approach has emerged from the preceeding discussion and the best method has been shown to depend on the fatigue regime of interest and the availability of cylinder fatigue data. It is therefore appropriate to summarise which approach should be taken in any particular situation.

If the vessel is elastic and of En25 steel then the fatigue behaviour is characterised in Fig. 12.1 by means of the range of shear stress and the mean shear stress. Conditions at the fatigue limit are also included in Fig. 12.1 from Burns and Parrys' (6) work, although this area was outside the scope of the present test programme.

If the vessel is to be designed in a material for which there are limited if any cylinder fatigue data then the fatigue limit conditions may be estimated from the rotating bending fatigue limit by an extension of Haslam's (37) method. This method accounts empirically for the effect of high pressure oil in contact with the cylinder bore by allowing the fluid pressure to augment the conventional Lamé hoop stress.

If the vessel is of En25 steel and yields on application of the working pressure the fatigue behaviour is characterised in Fig. 12.13 by means of the range of shear strain and the mean shear strain. The shear strains must be calculated by elastic plastic analysis based on the static properties of the cylinder material and the application of the Tresca yield criterion and associated flow rule as proposed by Koiter (67).

If the vessel is to be designed for the mortal range in a material other than En25 steel a simplified fracture mechanics approach can be used. The method is an extension of Haslam's work (38) on monobloc cylinders and requires only a limited amount of data already available for a wide range of materials.

12.6.1 Worked Example

As an example of fatigue analysis consider the case of an En25 steel static support vessel with an inner K ratio of 2. Let us assume that a repeated internal pressure of 35 $Tonf/in^2$ is to be contained and that a static external pressure of 10 $Tonf/in^2$ can conveniently be provided. We wish to know what life can be expected of the vessel. The following material properties are assumed,

Shear yield stress, τ_y = 26.4 $Tonf/in^2$

Shear modulus, G = 5,230 $Tonf/in^2$

The yield pressure of the inner cylinder with external pressure acting is given by equation (A1.5) as 29.8 $Tonf/in^2$. The working internal pressure of 35 $Tonf/in^2$ will therefore cause yielding and the simple shear stress basis of fatigue analysis can not be used. The fatigue life may either be predicted on the basis of shear strains from elastic-plastic analysis and the results of the present fatigue tests on En25, or if no such information were available the life may be predicted from the fracture mechanics approach. In this example both methods are demonstrated.

i) Shear strain analysis

Substituting the maximum internal and external pressure conditions in equation (A1.13) the elastic-plastic radius ratio may be calculated as 1.15. This value may be substituted in equation (A1.25) to give the maximum bore shear strain,

$$\gamma_{max} = 74.10^{-4}$$

The range of bore shear strain is purely elastic and therefore calculable from the bore shear stress range that is,

$$\gamma_{range} = \frac{1}{G}\left[\frac{K^2}{K^2-1}\,p_{i_{max}}\right] = 89.10^{-4}$$

The mean bore shear strain is given by

$$\gamma_{mean} = \gamma_{max} - \tfrac{1}{2}\gamma_{range} = 29.5.10^{-4}$$

We have now defined the fatigue cycle and can refer to the constant life curves in Fig. 12.13 to estimate the fatigue life. On this basis a fatigue life of 12,000 cycles is predicted.

ii) Fracture mechanics analysis

It is necessary first to calculate the repeated internal pressure at the fatigue limit for a cylinder having a K ratio of 2 and with 10 Tonf/in^2 external pressure. This is given by equation (12.13) as 20.4 Tonf/in^2. Substituting this figure in equation (12.11) gives an effective tensile hoop stress of 41.3 Tonf/in^2. We can now calculate the initial crack length a_o from equation (12.33) as $7.95 \cdot 10^{-5}$ in. Finally equation (12.32) gives the following relation between life and the maximum repeated internal pressure.

$$N = \frac{123}{(3.33p_i - 26.7)^3} \cdot 10^8 \text{ cycles}$$

For a repeated internal pressure of 35 Tonf/in^2 a fatigue life of 17,000 cycles is predicted.

Thus we have life estimates of 12,000 and 17,000 cycles from the respective approaches of shear strain analysis and fracture mechanics. In the present example the shear strain approach is backed by experimental cylinder fatigue data and must therefore be considered the more reliable method. However the example shows that in the absence of such information that the fracture mechanics approach would give a reasonable estimate of life within the order of accuracy usually associated with fatigue.

To conclude the example it remains to define the geometry of the outer vessel subject to a static internal pressure of 10 Tonf/in^2. For an economic design this cylinder should be as highly stressed as it is safe to do so even up to the collapse pressure if a ductile material were used. From equation (A1.32) an En25 steel cylinder of 1.25 K ratio has a collapse pressure of 11.8 Tonf/in^2. If this cylinder were used the nominal overall K ratio of the static support vessel would be 2.5 although this figure ignores the additional space required for the interface fluid and seals.

CHAPTER 13.

CONCLUSIONS.

1. A hydraulically operated fatigue press has been constructed to generate repeated fluid pressures within the bore of a test cylinder. Pressures up to 50 Ton/in^2 (772 MN/m^2) and frequencies up to 60 cycles per minute have been achieved in the present work. It was found that the variable decompression facility in the main control valve was essential to overcome problems in controlling the pressure cycle arising from the stored energy in a compressed volume of fluid.

2. A dynamic fluid support vessel system has been built to subject test cylinders to combined repeated internal and external pressure with the facility of changing the external pressure / internal pressure ratio. A ratio of about one third was employed in the present work and tests were carried out at repeated internal pressures up to 31 $Tonf/in^2$ (480 MN/m^2). Problems were encountered in clamping the moving cylinder / end-closure assembly together reliably for the whole fatigue life. A self clamping arrangement using the external fluid pressure provided a satisfactory solution. It was found that excessively large plunger displacements were necessary even at modest pressures and it is suggested that future work on dynamic support vessels would benefit from a less compressible pressure medium such as rubber.

3. A vessel rig has been built in conjunction with a 200,000 lbf/in^2 (1.4 GN/m^2) static pressure supply system to subject test cylinders to combined repeated internal pressure and static external pressure. Fatigue tests have been carried out at repeated internal pressures up to 50 $Tonf/in^2$ (772 MN/m^2) with static external pressures up to 21.25 $Tonf/in^2$ (328 MN/m^2). Fluctuations in the static support

pressure due to the cyclic elastic displacement of the test cylinder were minimised by the incorporation of a large capacity high pressure reservoir in the supply line. The static support rig was also used for fatigue tests on monobloc and high base pressure cylinders to supplement the results of the fluid supported tests.

4. Manganin pressure gauges were found to be entirely satisfactory for static and dynamic pressure measurements over long periods. Dynamic temperature variations were recorded in addition for the purpose of applying a temperature correction to the manganin gauge pressure signal. An important feature of the recording system was a slow speed continuous ultra-violet trace of the whole fatigue test. In some cases this provided the only record of the exact point of failure.

5. The performance of the Hallprene hydraulic seal as the dynamic plunger seal proved entirely satisfactory. Wear of the mitre ring was usually more severe than that of the seal itself. In some tests the fluid temperature reached the upper recommended limit for hydraulic seals of 120°C. Excessive temperatures are therefore likely to prove a serious limitation to sealing at substantially higher pressures if the present cycle conditions are reproduced. Seal friction at the plunger was low indicating some measure of hydrodynamic lubrication.

6. Elastic finite element stress analysis of necked and plain static support specimen designs showed that there was little to be gained from a necked design in the reduction of stress discontinuities at seals. Also true Lamé stresses were present for a greater proportion of the specimen length in the case of the plain design. If combined

internal and external pressure were applied the tensile axial discontinuity stresses could cause problems with high strength brittle materials used for very high pressure vessels.

The cyclic behaviour of a cylinder beyond yield was found by strain gauge tests to be predominantly elastic. Prediction of the steady state strains could be approximated by elastic-plastic analysis using static material properties.

7. The test material used throughout was En25 steel in the 56 $Tonf/in^2$ (781 MN/m^2) ultimate tensile strength condition. Monobloc fatigue tests carried out to supplement the tests on fluid supported cylinders agreed well with the results of earlier workers. The application of static external support pressure had the effect of increasing the maximum repeated internal pressure which a cylinder could withstand for a particular life. The higher the external pressure the greater the improvement even when the static pressure exceeded the reverse yield pressure. Significantly improved fatigue resistance also resulted from the application of dynamic support pressure. At first sight the performance of a dynamic support vessel appears better than an equivalent static support vessel with the same maximum external pressure say, but of course the outer vessel of a dynamic support system is itself subject to fatigue. The dynamic and static supported vessel tests showed that both were reliable practical systems of vessel design with good fatigue resistance meriting serious consideration for high pressure operation.

8. One of the most important aspects of the work is in the application of the fatigue results to design. A number of design approaches are necessary depending upon the vessel material and the fatigue regime of interest. If the vessel is of En25 steel then the fatigue behaviour is characterised in the elastic range by the range of shear stress and mean shear stress and a series of constant life curves provide a convenient basis

for design. If the vessel is of En25 steel and operates beyond yield then elastic-plastic analysis is necessary to characterise the fatigue conditions in terms of range of shear strain and mean shear strain. A second series of constant life curves are presented for design. If the vessel material is other than En25 steel then the fatigue limit conditions may be estimated by a method which accounts empirically for the oil effect in thick-walled cylinder fatigue. In the mortal region for other vessel materials a simplified fracture mechanics approach has been successfully applied to predict the fatigue behaviour.

LIST OF REFERENCES.

1. Alexander J.M. and Lengyel B., Semi-continuous hydrostatic extrusion of wire, Proc. Instn. Mech. Engrs., 1965-66, 180 (3I), 317.
2. Lengyel B, and Alexander J.M., Design of a production machine for semi-continuous hydrostatic extrusion, Proc. Instn. Mech. Engrs. 1967-68, 182 (3C), 207.
3. Lengyel B., A semi-continuous hydrostatic extrusion process, Metals and Materials 1968, Jan, 11.
4. Lengyel B, Burns D.J., and Prasad L.V., Design of containers for a semi-continuous hydrostatic extrusion production machine, Proc. 7th Int. M.T.D.R. Conf., 1967, 319.
5. Crossland B. and Burns D.J., Behaviour of compound steel cylinders subjected to internal pressure. Proc. Instn. Mech. Engrs., 1961, 175, 1083.
6. Burns D.J. and Parry J.S.C., Effect of mean shear stress on the fatigue behaviour of thick-walled cylinders. Proc. Instn. Mech. Engrs. 1967-68, 182 (3c), 72.
7. Harvey D.C. and Lengyel B., Pressure vessels under cyclic loading: test rig and initial results, Proc. 9th Int M.T.D.R. Conf., 1969, 495.
8. Crossland B., The effect of pressure on the fatigue of metals. The mechanical behaviour of Materials under Pressure, Elsevier, 1970, Chapter 7.
9. Plumbridge W.J. and Ryder D.A., The metallography of fatigue, Metallurgical Reviews No.136, 1969, 14.
10. Forsyth P.J.E., A two stage process of fatigue crack growth. Proc. Crack Propogation Symposium, Cranfield, 1961, 76.
11. Manson S.S., Thermal Stress and low-cycle fatigue, McGraw - Hill, 1966.

12 Forrest, P.G., Fatigue of Metals. Pergamon, 1962.

13. Heywood. R.B., Designing against fatigue.
Chapman and Hall, 1962.

14. Manson, S.S. Behaviour of materials under conditions of thermal stress, Heat Transfer Symp. Univ. Mech. Eng. Res. Inst., 1953, 9.

15. Gough H.J., Pollard H.V., and Clenshaw W.J., Some experiments on the resistance of metals to fatigue under combined stresses.
R. and M. 2522. Aeronautical Research Council, 1951.

16. Pascoe K.J., Low-cycle fatigue in relation to design.
Proc. 2nd. Int. Conf. Fracture, Brighton, 1969, Paper 59.

17. Paris P.C. and Sih G.C., Stress analysis of cracks.
Symp. Fracture Toughness Testing and its Applications.
A.S.T.M., 1965, STP 381.

18. Johnson H.H. and Paris P.C., Sub-critical flaw growth,
Eng. Fracture Mech., 1968, 1, 1.

19. Paris P.C., and Erdogan F., A critical analysis of crack propogation laws.
Trans. A.S.M.E., J. Bas. Engng., 1963, 85, 528.

20. Frost N.E., Pook L.P., and Denton K., A fracture mechanics analysis of fatigue crack growth for various materials.
Engng. Fracture Mech. (to be published).

21. Manning W.R.D., High Pressure Engineering.
Univ. Nottingham Bullied Memorial Lectures, 1963, V II.

22. Morrison J.L.M., Crossland B., and Parry J.S.C. [1], Fatigue under triaxial stress: development of a testing machine and preliminary results.
Proc. Instn. Mech. Engrs., 1956, 170, 697.

23. Parry, J.S.C.[1], Further results of fatigue under triaxial stress, Proc. Int. Conf. Fatigue, Instn. Mech. Engrs., 1956, 132.

24. Morrison J.L.M., Crossland B., and Parry J.S.C.[2], Strength of thick cylinders subjected to repeated internal pressure. Proc. Instn. Mech. Engrs. 1960 174 95.

25. Morrison J.L.M., Crossland B., and Parry J.S.C.[3], Fatigue strength of cylinders with cross-bores. J. Mech. Engng., Sci., 1959, 1, 207.

26. Davidson T.E., Eisenstadt R., and Reiner A.N., Fatigue characteristics of open-end thick-walled cylinders under cyclic internal pressure, Trans. A.S.M.E., J. Bas. Engng., 1963, 85, 55.

27. Austin B.A. and Crossland B., Low endurance fatigue strength of thick-walled cylinders : development of a testing machine and preliminary results. Proc. Instn. Engrs. (Mech)., 1965 - 66, 180, 43.

28. Parry J.S.C.[2], Fatigue of thick cylinders : further practical information, Proc. Instn. Mech. Engineers, 1965 - 66, 180 (I), 387.

29. Hannon B.M., Correlation of fatigue tests of thick-walled cylinders subjected to repeated internal pressure, Trans. A.S.M.E., J. Bas. Engng., 1965, 87, 405.

30. Blass J.J. and Findley W.N., The influence of the intermediate principal stress on fatigue under triaxial stress, Mat. Res., Stds., 1967, 7, 254.

31. Frost W.J. and Burns D.J., Effect of Oil and Mercury at high pressure on the fatigue behaviour of thick-walled cylinders of EN.25. Steel. Proc. Instn. Mech. Engrs., 1967-68, 182 (3C), 65.

32. Crossland B. and Skelton W.J., Effect of varying hardness on the fatigue strength of thick-walled cross-bore cylinders of EN.25. Proc. Instn. Mech. Engrs., 1967-68 182 (3C), 106.

33. Austin B.A., Reiner A.N., and Davidson T.E., Low cycle fatigue strength of thick-walled pressure vessels.
Proc. Instn. Mech Engrs., 1967-68, 182 (3C), 91.

34. Jones P.M. and Tomkins B., Low endurance fatigue of very thick-walled cylinders.
Proc. Instn. Mech Engrs., 1967-68, 182 (3C), 81.

35. Marsh K.J. and Haslam G.H., Fatigue of cylinders subjected to pulsating internal oil pressure NEL Report No.381, January 1969.

36. Haslam G.H. [1], Fatigue strength of thick-walled steel cylinders subjected to pulsating internal pressures,
N.E.L. Report No.444, 1970.

37. Haslam G.H.[2], The fatigue limit of cylinders subjected to repeated internal pressures.
High Temperatures - High Pressures, 1969, 1 , 705.

38. Haslam, G.H.[3], Estimation of the fatigue life of a thick-walled cylinder subjected to repeated internal pressure.
J. Mech Engng. Sci., 1971, 13 , 130.

39. Prasad L.V., Design concepts for Hydrostatic Extrusion Tooling Indian Institute of Technology, Delhi.

40. de Malherbe M.C. and Firth B.W., Ultra-high pressures; measuring devices and their calibration.
Metallurgical Reviews No.140, 1970 , 15 .

41. Fawcett J.R., Engineer, 1968, 226, 405.

42. Mason H.L., Sensitivity and life data on Bourdon tubes.
Trans. A.S.M.E., 1956, 78, 65.

43. Kudo H. and Nakane T., A method of strain measurement on the inner surface of high pressure vessels,
5th Japan Cong. Testg. Mtls., 1969, 153.

44. Newhall D.H. and Abbott L.H., The bulk modulus cell : new high - pressure measurement instrument.
Chem. Engng. Prog., 1960, 56, 112.

45. Bridgman P.W., The measurement of hydrostatic pressures up to 20,000 kilograms per square centimeter.
Proc. Amer. Acad. Arts. Sci., 1911, 47, 321.

46. Lisell E., On the effect of pressure on the electrical resistance of metals and the new methods of technique for measuring high pressures.
Upsal Univ. Arsskrift, 1903, No.1.

47. Darling H.E. and Newhall D.H., Trans. A.S.M.E., 1953, 75, 311.

48. Bundy F.P., Effect of pressure on emf of thermocouples.
J. Appl. Phys., 1961, 32, 483.

49. Chandler E.F., Tensile properties of a number of materials under hydrostatic pressure, NEL Report No. 306, 1967

50. Burton A.W., Direct reading pressure gauge for measurement of fluid pressure.
N.E.L. Report No.60, 1962.

51. Johnson D.P. and Newhall D.H., The piston gauge as a precise pressure-measuring instrument,
Trans. A.S.M.E., 1953, 75, 301.

52. Nadai A., The theory of flow and fracture of solids, 1, (1931)
McGraw-Hill, 1950.

53. Franklin G.J. and Morrison J.L.M., Autofrettage of cylinders : prediction of pressure / external expansion curves and calculation of residual stresses,
Proc. Instn. Mech. Engrs., 1960, 174, 947.

54. Kudo, H. and Matsubara S., Stress analysis in cylindrical dies of finite length subjected to a band of internal pressure. Jr. Japan Soc. for Technology of Plasticity, 1968, 9 86.

55. El-Behery, A.M. and Lamble, J.H., Stress distribution in an extrusion container found by the sandwich technique, Strain 1969 5 209.

56. Thick-walled Cylinder Handbook Report No. WAL 893/172, 1954, Watertown Arsenal Laboratory

57. Timoshenko S. and Goodier, J.N., Theory of Elasticity, McGraw-Hill, 1959, p.388.

58. Barton M.V., The circular cylinder with a band of uniform pressure on a finite length of surface, J. Applied Mechanics, Trans. A.S.M.E. 1941., 8 A-97.

59. Mohaupt, U.H. Pick, R.J. and Burns D.J., Bending stresses in elastic thick-walled cylindrical pressure vessels, First International Conf. Pressure Vessel Technology, Delft 1969, p. 195.

60. Simonen, F.A., Meyer, G.E. Fiorentino R.J., and Sabroff A.M., Design of containers for large scale hydrostatic extrusion, 25th National Conference of Fluid Power, 1969.

61. Hulbert, L.E. and Simonen, F.A., On the solution of axisymmetric elastic stress problems by the boundary point least squares technique, First International Conf. Pressure Vessel Technology, Delft 1969.

62. Hayes, D.J., Axisymmetric finite element stress analysis programme, Imperial College, Unpublished.

63. Zienkiewicz O.C., The finite element method in structural and continuum mechanics, McGraw-Hill, 1967.

64. Allen D.N. de G., and Sopwith D.G., The stresses and strains in a partly plastic thick tube under internal pressure and end load Proc. Roy. Soc. 1951, 205A, 69.

65. Steele M.C., Partially Plastic thick-walled cylinder theory, J. Appl. Mech, 1952, 19, 133.

66. Crossland B. and Bones J.A., Behaviour of thick-walled steel cylinders subjected to internal pressure. Proc. Instn. Mech Engrs., 1958, 172, 777.

67. Koiter W.T., On partially plastic thick-walled tubes, Biezeno Anniversary Volume, N.V. De Technische Uitgeverij, W. Stam, Amsterdam, 1953.

68. Bland D.R., Elastoplastic thick-walled tubes of work-hardening material subject to internal and external pressures and to temperature gradients, J. Mech Phys. Solids, 1956, 4, 209.

69. Manning W.R.D., The overstrain of tubes by internal pressure, Engineering, 1945, 159, 101.

70. Crossland B., The design of thick-walled closed-ended cylinders based on torsion data, Welding Research Council Bulletin No.94, February, 1964.

71. Mackenzie C.T., Burns D.J., and Benham P.P., A comparison of uniaxial low and biaxial low endurance fatigue behaviour of two steels. Proc. Instn. Mech. Engrs., 1965, 180 (3I), 414.

72. Frost N.E., A note on the behaviour of fatigue cracks, J. Mech. Phys. Solds 1961, 9, 143-151.

73. Frost N.E. and Greenan A.F., Effect of a tensile mean stress on the alternating stress required to propogate an edge crack in mild steel, J.Mech. Eng. Sci., 1967, 9, 234.

74. Pook, L.P. , Linear Fracture Mechanics - what it is, what it does, N.E.L. Report No. 465, 1970.

75. Coffin L.F., A study of cyclic-thermal stresses in a ductile metal.
Trans. A.S.M.E., 1954, 76, 931.

76. Mackenzie C.T. and Benham P.P., Push-Pull low endurance fatigue of En.25 and En.32B steels at 20°C and 450°C
Proc. Instn. Mech. Engrs. 1965, 180, 424.

77. White D.J., Crossland B., and Morrison J.L.M., Effect of hydrostatic pressure on the direct - stress fatigue strength of an alloy steel.
J. Mech. Engng. Sci., 1959, 1, 39.

78. Coffin L.F. and Tavernelli J.F., Cyclic straining and fatigue of metals.
Trans. Met. Soc. A.I.M.E. 1959, 215. 794.

79. Becker S.J. , An analysis of the yielded compound cylinder,
Trans. A.S.M.E., J. Engng. Ind., 1961, 83 43.

80. Hill R., The mathematical theory of plasticity.
Oxford, 1950.

APPENDIX 1

STRESS ANALYSIS OF THICK WALLED CYLINDERS

1.1 Elastic Thick-Walled Cylinders

The Lamé equations for an open-ended cylinder are,

$$\sigma_r = \frac{p_i - K^2 p_o}{K^2 - 1} - \frac{p_i - p_o}{K^2 - 1}\left(\frac{b}{r}\right)^2 \tag{A1.1}$$

$$\sigma_\theta = \frac{p_i - K^2 p_o}{K^2 - 1} + \frac{p_i - p_o}{K^2 - 1}\left(\frac{b}{r}\right)^2 \tag{A1.2}$$

$$\sigma_z = 0 \tag{A1.3}$$

$$\tau = \frac{\sigma_\theta - \sigma_r}{2} = \left(\frac{p_i - p_o}{K^2 - 1}\right)\left(\frac{b}{r}\right)^2 \tag{A1.4}$$

1.2 Yield Pressure of a Thick-Walled Cylinder

Yield occurs at the bore of a cylinder when the shear stress at the bore reaches the yield stress in simple shear obtained from a torsion test.

$$p_i = \frac{K^2 - 1}{K^2}\tau_y + p_o \tag{A1.5}$$

1.3 Elastic-Plastic Thick-Walled Cylinder

1.3.1 General

The equilibrium equation for a cylinder gives,

$$\frac{d\sigma_r}{dr} = \frac{\sigma_\theta - \sigma_r}{r} \tag{A1.6}$$

As $\sigma_\theta - \sigma_r = 2\tau$ equation (A1.6) becomes

$$\int_{-p_i}^{-p_o} d\sigma_r = 2\int_a^b \frac{\tau}{r}\, dr \qquad \text{(A1.7)}$$

If the cylinder material strain hardens then $\int_a^b \frac{\tau}{r}$ dr may be evaluated numerically providing the distribution of shear strain across the cylinder wall is known.

1.3.2 Franklin and Morrison Approach

The basic assumption of the Franklin and Morrison (53) method of analysis of elastic plastic cylinder behaviour is that shear strain is inverseley proportional to the square of the cylinder radius,

$$\gamma_r = \gamma_o \left(\frac{r_o}{r}\right)^2 \qquad \text{(A1.8)}$$

It can be shown that at the outer surface of a cylinder,

$$\gamma_o = \frac{\epsilon_{\theta_o} + \nu\,\epsilon_{z_o}}{1-\nu} \qquad \text{(A1.9)}$$

Combining (A1.8) and (A1.9)

$$\gamma_r = \frac{\epsilon_{\theta_o} + \nu\epsilon_{z_o}}{1-\nu}\left(\frac{r_o}{r}\right)^2 \qquad \text{(A1.10)}$$

If a value of the function $(\epsilon_{\theta_o} + \nu\,\epsilon_{z_o})$ is assumed then the shear strain distribution through the cylinder wall is known. The shear stress distribution through the wall can then be found using shear stress-strain from a torsion test, and the integration of equation (A1.7) carried out to calculate the internal pressure corresponding to the initial assumed external strains. By taking a series of assumed strains it is possible to build up the complete pressure expansion curve.

1.3.3 Simplified Approach

If strain-hardening can be ignored the use of a constant shear yield stress simplifies the analysis considerably. The following equations may be derived.

In the plastic region,

$$\sigma_r = 2\tau_y \ln\frac{r}{c} + \tau_y\left[\left(\frac{c}{b}\right)^2 - 1\right] - p_o \qquad \text{(A1.11)}$$

$$\sigma_\theta = 2\tau_y \ln\frac{r}{c} + \tau_y\left[\left(\frac{c}{b}\right)^2 + 1\right] - p_o \qquad \text{(A1.12)}$$

The bore pressure may be expressed in terms of the elastic-plastic interface radius from equation (A1.11).

$$p_i = 2\tau_y \ln\frac{c}{a} + \tau_y\left[1 - \left(\frac{c}{b}\right)^2\right] + p_o \qquad \text{(A1.13)}$$

In the elastic region,

$$\sigma_r = \tau_y\left[\left(\frac{c}{b}\right)^2 - \left(\frac{c}{r}\right)^2\right] - p_o \qquad \text{(A1.14)}$$

$$\sigma_\theta = \tau_y\left[\left(\frac{c}{b}\right)^2 + \left(\frac{c}{r}\right)^2\right] - p_o \qquad \text{(A1.15)}$$

$$\tau = \left(\frac{c}{r}\right)^2 \tau_y \qquad \text{(A1.16)}$$

The simplified analysis provides no information about the distribution of shear strain within the plastic region unless the assumption is made as in the previous section that shear strain is inversely proportional to the square of the radius.

1.3.4 Koiter Approach

The following analysis treats the problem of elastic-plastic behaviour by the Tresca yield criterion and associated flow rule approach developed by Koiter (67) and Bland (68). The present analysis is concerned with the specific case of a cylinder of non strain-hardening material with both internal and external pressure.

If it is assumed that the axial stress is always the intermediate principal stress then Tresca yield criterion gives,

$$\sigma_\theta - \sigma_r = 2\tau_y \qquad \text{(A1.17)}$$

Using equilibrium equation (A1.6) the same equations (A1.11), (A1.12), and (A1.13) are obtained in the plastic region. It was not necessary to invoke a yield criterion previously as it was assumed that a torsion test exactly described the shear stress-strain behaviour of a cylinder. The validity of the axial stress assumption is examined later.

The stress-stain relations (80) associated with Tresca's yield criterion require

$$\dot{\epsilon}_{\theta_p} = -\dot{\epsilon}_{r_p} \geqslant 0 \; , \; \dot{\epsilon}_{z_p} = 0 \qquad \text{(A1.18)}$$

where $\dot{\epsilon}_{\theta_p}$, $\dot{\epsilon}_{r_p}$, and $\dot{\epsilon}_{z_p}$ are the principal plastic strain rates. It follows from (A1.18) that

$$\epsilon_{z_t} = \epsilon_{z_e} \qquad \text{(A1.19)}$$

$$\therefore \quad \epsilon_{z_t} = \frac{1}{E}\left[\sigma_z - \nu(\sigma_r + \sigma_\theta)\right]$$

Substituting from (A1.11) and (A1.12)

$$\sigma_z = 4\nu\tau_y \ln\frac{r}{c} + 2\nu\tau_y\left(\frac{c}{b}\right)^2 - 2\nu p_o + E\,\epsilon_{z_t} \qquad \text{(A1.20)}$$

The elastic dilatation is given by

$$\epsilon_r + \epsilon_\theta + \epsilon_z = \frac{1-2\nu}{E}\left(\sigma_r + \sigma_\theta + \sigma_z\right) \qquad \text{(A1.21)}$$

Hence $$\epsilon_r + \epsilon_\theta = \frac{\partial u}{\partial r} + \frac{u}{r} = \frac{1-2\nu}{E}\left(\sigma_r + \sigma_\theta + \sigma_z\right) - \epsilon_z \qquad \text{(A1.22)}$$

Substituting in (A1.22) from (A1.11), (A1.12), and (A1.20)

$$\frac{\partial u}{\partial r} + \frac{u}{r} = \frac{1-2\nu}{E}\left[4\tau_y \ln\frac{r}{c} + 2\tau_y\left(\frac{c}{b}\right)^2 - 2p_o + 4\nu\tau_y\ln\frac{r}{c} + 2\nu\tau_y\left(\frac{c}{b}\right)^2 - 2\nu p_o + E\epsilon_z\right] - \epsilon_z \qquad \text{(A1.23)}$$

The solution to this differential equation is finally

$$u_r = \frac{1-2\nu}{G}\tau_y r\left[\ln\frac{r}{c} + \frac{1}{2}\left\{\left(\frac{c}{b}\right)^2 - 1 - \frac{p_o}{\tau_y}\right\}\right] - \nu\epsilon_z r + \frac{1-\nu}{G}\tau_y\frac{c^2}{r} \qquad \text{(A1.24)}$$

$$\gamma = \epsilon_\theta - \epsilon_r = \frac{u}{r} - \frac{\partial u}{\partial r}$$

Substituting from (A1.24) gives

$$\gamma = 2(1-\nu)\frac{\tau_y}{G}\left(\frac{c}{r}\right)^2 - (1-2\nu)\frac{\tau_y}{G} \qquad \text{(A1.25)}$$

To determine ϵ_z; consider axial equilibrium for tube with open ends,

$$0 = 2\pi\left[\int_a^c \sigma_z\, r\,dr + \int_c^b \sigma_z\, r\,dr\right] \qquad \text{(A1.26)}$$

Substituting for σ_z from (A1.20) gives

$$E\epsilon_z = -2\nu\tau_y \frac{a^2}{b^2-a^2}\left[2\ln\frac{c}{a}+1-\left(\frac{c}{b}\right)^2\right]+2\nu p_o \qquad \text{(A1.27)}$$

To determine validity of the assumption that the axial stress is the intermediate principal stress; consider first the situation at the elastic-plastic interface.

From (A1.11) $\qquad \sigma_r = \tau_y\left[\left(\frac{c}{b}\right)^2-1\right]-p_o$

From (A1.20) $\qquad \sigma_z = 2\nu\tau_y\left(\frac{c}{b}\right)^2+E\epsilon_z-2\nu p_o$

The inequality, $\sigma_r < \sigma_z$ must be satisfied that is,

$$-1+\left(\frac{c}{b}\right)^2+2\nu\frac{a^2}{b^2-a^2}\left[\ln\left(\frac{c}{a}\right)^2+1-\left(\frac{c}{a}\right)^2\right]-\frac{p_o}{\tau_y}<0 \qquad \text{(A1.28)}$$

As $c \leqslant b$ and $\left(\frac{c}{a}\right)^2-\ln\left(\frac{c}{a}\right)^2-1>0$ the inequality is satisfied.

In the plastic region $\sigma_\theta - \sigma_z \geqslant 0$ must be satisfied, considering conditions at the bore where $(\sigma_\theta - \sigma_z)$ is minimum.

From (A1.12), (A1.20) and (A1.27) inequality is,

$$\left(\ln\left(\frac{a}{c}\right)^2+\left(\frac{c}{b}\right)^2\right)\left(1-2\nu\frac{b^2}{b^2-a^2}\right)\geqslant -1-2\nu\frac{a^2}{b^2-a^2}+\frac{p_o}{\tau_y} \qquad \text{(A1.29)}$$

For thick tubes having $\frac{b^2}{a^2}>\frac{1}{1-2\nu}$, that is $\frac{b}{a}>1\cdot5$ for $\nu=0\cdot28$, then the minimum value of the left hand side of equation (A1.29) is given when c = b that is,

$$\left[1-\ln\left(\frac{b}{a}\right)^2\right]\left(1-2\nu\frac{b^2}{b^2-a^2}\right)\geqslant -1-2\nu\frac{a^2}{b^2-a^2}+\frac{p_o}{\tau_y} \qquad \text{(A1.30)}$$

which reduces to

$$\ln K \geqslant 0\cdot5+\frac{K^2-0\cdot44-(K^2-1)\frac{p_o}{\tau_y}}{0\cdot88K^2-2} \qquad \text{(A1.31)}$$

This inequality is expressed graphically in Fig A1.1 in terms of the ratio p_c / τ_y and the corresponding permissible K ratios for which the axial stress is in fact intermediate. It can be seen that if no external support pressure is applied then the analysis is valid for K ratios up to 5.65 but if $p_o = \tau_y / 2$ then only K ratios up to 3.38 are permissible. In the present work the maximum p_o / τ_y ratio occurred with p_o = 21.25 Tonf/in^2, that is p_o / τ_y = 21.25/26.4 = 0.805 and the limiting K ratio would be approximately 2.5.

Collapse Pressure of a Thick-Walled Cylinder

The collapse pressure of a cylinder is defined as that pressure which will just cause the entire cylinder wall to yield. Depending on the cylinder K ratio and material properties further expansion of the cylinder may then take place without any increase in pressure.

From equation (A1.13)

$$p_{collapse} = 2 \tau_y \ln K + p_o \qquad \text{(A1.32)}$$

In the case of K = 1.75 and En25 as cylinder material with an average τ_y of 26.8 Tonf/in^2,

$$p_{collapse} = 30 + p_o$$

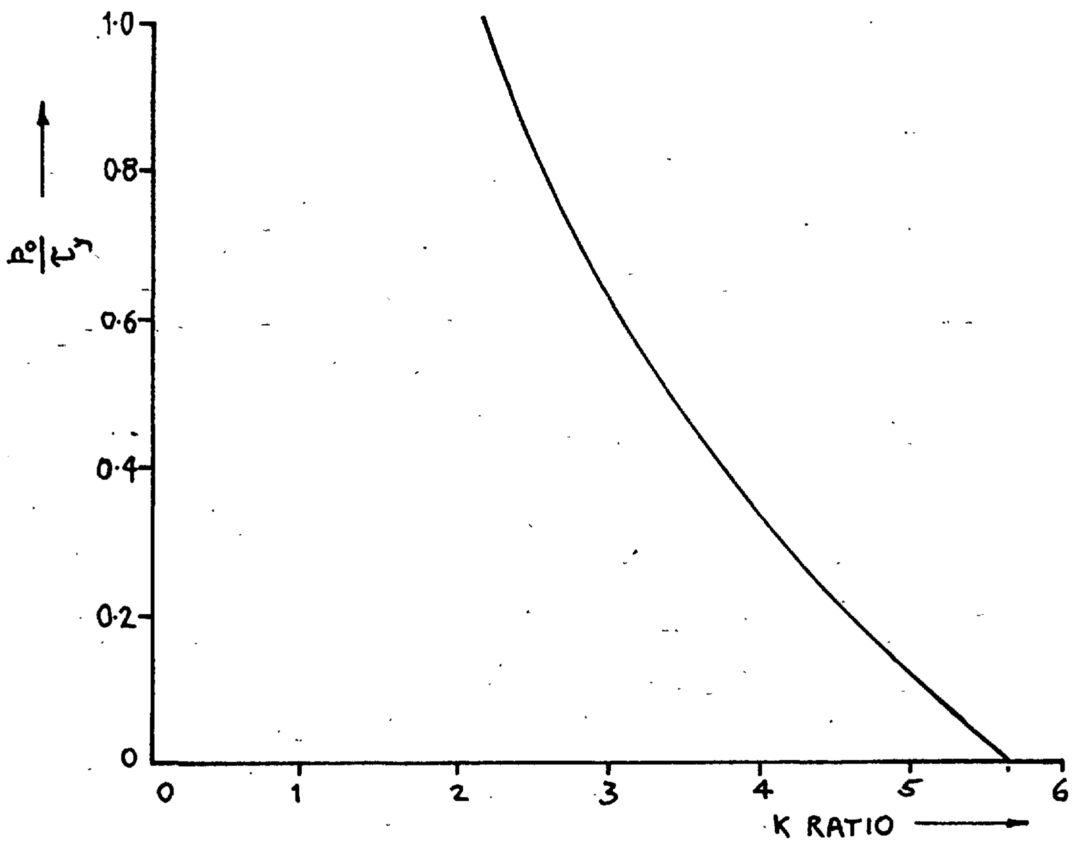

FIG. A1.1 LIMITING K RATIOS FOR THE VALIDITY OF THE KOITER APPROACH TO CYLINDERS WITH EXTERNAL PRESSURE

APPENDIX 2

INSPECTION CERTIFICATE OF EN 25 STEEL

Test No. 2099/2

Specification 2.S.96.B
SIZE 2.1/2" dia

	0.1% Proof Stress Tons per Sq. In.	Maximum Stress Tons per Sq. In.	Elongation per cent.	Reduction of Area per cent.	Izod Impact Value Foot Lbs.			Brinell
	49.2	58.8	21.0	65.8	71	77	75	269

HEAT TREATMENT to which Test Samples have been submitted.

Heated to 840oC., Cooled in Oil
Heated to 660oC., Cooled in Air

CAST No.	ANALYSIS C.	Si.	Mn.	S.	P.	Ni.	Cr.	Mo.
4C9493	.33	.30	.55	.010	.0[illegible]7	2.44	.64	.48

Condition of Material as supplied BLACK. HARDENED & TEMPERED

Identification Marks 4C.9493 Z.463

Brinell Range 269/285

APPENDIX 3

VACUUM STRESS RELIEVING TREATMENT CYCLE

Sample Nos. SS7, SS9, SS11

Samples were protected by molybdenum shields

TIME MINS:	PRESSURE.		POWER.		TEMPERATURE.			REMARKS.
	BACKING	CHAMBER	I	V	T_T	T_C	T_B	
11.0	.15	9×10^{-6}	50	10		30		Power on - manual control
12.30	.17	7×10^{-5}	45	10		360		Check
2.00	.19	6×10^{-5}	60	15		600		Auto control
2.15	.18	4×10^{-5}	55	14		595		Controlling
3.00	.16	5×10^{-6}	45	10		602		Power off - cooling
	Max. & min. temperature during control period							595°C & 610°C
4.30	.16	2×10^{-6}	-	-		440		Cooling naturally
9.00 a.m.	January 4th 1969					30		Work removed from furnace

APPENDIX 4

Fluctuation of Static Support Pressure

1. Displacement of specimen

When $p_i = 0$ and p_o = nominal static value,

At outer surface of specimen, $\epsilon_\theta = \frac{u}{r} = \frac{1}{E}\left[-\frac{1+K^2}{K^2-1}\,p_o + \nu p_o\right]$

When $p_i = p_{i\,max}$ and $p_o = p_o + \Delta p_o$

where Δp_o = increase in p_o due to elastic expansion

At outer surface of specimen, $\epsilon_\theta = \frac{u}{r} = \frac{1}{E}\left[\frac{2p_i}{K^2-1} - \frac{1+K^2}{K^2-1}\left(p_o + \Delta p_o\right) + \nu\left(p_o + \Delta p_o\right)\right]$

Thus the net cyclic displacement $u = \frac{r}{E}\left[\frac{2p_i}{K^2-1} - \frac{1+K^2}{K^2-1}\,\Delta p_o + \nu\,\Delta p_o\right]$

and cyclic volume change $dV_s = 2\pi r u l_s$

where l_s = specimen length subjected to pressure

$$\therefore \quad dV_s = \frac{2\pi r_s^2 l_s}{E}\left[\frac{2p_i}{K^2-1} - \left(\frac{1+K^2}{K^2-1} - \nu\right)\Delta p_o\right]$$

2. Displacement of containing vessels

The net displacement for a cyclic pressure change p_o is given by,

$$u = \frac{r}{E}\left[\frac{K^2+1}{K^2-1}\,\Delta p_o + \nu\,\Delta p_o\right]$$

and the cyclic volume change by,

$$dV_v = \frac{2\pi r_v^2 l_v}{E}\left(\frac{K^2+1}{K^2-1} + \nu\right)\Delta p_o$$

where l_v = effective length of containing vessel subjected to pressure

3. Substitution of rig geometry and elastic constants

For specimen, $K = 1.75 \quad r_s = 0.875$ in $\quad l_s = 4.5$ in

$$E = 13{,}200 \text{ Tonf/in}^2 \quad \nu = 0.28$$

$$dV_s = (1.59\, p_i - 2.77\, \Delta p_o)\, 10^{-3} \text{ in}^3$$

For static support outer vessel, $K = 3.0 \quad r_v = 1.0$ in $\quad l_v = 4.5$ in

$$dV_v = 3.28\, \Delta p_o . 10^{-3} \text{ in}^3$$

For accumulator, $K = 3.33 \quad r_v = 0.375$ in $\quad l_v = 10.0$ in

$$dV_v = 0.99\, \Delta p_o . 10^{-3} \text{ in}^3$$

Net reduction in volume, $dV = dV_s - dV_v = (1.59\, p_i - 7.04\, \Delta p_o)\, 10^{-3} \text{ in}^3$

Working volumes of fluid are,

(a) between specimen and bore of outer vessel	3.3 in^3
(b) in accumulator	4.4
(c) in high pressure tubing, fittings etc.	0.3
Total V_o	$= 8.0 \text{ in}^3$

4. Calculation of pressure fluctuation

As an example consider conditions in Test No. 7,

$$p_{i\,max} = 24.1 \text{ Tonf/in}^2 , \quad p_o = 17.0 \text{ Tonf/in}^2$$

To a first approximation the Δp_o term may be neglected in the calculation of dV, then $dV = 38.3 . 10^{-3} \text{in}^3$ and $\frac{dV}{V_o} = 0.48\%$.

From the compressibility curve for Tellus 27 at $p_o = 17.0 \text{ Tonf/in}^2$ $\frac{dV}{V_o} = 9.4\%$, and as a result of elastic displacements this must rise to

$9.4 + 0.91 \times 0.48 = 9.84\%$. From the compressibility curve the corresponding pressure $= 18.2 \text{ Tonf/in}^2$.

Thus $\Delta p_o = 18.2 - 17.0 = 1.2 \text{ Tonf/in}^2$.

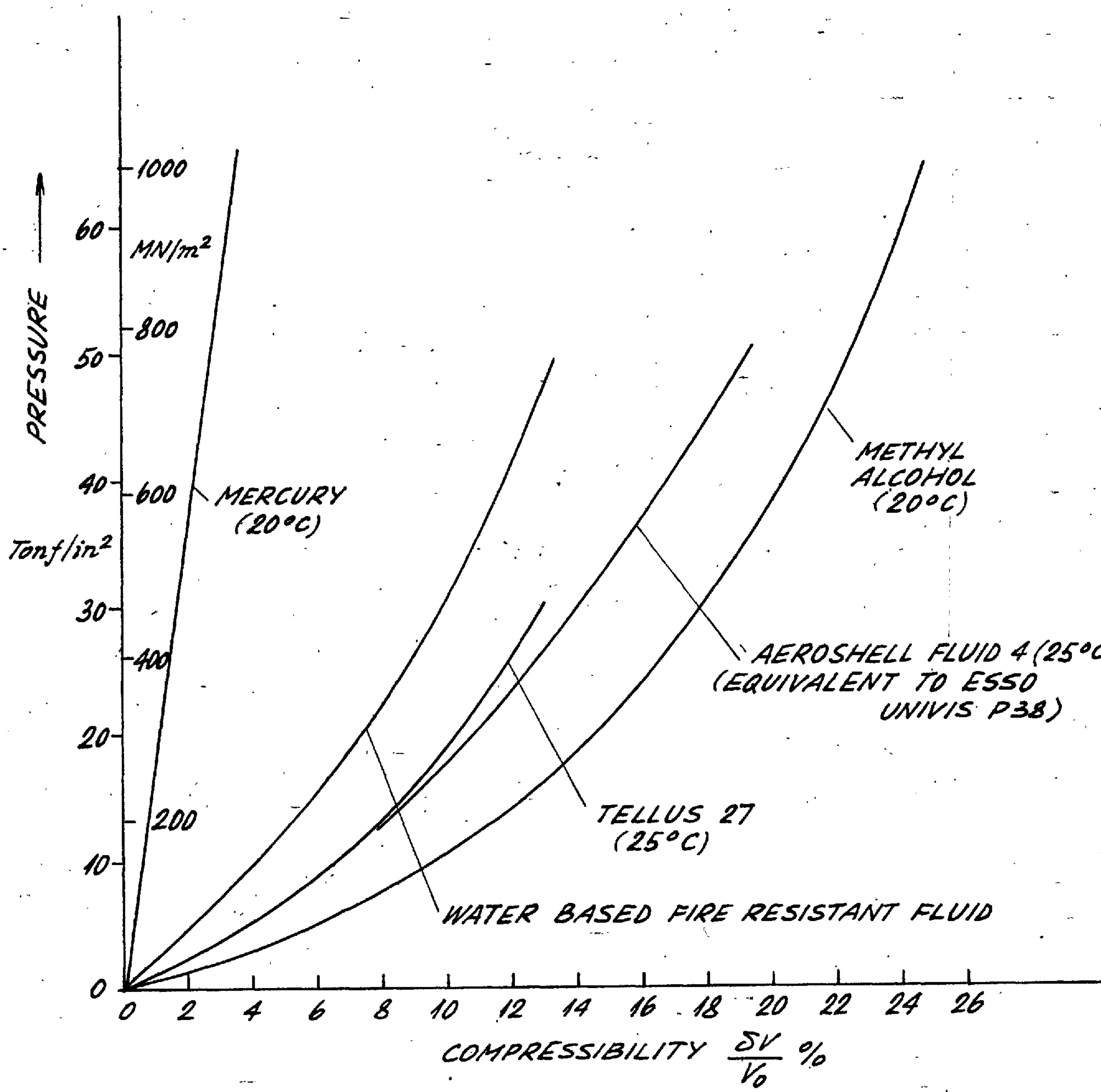

FIG.A4.1 COMPRESSIBILITY CURVES FOR VARIOUS LIQUIDS.

We can now try a trial value for Δp_o in the calculation of dV. The value must be less than 1.2 $Tonf/in^2$, and 1.0 $Tonf/in^2$ is suitable.

Then $\quad dV = 31.3.10^{-3} in^3$ and $\frac{dV}{V_o} = 0.39\%$

Overall $\frac{dV}{V_o}$ rises to $9.4 + 0.91 \times 0.39 = 9.76\%$

From compressibility curve corresponding pressure = 18.0 $Tonf/in^2$ giving $\Delta p_o = 1.0$ $Tonf/in^2$ which was the trial value and is therefore correct.

HARVEY D.C.
PH.D.
FIG. 5.4P

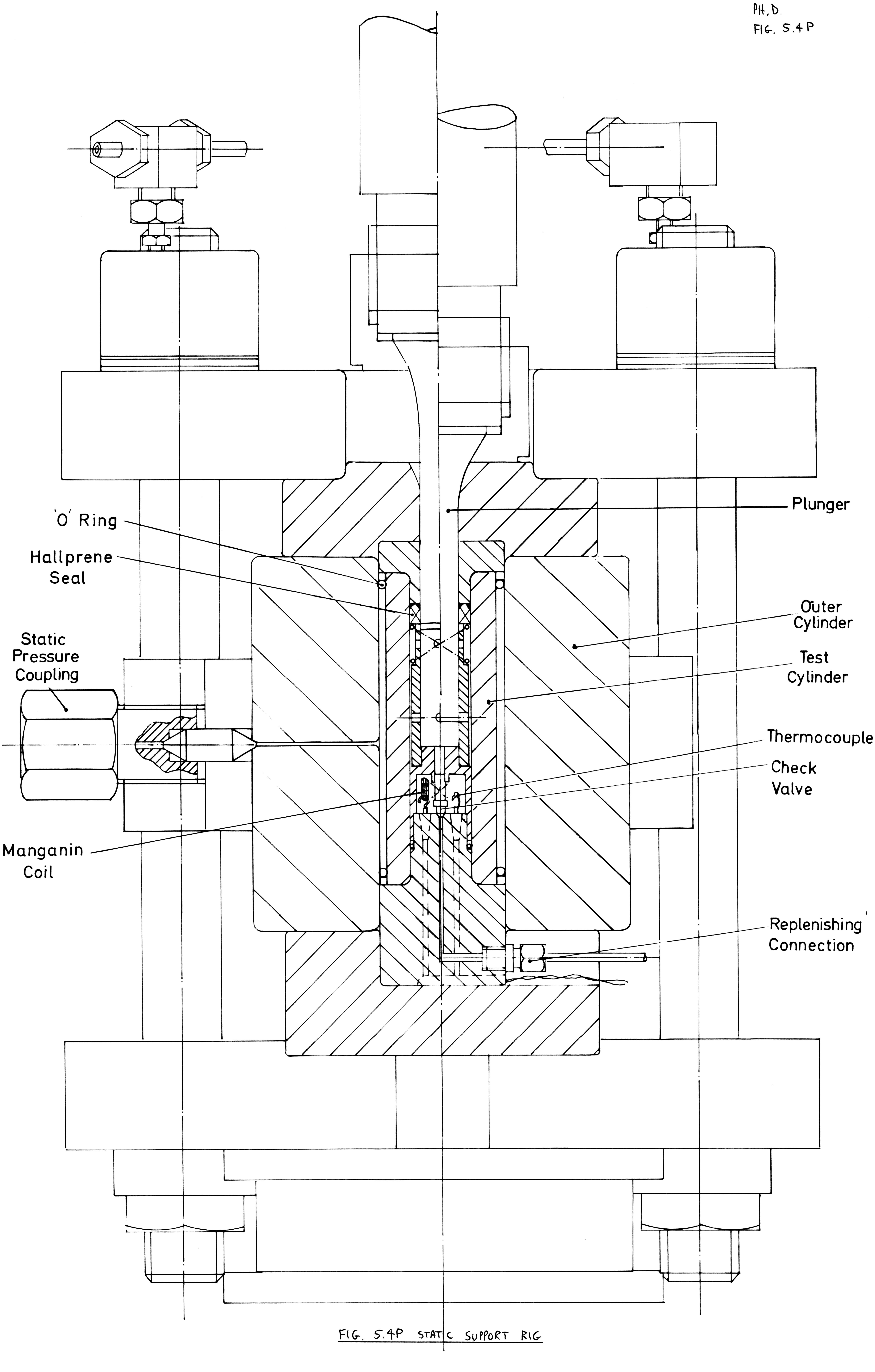

FIG. 5.4P STATIC SUPPORT RIG

HARVEY D.C.
PH.D.
FIG. 3.1P

Fig 3.1P HIGH PRESSURE PUMPING RIG

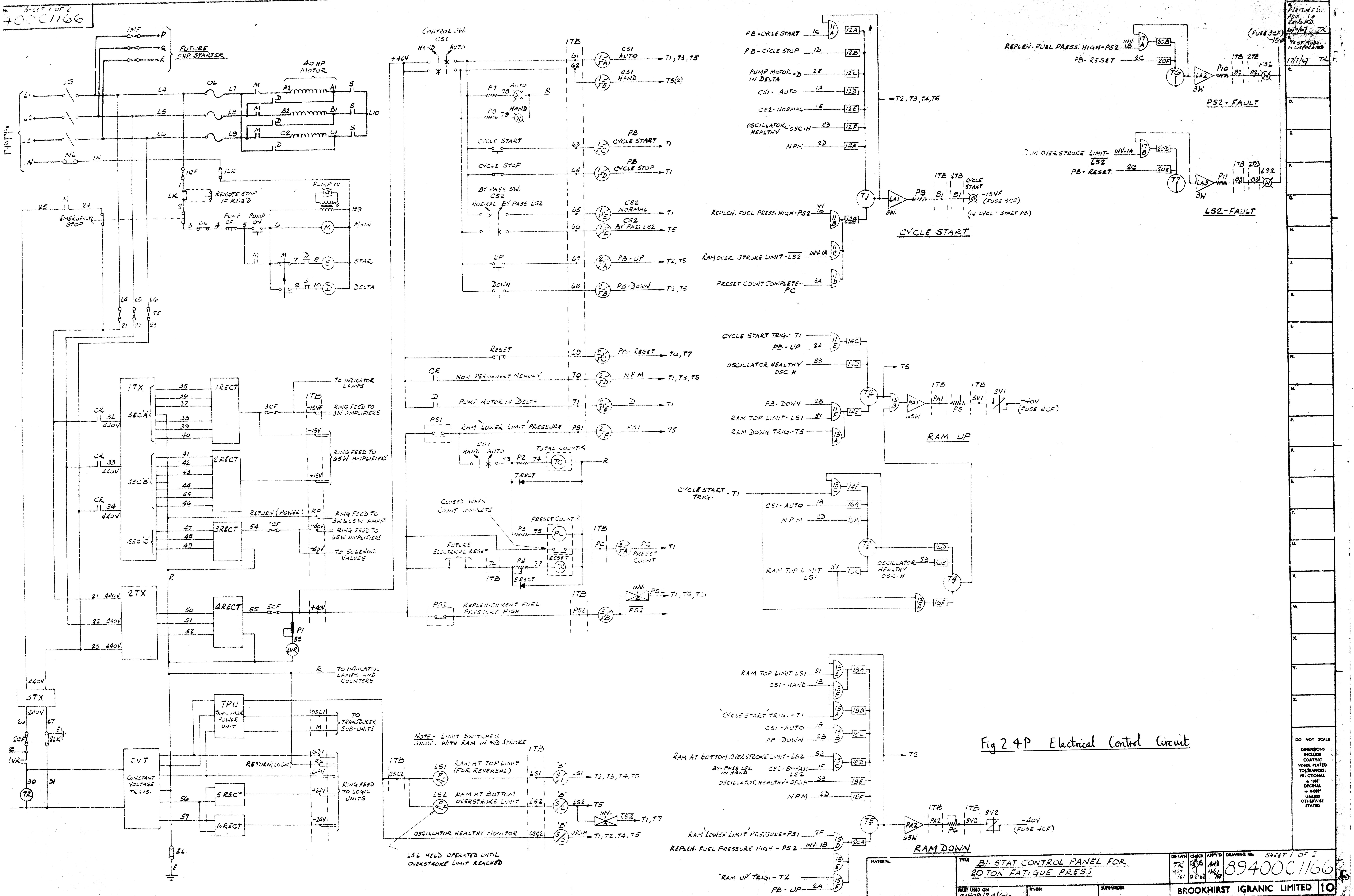

Fig 2.4P Electrical Control Circuit

TITLE	B1- STAT CONTROL PANEL FOR 20 TON FATIGUE PRESS
PART USED ON	C1509/7A/66
DRAWING No.	89400C1166 SHEET 1 OF 2
	BROOKHIRST IGRANIC LIMITED 10